Dissection of the key molecular pathways for muscle regeneration in the zebrafish in vivo model

Sultan, Sami

Awarding institution:
King's College London

Dissection of the key molecular pathways for muscle regeneration in the zebrafish *in vivo* model

By
Sami Hassan Ali Sultan

A thesis submitted to King's College London in partial fulfilment for the degree of
Doctor of Philosophy
Stem Cells & Regenerative Medicine

December 2021

Centre for Craniofacial and Regenerative Biology
Dental Institute
King's College London

Abstract

In mouse, Notch signalling is important for the maintenance of the muscle stem cell (muSC) niche during muscle development and regeneration. Inhibition of Notch signalling in Pax7+ cells leads to the loss of the muSC pool due to premature differentiation, perturbing muscle repair. Following muscle damage, an influx of immune cells generates a pro-inflammatory microenvironment. Murine macrophage ablation studies have demonstrated the importance of macrophages in successful muscle repair. Following macrophage ablation, neutrophilic mediated inflammatory microenvironment is prolonged, leading to increased muscular necrosis and fibrosis, not seen in normal regeneration. Furthermore, it has been shown that pro-inflammatory macrophages inhibit myogenic precursor cell (MPC) fusion and promote proliferation, whereas anti-inflammatory macrophages promote differentiation. Moreover, it has been shown in mouse that both anti- and pro-inflammatory macrophages inhibit Notch activity in muSCs. The activity of Notch signalling in muSC during muscle repair is still poorly defined *in vivo*, and it is not understood if Notch regulates muscle regeneration in zebrafish. Moreover, it is not known if infiltrating immune cells, macrophages and neutrophils, and the inflammatory microenvironment are important for regulating Notch activity during regeneration. Therefore, I aim to determine how Notch signalling regulates muSC biology in zebrafish. Additionally, I aim to understand if the inflammatory microenvironment influences the Notch-dependent regulation of muSCs.

To understand the importance of Notch signalling for the muSC response to injury in zebrafish, I used transgenic zebrafish to visualise muSCs in conjunction with pharmacological (DAPT) and genetic (dnsu[h]) tools to globally inhibit Notch. I found that fewer proliferating *pax7a*-expressing muSCs were present following injury in the absence of Notch, which was associated with an increase in the proportion of differentiating muSCs. Moreover, I found that in the myosepta, described as the muSC niche, there was an increase in the number of proliferating *pax7a*-expressing muSCs in the absence of injury. This suggests that Notch signalling is important to promote proliferation following injury, and limit proliferation in the absence of injury. A dynamic reporter of Notch activity revealed that proliferating *pax7a*+ cells

express Notch (*Tp1*:VenusPEST). Additionally, by immunolabelling I also found that very few Pax7+ cells express a stable reporter for Notch activity (*Tp1:H2BmCherry*) at 24 hpi. Moreover, the proportion of *Tp1:H2BmCherry*+ cells expressing *pax7a* increased over time following injury. Taken together, I concluded that the majority of *Tp1*+ nuclei reside in myofibers and do not contribute to muscle repair. Contrastingly, *Tp1*+ cells which upregulate *pax7a* expression, respond to muscle injury. Moreover, I found that these *Tp1:H2BmCherry*+ cells are controlled by Notch signalling. DAPT treatment resulted in more *Tp1:H2BmCherry*+ cells after injury. Using a pharmacogenetic method to ablate macrophages, DEX (steroid) and a TNF-α receptor mutant zebrafish line, I showed that reducing inflammatory signalling following injury resulted in more Pax7+ muSCs. Additionally, I found that macrophages express DeltaD suggesting that macrophages can signal to adjacent cells via Notch. Together my data shows that muSCs are regulated by Notch signalling and the inflammatory microenvironment. I propose that pro-inflammatory macrophages signal via DaltaD to limit Pax7+ and *Tp1*+ cell proliferation. Moreover, as macrophage ablation and Notch inhibition have opposing effects on the Pax7+ cell population, Notch activity is also important to limit Pax7-expressing muSC differentiation and promote proliferation.

Acknowledgments

Robert, thank you for not only giving me the opportunity to carry out a PhD within your lab, but for also being a great supervisor and mentor. Whilst working with you, I gained valuable lab and written skills, I experienced a fellowship application, and I have had the opportunity to work towards multiple publications. This is more than I could have asked for during this training period of my career and I will be forever grateful.

Christer, although our contact was limited due to the Covid-19 pandemic, your encouragement at the beginning of my PhD and whilst writing this thesis means more to me than you could imagine. Both starting and finishing a PhD are arguably some of the more stressful times during a PhD, and you made the transition periods a lot easier. Also, I would like to thank you for reading my entire results and discussion chapters in just a week, whist juggling other deadlines.

Mum, Dad, and Nadia. Thank you for putting up with me the last four years, you have really helped me get through this PhD. Picking me up from the station after a long day of work, having our morning chats, and the daily encouragement and motivation, have all kept me alive and well during my PhD. This work is as much yours as it is mine. Thank you so much.

Barbara, where even to begin. Since starting your Post-doc you have been by my side, both in lab and whilst writing my thesis. I am still amazed that you managed to proof read my entire thesis in a week whilst working a 9-5 job. With your help, not only have I produced a better thesis, but I have definitely become a better researcher. I am honoured by the amount of time you set aside to help me, and I just hope I will have the opportunity to do the same for you.

The Knight lab, old and new. **Carly** and **Mirco**, I am not sure how I would have survived during the early days in lab without your kindness and patience. You both taught me everything I needed to know from lab work, to fish handling and even the confocal and multiphoton microscopes. Thank you for answering all of my stupid questions and keeping me on track. **Camilla**, my big sister. Thank you for all the jokes and love you have shown me, some of my best laughs during my PhD were with you, and it kept me alive. You, **Johan**, and **little Madeleine** have become like family to me and I cannot wait for all the future adventures! **Klairy** and **Pia**, thank you for your

immunity knowledge. It was extremely helpful to learn from both of you to progress through my PhD. To Pia I also thank you for all the hard work you accomplished during your PhD, as my project is a direct link to yours, I gained a lot from your hard work. **Chantal**, a very special thank you. You have been amazing, not only do you work above and beyond for everyone, but you have been so kind (in your own way) showing an interest in my project any time you get a chance. **MC**, although our time together was short, you made a big impact on me. Your hard work ethic and encouraging words and advice definitely helped me during the later stages of my PhD.

Dom, **Juan, Suveer**, and **Anna**, thank you for always being there for me. Taking me down for coffee breaks, giving me great advice, making me laugh or telling me cool facts about the world, always helping me de-stress. I really appreciate it, you all made my PhD that little bit more enjoyable.

Davide, you have been by my side throughout my PhD, writing your thesis at the same time as me. I honestly do not know what I would have done without you. You have been amazing, and I am so thankful that I got to experience this with you. I hope our paths cross again in the future!

Finally, I would like to thank **Angela** and the wider **CCRB**. Angela you have been amazing, always there to support everyone. Having you by our side is empowering, thank you so much. Working in such a friendly environment has made my PhD experience so much better. Thank you to everyone!

Table of Contents

List of figures

List of tables

List of movies

List of files

Abbreviations

ADAMTS1	A Disintegrin-Like And Metalloproteinase With Thrombospondin Type 1 Motif
ALM	Anterior lateral mesoderm
AMPK	AMP-activated protein kinase
ANOVA	Analysis of variance
Arg	Arginase
ART	Align Rank transform
ATP	Adenosine triphosphate
bh	Benjamini and Hochberg
BMP	Bone Morphogenetic Protein
BrdU	Bromodeoxyuridine
CCR	Chemokine receptor
CD	Cluster of differentiation
cDNA	Complementary DNA
CHT	Caudal hematopoietic tissue
CI	Confidence interval
CIITA	Class II transactivator
CINC	Neutrophil chemoattractant
CREB	cAMP response element-binding protein
CTX	Cardiotoxin
DEX	Dexamethasone
DHM	Dorsal horizontal myoseptum
Dll	Delta like ligand
DMB	Decamethonium bromide
DMSO	Dimethyl sulfoxide
DN	Dominant negative
DNA	Deoxyribonucleic acid
dpf	Days post fertilisation
dpi	Days post injury

ECL	External cell layer
ECM	Extracellular matrix
EN	Engrailed
FACS	Fluorescence activated cell sorted
FAP	Fibro-adipogenic progenitor
Fzd	Frizzled
H2K27me3	Trimethylation of lysine 27 on histone 3
H4	Histone 4
HCL	Hydrochloric acid
HGF	Hepatocyte growth factor
Hh	Hedgehog
HIF	Hypoxia induced factor
HM	Horizontal myoseptum
hpa	Hours post amputation
hpf	Hours post fertilisation
hpi	Hours post injury
ICM	Intermediate cell mass
IFN	Interferon
IGF	Insulin like growth factor
IL	Interleukin
iNOS	Nitric oxide synthase
IRF	IFN regulatory factor 1
LPS	Lipopolysaccharide
M-CSF	Macrophage colony stimulating factor
MCP	Monocyte chemoattractant protein
MEF2	Myocyte enhancer factor-2
MIP	Macrophage inflammatory protein
MO	Morpholino antisense oligonucleotides
MPC	Muscle precursor cell
Mpx	Myeloperoxidase
MRF	Myogenic regulatory factor

mRNP	Messenger ribonucleotide protein
MTZ	Metronidazole
muSC	Muscle stem cell
MYHC	Myosin heavy chain
Myog	Myogenin
NBCS	New born calf serum
NICD	Notch intracellular domain
NMJ	Neuromuscular junctions
NO	Nitric oxide
N	Number of samples per group
N	Total number of samples
PBI	posterior blood island
PBS	Phosphate buffered saline
PBT	Phosphate buffered saline with Tween 20
PBTx	Phosphate buffered saline with Triton x-100
PCP	Planar cell polarity
PCR	Polymerase chain reaction
PDMS	Polydimethylsiloxane
PFA	Paraformaldehyde
PICs	Pw1+ interstitial cells
PKA	protein kinase A
PLM	Posterior lateral mesoderm
POCG2	Polycomb group 2
PRE	Polycomb-response element
PTU	N-Phenylthiourea
PICs	Pw1+ interstitial cells
RNA	Ribonucleic acid
SC	Satellite cell
SHG	Second harmonic generation
Shh	Sonic hedgehog
SNP	Single nucleotide polymorphism

Su(H)	Suppressor of hairless
T cells	T lymphocytes
TGF	Transforming growth factor
TNF	Tumour necrosis factor
TrA	Transverse abdominis
Transgenic	Tg
Tregs	Regulatory T-cells
Tricane	Tricaine methanesulfonate
UAS	Upstream Activation Sequence
V/V	Volume per volume
VCAM	Vascular cell adhesion molecule
VEGF	Vascular endothelial growth factor
VHM	Vertical horizontal myoseptum
VM	Vertical myoseptum
WISP1	Wnt inducible signalling pathway protein 1
WMW	Wilcoxon Mann Whitney U rank sum test
WT	Wild type

Chapter 1 Introduction

Constituting 30-40% body mass (Relaix *et al*., 2021), skeletal muscle controls body movement, posture, breathing and lipid metabolism. Although post-mitotic in nature, skeletal muscle has a remarkable regenerative capacity, facilitated by the activity of resident muSCs, interstitial cells and the propagation of an immune response. To understand how muSC activity is controlled in homeostasis and regeneration, a comprehensive understanding of the development of muscle and the emergence of the muSC population is required. Moreover, a detailed description of the interplay of signalling pathways which orchestrate the process of myogenesis is necessary to dissect the processes controlling postnatal regeneration. Therefore, I begin by describing the process of amniote muscle development and how these processes are similar or different from zebrafish. I subsequently describe how muSC quiescence and activation is regulated by Notch signalling. Finally, I introduce the importance of the immune response, particularly the activity of pro- and anti-inflammatory macrophages, on the muSC response to injury.

1.1 Amniote muscle development

Although the processes of muscle development and regeneration are fundamentally different, several mechanisms which are important for regulating MPCs during muscle development, are also key for the activation and activity of muSCs in repair. Moreover, it is important to account for the developmental mechanisms of muscle formation and growth when using the developing zebrafish to dissect the mechanisms controlling muSC activity following injury.

1.1.1 Formation of the myotome

Embryonic somites are derived from the paraxial mesoderm controlled by morphogen gradients and 'clock' gene expression (reviewed by Aulehla and Pourquié, 2006). The paraxial mesoderm begins to undergo somitogenesis, the prerequisite to myotome formation. Under the influence of 'clock' transcription factors (Hairy in chick, *Hes* in mouse, and *her* in zebrafish; reviewed by Maroto *et al.*, 2012), somitogenesis follows an orderly programme. Epithelialization of the

mesoderm into somites starts at the anterior/cranial end of the body axis; simultaneously, a constant supply of stem-like mesenchymal cells enter the posterior/caudal end (Christ *et al.*, 1992; Cossu *et al.*, 1995; Kiefer and Hauschka, 2001).

The most dorsal structure of the somite is the dermomyotome. The dermomyotome contains MPCs responsible for the formation of skeletal muscle (Christ *et al.*, 1992). Embryonic myogenesis occurs in two successive waves (reviewed by Chal and Pourquié, 2017; Fig. 1.1). The initial wave forms template myotubes within the primitive myotome, contributing to muscle growth. During the 2nd wave, the dermomyotome de-epithelializes, and proliferative MPCs expressing *Pax3* and *Pax7* migrate towards the primitive myotome (Relaix *et al.*, 2005). These cells form additional myofibers along the initial template fibres whilst establishing the muSC population (Gros *et al.*, 2005; Manceau *et al.*, 2008). Using fate mapping techniques in chick (Ben-Yair and Kalcheim, 2005; Manceau *et al.*, 2008) and the engrailed (*En*) 1 reporter mouse (specifically expressed in the central dermomyotome; Atit *et al.*, 2006), cells become a triangular domain below the dermomyotome by E10.8, differentiating into trunk muscle by E16.5. By tracking injected dye, it has been shown that cells residing in the lateral and medial dermomyotome lips contribute to the primary wave of myogenesis (Denetclaw *et al.*, 2001). Once the cells have migrated beneath the dermomyotome, they divide vertically, generating the typical triangular mature myotome structure (Gros *et al.*, 2005).

Myf5 transcript is the first MRF expressed transiently in the paraxial mesoderm (Ott *et al.*, 1991), with high *Myod* and *Myf5* transcript expression within the dermomyotomal lips (Kiefer and Hauschka, 2001). Cells which delaminate from the epaxial (dorsal) and hypaxial (ventral) lips of the dermomyotome, seeding the formation of the myotome, sequentially express *Myf5*, *Myod*, *Myogenin*, *MRF4*, and myosin heavy chain (MYHC; Gros *et al.*, 2005; Manceau *et al.*, 2008). Additionally, MRF activation also results in the upregulation of transcription factors such as myocyte enhancer factor-2 (*Mef2*) which enhances the function of MRFs through the process of transcriptional cooperation (Molkentin *et al.*, 1995). *Myod* upregulates MiR-1, repressing HDAC4 which sequentially downregulates *Mef2*, promoting differentiation (Chen *et al.*, 2006).

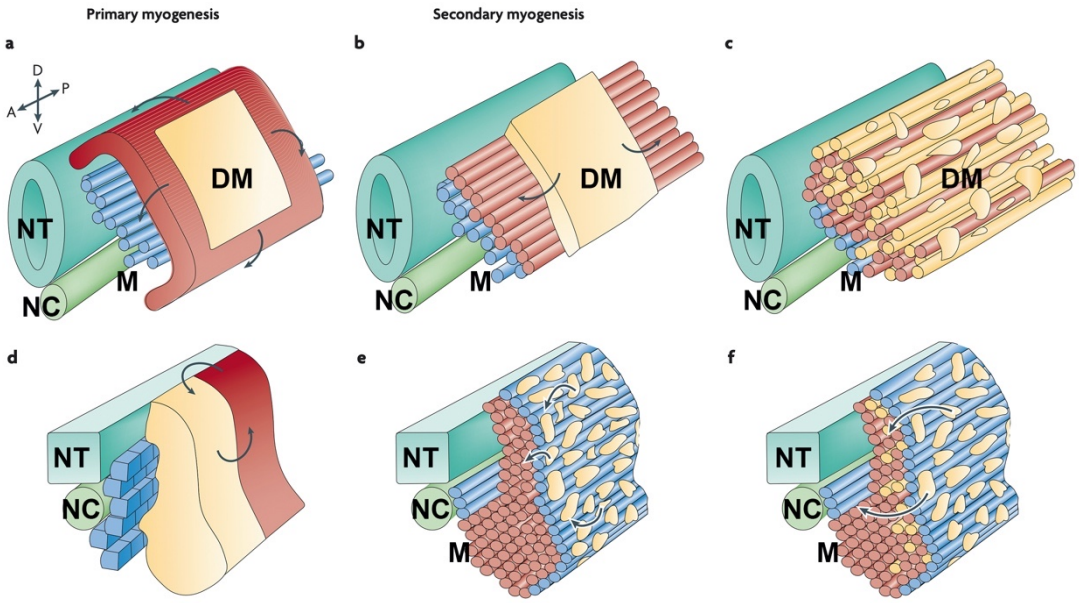

Figure 1.1. Amniote and zebrafish muscle development

In amniotes, pioneer fibres (blue) are formed by cells originating from the dorsal-medial somite (a), acting as a template for the formation of the primary myotome. Cells subsequently delaminate from the dermomyotome lips forming additional myofibers and the primary myotome (b). Secondary myogenesis in amniotes occurs following the de-epithelializes of the central region of the dermomyotome (c). In the zebrafish, the early myotome is organised anteriorly-posteriorly (d). Adaxial cells are the first cell to differentiate and migrate into the myotome (blue; e). The adaxial cells will migrate to the lateral surface forming a monolayer of slow muscle (f). The muscle pioneer cells are a subset of adaxial cells which stay near the notochord (f). During the migration of the adaxial cells, fast muscle fibres begin to elongate and differentiate into the fast muscle (f). Due to a rotation event mid-segmentation, anterior cells of the somite (yellow) migrate to the lateral edge, forming the ECL (f). A, anterior; D, dorsal; P, posterior; V, ventral; NT, neural tube; NC, notochord; DM, dermomyotome; M, myotome (Adapted from Bryson-Richardson and Currie, 2008).

1.1.2 Myogenic regulatory factors

Myogenic regulatory factors (MRFs) regulate the commitment, activation, and fusion of MPCs (Fig. 1.2). MRFs are members of the basic helix-loop-helix transcription factor family (Fong *et al.*, 2012; Conerly *et al.*, 2016). The expression of each MRF in muSCs follow a sequential pattern during development and regeneration, initiated by the expression of *Myf5* and *Myod*, followed by *Myogenin* and a transient expression of *MRF4* (Fig. 1.2; reviewed by Ruparelia *et al.*, 2020).

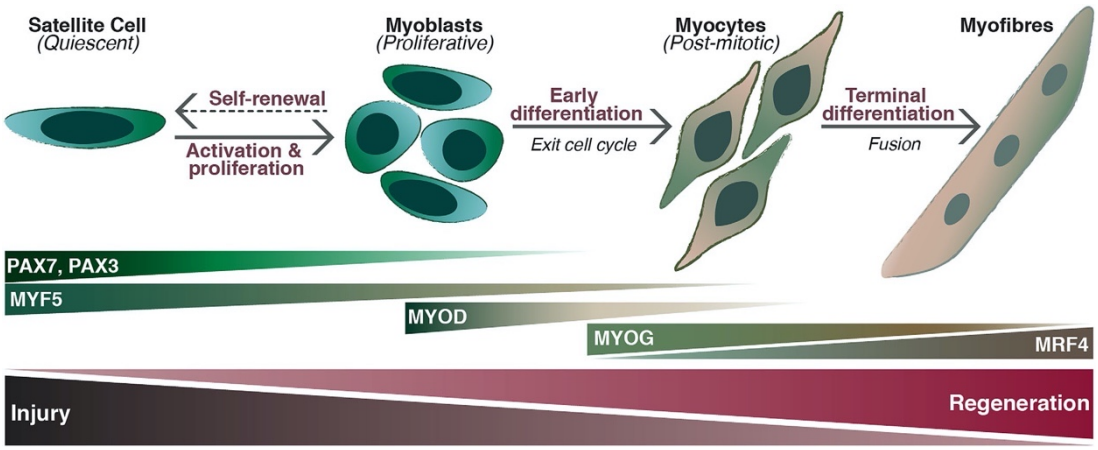

Figure 1.2 Sequential expression of *pax* genes and MRFs following muSC activation.
Following activation, muSCs proliferate, differentiate and fuse into damaged or new myofibers. This sequential program is facilitated by the expression of myogenic regulatory factors (MRFs). PAX3+PAX7+ muSCs commit to the myogenic lineage and proliferate, expressing both MYF5 and MYOD. Subsequently, muSCs express Myogenin (MYOG) and MRF4, terminally differentiating and fusing into myofibers (Ruparelia *et al.,* 2020).

Myf5 and *Myod*

Myf5 and *Myod* are described as markers of terminal specification of cells into the myogenic lineage (reviewed by Pownall *et al.*, 2002), shown to convert cultured cells into the myogenic fate (Lassar *et al.*, 1986; Braun *et al.*, 1989; Olson, 1990). *Myf5*:*Myod* double-null mice revealed that *Myf5* and *Myod* are critical for the formation of muscle (Rudnicki *et al.*, 1993); however, they are functionally redundant. Although muscle development is delayed, mice lacking *Myf5* expression still develop muscle, expressing *Myod*, *Myogenin* and *MRF4* mRNA (Braun *et al.*, 1992). Moreover, prolonged *Myf5* expression compensates for a lack of *Myod* expression, developing phenotypically normal muscle (Rudnicki *et al.*, 1992). Although *Myf5* and *Myod* are redundant during muscle development, they also display specific functions. Using a mouse fibroblast line lacking *Myod* or *Myf5* expression, Conerly *et al.,* (2016) demonstrated that *Myod* and *Myf5* show different transcriptional abilities. MYF5 binds heterochromatin, acetylating histone 4 (H4) conferring a euchromatin configuration. This allows MYOD to bind interim, which can further acetylate H4 in addition to initiating transcription through polymerase II recruitment (Conerly *et al.*, 2016).

Myogenin

Myogenin transcript can be detected as early as E8.5-9.5 (Sassoon *et al.*, 1989). Cusella-DeAngelis *et al.,* (1992) concludes that although *Myogenin* transcript is synthesized, it is associated with the polysome complex, suggesting it subsequently undergoes cytoplasmic degradation (Cusella-De Angelis *et al.*, 1992). *Myogenin* mutations do not affect *Myod* transcript levels so mutants can initiate myogenic lineage specification. However, in *Myogenin* mutants, MPCs lack the ability to fuse resulting in reduced myofiber density (Hasty *et al.*, 1993). This lack of fusion of MPCs results in an increase of mononuclear myoblasts with diffuse myofiber formation during the later stages of muscle development (Hasty *et al.*, 1993). Although *Myod* and *Myogenin* positively regulate one another, suggesting possible redundancy (Thayer *et al.*, 1989), *Myod* expression is unable to compensate for the lack of *Myogenin* (Hasty *et al.*, 1993).

MRF4

MRF4, also known as *Myf6*, is transiently activated during myogenesis, contributing to the specification and fusion of MPCs (Rhodes and Konieczny, 1989; Braun *et al.*, 1990; Kassar-Duchossoy *et al.*, 2004). *MRF4* was found to convert C3H10T1/2 mouse fibroblasts into a myogenic lineage, similar to *Myod* or *Myogenin* transfections (Rhodes and Konieczny, 1989). In light of the observation that *Myf5:MyoD* mouse double mutants were in fact *Myf5:MyoD:MRF4* triple KOs (*Myf5* and *MRF4* are genetically linked), Kassar-Duchossoy *et al.,* (2004) shows that mice lacking both *Myf5* (where *MRF4* expression is maintained) and *Myod*, still show early robust skeletal muscle determination (Kassar-Duchossoy *et al.*, 2004). Furthermore, using previously described *Myf5* mutant mice which lack *MRF4* expression ($Myf5^{nlacZ/nlacZ}$), and two newly designed mice lines which show normal ($Myf5^{loxP/loxP}$) and delayed ($Myf5^{GFP\text{-}P/GFP\text{-}P}$) MRF4 expression, they find that *Myf5*:*Myod*:*MRF4* triple mutants have drastically reduced musculature in an MRF4-dependent manner ($Myf5^{nlacZ/nlacZ} > Myf5^{GFP\text{-}P/GFP\text{-}P} > Myf5^{loxP/loxP}$; Kassar-Duchossoy *et al.*, 2004). They conclude that *MRF4* plays a role upstream of *Myod* during the early stages of skeletal muscle determination in tandem with *Myf5*, and a secondary key role during the later differentiation events (Kassar-Duchossoy *et al.*, 2004).

1.1.3 *Pax* genes

Pax genes are characterised by their paired homeobox Deoxyribonucleic acid (DNA)-binding domain, important for the survival, proliferation, motility, and differentiation of various somitic stem cell populations (reviewed by Buckingham and Relaix, 2007). *Pax3* and *Pax7* are important for the migration, self-renewal, and quiescence of MPCs during embryonic and postnatal myogenesis (reviewed by Buckingham and Relaix, 2007).

Both *Pax3* and *Pax7* are expressed by cells of the dermomyotome; *Pax7* is highly expressed centrally while *Pax3* expression is higher at the dermomyotomal lips (Jostes *et al.*, 1990; Kiefer and Hauschka, 2001; Kassar-Duchossoy *et al.*, 2004; Relaix *et al.*, 2005). *Pax3* and *Pax7* reporter line studies have shown that cells expressing both Pax3 and Pax7 divide vertically, generating a population of “inner cells” which

constitute the early myotome (Relaix *et al.*, 2005). Although *Pax3*:*Pax7* double knockouts successfully initiate and complete the first early wave of myogenesis under the control of MRFs, they fail to generate additional myogenic cells leading to the reduction and disorganization of trunk musculature (Relaix *et al.*, 2005). This suggests that cells expressing *Pax3* and *Pax7* drive secondary myogenesis and the growth of the myotome (Relaix *et al.*, 2005). Interestingly, although *Pax7-/-* knock-out mice are significantly smaller with smaller myofibers, *Pax7* expression is dispensable for embryonic myogenesis (Seale *et al.*, 2000). Contrastingly, the conditional loss of *Pax3*-expressing cells results in the loss of PAX7+ progenitors, MYOD+ myoblasts, and Myosin+ myofibers, subsequently leading to embryonic lethality by E12.5 (Hutcheson *et al.*, 2009). Although *Paix3* and *Pax7* appear to have separate roles during embryonic myogenesis, *Pax7* knock-in expression within the *Pax3* locus partially rescues the functions of *Pax3*, leading to the successful development of somites (Relaix *et al.*, 2004). This suggests that *Pax3* and *Pax7* are functionally redundant.

Pax3 is initially expressed in the presomitic mesoderm. To assess the contribution of *Pax3*-expressing MPCs to muscle development, *Pax3*-GFP lineage tracing has been conducted (Schienda *et al.*, 2006). These lineage tracing experiment have shown that *Pax3*-expressing MPCs contribute to limb and ventral body wall muscle (Schienda *et al.*, 2006). The ventrolateral lips of the dermomyotome undergoes epithelial-to-mesenchymal transition giving rise to long-range migratory MPCs (reviewed by Buckingham *et al.*, 2003). *Splotch* mutant mice, devoid of *pax3* expression, do not develop limb musculature (Bober *et al.*, 1994). The delamination and migration of *pax3*-expressing cells is controlled by Hepatocyte growth factor (HGF) and its receptor C-MET (Bladt *et al.*, 1995), which is upregulated by *Pax3* (Epstein *et al.*, 1996). These cells constitute the development of the limb musculature, contributing to the formation of the *Pax7*+ muSC niche (Schienda *et al.*, 2006). Contrastingly, *Pax7*-expressing cells play an important role in postnatal growth and the establishment of the muSC population (Lepper *et al.*, 2009). *Pax3* and *Myf5* are expressed in tandem upstream of *Myod* and *Myogenin*, a conclusion substantiated by Pax3:Myf5 double knock-out mice (Tajbakhsh *et al.*, 1997). These double mutant mice are devoid of *MyoD* and *Myogenin* expression and all skeletal muscle,

demonstrating the importance of *Pax3* and *Myf5* expression for successful muscle development (Tajbakhsh *et al.*, 1997).

Six genes, particularly, *Six1* and *Six4*, have been dubbed the apex of myogenic genetic regulation, working in concert with *Pax* genes and MRF to orchestrate embryonic myogenesis. Six genes regulate *Pax3*, *Myf5*, *Myod*, *MRF4*, and *Myogenin* expression important for somitogenesis and limb formation (Grifone *et al.*, 2005). Mice lacking *Six4* develop muscle normally (Laclef *et al.*, 2003; Grifone *et al.*, 2005), and MPCs differentiate and migrate normally in *Six1-/-* knock-out mice, expressing normal levels of *Six4* (Laclef *et al.*, 2003). *Six1-/-Six4-/-* double knock-out mice have severe skeletal and muscular defects, characterised by myotomal disorganisation, increased apoptosis and the decrease of *pax3, Pax7 and c-met* expression within the limb (Grifone *et al.*, 2005). Although *Six4* can partially compensate for the loss of *Six1* suggesting functional redundancy, *Six1-/-Six4-/+* mice have severely reduced *Pax3*+*Myf5*+ MPCs within the limb (Giordani *et al.*, 2007). Moreover, *Eya1−/−Eya2−/−* (downstream target of *Pax3*, *Six4*, *Six1* and *Six5*) double mutant mice do not develop most trunk hypaxial muscles, or limb muscles (Grifone *et al.*, 2007). This is caused by a reduced *Pax3* expression at the hypaxial dermomyotome lips (Grifone *et al.*, 2007). Epaxial dermomyotome and muscle, which forms independently of *Pax3* expression, are unaffected by *Six* gene pathway manipulations (Grifone *et al.*, 2005, 2007). This shows the importance of *Six* expression for the regulation of *Pax3* expression during the development of hypaxial musculature.

Summary

Together, studies investigating the development of muscle in mouse and chick have demonstrated that myogenesis occurs in two waves (Fig. 1.1). During the first wave, dermomyotomal *En1*+ cells migrate into the nascent myotome to form template myofibers. Subsequently, during the second wave, the dermomyotome de-epithelializes, and proliferative *Pax3*- and *Pax7*- expressing MPCs form additional myofibers. Although *Pax3* expression is critical for muscle development, *Pax7* is dispensable, instead required for post-natal myogenesis. The activity of MPCs during

myogenesis is controlled by the sequential expression of MRFs. *Myf5* and *Myod* promote myogenic commitment and *Myogenin* and *MRF4* promote differentiation.

1.2 Zebrafish muscle development

Unlike amniotes, zebrafish are externally fertilised and so have an early requirement to swim to survive. Consequently, myogenesis is initiated at an earlier stage relative to amniotes, and the muscle architecture is suited to meet the requirements needed to generate force whilst swimming (reviewed by Johnston *et al.*, 2011). In addition to swimming, fish muscle growth is influenced by the habitat. Factors such as hydrodynamic flow and temperature can affect muscle development (reviewed by Johnston *et al.*, 2011). Thermal imprinting in the developing fish has been shown to negatively affect the number and size of muscle fibres in juvenile and adult Atlantic salmon (Macqueen *et al.*, 2008; Clarkson *et al.*, 2021) and zebrafish (Johnston *et al.*, 2009). Like amniote muscle development, zebrafish muscle development is co-ordinated by the sequential activation of MRFs in MPCs. This MRF expression pattern is important for the formation of both fast (deep; Devoto *et al.*, 1996; Stellabotte *et al.*, 2007) and slow (superficial; Devoto *et al.*, 1996; Hirsinger *et al.*, 2004; Stellabotte *et al.*, 2007) myofibers.

1.2.1 Formation of the myotome

Like amniotes, all muscle in the developing zebrafish trunk is derived from somites, found in pairs separated by the notochord and neural tube (reviewed by Johnston *et al.*, 2011). In zebrafish, the MPCs which are responsible for the development of slow or fast muscle occupy specific locations around the marginal zone of the zebrafish embryo prior to somitogenesis (Hirsinger *et al.*, 2004). However, these cells are still plastic, retaining the ability to succumb to either cellular fate. The initiation of gastrulation leads to the involution and convergence of cells proximal to the developing notochord; fast precursors found superficially and adaxial cells deeper relative to the notochord. Although not yet committed, adaxial cells are precursors of slow muscle (Devoto *et al.*, 1996). During somitogenesis, *Myf5*+*Myod*+ adaxial cells elongate and span the length of the somite before migrating through the somite towards the lateral surface of the embryo forming a monolayer of muscle cells

committed to the slow musculature lineage (Devoto *et al.*, 1996; Hirsinger *et al.*, 2004; Stellabotte *et al.*, 2007; Fig. 1.1). The commitment of cells towards the slow lineage is mediated by Hedgehog signalling (Hirsinger at al., 2004). Some adaxial cells remain proximal to the notochord, developing into an intermediate muscle group referred to pioneer cells. *En1*-expressing pioneer cells remain proximal to the notochord and expand to the lateral surface of the somite at the level of the horizontal myosepta (Devoto *et al.*, 1996). These cells will form neuromuscular junctions (NMJs) with primary motor neurons (Melançon *et al.*, 1997). The final cellular event is the establishment of fast muscle in the now deeper part of the somite. The elongation of the fast fibre cells is promoted by the migration of adaxial cells (Henry and Amacher, 2004). Fast fibres arise from the lateral presomitic *Myod*+*Myogenin*- cells (Devoto *et al.*, 1996; Weinberg *et al.*, 1996; Fig. 1.1), constituting most of the mature zebrafish myotome (Devoto *et al.*, 1996; Stellabotte *et al.*, 2007).

1.2.2 External cell layer

During mid-segmentation, the zebrafish somite undergoes a re-arrangement event. The cells 'rotate' so that the anterior border cells translocate laterally towards the periphery of the somite (Hollway *et al.*, 2007; Stellabotte *et al.*, 2007). It has been demonstrated in the pearlfish that this cellular migration forms the external cell layer (ECL), which is analogous to the amniote dermomyotome (Marschallinger *et al.*, 2009). The ECL persists throughout the entire life of the fish, and is important for post-embryonic growth (Marschallinger *et al.*, 2009; Nguyen *et al.*, 2017). The ECL can be further subdivided into the horizontal myosepta and the vertical myosepta. The horizontal myosepta comprises a reservoir of low-cycling muSCs (Nguyen *et al.*, 2017; Fig. 1.3). Subsequently, a sub-set of these cells migrate to the vertical myosepta, where they proliferate and contribute to muscle growth (Nguyen *et al.*, 2017; Fig. 1.3). These proliferative MPCs which migrate through the developing somite, contributing to secondary myogenesis and the growth of fast muscle during the later stages of embryonic (Hollway *et al.*, 2007; Marschallinger *et al.*, 2009). The ECL also give rise to the population of quiescent MPCs which proliferate and

differentiate following activation, contributing to adult fish growth and regeneration (Hollway *et al.*, 2007).

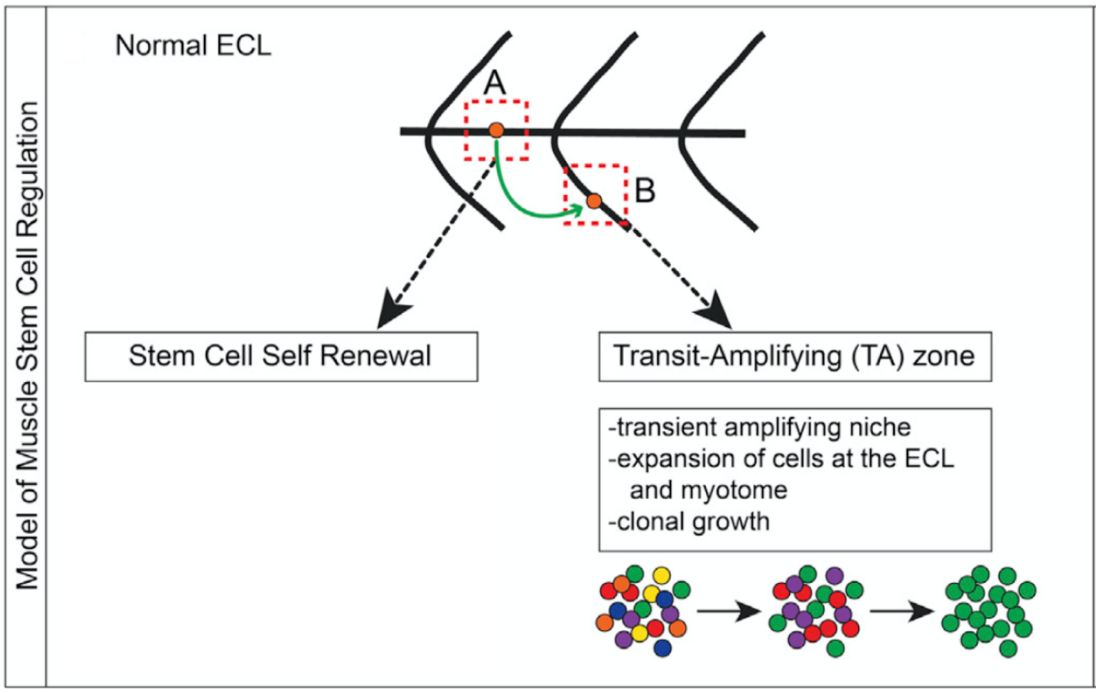

Figure 1.3 Growth specific muSC regulation.
Slow cycling muSCs are located within the horizontal myoseptum (A). These cells act as the reservoir, maintaining the muSC population. A proportion of these muSCs migrate to the vertical myoseptum, also referred to as the transit-amplifying zone (B) where they hyper-proliferate. A single muSC is randomly assigned to migrate from the horizontal to vertical myoseptum. This muSC will undergo successive proliferative events eventually constituting an entire myofiber. This process has been termed clonal drift (adapted from Nguyen et al., 2017).

1.2.3 Myogenic regulatory factors

Like amniotes, zebrafish MPCs are under the control of the same conserved MRF master-transcription factors which show both specific and redundant functions during muscle development (reviewed by Rossi and Messina, 2014). Due to the evolutionary duplication of the zebrafish genome, there are often multiple paralogs per mammalian gene (Jaillon *et al.*, 2004). Although zebrafish have undergone this whole genome duplication, MPCs in zebrafish are controlled by the temporal activation of *myf5*, *myod* and then *myogenin* during embryonic myogenesis. Using a combination of morpholino antisense oligonucleotides (MO) injections to limit MRF translation and *myf5* homozygote zebrafish mutants, Hinits *et al.,* (2009) characterised the function of MRFs on the development of slow and fast muscle. They find that, although *myod* MO leads to delayed slow muscle fibre formation, *myf5* and *myod* are redundant for the formation of slow fibre formation (Hinits *et al.*, 2009). Only when both *myf5* and *myod* MOs are injected or when the *myod* MO is injected into *myf5* mutants is there a loss of slow muscle differentiation markers and slow muscle fibres (Hinits *et al.*, 2009). Contrastingly, it appears that *myod* is critical for the development of fast muscle fibres. Fast muscle markers are overtly normal in *myf5* mutants, reduced in *myod* morphants and ablated in *myf5* mutants injected with *myod* MO (Hinits *et al.*, 2009). This is associated with a loss of *myogenin* expression in fast muscle (Hinits *et al.*, 2009). Although *myod*, *myogenin* double morphants have a loss of most fast fibres, loss of *myogenin* and *myf5* expression has no effect, suggesting that the development of fast muscle is mediated by *myod* (Hinits *et al.*, 2009). Unsurprisingly, *myf5*, *myod* and *myogenin* are devoid of muscle (Hinits *et al.*, 2009). Although MRF4 is important for the determination of MPCs in mammals, this does not appear to be conserved in zebrafish. Hinits *et al.,* (2009), shows that *mrf4* mutant injected with *myf5* and *myod* MOs fail to stop the development of all muscle (regardless of the *mrf4* genotype; Hinits *et al.*, 2009). Moreover, *mrf4* is concomitantly expressed with *myogenin* suggesting a role in differentiation (Hinits *et al.*, 2009). Additionally, *myogenin* and *myod* work in concert to induce fast muscle differentiation (Maves *et al.*, 2007). Hinits *et al*., (2011) reports that although *myogenin* mutant zebrafish successfully complete primary myogenesis, larvae were no longer detected (by genotyping) from 10 weeks post

fertilisation (Hinits *et al.*, 2011). More recently, *myogenin* has also been shown to be an essential regulatory of adult zebrafish muscle growth (Ganassi *et al.*, 2020). Ganassi *et al.,* 2020 show that myofibers isolated from *myogenin*-/- knock-out adult fish have smaller myofibers with more proliferating muSCs (Ganassi *et al.*, 2020). In addition to MRFs, *mef* expression shows a conserved importance during zebrafish embryonic development. MO knockdown of *mef2c* and *mef2d* leads to a disorganised slow and fast myofibril assembly (Hinits and Hughes, 2007).

Summary

In summary, *myf5* and *myod* show a redundant requirement for the development of slow muscle fibres. Contrastingly, *myod* expression is critical for the formation of fast myofibers. Unlike amniote muscle development, *myogenin* and *mrf4* are not required for zebrafish muscle development, but rather show importance for the post-embryonic growth of muscle. Finally, *mef* expression shows a conserved key role during muscle development in both amniotes and zebrafish.

1.2.4 *Pax* genes

Like amniotes, the zebrafish ECL is defined by the expression of *pax3* and *pax7*, both of which are expressed in growth specific MPCs (Hollway *et al.*, 2007; Stellabotte *et al.*, 2007; Nguyen *et al.*, 2017). Histology in pearlfish has shown that Pax7-expressing cells, which lie within the ECL, migrate via the posterior lip to populate the myotome (Marschallinger *et al.*, 2009). These Pax7-expressing cells have also previously been described in the zebrafish ECL by immunohistochemistry (Hollway *et al.*, 2007; Stellabotte *et al.*, 2007). Interestingly, although both mammal and zebrafish secondary myogenesis is dependent on the dermomyotome and ECL, respectively, adaxial cells express MRFs void of any *Pax* expression prior to the formation of the ECL (Devoto *et al.*, 1996; Stellabotte *et al.*, 2007). This suggests that primary myogenesis develops independently of the ECL in zebrafish (Devoto *et al.*, 1996; Stellabotte *et al.*, 2007). Using zebrafish *pax3* and *pax7* MO knockdowns to study the xanthophore lineage, it was found that although zebrafish lacking *pax3* expression have reduced *pax7* expression like mouse mutants (Seale *et al.*, 2000; Hutcheson *et al.*, 2009), they are viable with normal musculature (Minchin and Hughes, 2008).

Nguyen *et al.,* (2017) has shown that 1-3 days post fertilisation (dpf) *Meox1* mutants (which lack slow-cycling Pax3-expressing cells) display perturbed muscle growth (Nguyen *et al.*, 2017). Like mammals, *six* genes are important during embryonic myogenesis, as *six1a* and *b* are expressed in zebrafish musculature (Nord *et al.*, 2013). Inhibition of Six genes in zebrafish leads to smaller disorganised muscle, whereas overexpression keeps Pax7-expressing cells in a proliferative, undifferentiated state (Nord *et al.*, 2013). Taken together, this data suggest that *pax* genes do not have a conserved importance during primary myogenesis in the developing zebrafish embryo, but are critical for the subsequent growth of the fish during the post-embryonic stages.

Summary

Investigations in zebrafish have revealed that developmental myogenesis occurs in two steps (Fig. 1.1). Initially, adaxial cells which are located deep relative to the notochord, elongate, and span the entire somite. The adaxial cells then migrate to the lateral surface forming a monolayer of slow muscle. During this migration, fast fibres begin to elongate, constituting the bulk of the myotome. Around mid-segmentation, a rotation even occurs where anterior border cells translocate to the periphery. This form the ECL, a structure which persists throughout the lifetime of the fish, important for post-embryonic growth. like amniote muscle development, zebrafish muscle development is co-ordinated by the expression of MRFs. *myf5* and *myod* are important for the development of slow muscle fibres. *myod* expression is critical for the formation of fast myofibers. In contrast, unlike amniote muscle development, *myogenin* and *mrf4* are not required for zebrafish muscle development, but rather show importance for the post-embryonic growth of muscle. Finally, *pax* genes are not critical during primary myogenesis in the developing zebrafish embryo.

1.3 Signals controlling embryonic myogenesis

An early transplantation study has shown that disruption of the somatic orientation reveals that myogenesis is controlled by morphogenic gradients (Aoyama and Asamoto, 1988). Since this study, a fine-tuned network of intrinsic and extrinsic

signals, acting as anti- or pro-commitment, have been identified as important for self-renewal and differentiation of MPCs. Embryonic myogenesis and the subsequent growth of muscle are tightly controlled by many processes which can be broadly characterised as mitochondrial and protein metabolism, as well as transcriptional regulators (reviewed by Johnston *et al.*, 2011; Vainshtein and Sandri, 2020). Among these pathways, Notch signalling has been well characterised during the early stages of embryonic myogenesis (reviewed below). Notch signalling functions in concert with Wnt, hedgehog (Hh), and Bone Morphogenetic Protein (BMP) signalling for successful muscle development and growth.

1.3.1 Notch signalling

The Notch signalling pathway is contact-dependent, meaning it is activated once cell surface ligands, such as Delta, Jagged, and Serrate, bind the Notch receptor (reviewed by Luo *et al.*, 2005; Osipo *et al.*, 2008). Upon binding, the Notch receptor undergoes two proteolytic cleavages by ADAM10 and γ-secretase, resulting in the release of the Notch intracellular domain (NICD; reviewed by Luo *et al.*, 2005; Osipo *et al.*, 2008). NICD then translocates to the nucleus interacting with CSL (CBF1/RBP-Jk in mammals and Suppressor of hairless [Su(H)] in zebrafish) repressors, converting them into transcriptional activators (reviewed by Luo *et al.*, 2005; Osipo *et al.*, 2008). Releasing CSL repression promotes the transcription of Notch target genes such as *her, hes* and *hey* genes (Fig. 1.4). During early embryogenesis, Notch signalling promotes the amplification and self-renewal of the MPC population whilst inhibiting differentiation (reviewed below; fig. 1.5). The requirement of Notch signalling during muscle development and growth is conserved in both mammals and zebrafish.

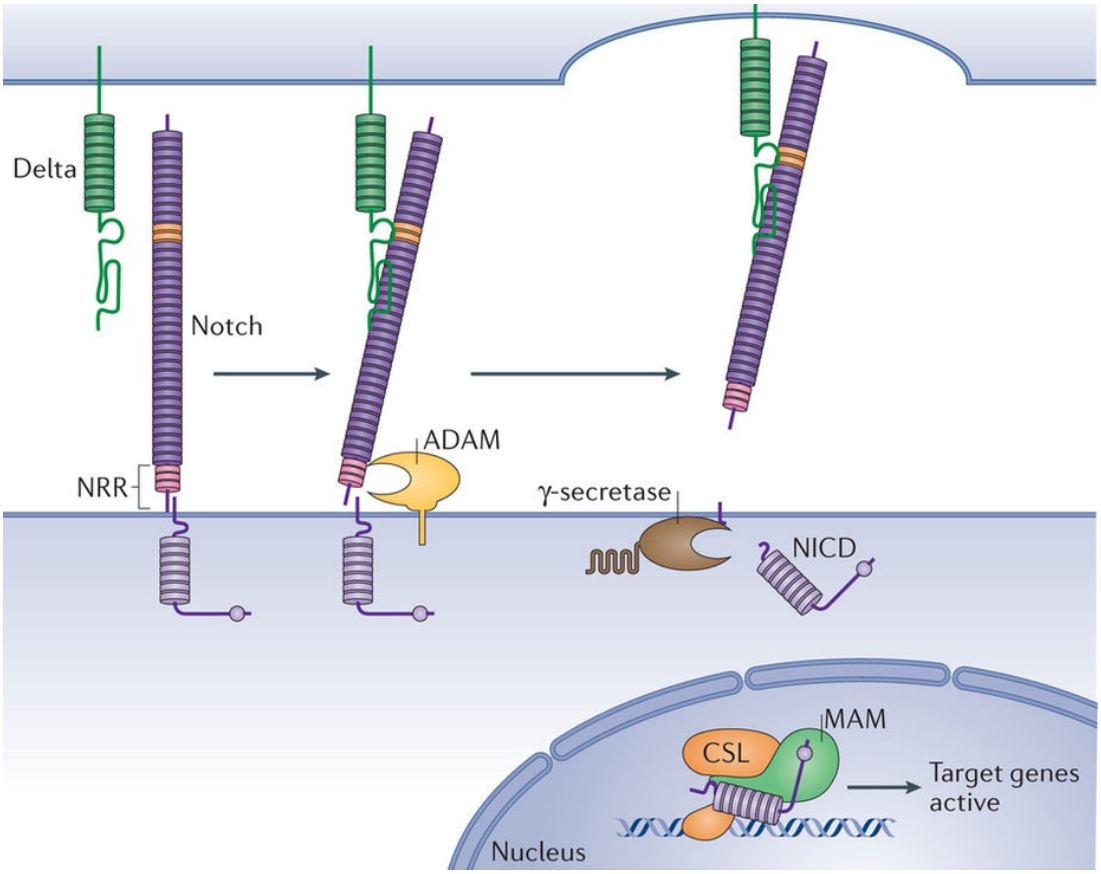

Figure 1.4. Notch signalling pathway.
Notch signalling is a cell contact-dependent pathway. Notch ligands (Delta) and receptors (Notch) are expressed on the cell membrane. Following ligand-receptor interaction, the receptor undergoes two sequential proteolytic cleavages by ADAM and then γ-secretase. The Notch intracellular domain (NICD) then translocates to the nucleus, binding the CBF1/RBP-Jk (Suppressor of hairless [Su(H)] in zebrafish) repressor, switching it into a transcriptional activator (Bray, 2006).

The requirement for Notch signalling to promote myogenic commitment has been supported by Notch inhibition (Schuster-Gossler *et al.*, 2007; Vasyutina *et al.*, 2007) and overactivation (Hirsinger *et al.*, 2001; Mourikis, Gopalakrishnan, *et al.*, 2012) studies. In murine En1+ dermomyotome cells, overexpression of NICD results in more *Pax3*-expressing cells in the dermomyotome and *Pax3*; *Pax7*-expressing cells in the myotome (Mourikis, Gopalakrishnan, *et al.*, 2012). This was associated with no change to the expression of *Myf5* (Mourikis, Gopalakrishnan, *et al.*, 2012). Furthermore, grafting transfected cells overexpressing Delta into the developing chick has demonstrated that Notch overexpression increased *Pax3* transcript expression within the somite, and decreased *Myod* and *Serrate2* transcript expression in the myotome (Hirsinger *et al.*, 2001). Overexpression of Notch is associated with no change in the number of proliferating cells or *Myf5* transcript expression in the myotome, ultimately resulting in loss of muscle formation due to a failure to differentiate down the myogenic lineage (Hirsinger *et al.*, 2001). Moreover, mouse embryos lacking the Notch ligand, Delta like ligand 1 (Dll1) or RBP-Jk, initially have a normal number of *Pax3*- and *Pax7*-expressing cells, but over time these cells are lost due to precocious differentiation (Schuster-Gossler *et al.*, 2007; Vasyutina *et al.*, 2007). This result highlights the role of Notch signalling in the expansion of MPCs whilst preventing early differentiation. *Delta-1*-expressing D10 cells and C2C12 myoblasts *in vitro* demonstrates that Notch signalling prevents differentiation through increased expression of RBP-Jk and *Hes1*, a transcriptional repressor, supressing *Myod* expression (Jarriault *et al.*, 1995; Kuroda *et al.*, 1999).

Notch signalling is also important later in development and growth, during the establishment of the muSC population (Delfini *et al.*, 2000; Mourikis, Gopalakrishnan, *et al.*, 2012; Verma *et al.*, 2018). *In silico* studies have shown that muSCs express *Notch1, 2* and *3* transcripts by RNAseq (Verma *et al.*, 2018). This expression of Notch later in development has also been shown in chick wing (Delfini *et al.*, 2000). In the wing, MPCs express *Delta1*+*MyoD*+, *Notch1*+ and *Serrate2*+*MF20*+ transcripts (Delfini *et al.*, 2000). MF20 stains MYHC, a marker of mature myoblasts (Delfini *et al.*, 2000). In mouse, following MPC sorting, $Pax7^{high}$ cells express more *HeyL*, *Hey1*, *Notch1*, *Notch3*, *Jagged1* and *Dll1* transcripts relative to $PAX7^{low}$ cells (Mourikis, Gopalakrishnan, *et al.*, 2012). This demonstrates that the MPC population expresses

Notch activity during muscle development. Notch signalling is then subsequently downregulated in differentiated MPCs.

Delta overexpression in the chick limb bud results in reduced *Myod*, and increased *Notch1* transcript but, does not change *Myf5* and *Pax3* transcript expression or Bromodeoxyuridine (BrdU) incorporation. Delta overexpression was associated with less MF20+ cells as well as, disorganised and absent muscle (Delfini *et al.*, 2000). NICD overexpression in *Myf5*+ cells in mouse results in an inhibition of cell differentiation in the limb, suggesting cells are entering a state of quiescence (Mourikis, Gopalakrishnan, *et al.*, 2012). Moreover, following NICD overexpression in *Myf5*+ cells, there is a total lack of muscle and PAX7+MYF5+MYOGENIN- cells in the head and limb are able to self-renew in the head and limb muscles (Mourikis, Gopalakrishnan, *et al.*, 2012). This phenotype is associated with an upregulation of foetal markers (such as *Nfix*), suggesting a block in myogenic progression (Mourikis, Gopalakrishnan, *et al.*, 2012). Forced overexpression of NICD in *Myf5*-expressing cells promotes an undifferentiated state, surrounded by laminin mimicking the quiescent stem cell niche (Mourikis, Gopalakrishnan, *et al.*, 2012). Interestingly, concomitant NICD overexpression and Rbp-jk suppression in *Myf5*+ cells, results in myoblast differentiation confirming this is an RBP-Jk-dependent pathway (Mourikis, Gopalakrishnan, *et al.*, 2012).

During embryonic myogenesis, *Myod*-induced expression of *Dll1* in committed myoblasts plays an important role in the expansion of the MPC population (reviewed by Mourikis and Tajbakhsh 2014). *Pax3*-specific RBP-Jk mutant or global loss of *Dll1* results in reduced muscle mass in mouse limb due to premature differentiation (Bröhl *et al.*, 2012). In conditional RBP-Jk mutants, this loss of muscle mass is a consequence of fewer proliferating PAX3+ cells and fewer MYF5+ cells (Bröhl *et al.*, 2012), and increased MPC differentiation (Vasyutina *et al.*, 2007). Additionally, Notch 1 and Notch 2 inhibition in *Pax7*-expressing cells leads to smaller Transverse abdominis (TrA) muscle, a consequence of reduced PAX7+ cells (Fujimaki *et al.*, 2018). *In vitro*, following *Notch 1* and *Notch 2* inhibition in *Pax7*-expressing cells leads to an increase in the proportion of PAX7+ cells expressing MYOD, reduced Ki67+ (proliferating) cells, and more MYOGENIN+ cells (Fujimaki *et al.*, 2018), suggesting PAX7+ cells loose the capacity to self-renew, terminally differentiating.

Although not well characterised, the requirement for Notch signalling during zebrafish muscle development and growth has also been demonstrated (Pascoal *et al.*, 2013; Palstra *et al.*, 2014; Lleras-Forero *et al.*, 2020). In pectoral fin musculature development, inhibition of Notch leads to a loss in muscle fibre mass (Pascoal *et al.*, 2013). More recently, a study has demonstrated that zebrafish adults lacking both *her1* and *her7* expression show a marked loss of muscle mass (Lleras-Forero *et al.*, 2020). Moreover, *her1*:*her7* zebrafish mutant larvae (32 hours post injury [hpi]) loose fast and slow muscles associated with cavity formation within the myotome (Lleras-Forero *et al.*, 2020). As stated earlier, the growth of zebrafish musculature is influenced by extrinsic factors, such as swimming force (reviewed by Johnston *et al.*, 2011). Transcriptional analysis has shown that swimming-induced exercise in zebrafish promotes Wnt and Notch signalling important for controlling muscle mass, myogenesis and muSC activation, and angiogenesis (Palstra *et al.*, 2014). Palstra *et al.*, (2014) has shown that swimming-induced exercise results in increased *notch1*, *jagged1* and *hey1* expression and decreased *notch2* expression (Palstra *et al.*, 2014). This need for contractile force to promote embryonic myogenesis has been shown in chick, and involves a Notch-YAP axis (de Lima *et al.*, 2016). Immobilisation of the muscle using Decamethonium bromide (DMB) reduced *Jag2, Hes5* and *HeyL* transcript expression, and led to reduced muscle mass (de Lima *et al.*, 2016). YAP (Yes-Associated Protein) is a sensor of mechanical activity (de Lima *et al.*, 2016). DMB treatment combined with YAP overexpression in *Myhc*-expressing cells, increased *JAG2* transcript expression and an increased number of undifferentiated PAX7+ cells could be detected in the limb bud, similarly to Delta overexpression (de Lima *et al.*, 2016). Chip analysis confirms that YAP binds the regulatory region one of JAG2 promoters via the TEAD domain (CATTCC; de Lima *et al.*, 2016). This shows that YAP can directly regulate Notch activity in MPCs.

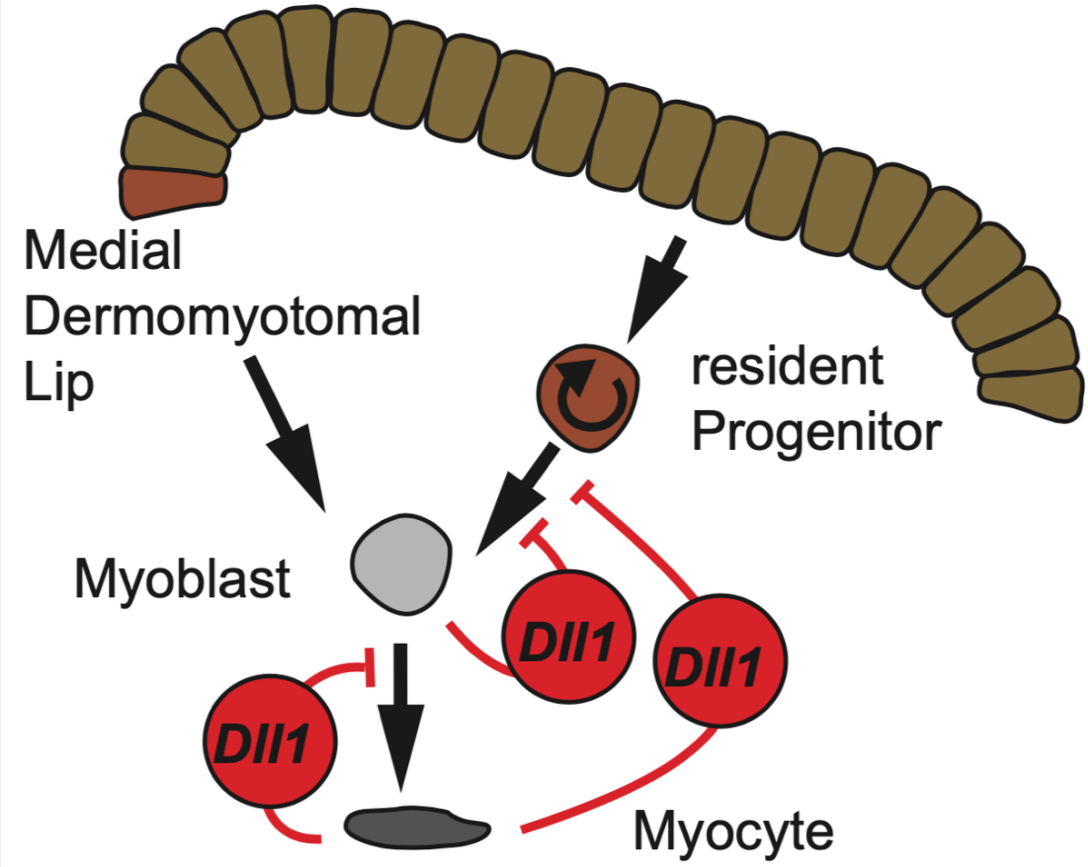

Figure 1.5 Notch signalling in MPCs during development.
Resident myogenic progenitor cells (MPCs) are Notch active, committing to the myogenic lineage. Following the migration from the dermomyotome, MPCs differentiate into myoblasts and then myocytes, upregulating Notch ligands such as *Dll1* expression. These differentiated cells signal back to non-differentiated cells to over-activate Notch and inhibit MPC differentiation (modified from Schuster-Gossler et al., 2006).

1.3.2 Wnt signalling

Wnt signalling plays a dual role during myogenesis. Wnt is important for the commitment to the myogenic program and subsequent differentiation and fusion of MPCs into mature myofibers of the developing myotome (reviewed below).

Cells within the paraxial mesoderm express *Wnt3a* in the chick tail bud, remaining in an undifferentiated mesenchymal state (Aulehla and Pourquié, 2010). *Wnt1-/- Wnt3a-/-* double mouse knock-outs embryos have reduced expression of *Pax3* and *Myf5* transcript in the medial dermomyotome, resulting in a smaller dermomyotome (Ikeya and Takada, 1998). *Wnt1-/-Wnt3a-/-* knock-out mice no longer expresses *noggin* (an inhibitor of the Bone Morphogenetic Protein [BMP] signalling pathway) and *Notch2* in the medial lip, or *En-1* in the central compartment of the dermomyotome (Ikeya and Takada, 1998). This demonstrates that Wnt is required for the early specification of dermomyotome cells during muscle development, working in concert with Notch and BMP signalling.

The key role of Wnt signalling in early embryonic muscle development has been shown by β-catenin knock-out mice (downstream effector of the canonical Wnt pathway) in the presomitic mesoderm resulting in segmentation defects due to oscillating clock genes (important for controlling temporal somitogenesis; Dunty *et al.*, 2008). Borello *et al.,* (1999) further characterised Frizzled (*Fzd*), Wnt ligand, in the developing chick. They found that *Fzd3* and *Fzd7* are expressed in the presomitic mesoderm, whilst *Fzd1*, *Fzd3*, *Fzd6*, *Fzd7*, and *Fzd8* are expressed in the developing somite (Borello, Buffa, *et al.*, 1999). This highlights that different Wnt ligands may function at different time points during muscle development, promoting both early cell specification, and late differentiation. Mouse *ex-vivo* cultures have demonstrated that *Wnt1* and *Wnt4* overexpression increases *Myf5* expression whereas Wnt7a induces *Myod* expression (Tajbakhsh *et al.*, 1998). Moreover, the interaction of Wnt1 with Fzd1 or Fzd6 appears to regulate *Myf5* expression through the canonical Wnt pathway (via β-catenin; Borello *et al.*, 2006), while Wnt7a-Fzd7 regulates *MyoD* expression in a non-canonical fashion relaying on PKC activity (Brunelli *et al.*, 2007). Wnt can act through Gα-adenylyl cyclase- protein kinase A (PKA) activity to phosphorylate cAMP response element-binding protein (CREB), a

transcription factor, promoting MRF and *Pax* expression (Chen *et al.*, 2005). Data from CREB-/- mouse has shown that a loss of CREB expression leads to reduced *Myf5*, *MyoD* and *Pax3* expression within the trunk somites (Chen *et al.*, 2005). This suggests that CREB regulates *Myf5*, *Myod* and *Pax3* expression.

Wnt signalling inhibition of myogenic specification has been further characterised by inactivating β-catenin in En1 dermomyotomal cells (Atit *et al.*, 2006). This inactivation of β-catenin results in an increased number of Myog-expressing myogenic cells, highlighting the inhibitory role of Wnt signalling in MPC specification during secondary myogenesis (Atit *et al.*, 2006). However, β-catenin inactivation in *Pax7*+ cells, leads instead to a reduction of slow myosin-expressing myofiber (Hutcheson *et al.*, 2009). Transplacental delivery of sFRP3 (a Wnt antagonist) results in the development of fewer smaller somites in a dose-dependent manner (Borello, Coletta, *et al.*, 1999). The inhibition of Wnt signalling also caused a decrease in *noggin, Myf5, En-1*, and *Myhc* gene expression (Borello, Coletta, *et al.*, 1999). Co-culture experiments also showed an increased expression *of Myf5, MydD, Pax3* and *Pax7* in somitic cells following exposure to Wnt (Fan *et al.*, 1997; Tajbakhsh *et al.*, 1998; Chen *et al.*, 2005).

Wnt signalling antagonises Notch expression through *Dll1* regulation, allowing MPCs to specify into a myogenic fate. Subsequently, Notch signalling promotes the self-renewal and amplification of MPCs during muscle development (Hofmann *et al.*, 2004).

1.3.3 Hedgehog and Bone Morphogenetic Protein signalling

Sonic hedgehog (Shh) is essential for the differentiation and fusion of MPCs following their amplification. Shh or smoothened null mice (downstream Shh transcription factor), despite developing normal skeletal muscle, display delayed expression of *Myf5* (Chiang *et al.*, 1996; Zhang *et al.*, 2001). Moreover, following Shh knock-out, a lack of *MyoD* is observed in chick somites (Borycki *et al.*, 1998). Consistently, ectopic Shh gain-of-function in chick increases *Pax3* and *Myod* expression (Johnson *et al.*, 1994). Borello *et al.,* (2006) show that the Myf5 gene contains Shh- and Wnt-binding sites suggesting Shh and Wnt can directly regulate the expression of *Myf5* during muscle development (Borello *et al.*, 2006).

In contrast, like Notch signalling, BMP amplifies MPC population prior to its differentiation and fusion. Bmp4 has been identified in the lateral mesoderm. Bmp4 is expressed in the lateral mesoderm, promoting *Pax3* expression and inhibiting *Myf5* and *Myod* expression in MPCs, keeping them in an undifferentiated state (Pourquié *et al.*, 1995; Hirsinger *et al.*, 1997; Bentzinger *et al.*, 2012). Transplantation studies revealed that Wnt and Shh antagonise BMP through Noggin expression in the dorsomedial lips of the dermomyotome (Hirsinger *et al.*, 1997). This antagonism allows for Wnt- and Shh-mediated regulation of *Myod* expression, MPCs differentiation and formation of mature myotomes. Noggin null mice do not express dermomyotomal Bmp4 and En-1 nor do they develop somites (McMahon *et al.*, 1998). The somite instead remains in an epithelial state (McMahon *et al.*, 1998).

Hh signalling has also been well characterised during early zebrafish myogenesis. Shh is secreted by the proximal notochord (Wolff *et al.*, 2003). Pharmacological inhibition of the Shh signalling pathway using Cyclopamine blocks the specification of *En1*-expressing pioneer cells (Wolff *et al.*, 2003). *smu*-/- (smoothened) null mutant lack slow MYHC expression in the myotome (Baxendale *et al.*, 2004). Additionally, Henry and Amacher, (2004), found that *smu*-/- mutant lack F59 (marker of slow myosin) expression and, therefore, slow muscle fibres by 19 hpf, presenting a delayed elongation of fast muscle fibres (although these are disorganised; Henry and Amacher, 2004). However, following transplantation of *smu*-/- cells into wild type (WT) fish, fast muscle cells are still able elongate, whereas slow fibres do not form (Henry and Amacher, 2004). Although, at later time point (> 24 hpf), Barresi *et al.,* (2001) found a population of slow muscle fibres eventually developed with a normal *myod* expression pattern (Barresi *et al.*, 2001). In conclusion, Hh inhibits the emergence of Pax3- and Pax7-expressing cells (Feng *et al.*, 2006; Hinits *et al.*, 2009) post slow muscle fibre formation (Feng *et al.*, 2006).

Summary

Studies investigating the importance of morphogens on the development of muscle have shown that Notch signalling functions in concert with Wnt, Shh, and BMP signalling to orchestrate MPCs commitment, proliferation, and differentiation. Together, it has been shown that Wnt plays a dual role, first promoting myogenic

commitment via the canonical pathway. Notch and BMP then promote MPC proliferation and expansion. Finally, non-canonical Wnt signalling and Shh inhibit Notch and BMP signalling, promoting differentiation. Hh signalling is also important for the timely development of slow and fast muscle fibres in zebrafish. There are currently no descriptions on the importance of Notch and Wnt signalling on the development of zebrafish muscle.

1.4 The muSC population

Postnatal muscle regeneration is mediated by the interplay between resident muSCs, interstitial cells, and immune cells (reviewed by Rossi and Messina, 2014). The three major stages for successful muscle regeneration are inflammation followed by tissue reconstruction and remodelling (reviewed by Rossi and Messina, 2014). The latter stages of muscle regeneration are primarily mediated by the activity of muSCs, also called satellite cells (SCs) reflecting their anatomical location (Mauro, 1961). In the proceeding sections, I will discuss how the muSC population is established in both amniotes and zebrafish and how this stem cell population contributes to muscle regeneration in the changing inflammatory environment.

1.4.1 Amniotes

Using the tibialis anticus muscle of the frog, Mauro (1961) was the first to identify a peripherally located cell. “Wedged” between the plasma membrane of muscle fibres and surrounding basement membrane, exhibiting a scant cytoplasm, and relatively enlarged nucleus (Mauro, 1961). These cells were termed SCs, theorised to mediate muscle regeneration (Mauro, 1961). A subsequent study in mouse demonstrates SCs display Pax7 immunoreactivity, important for self-renewal following injury (Oustanina *et al.*, 2004). MuSCs are a heterogeneous population expressing markers such as, PAX3, MYF5, MET, cluster of differentiation (CD) 34, M-cadherin, syndecan-3, syndecan -4, and SOX8 (reviewed by Ruparelia *et al.*, 2020). The level of heterogeneity has been further characterised between different muscle cells and within the muSC population, in the context of injury or homeostasis, using single cell RNAseq analysis (Giordani *et al.*, 2019; Orso *et al.*, 2019; De Micheli *et al.*, 2020) and single cell mass cytometry (Porpiglia *et al.*, 2017). This heterogeneity has also been

defined in function of muSC self-renewal capacity (Mourikis, Gopalakrishnan, *et al.*, 2012), migration (Epstein *et al.*, 1996; Vasyutina and Birchmeier, 2006), and survival (Oustanina *et al.*, 2004; Relaix *et al.*, 2006; Von Maltzahn *et al.*, 2013; Der Vartanian *et al.*, 2019). Although muSCs express a multitude of markers, Pax7 is expressed on all quiescent muSCs (Seale *et al.*, 2000).

Adult muSCs are derived from a multipotent *Pax3*+*Pax7*+ somitic population (Gros *et al.*, 2005; Relaix *et al.*, 2005). These multipotent stem cells originate from the dermomyotome as shown by lineage tracing in chick and mouse (Gros *et al.*, 2005; Relaix *et al.*, 2005; Hutcheson *et al.*, 2009; Lepper and Fan, 2010) and can differentiate into muscle, bone, and brown fat (reviewed by Lepper *et al.*, 2011; Bentzinger *et al.*, 2012). Moreover, *Pax3*+*Pax7*+ cells originate from *Myf5*-expressing progenitor cells (Kuang *et al.*, 2007) suggesting their commitment to the myogenic lineage in adults.

The myogenic potential of muSCs has been demonstrated through transplantation studies (Collins *et al.*, 2005; Montarras *et al.*, 2005; Sacco *et al.*, 2008). PAX3+ (Montarras *et al.*, 2005), MYF5+ (Collins *et al.*, 2005) and integrinα7+CD34+PAX7+MYF5+ (which are negative for CD45, SCA1, CD11b, and CD31; Sacco *et al.*, 2008) muSCs give rise to many new myonuclei and muSCs following transplantations into muscle. The importance of the Pax7-expressing muSC population during embryonic, foetal and, adult myogenesis has been well characterised (Hutcheson *et al.*, 2009; Lepper and Fan, 2010). Lineage tracing experiments in mouse showed that embryonic myogenesis and the establishment of *Pax7*+ population arise from *Pax3*+*Pax7*- cells (Hutcheson *et al.*, 2009), whereas foetal muscle development and regeneration is mediated by *Pax7*+ cells (Lepper and Fan, 2010). Moreover, *Pax7*+ cells are critical for the establishment of the quiescent muSC population (Lepper and Fan, 2010). Further studies have revealed that *Pax7* is pivotal for muSC survival, myogenic commitment and proliferation whilst inhibiting differentiation (Oustanina *et al.*, 2004; Relaix *et al.*, 2006; Kuang *et al.*, 2007). In homeostatic conditions, MPCs arrest at G0/G1 phase of the cell cycle, whereas upon injury, MPCs can enter G_{alert}. G_{alert} cells are slightly bigger, primed to enter the cell cycle and contribute to adult myogenesis (Rodgers *et al.*, 2014).

1.4.2 Zebrafish

The zebrafish ECL contains a population of muSCs analogous to mammalian SCs (Hollway *et al.*, 2007; Stellabotte *et al.*, 2007). These cells are found in a quiescent state; they proliferate, and contribute to muscle growth and regeneration following activation (Hollway *et al.*, 2007; Stellabotte *et al.*, 2007). Similar to mammalian SCs, the zebrafish muSC population is heterogeneous, expressing *pax3*, *pax7a*, *pax7b*, *c-met* and *meox1* (Rowlerson *et al.*, 1997; Hollway *et al.*, 2007; Seger *et al.*, 2011; Gurevich *et al.*, 2016; Pipalia *et al.*, 2016).

Subsequent studies have revealed that that zebrafish have two populations of muSCs which are differentially distributed within the muscle (Seger *et al.*, 2011; Knappe *et al.*, 2015; Pipalia *et al.*, 2016; Nguyen *et al.*, 2017). The first population resides juxtaposed to the myotomal myofibers, like mammalian SCs, and is important for muscle regeneration (Knappe *et al.*, 2015; Pipalia *et al.*, 2016). The second population is restricted to the ECL, and is critical during zebrafish post-embryonic growth (Seger *et al.*, 2011; Nguyen *et al.*, 2017). The ECL has been further subdivided into horizontal and vertical myosepta. Low-cycling muSCs are found within the horizontal myosepta. These cells migrate to the vertical myosepta where they proliferate before migrating into the myotome to support muscle growth (Knappe *et al.*, 2015; Nguyen *et al.*, 2017).

Lineage tracing experiments in zebrafish have shown that a single muSC, derived from a heterogenous population, is 'randomly' assigned to contribute towards muscle growth (Nguyen *et al.*, 2017). Over successive self-renewal events, this muSC will constitute an entire myofiber (Nguyen *et al.*, 2017). This process has been termed 'clonal drift', dependent on the horizonal myosepta derived *meox1*+ low-cycling muSCs (Nguyen *et al.*, 2017). Although critical for muscle repair in larval (Knappe *et al.*, 2015; Pipalia *et al.*, 2016) and adult (Berberoglu *et al.*, 2017) zebrafish, the origin and contribution of the myotomal muSC population towards growth is less understood.

Summary

Taken together, studies investigating the activity of muSCs during muscle repair have shown that muSCs are a heterogeneous population, expressing markers such as, PAX3, MYF5, MET, cluster of differentiation (CD) 34, M-cadherin, syndecan-3, syndecan-4, and SOX8. Although muSCs express a multitude of markers, all adult muSCs express Pax7, derived from a multipotent Pax3+Pax7+ somatic population. The zebrafish muSC population is also heterogeneous, expressing *pax3*, *pax7a*, *pax7b*, *c-met* and *meox1*. Unlike amniotes, zebrafish undergo post-embryonic growth, and so two populations of muSCs exist which are differentially distributed within the muscle. The first population resides juxtaposed to the myotomal myofibers, important for muscle regeneration. The second population is restricted to the ECL, and is critical for post-embryonic growth.

1.5 muSCs: Muscle regeneration

The contribution of PAX7-expressing muSCs towards muscle regeneration has been shown in both amniotes and zebrafish (Lepper *et al.*, 2009; Knappe *et al.*, 2015; Pipalia *et al.*, 2016). Following cardiotoxin (CTX; results in widespread muscle cell membrane disruption) treatment, lineage tracing following revealed that PAX7-expressing muSCs can self-renew to maintain the muSC population whilst contributing towards the regeneration of myofibers (Lepper *et al.*, 2009). It has been demonstrated that *Pax7* is critical for the survival of the proliferative muSC population (Oustanina *et al.*, 2004; Von Maltzahn *et al.*, 2013), and *Pax7* null mice fail to repair muscle in response to injury (Von Maltzahn *et al.*, 2013). A tamoxifen-induced ablation of *Pax7* specifically in adult mice, muscle regeneration appears overtly normal and MPCs reconstitute the muSC niche, sustaining additionally rounds of injury and regeneration (Lepper *et al.*, 2009). The authors conclude that there is an age-dependent requirement of *Pax7* to repair damaged muscle. Subsequent studies investigating the importance of the PAX7-expressing cells for muscle regeneration in mice have provided definitive evidence for their essential role (Lepper *et al.*, 2011; Sambasivan *et al.*, 2011; Von Maltzahn *et al.*, 2013). They show that a loss of PAX7-expressing cells leads to a failure to repair damaged muscle (Lepper *et al.*, 2011; Sambasivan *et al.*, 2011; Von Maltzahn *et al.*, 2013).

The contribution of *pax7a*- and *pax7b*-expressing cells towards muscle regeneration has been observed in zebrafish (Pipalia *et al.*, 2016). Using zebrafish reporter lines, Pipalia *et al.,* (2016) has shown that *pax7a*-expressing cells orchestrate nascent fibre formation, whereas *pax7b*-expressing cells fuse to existing myofibers (Pipalia *et al.*, 2016). The regenerative capacity of *pax7a*+ population has also been demonstrated in adult zebrafish (Berberoglu *et al.*, 2017). Moreover, Knappe *et al.,* 2015 demonstrated that *pax7a*-expressing cells exclusively contribute to the repair of larger injuries (Knappe *et al.*, 2015). Contrary to mammalian muSC, muSC within the ECL of zebrafish arrest at G2, suggesting that zebrafish muCSs are primed to better respond to growth stimuli (Nguyen *et al.*, 2017).

1.5.1 MRFs

Following injury, the muSC niche is disrupted leading to the activation and suppression of intrinsic and extrinsic pathways, ultimately leading to the activation of muSCs. muSCs will proliferate, migrate, differentiate and fuse into mature myofibers, controlled by a conserved set of MRFs employed during embryonic myogenesis (Fig. 1.2). In mouse, post-transcriptional sequestration (fragmented within messenger ribonucleotide protein [mRNP] granules) of *Myf5* transcript has been identified maintaining a quiescent cellular state (Crist *et al.*, 2012). Following injury, disrupted mRNPs release the *Myf5* into the cytoplasm initiating the myogenic program (Crist *et al.*, 2012). muSCs subsequently downregulate *Pax7*, promoting *Myf5*, *Myod*, and then *MRF4* and *Myogenin* expression, differentiating into mature myotubes (reviewed by Dumont *et al.*, 2015). While *Myod* was shown to be dispensable and *Myogenin* is required for successful embryonic myogenesis, the reverse is not true during adult myogenesis. In an homeostatic state, *Myod*-/- mice exhibit reduced *MRF4* and *Myogenin* and increased *Myf5* in muSCs leading to a disrupted differentiation (Cornelison *et al.*, 2000). Following injury, although muSCs appear normal by electron microscopy in *Myod*-/- mice, muSCs fail to regenerate due to their inability to proliferate (Megeney *et al.*, 1996).

Summary

Together, these studies have shown that although MRFs fundamentally function in the same way during embryonic myogenesis and regeneration, not all are conserved between the two processes. This is likely due to the complex feedback and feedforward signalling networks which function in the changing microenvironment to finetune the intricate process of muSC activation and self-renewal.

1.5.2 Importance of the muSC niche

The muSC niche maintains quiescence and self-renewal whilst preventing ectopic differentiation (reviewed by Bentzinger *et al.*, 2012; Fig. 1.6). HGF, released into the muscle following injury, primes quiescent muSCs into a G_{alert} state, a prerequisite to muSC activation (Rodgers *et al.*, 2017).

Collagen and laminin are critical ECM derived regulators of muSC self-renewal. Collagen V treatment supressed muSC differentiation, whereas *Pax7*-specific knockdown of *Col5a1* results in depletion of muSC population due to premature muSC activation (Baghdadi, Castel, *et al.*, 2018), modulated by calcitonin receptor in an autocrine fashion (Baghdadi, Castel, *et al.*, 2018). Integrin has been described as an important niche sensing protein, expressed on the cell surface of muSCs (Rayagiri *et al.*, 2018). Signalling via muSC-expressed integrin-α6β1, laminin-111 mediates muSC polarity and subsequent asymmetric proliferation (Rayagiri *et al.*, 2018). laminin-111 treatment increases planar proliferation (symmetrical division) and decreases apico-basal proliferation (asymmetrical division; Rayagiri *et al.*, 2018). Mature myofibers are an important signal-presenting structure for the maintenance of quiescent muSCs and promotion of self-renewal (Goel *et al.*, 2017). Such interaction occurs through myofiber-derived cadherin (Goel *et al.*, 2017). Global suppression of *M-cadherin* in mouse leads to increased muSC proliferation, displaying activation markers such as increased *Myod* expression and decreased mRNP granules (Goel *et al.*, 2017). Furthermore, muSC-specific cadherin knock-out leads to the disruption of the myofiber-muSC adhesive junction, skewing muSCs towards a G_{alert} state (Goel *et al.*, 2017).

There is increasing evidence demonstrating the muSCs ability to modulate the environment in response to injury. Activated muSCs transiently express fibronectin

which can autonomously activate Wnt to expand the muSC population (Bentzinger, Wang, Von Maltzahn, *et al.*, 2013). Moreover, as muSCs differentiate, they deposit laminin (α1 and 5) into the niche, promoting proliferation and self-renewal of surrounding muSCs (Rayagiri *et al.*, 2018). muSCs also prevent collagen disposition by fibroblasts via secretory exosomes containing *miR-206*, contributing to muSC exit from quiescence (Fry *et al.*, 2017). The muCSs modulation of their own environment has been exemplified by the loss of α7β1 integrin which leads to reduced laminin-α2 (Rooney *et al.*, 2006), and the absence of muscle repair due to delayed muSC proliferation and differentiation (Rooney *et al.*, 2009).

In zebrafish, Pax3+ and Pax7+ are located within the ECL (Seger *et al.*, 2011; Nguyen *et al.*, 2017). The ECL is enriched in molecules associated to the ECM such as β-catenin, Laminin and Fibronectin (Seger *et al.*, 2011; Knappe *et al.*, 2015; Gurevich *et al.*, 2016; Pipalia *et al.*, 2016). Although the role of Laminins (such as Laminin 2) in adhesion and survival of zebrafish myofibers in the context of muscular dystrophy (Hall *et al.*, 2019), growth, and injury (Gupta *et al.*, 2012) has been shown, the potential involvement of the muSC niche in cellular quiescence and regenerative responses remains unexplored.

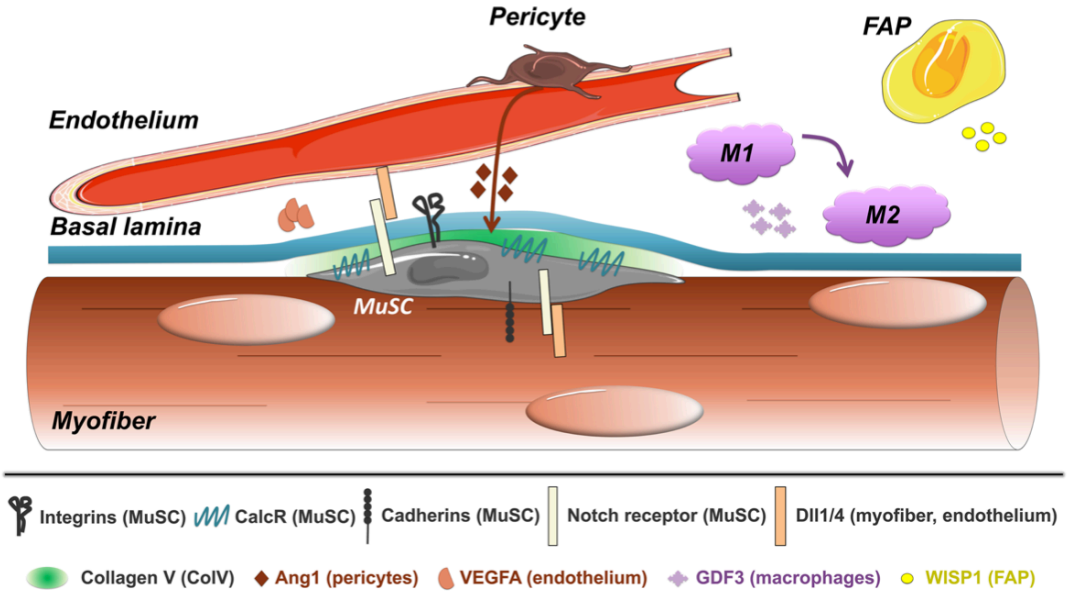

Figure 1.6. The importance of the muSC niche.
muSCs are located beneath the basal lamina proximal to the myofiber, anchored by integrin and cadherin. Myofiber derived Notch ligand and Collagen V, endothelium derived Notch ligand, and pericyte derived Angiopoietin-1 maintains muSC quiescence. Following injury, macrophages and Fibro-adipogenic progenitors (FAPS) contribute to muSC activation via GDF3 (transforming growth factor-β [TGF-β] family member) and WNT1-inducible-signaling pathway protein 1 (WISP1) expression, respectively. The former is synthesised by pro- (M1) and anti- (M2) inflammatory macropahges. (Relaix *et al.*, 2021).

1.5.3 Symmetric and asymmetric proliferation

muSCs proliferate in both a symmetrical and asymmetrical manner (Fig. 1.7). Asymmetrical proliferation results in the generation of two distinct daughter cells, one of which reconstitutes the muSC niche, and other differentiates down the myogenic lineage (Shinin *et al.*, 2006; Conboy *et al.*, 2007; Kuang *et al.*, 2007). Contrastingly, symmetrical division will only expand the stem cell or progenitor cell populations (Shinin *et al.*, 2006; Conboy *et al.*, 2007; Kuang *et al.*, 2007). Asymmetrical proliferation maintains the muSC pool whilst repairing damaged tissue (Shinin *et al.*, 2006; Conboy *et al.*, 2007; Kuang *et al.*, 2007).

The first reported evidence of a dual muSC compartment was described by Schultz *et al.,* (1996) who used BrdU and [3H] thymidine labelling in the rat skeletal muscle to show that ~80% of muscle cells are fast cycling (BrdU+) and the remaining ~20% are slow cycling (BrdU-; Schultz, 1996). Advancements in reporter lines and lineage tracing showed that *Myf5* is asymmetrically distributed following muSC proliferation (Shinin *et al.*, 2006; Conboy *et al.*, 2007; Kuang *et al.*, 2007). *Myf5*-cre mice to label Pax7+MYF5+ muSCs with YFP, studies have shown that planar symmetric cell division (along the plane of the myofiber) leads to two identical daughter cells expressing PAX7+YFP- or PAX7+YFP+ (Shinin *et al.*, 2006; Conboy *et al.*, 2007; Kuang *et al.*, 2007). Contrastingly, asymmetric division occurs along the apical-basal plane, the cell dividing away from the basal lamina is YFP+, whereas the basal sister cell YFP- remains in the muSC compartment (Shinin *et al.*, 2006; Conboy *et al.*, 2007; Kuang *et al.*, 2007). In addition to *Myf5*, DEK (cell-cycle negative regulator) is also asymmetrically distributed into the MYOD+ committed cell (Cheung *et al.*, 2012). Further analysis has revealed that grafted YFP- cells relocate to the muSC niche, whereas YFP+ cells contribute to new myofibers (Cheung *et al.*, 2012). Moreover, YFP+ cells cannot re-constitute the YFP- cell population, but YFP- cells can upregulate *myf5* (Cheung *et al.*, 2012). Asymmetrical division has also been observed in committed MYOD-expressing cells (Zammit *et al.*, 2004). Proliferating MyoD+Pax7+ muSCs are able to give rise to PAX7+MYOD- cells through asymmetric division (Zammit *et al.*, 2004). Additionally, in zebrafish, *met*+ *pax7*+ muSC asymmetrically generate $met^{hi}pax7^{lo}$ muSCs and $met^{lo}pax7^{hi}$ progenitor cells which contribute to repair and muSC niche, respectively (Gurevich *et al.*, 2016). Interestingly, it has been

shown that the daughter cell, which remains stem-like, retains the parental DNA strand, reducing replication-induced error, thought to be key for the long-term survival of muSC population (Rocheteau *et al.*, 2012).

Following activation of muSCs, symmetrical proliferation dominates to generate two identical daughter cells (Shinin *et al.*, 2006; Conboy *et al.*, 2007; Kuang *et al.*, 2007). Intravital imaging has shown proliferation and subsequent migration occur along ghost fibres, remnants of damaged fibres which act as scaffolds (Webster *et al.*, 2016).

Planar cell polarity (PCP) is a critical mechanism for asymmetrical proliferation of muSCs. The PAR complex (a regulatory of PCP) asymmetrically distributes to one daughter cell, activating p38α/β MAPK pathway, increasing MYOD, supressing PAX7, and reducing muSC proliferation, to promote the entry into the myogenic program (Perdiguero *et al.*, 2007; Palacios *et al.*, 2010; Troy *et al.*, 2012).

Summary

Studies investigating the contribution of muSCs during muscle regeneration have revealed that the PAX7-expressing cells are indispensable for successful muscle repair in mammals. Similarly, investigation in zebrafish have shown the contribution of *pax7a*- and *pax7b*-expressing cells towards muscle repair. MuSCs reside within the muSC niche, important for the maintenance of quiescence and self-renewal whilst preventing ectopic differentiation. Following injury and the disruption of the niche, muSCs activity is controlled by the sequential expression of MRFs, promoting commitment (MYF5 and MYOD) and differentiation (MYOGENIN). MuSCs also proliferate in both a symmetrical and asymmetrical manner. Symmetrical proliferation yields two identical stem cell daughter cells. Asymmetrical proliferation leads to the formation of one stem cell, and one *Myf5*+ progenitor cell. This allows one cells to differentiate down the myogenic lineage to contribute towards muscle repair, whilst maintaining the muSC population.

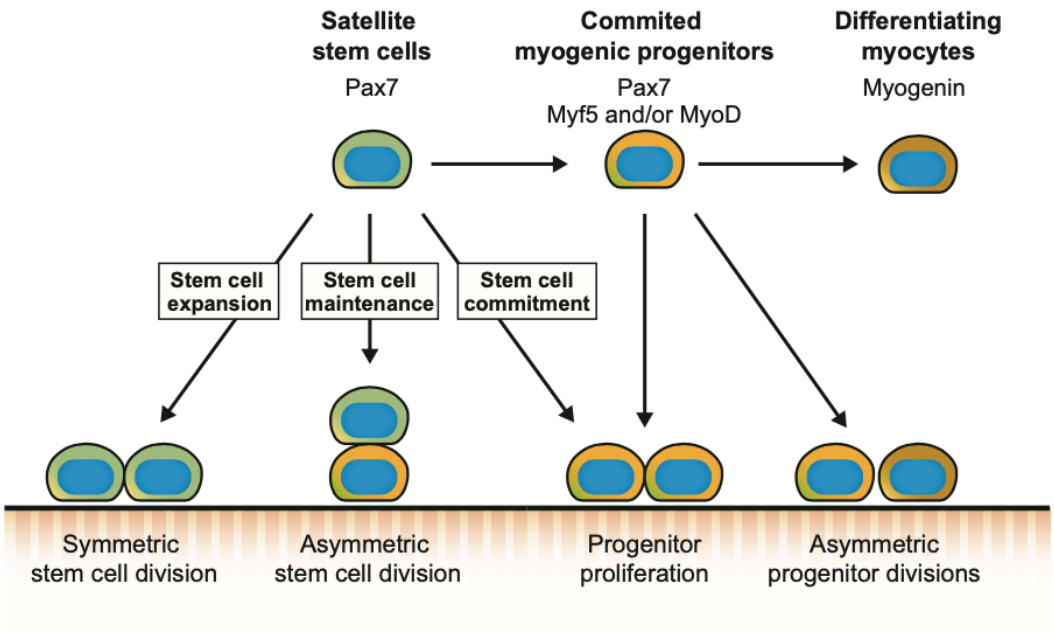

Figure 1.7. Satellite cell fate following muscle injury.
Satellite cells are able to both symmetrically and asymmetrical proliferate. Symmetrical proliferation yields two identical stem cell daughter cells, expanding the stem cell population. Asymmetrical proliferation leads to the formation of one stem cell maintaining the stem cell niche, and one Myf5+ progenitor cell differentiating down the myogenic lineage to contribute towards muscle repair. The progenitor cell can then either asymmetrically proliferate, or directly differentiate, expressing MyoD and Myog, fusing into new myofibers (Dumont *et al.*, 2015).

1.6 Notch signalling controls muSC activity during regeneration

1.6.1 Notch signalling maintains muSC quiescence

It was initially thought that the role of Notch signalling during postnatal muscle growth and regeneration was reminiscent of its developmental role. Notch signalling in development leads to proliferation and self-renewal of MPCs (reviewed by Mourikis and Tajbakhsh, 2014). However, Mourikis, Sambasivan, *et al.,* (2012) and Bjornson *et al.,* (2012) challenged this hypothesis, demonstrating a loss of Notch target genes (*Hey1*, *Hey2*, *HeyL*, *Hes5* and *Hes1*) in muSCs following injury (Bjornson *et al.*, 2012; Mourikis, Sambasivan, *et al.*, 2012). This result demonstrated the role of Notch in adult muscle regeneration is more complex than what was initially believed. Adult quiescent muSC express *Notch1*, *Notch2*, and *Notch* 3, as well as high levels of Rbp-jk target genes *Hey1*, *HeyL*, and *Hes1*. *Pax7*-specific Rbp-jK knock-outs leads to reduced proliferation and spontaneous differentiation of muSCs (Bjornson *et al.*, 2012; Mourikis, Sambasivan, *et al.*, 2012). Consistently with Notch signalling maintaining muSC in a quiescent state, constitutively active Notch1 in mouse muSCs results in early cell cycle exit, characterised by the expression of quiescent genes (upregulation of *Pax7*, *Calr*, and downregulation of *Myod*; Mourikis, Sambasivan, *et al.*, 2012). Interestingly Notch3 and Hes6 seem to play an opposing role following muscle injury, acting as negative regulators of the muSc niche (Kitamoto and Hanaoka, 2010; Bjornson *et al.*, 2012). Following injury, *Hes6* expression is upregulated, and Notch3 null mice have increased muSC numbers and hypertrophic regenerating muscle. This implies that *Notch3* and *Hes6* promote muSC activation rather than quiescence.

1.6.2 Notch signalling is downregulated following injury

Although upregulation of Notch target genes is important for the proliferation of cultured myoblasts (Conboy and Rando, 2002), this does not seem to entirely represent what has been observed *in vivo*. As previously mentioned, fluorescence activated cell sorted (FACS) and quantitative polymerase chain reaction (qPCR) analysis has revealed that *Pax7*-expressing muSCs downregulate Notch target genes

following injury (Bjornson *et al.*, 2012; Mourikis, Sambasivan, *et al.*, 2012; Fig. 1.8). Notch activity is then transiently upregulated around the time *Myogenin* is expressed (Mourikis, Sambasivan, *et al.*, 2012). This temporal increase of Notch has been attributed to the emergence of *Dll1*-expressing mature myoblasts (Mourikis, Sambasivan, *et al.*, 2012; Fig. 1.5, 1.8). Tamoxifen induced *Pax7*-specific Rbp-jk depletion in injured mouse has demonstrated that although Notch activity is downregulated in muSCs following injury, Notch activity is still required for successful muscle repair (Bjornson *et al.*, 2012; Mourikis, Sambasivan, *et al.*, 2012; Fig. 1.8). In contrast, short-term tamoxifen treatment (16 days) results in overtly normal tissue repair with slightly smaller myofibers (Mourikis, Sambasivan, *et al.*, 2012; Mourikis and Tajbakhsh, 2014); however, this partial rescue is due to incomplete depletion of Rbp-jk. In fact, prolonged tamoxifen treatment (28-32 days), ensuring the efficient depletion of Rpb-jk, results in no muscle repair (Bjornson *et al.*, 2012; Mourikis, Sambasivan, *et al.*, 2012). Moreover, although cultured Rbp-jk-/- muSC undergo the first mitosis event in a timely manner equal to control muSCs, mutant cells fail to keep proliferating over time, prematurely expressing commitment (MYOD) and differentiation (MYOGENIN) markers (Mourikis, Sambasivan, *et al.*, 2012). *Dll1* knock-out mice also exhibit accelerated myoblast differentiation forming excess fibres, and depleting *Pax3*+*Pax7*+ muSCs (Schuster-Gossler *et al.*, 2007). Additionally, muSC expressing constitutively active Notch1 (NICD) in mice can successfully self-renew but fail to exit from quiescence, inhibiting the expression of differentiation associated MRFs (Wen *et al.*, 2012). Bi *et al.,* (2016) demonstrated that overexpressing NICD leads to upregulation of quiescent markers in differentiated myoblasts (*Pax7*; Bi *et al.*, 2016). It is now appreciated that, following injury, proliferating muSCs show low Notch activity, and, in homeostasis, the depletion of Rbp-jk in *Pax7*-expressing muSCs results in an S-phase-independent differentiation of muSCs (Bjornson *et al.*, 2012; Mourikis, Sambasivan, *et al.*, 2012). Therefore, although Notch signalling may not directly influence the proliferation of muSCs, Notch signalling inhibition of differentiation indirectly affects the proliferative state of muSCs. This is demonstrated in the context of injury where *Pax7*-specific Rbp-jk-/- mice have a reduced proliferation of muSCs (Bjornson *et al.*, 2012; Mourikis, Sambasivan, *et al.*, 2012). Notch signalling negatively regulates proliferation by

upregulating *miR-708*, a mirtron which is upregulated in quiescent muSCs and downregulated in activated muSCs (Baghdadi, Firmino, *et al.*, 2018). *miR-708* inhibits cell migration by supressing the synthesis of focal-adhesion associated protein TENSIN3 (Baghdadi, Firmino, *et al.*, 2018). Additionally, Notch upregulates p21 expression (cell cycle inhibitor) promoting muSC cell cycle arrest (Wang *et al.*, 2016). Notch signalling can also limit differentiation by supressing of p38α/β and *Myod* expression in muSCs (Kondoh *et al.*, 2007; Mourikis, Sambasivan, *et al.*, 2012). Together this shows that Notch signalling regulates quiescence, migration, proliferation, and differentiation of muSCs.

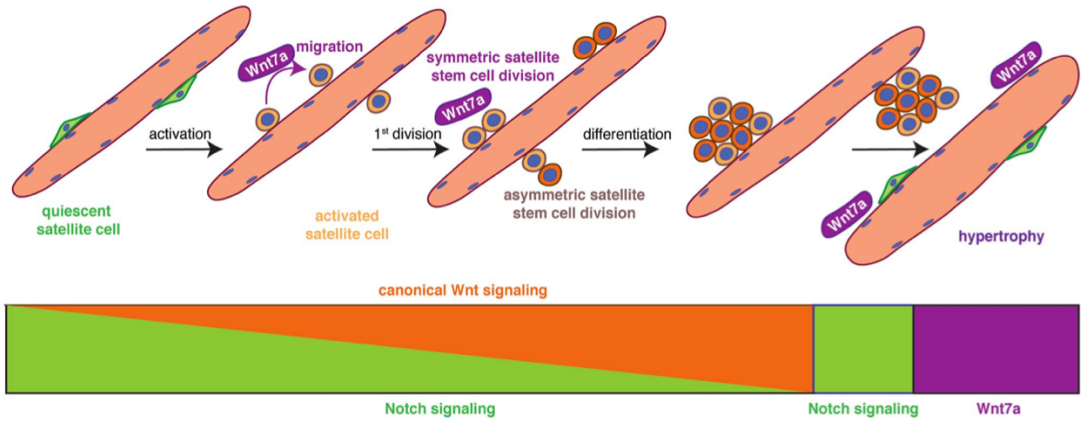

Figure 1.8. Balanced Notch and Wnt signalling required for muSC activity following injury. Following injury, quiescent muSCs downregulate Notch activity and upregulate Wnt7a. Non-canonical Wnt7a facilitates muSC migration and symmetric division. Upon re-entry into quiescence, muSCs show Notch activity. Wnt7a is important for the subsequent hypertrophic growth (Schmidt *et al.*, 2019).

1.6.3 Notch signalling controls Asymmetrical division

In addition to the regulation of quiescence, Notch signalling has also been associated with asymmetric proliferation (Kuang *et al.*, 2007). Following asymmetric division, the distribution of Numb, a negative regulator of Notch, differs between daughter cells. Numb is asymmetrically distributed between daughter cells. During self-renewal, Numb is expressed in the Pax7+ progenitor daughter cell and not the committed differentiating daughter cell (Conboy and Rando, 2002; Shinin *et al.*, 2006). Following injury, ablation of Numb in Pax7-expressing cells inhibits proliferation and muscle regeneration (George *et al.*, 2013). Moreover, following asymmetrical division, the basal progenitor cell expresses *Notch3,* whereas the committed muSC expresses *Delta-1*, suggesting a lateral inhibition feedback mechanism (Kuang *et al.*, 2007). Together these findings highlight a potential role of Notch signal regulation in asymmetrical division to balance between renewal and differentiation.

1.6.4 muSC-niche interaction

Various studies have described a crosstalk between Notch-expressing muSCs and the surrounding niche (Bjornson *et al.*, 2012; Bröhl *et al.*, 2012; Mourikis, Gopalakrishnan, *et al.*, 2012; Baghdadi, Castel, *et al.*, 2018). ChIP-Seq analysis has revealed that NICD enhancers are associated with genes encoding ECM proteins, suggesting adult muSCs contribute to the composition of their own niche (Bröhl *et al.*, 2012). Notch signalling directly activates collagen production by muSCs (Baghdadi, Castel, *et al.*, 2018) consistently with the overexpression of NICD increasing CALCR and laminin expression by muSCs (Mourikis, Gopalakrishnan, *et al.*, 2012). Interestingly, in *Pax7*-specific Rbp-jk-/- knock-out mice, mutant cells relocate from under the basal lamina to the interstitial space (Bröhl *et al.*, 2012). Similarly, also in mouse, proliferating *Pax7* Rbp-jk-/- mutant cells reside above the basement membrane (Bjornson *et al.*, 2012). This suggests that following Notch inhibition, activated muSCs exit from their niche.

Notch-dependent muSCs interaction with surrounding cells is important for the maintenance of a quiescent state. In mouse, PAX7+ Vascular endothelial growth

factor+ (VEGF) muSCs lie in proximity to vessels (Verma *et al.*, 2018). Following injury, muSCs closer to vessels proliferate more in a NOTCH1/NOTCH2 (muSC)- or DLL4 (blood vessel)-dependent manner (Verma *et al.*, 2018). Moreover, *in vitro,* muSCs express NOTCH1 and NOTCH3, while ligands DLL1 and DLL4 are found on committed myoblasts and mature myofibers (Low *et al.*, 2018). These results suggest that cells commit to the myogenic lineage, signalling to progenitor cells in a Notch-dependent manner, limiting differentiation whilst maintaining quiescence, preventing the depletion of the muSC pool.

Summary

Taken together, studies investigating the importance of Notch signalling on the activity of muSCs have shown that in homeostatic conditions Notch functions to keep cell in a quiescent state. MuSCs make contacts with their surrounding niche in a Notch dependent manner to maintain quiescence. Following injury, Notch expression is downregulated in activated *Pax7*-expressing cells. *In vitro* it has been shown that a *Pax7*+ cell-specific Notch mutation results in premature S-phase independent differentiation. This suggests that although Notch signalling is downregulated following injury, Notch is still important to limit differentiation and promote proliferation. Additionally, Notch has been implemented in the process of asymmetric division, active in the stem cell to maintain quiescence, and supressed in the progenitor cell to promote differentiation.

1.7 Interstitial cells

In addition to muSCs, different interstitial cells contribute towards muscle repair (reviewed by Bentzinger *et al.*, 2012; Schmidt *et al.*, 2019; Fig. 1.9). These interstitial cells can be broadly categorised in cells with or without myogenic potential, directly or indirectly influencing postnatal myogenesis, respectively (reviewed by Bentzinger *et al.*, 2012; Schmidt *et al.*, 2019). Interstitial cells with myogenic potential include: pericytes, Pw1+ interstitial cells (PICs), and *Twist2*+ cells, all of which can differentiate into the myogenic lineage (reviewed by Bentzinger *et al.*, 2012; Schmidt *et al.*, 2019). Although many cells can contribute to myogenesis, interstitial cells

cannot compensate for a lack of embryonically derived Pax7-expressing cells following injury (Lepper *et al.*, 2011).

***Pw1*+ interstitial cells**

Pw1+ interstitial cells (PICs) are an emerging population of interest due to their putative myogenic potential. In culture, PICs convert to skeletal myogenic cells, expressing *Myod* in a *Pax7*-dependent manner (Mitchell *et al.*, 2010). In mice, *Pax7*-/- knockout results in more PICs, whereas, *in vitro*, PICs displaying perturbed proliferation, differentiation and fusion (Mitchell *et al.*, 2010). Following transplantation, PICs reconstitute the muSC niche around muscle fibres beneath the basement membrane (Mitchell *et al.*, 2010). PICs can commit to the myogenic lineage, expressing *Pax7*, *Myf5* and *Myod*, and, *in vitro,* can differentiate into muscle fibres expressing MYOGENIN and MYHC (Lewis *et al.*, 2017). Moreover, following CTX injury, muscle transplanted with exogenous PICs display improved muscle regeneration associated with increased cell proliferation, capillary density, muscle fibre diameter and cross-section area (Lewis *et al.*, 2017). Additionally, PICs express growth factors and cytokines promoting muSC activity and immune response (Lewis *et al.*, 2017).

***Twist2*+ interstitial cells**

Twist2+ interstitial cells differ from PAX7-expressing cells and are found above the basement membrane of type II myofibers (Liu *et al.*, 2017). *Twist2*+ interstitial cell contribution to type II myofiber growth is substantiated by *Twist2*+ lineage depletion leading to type II fibre atrophy (Liu *et al.*, 2017). Moreover, *Twist2*+ interstitial cells express Desmin (marker of muscle differentiation), and fuse to damaged myofibers (>90 % of fusion events), as well as fusing to one another to initiate *de novo* myogenesis (Liu *et al.*, 2017). Following *Twist2*+ cell isolation, and presumably activation, *Twist2*+ cells downregulate *Twist* genes and upregulate *Pax7* (Liu *et al.*, 2017). *In vitro*, in growth medium, *Twist2*+ cells upregulate *Pax7* expression to enter the myogenic lineage (Liu *et al.*, 2017). In differentiation medium, *Pax7* is downregulated, and *Myogenin* and *Myosin* are upregulated, resulting in terminal differentiation (Liu *et al.*, 2017).

Pericytes

Co-culture experiments revealed a cross-talk between the processes of myogenesis and angiogenesis (Latroche *et al.*, 2017). Proliferating MYF5+ muSCs are found within close proximity with laminin+ capillaries (Chiristov *et al.*, 2007). This proximity of muSCs with capillaries has also been shown in human deltoid muscle (Chiristov *et al.*, 2007). Pericytes are contractile cells found on the vasculature of mammalian skeletal muscle (Dellavalle *et al.*, 2007). Co-culture experiments have been used to assess the cross-talk between pericytes and MPCs (Dellavalle *et al.*, 2007). Pericytes in co-culture with C2C12 cells leads to multi-nucleated myotube formation (myosin-expressing; Dellavalle *et al.*, 2007). This suggests that pericytes can promote MPC activation and differentiation. Pericytes in myogenic-promoting conditioned media upregulate MYOD, MYOGENIN and MYHC by 3 days, and MYF5 by 4 days (Dellavalle *et al.*, 2007); however, pericytes do not express Pax7 (Dellavalle *et al.*, 2007). Contrastingly, Following CTX mucle injury, pericytes contribute to muscle repair, progressively expressing Pax7 and MYHC (Dellavalle *et al.*, 2007). Two population of muscle-associated pericytes exist, NG2+NESTIN+ and NG2+NESTIN- pericytes (Birbrair *et al.*, 2013). The former contributes to myogenesis and the latter fibrosis (Birbrair *et al.*, 2013). Moreover, NESTIN+ pericytes make contacts with PAX7+ muSCs (Kostallari *et al.*, 2015). Co-culture of pericytes with PAX7+ muSCs has shown that pericytes promote increased EdU retention, MHC+ myotube formation, PAX7, MYOD and MYOGENIN expression in MPCs (Kostallari *et al.*, 2015). MPCs found on Myofibers which had been cultured in pericyte-conditioned media showed an increase differentiation (PAX7 negative; Kostallari *et al.*, 2015). Moreover, loss of pericytes leads to hypotrophy (Kostallari *et al.*, 2015). Further investigations have demonstrated that pericytes have a dual role, influencing both muSC quiescence and myogenesis (Kostallari *et al.*, 2015).

Fibro-adipogenic progenitors

Although they do not have myogenic potential, fibro-adipogenic progenitors (FAPs) have been identified during the inflammatory phase of muscle repair (Joe *et al.*,

2010). Quiescent in uninjured muscle, FAP readily activate and proliferate following muscle injury, peaking by 3 dpi before drastically declining to homeostatic levels (Joe *et al.*, 2010). This peak in FAP number coincides with the peak in macrophage number during the inflammatory response (reviewed by Bentzinger, Wang, Dumont, *et al.*, 2013). In mouse, macrophage depletion models demonstrated the importance of pro- *versus* anti-inflammatory macrophages for the survival of FAPs and the consequences on muscle repair.

Following injury-induced FAP proliferation, FAPs begin to undergo apoptosis and are subsequently cleared by pro-inflammatory macrophages (Lemos *et al.*, 2015). Following diptheria toxin-induced macrophage ablation, a prolonged VCAM+ FAP response is observed (Malecova *et al.*, 2018). The absence of macrophage in chemokine receptor (CCR) 2-/- mice inhibits the clearing of FAPs from damaged tissue and is associated with an increase in fibrogenic- and ECM-associated markers (Lemos *et al.*, 2015). Co-culture with FAPs and pro-inflammatory macrophages demonstrated that macrophage-derived tumour necrosis factor (TNF) α is responsible for increased FAP death, a phenotype rescued through TNF-α blockade (Lemos *et al.*, 2015). Mice treated with anti-TNF-α showed an increase in FAPs by 7 dpi, a reduction of Caspase3-expressing FAPs, and an increase in collagen deposition, a hallmark of fibrosis (Lemos *et al.*, 2015). *In vitro* co-culture analysis showed an interaction between TNF-α-expressing macrophages and FAPs (Lemos *et al.*, 2015). Furthermore, in Mdx mice, nitric oxide (NO) treatment leads to reduced FAP numbers associated with reduced collagen and fat deposition (Cordani *et al.*, 2014). This phenotype is due to NO inhibition of adipogenic differentiation of FAPs.

Contrastingly, anti-macrophage-derived transforming growth factor (TGF) β counters the apoptotic effects of TNF-α via the p38 kinase and NF-κβ pathways (Lemos *et al.*, 2015). In addition to anti-inflammatory macrophages, eosinophils also promote the survival of FAPs Heredia *et al.*, 2013). FAP proliferation is enhanced by eosinophil-derived interleukin (IL)-4, aiding in the removal of necrotic tissue and cellular debris (Heredia *et al.*, 2013). FAPs can also directly influence muSCs (Joe *et al.*, 2010). FAPs express IL-6 and insulin like growth factor (IGF) 1 that directly stimulate muSC differentiation during muscle repair, as well as potentiating the inflammatory response (Joe *et al.*, 2010). Moreover, FAP-derived Wnt inducible signalling pathway

protein 1 (WISP1) promotes muSC expansion and commitment following injury (Lukjanenko *et al.*, 2019).

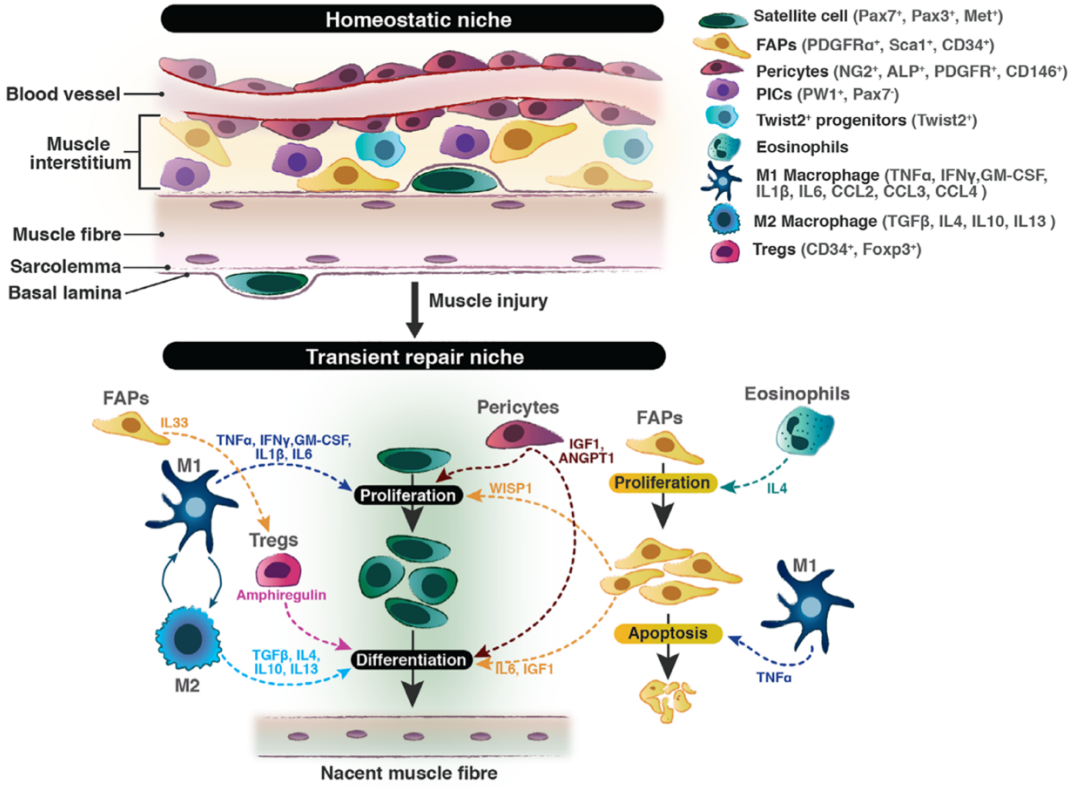

Figure 1.9. Interstitial cells regulate satellite cell proliferation and differentiation following injury.

Following muscle injury, the stem cell niche is disrupted resulting in satellite cell activation. Interstitial cells are activated and recruited to the site of injury contributing towards muscle repair. Pericytes, *Pw1*+ interstitial cells (PICs), and *Twist2*+ cells can directly contribute to the formation of new myofibers. Fibro-adipogenic progenitors (FAPs) and the recruited immune cells such as eosinophils, macrophages, and regulator T-cells (Tregs), promote resident satellite cell activation (Ruparelia *et al.*, 2020).

1.8 The immune response during amniote muscle repair

As previously mentioned, there are three major phases for mammalian muscle repair: immune infiltration, tissue reconstruction and remodelling, the latter mediated by the interplay between tissue resident muSCs and interstitial cells (reviewed by Rossi and Messina, 2014). It is now understood that there are three immunological phases temporally controlled relative to myoblast activation, proliferation and differentiation (reviewed by Yang and Hu, 2018; Fig. 1.10). Moreover, this fine-tuned cascade of immune activation both indirectly and directly contributes to myogenesis following muscle injury (reviewed by Tidball, 2017; Yang and Hu, 2018; Dort *et al.*, 2019).

The mammalian immune system is sophisticated and can be broadly categorised as innate and adaptive. Both innate and adaptive immunity coordinate to amplify a pro-inflammatory response through the secretion of cytokines and chemokines (chemoattractant cytokines), subsequently supressing a prolonged pro-inflammatory response by generating an anti-inflammatory environment (reviewed by Tidball, 2017; Yang and Hu, 2018; Dort *et al.*, 2019). The anti-inflammatory environment supports tissue repair and growth through direct interactions or secreted factors (reviewed by Tidball, 2017; Yang and Hu, 2018; Dort *et al.*, 2019). Although the anti-inflammatory response is typically associated with the repair of tissue following injury, a balanced pro- and anti-inflammatory immune response is required for successful tissue regeneration (Thornton, 1949; Mathew *et al.*, 2007).

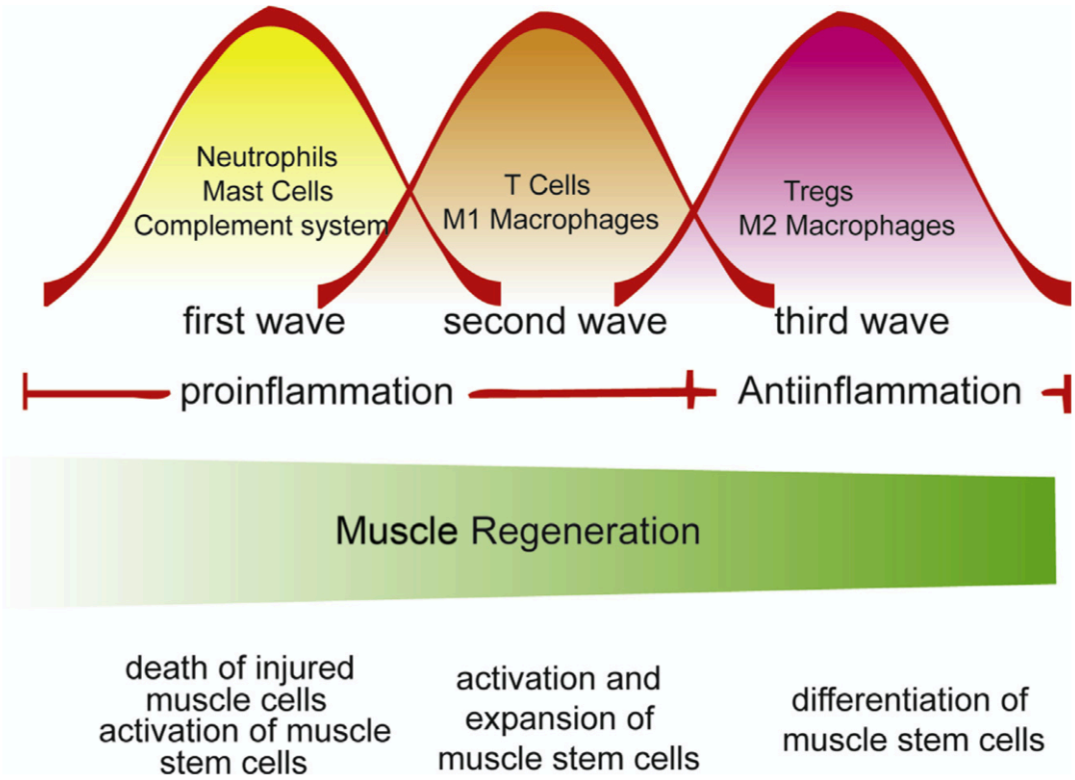

Figure 1.10. The three immunological phases of muscle repair.
The complement system, resident mast cells and neutrophils respond to tissue damaged immediately after muscle injury. This first wave initiates the pro-inflammatory response, facilitates the degeneration of damaged muscle and promotes stem cell activation. Following the initial response, Cytotoxic T-cells and pro-inflammatory (M1) macrophages are recruited as part of the second wave. These cells aid in the clearance of muscle debris, propagating the pro-inflammatory response, and promoting stem cell expansion. Finally, regulatory T-cells (Tregs) and anti-inflammatory macrophages (M2) are recruited, supressing the pro-inflammatory response. This third wave marks the end of the inflammatory response, promoting stem cell differentiation (Yang and Hu, 2018).

The mammalian immune response in damaged muscle is predominantly facilitated by macrophages and monocytes, as well as, their interaction with complement, granulocytes (neutrophils and mast cells), and lymphocytes (cytotoxic and regulatory).

The immune response can be compartmentalised into three phases. The first wave is mediated by the recruitment of the complement system, mast cells and neutrophils (reviewed by Tidball, 2017; Yang and Hu, 2018; Dort *et al.*, 2019). In conjunction with locally produced damage-associated molecular patters (DAMPs) and chemokines (also referred to as myokines in the context of skeletal muscle), this first phase functions to initiate the pro-inflammatory response (reviewed by Tidball, 2017; Yang and Hu, 2018; Dort *et al.*, 2019). The early response results in the secondary recruitment of pro-inflammatory macrophages and cytotoxic T lymphocytes (T cells) which propagate the pro-inflammatory response (reviewed by Tidball, 2017; Yang and Hu, 2018; Dort *et al.*, 2019). Finally, the third wave constitutes a switch to an anti-inflammatory environment characterised by the recruitment of anti-inflammatory macrophages and regulatory T-cells (Tregs; reviewed by Tidball, 2017; Yang and Hu, 2018; Dort *et al.*, 2019).

1.8.1 Phase I

The complement system

The complement system consists of more than 30 surface and soluble factors (reviewed by Klos *et al.*, 2009). Although the complement system is classically associated with the clearance of pathogenic microorganisms, studies highlighted its role in tissue repair (reviewed by Klos *et al.*, 2009). C3a and C5a are by-products of the complement system (also known as anaphylatoxins), capable of inducing vasodilation, recruiting macrophages, neutrophils, basophils, mast cells, B- and T-cells (reviewed by Klos *et al.*, 2009). Following injury, the complement system is activated, recruiting pro-inflammatory leukocytes to the site of injury (Frenette *et al.*, 2000). In rat, blockade of the classical and alternative complement system inhibits early recruitment of pro-inflammatory macrophages (ED1+) and neutrophils in damaged muscle without effecting resident macrophages (ED2+; Frenette *et al.*, 2000). The later pro-inflammatory response still activates, likely due to the activity

of resident immune cells (Frenette *et al.*, 2000). Moreover, both C3a and are upregulated in circulation following extensive exercise in humans, suggesting that the complement system can act as a muscle damage sensor in humans (Dufaux and Order, 1989). Following CTX-induced muscle injury, C3b was observed at the injury site, suggesting the activation of the alternative complement system (Zhang *et al.*, 2017). The alternative, but not the classical, complement pathway is critical for C3-dependent monocyte recruitment and repair of skeletal muscle (Zhang *et al.*, 2017).

Mast cells

In addition to the complement system, mast cells are rapidly recruited and activated, amplifying the early recruitment of pro-inflammatory lymphocytes (Gorospe *et al.*, 1996). Mast cells are fast responding granulocytes which degranulate, releasing pro-inflammatory cytokines such as TNF-α, IL-1β, and histamine following muscle injury (Gordon and Galli, 1990). Pro-inflammatory cytokines induce vasodilation and the recruitment of pro-inflammatory leucocytes, as well as additional mast cells to the site of injury (reviewed by Tidball, 2017; Yang and Hu, 2018; Dort *et al.*, 2019). In myopathies, aberrant mast cell activation contributes to necrosis and dystrophic muscle; the phenotype was rescued by limiting mast cell granulation (reviewed by Radley and Grounds, 2006).

Neutrophils

The most important immune cell in phase I and the priming of the pro-inflammatory microenvironment are neutrophils (reviewed by Tidball, 2017; Yang and Hu, 2018; Dort *et al.*, 2019). Neutrophils are readily recruited and activated following muscle damage. Neutrophils are observed immediately after exercise-induced damaged in humans, releasing an increasing amount of IL-1β (Fielding *et al.*, 1993). Neutrophils are a potent source of pro-inflammatory cytokines, including TNF-α, interferon (IFN) γ, IL-1β, macrophage inflammatory protein 1 (MIP-1α), and monocyte chemoattractant protein 1 (MCP-1; reviewed by Scapini *et al.*, 2000; Dort *et al.*, 2019). The production of pro-inflammatory cytokines results in the recruitment of peripheral neutrophils, mast cells, monocytes and macrophages, further exacerbating the pro-inflammatory microenvironment.

1.8.2 Phase II

Neutrophils

Following the initial pro-inflammatory priming, peripheral neutrophils (Ly6C+CD11b+) are quickly recruited to muscle injury (Fielding *et al.*, 1993; Belcastro *et al.*, 1996), peaking by 24 hpi, before declining to homeostatic levels by 14 dpi (Dumont *et al.*, 2008). Neutrophils play a dual role; neutrophils break down damaged myofibers before phagocytosing cellular debris and necrotic tissue leading to secretion of oxidative factors (ROS), enzymes (proteases) and pro-inflammatory cytokines (reviewed by Nathan, 2006; Dumont *et al.*, 2008; Tidball, 2017; Yang and Hu, 2018; Dort *et al.*, 2019). In canine *Gracilis* skeletal muscle, neutrophils promote ROS-mediated vascular permeability following ischemia-induced injury (Korthuis *et al.*, 1988). This suggests that a chronic neutrophilic response is associated with worsened muscle damage, delaying the regenerative program (reviewed by Yang and Hu, 2018).

Monocytes and pro-inflammatory macrophages

Blood monocytes and tissue macrophages are crucial during the early pro-inflammatory phase, following tissue damage, and the later anti-inflammatory pro-regenerative stage (reviewed by Ginhoux and Jung, 2014). Monocytes, predominantly found in circulation, display determinant surface receptors key to identifying their respective immune roles: CD14 (lipopolysaccharide [LPS] co-receptor) and CD16 (FCγRIII) in human, and Ly6C in mouse (reviewed by Ginhoux and Jung, 2014). Three major monocytic subsets exist: classical ($CD14^{++}CD16^{-}$/ $Ly6C^{hi}$), intermediate ($CD14^{++}CD16^{+}$), and non-classical ($CD14^{+}CD16^{++}$/ $Ly6C^{low}$) (reviewed by Ginhoux and Jung, 2014).

The polarisation states of macrophages add another layer of complexity to the roles macrophage play during tissue repair (Arnold *et al.*, 2007; Heredia *et al.*, 2013; Varga *et al.*, 2016). Initially macrophages were classified into pro-inflammatory (also called classically activated or M1) and anti-inflammatory (also called alternatively activated or M2; Arnold *et al.*, 2007). However, although macrophages can polarise towards the extreme M1 or M2 phenotype, they can also polarise towards a hybrid phenotype (Heredia *et al.*, 2013). During the process of muscle repair, pro- and anti-

inflammatory macrophages are both present within the injured muscle. Both pro- (*Nos2*, *Il6*, and *Tnfα*) and anti-inflammatory (*Arg1* and *Ym1*) markers are expressed concurrently following injury within individual macrophages (Heredia *et al.*, 2013). Furthermore, *in vivo,* the classical Ly6C^{hi} and non-classical Ly6C^{lo} macrophages only partially overlap with the expression of pro- and anti-inflammatory-associated genes following muscle injury (Varga *et al.*, 2016). Although macrophages are extremely plastic, studies often simplify the nomenclature, referring to macrophages as M1 or M2. Therefore, following muscle injury, pro-inflammatory Ly6C^{hi} macrophages are recruited to the injury, which subsequently switch to anti-inflammatory Ly6C^{lo} macrophages (Arnold *et al.*, 2007). This phenotypic switch occurs in response to phagocytosis and the release of anti-inflammatory cytokines (reviewed by Mantovani *et al.*, 2004).

Following notexin-induced muscle injury, resident tissue macrophages release neutrophil chemoattractant 1 (CINC-1) and MCP-1, required to recruit bone marrow-derived monocytes and neutrophils (Brigitte *et al.*, 2010). Post-injury, monocytes migrate towards tissue damage at 1 hpi (Finsterbusch *et al.*, 2016), and bone marrow-derived macrophages increase within the first 12 hpi (Brigitte *et al.*, 2010), acting as the primary source of TNF-α.

Following the priming of the immune environment, the major leukocyte is the pro-inflammatory macrophage (reviewed by Tidball, 2017; Yang and Hu, 2018; Dort *et al.*, 2019). Muscle derived CLL2 promotes the recruitment and differentiation of CCR2-expressing bone marrow-derived monocytes into tissue macrophages (Lu, Huang, Ransohoff, *et al.*, 2011). Pro-inflammatory macrophages are observed in injured muscle by 24 hpi, peaking by 3 dpi (Arnold *et al.*, 2007; Lu, Huang, Ransohoff, *et al.*, 2011) around the time neutrophils begin to decline. The primary function of pro-inflammatory macrophages is to phagocytose cell debris and secrete pro-inflammatory cytokines (such as TNF-α, IFN-γ, IL-6 and IL-1β) to promote the primary pro-inflammatory microenvironment.

Cytotoxic T-cells

Originally both CD4+ helper and CD8+ cytotoxic T-cells were thought to be within injured and regenerating muscle (McLennan, 1996), there is now evidence that cytotoxic T-cells contribute to the propagation of the pro-inflammatory microenvironment (Cheng *et al.*, 2008; Zhang *et al.*, 2014; Fu *et al.*, 2015). Recruited T-cells at the site of injury secrete cytokines such as MCP-1 (Zhang *et al.*, 2014) and IFN-γ (Cheng *et al.*, 2008), contributing to macrophage recruitment and muscle repair. *Rag1*-/- null mice, lack T-cell due to a loss in V(D)J recombination, and are unable to regenerate muscle (Fu *et al.*, 2015), a phenotype rescued by muscle transplantation of CD3+ cells or by injection of pro-inflammatory cytokines (IL-1α, IL-13, TNF-α and IFN-γ; Fu *et al.*, 2015). *In vitro*, T-cells secretion of IL-1α, IL-13, TNF-α and IFN-γ is sufficient to promote muSC proliferation (Fu *et al.*, 2015). Transplantation of these muSC *in vivo*, shows they can populate the muSC niche and repair secondary injuries (Fu *et al.*, 2015).

1.8.3 Phase III

Monocytes and anti-inflammatory macrophages

The third phase of inflammation is associated with the phenotypic switch of macrophages from pro- to anti-inflammatory (reviewed by Tidball, 2017; Yang and Hu, 2018; Dort *et al.*, 2019). In mouse, anti-inflammatory macrophages are classified in M2a, b and C and activated by IL-1R, IL-4, IL-10, IL-13 *in vitro* (defined and reviewed by Mantovani *et al.*, 2004). Macrophage are skewed towards an anti-inflammatory phenotype by the surrounding ECM (Joshi *et al.*, 2014). In cancer, interactions between ECM components, fibronectin and vascular cell adhesion molecule-1 (VCAM-1), and macrophage-expressing α4β1 integrin promote an anti-inflammatory phenotype (Joshi *et al.*, 2014). Moreover, macrophage polarisation is associated with mechanical stress, for instance, high strain results in more anti-inflammatory macrophages, characterised by increased IL-10 (Ballotta *et al.*, 2014). During this phenotypic switch, macrophage's metabolic activity change from glycolytic to oxidative (reviewed by O'Neill and Hardie, 2013). This shift is associated with AMP-activated protein kinase α (AMPKα) inhibiting Adenosine triphosphate (ATP)-consuming processes (Zhu *et al.*, 2015). Anti-inflammatory cytokines, such as

IL-10, activates AMPK, promoting the expression of Akt/mTORC1 and JAK/STAT signalling pathways (Zhu *et al.*, 2015). Akt/mTORC1 and JAK/STAT in turn supresses pro-inflammatory pathways such as, NF-κβ and the synthesis of TNF-α and IL-6 by bone marrow-derived macrophages (Zhu *et al.*, 2015). *In vitro*, macrophages-derived from AMPKα-/-mice are pro-inflammatory as expected, displaying reduced expression of anti-inflammatory markers (CD163, CD206 and TFGB1) and increased expression of pro-inflammatory markers (CCL2 and Nitric oxide synthase [iNOS]; Mounier *et al.*, 2013). A phenotype substantiated by *in vivo* data following muscle injury (Mounier *et al.*, 2013). The AMPK-mediated switch to an anti-inflammatory phenotype has also been attributed to the phagocytosis of cellular debris or necrotic neutrophils (Arnold *et al.*, 2007; Bae *et al.*, 2011; Mounier *et al.*, 2013). AMPK is active in phagocytic macrophages and important for microtubule re-organisation (Bae *et al.*, 2011), biasing macrophages towards an anti-inflammatory phenotype (Arnold *et al.*, 2007; Mounier *et al.*, 2013). Macrophages isolated from AMPKα-/- knock-down mice do not upregulate anti-inflammatory markers CD163, CD206 (decreased), or TGF-β following phagocytosis (Mounier *et al.*, 2013). Anti-inflammatory macrophages subsequently propagate the anti-inflammatory microenvironment by secreting anti-inflammatory cytokines whilst supressing the pro-inflammatory immune response (reviewed by Tidball, 2017; Yang and Hu, 2018; Dort *et al.*, 2019).

Regulatory T-cells

The anti-inflammatory stage of inflammation is also characterised by the recruitment of Tregs (CD4+CD25+Foxp3+) characterised by a potent immune suppression ability (Fontenot *et al.*, 2017). Tregs are already found within homeostatic muscle in young and old mice (Burzyn *et al.*, 2013; Wang *et al.*, 2015), and at low levels in early stages of muscle repair (Burzyn *et al.*, 2013). Tregs increases at later stage of inflammation (4 dpi), proliferating and peaking around 8 dpi, coinciding with the switch from pro- to anti-inflammatory myeloid mononuclear cells (Burzyn *et al.*, 2013). Following muscle injury, Tregs upregulate *il10,* which may regulate the conversion of pro- to anti-inflammatory macrophages (Burzyn *et al.*, 2013), and reduce CD8+ T-cells (Villalta, Rinaldi, *et al.*, 2011), inhibiting myoblast proliferation and promoting differentiation. Interestingly, a sub-population of Tregs with identical specific

complementary determining region 3 sequences (CDR3) in the T-cell receptors (TCR) have been identified in multiple mice following muscle injury (Burzyn *et al.*, 2013), suggesting that Tregs develop an immunological memory towards muscle damage. These cells express amphiregulin (epidermal growth factor receptor ligand), which promote myoblast activation (Burzyn *et al.*, 2013). Treg knockouts mice have a prolonged inflammatory response, resulting in a failure to repair damaged muscle (Burzyn *et al.*, 2013).

1.8.4 Cytokines

The mammalian immune response towards muscle injury constitutes the activation and crosstalk of a diverse pool of monocytes, granulocytes, and lymphocytes. Moreover, a sequential switch from a pro- to anti-inflammatory microenvironment is critical for successful muscle repair. This complex multi-phase response is coordinated by the expression of numerous cytokines by resident and infiltrating leukocytes Schuster-Gossler *et al.*, 2007; Pedersen, 2011; Pillon *et al.*, 2013). In addition to leukocyte-derived cytokines, muscle cells can also locally synthesise cytokines (termed myokines; Table 1.1). Moreover, cytokines can directly modulate the muSC response, facilitating muscle repair Schuster-Gossler *et al.*, 2007; Pedersen, 2011; Pillon *et al.*, 2013).

Interactions	Model	Condition	Source
IL-6	Rat	ATP treatment	Primary myotubes
	Murine	limb ischemia	Muscle (general)
	Human	LPS treatment	Skeletal muscle Primary quadriceps muscle
	C_2C_{12} (murine)	LPS treatment	Immortalised myoblast cell culture
IL-8	Human	Exercise	Skeletal muscle
IL-15	Human	Exercise	Skeletal muscle
TNF-α	Human	LPS treatment	Skeletal muscle Primary quadriceps muscle
	C_2C_{12} (murine)	LPS treatment	Immortalised myoblast cell culture
CCL2	C_2C_{12} (murine)	LPS treatment	Cell culture
CCR2	Human	TNF-α	Skeletal myocytes
	Rat	Endotoxin	Skeletal muscle (general)
	L6 myotubes (rat)	TNF-α and IFN-γ	Immortalised myotubes cell culture
	Murine	LPS	Diaphragm

Table 1.1. List of myokines, the conditions in which they are produced and the cell type which produces them.
Myokines have mostly been defined in the context of exercise, insulin resistance and infection (Schuster-Gossler *et al.*, 2007; Pedersen, 2011; Pillon *et al.*, 2013). Lipopolysaccharide (LPS), adenosine triphosphate (APT), tumor necrotic factor alpha (TNF-α), and interferon gamma (IFN-γ).

IL-6 and IL-1β

IL-6 is a putative pro-inflammatory cytokine secreted by multiple leukocytes including macrophages and T-cells, characterised during the processes of myogenesis (reviewed by Muñoz-Cánoves *et al.*, 2013). Following muscle insult in rat, *Il6* is expressed in both mononucleated and damaged muscle cells at 3 hpi (Kami and Senba, 1998). Although muscle cells are able to synthesise local IL-6, macrophage-derived IL-6 is pivotal for myogenic cell determination and proliferation (Zhang *et al.*, 2013). In *Il6*-/- mice, muscle repair is impaired, associated with decreased *MyoD*, *Myogenin*, myofiber size and macrophage infiltration (Zhang *et al.*, 2013). This phenotype is rescued by transplanting bone marrow-derived macrophages from WT animals (Zhang *et al.*, 2013). Moreover, co-culturing macrophages from *il6*-/- mice and C2C12 myoblasts results in reduced myoblast proliferation (Zhang *et al.*, 2013).

In the pro-inflammatory microenvironment, IL-1β is produced by many pro-inflammatory leukocytes (reviewed by Tidball, 2017; Yang and Hu, 2018; Dort *et al.*, 2019). In addition to acting as a potent leukocyte chemoattractant, IL-1β inhibits myotube formation in culture, suggesting an inhibitory role on differentiation (Saclier, Yacoub-Youssef, *et al.*, 2013). IL-1β has also been shown to stimulate the production of myoblast-derived IL-6 via the NF-κβ pathway *in vitro* (Luo *et al.*, 2003), potentiating the IL-6 driven commitment and proliferation of myoblasts. In a positive feedback mechanism, IL-6 promotes increased macrophage-derived IL-1β production (Zhang *et al.*, 2013).

CCL2-CCR2

CLL2, also known as MCP-1, is predominantly produced by monocytes and macrophages (reviewed by Tidball, 2017; Yang and Hu, 2018; Dort *et al.*, 2019). CCL2 is a chemokine, recruiting monocytes to the site of inflammation, signalling through CCR2 (reviewed by Tidball, 2017; Yang and Hu, 2018; Dort *et al.*, 2019). CCR2 deficient mice have demonstrated the importance of the CCL2-CCR2 axis during successful muscle repair (Warren *et al.*, 2005; Contreras-Shannon *et al.*, 2007; Martinez *et al.*, 2010). The principal defect following CCR2 mutation is the reduced monocytic recruitment to damaged muscle (Warren *et al.*, 2005; Contreras-Shannon *et al.*, 2007; Martinez *et al.*, 2010). CCR2-/- mice fail to regenerate muscle associated with increased necrosis (Contreras-Shannon *et al.*, 2007; Martinez *et al.*, 2010), fat (Warren *et al.*, 2005; Contreras-Shannon *et al.*, 2007), collagen (Warren *et al.*, 2005) and calcium (Warren *et al.*, 2005) deposition. This inability to regenerate muscle leads to increased fat area (Contreras-Shannon *et al.*, 2007), total weight (Contreras-Shannon *et al.*, 2007), and reduced MYOD and MYOGENIN expression (Contreras-Shannon *et al.*, 2007; Sun *et al.*, 2009), myofiber cross-section area (Warren *et al.*, 2005; Contreras-Shannon *et al.*, 2007; Martinez *et al.*, 2010) and the formation of blood vessels (Contreras-Shannon *et al.*, 2007). This ultimately reduces the functionality of the muscle, exhibiting reduced strength (Warren *et al.*, 2005). Interestingly, pro-inflammatory signals increase in CCR2-/- mice (Warren *et al.*, 2005), likely due to the increased early neutrophilic response (Warren *et al.*, 2005; Contreras-Shannon *et al.*, 2007; Martinez *et al.*, 2010). The number of recruited

tissue neutrophils are unaffected, therefore the increased neutrophilic response is likely due to the perdurance rather than recruitment (Contreras-Shannon *et al.*, 2007). The incapacity to regenerate muscle has been attributed to the failure to mount a monocytic response (Warren *et al.*, 2005; Contreras-Shannon *et al.*, 2007; Sun *et al.*, 2009; Martinez *et al.*, 2010). Reduced monocytic infiltration and regenerative capacity in CCR2-/- mice is rescued following bone-marrow transplantation from healthy mice (Sun *et al.*, 2009). The loss of macrophages is associated with increased MYOD and MYOGENIN expressing muSCs *in vivo* and improves myogenic potential of fibres *in vitro* (MYHC and MYOD positive cultured fibres; Sun *et al.*, 2009).

The absence of muscle regeneration, characterised by reduced muscle volume and fibre cross-section area following muscle injury, has also been observed in Ccl2-/- mice (Lu, Huang, Ransohoff, *et al.*, 2011). These mice also have a reduced monocytic response and an increased early neutrophil response which gradually subsides (Lu, Huang, Ransohoff, *et al.*, 2011). Moreover, immune infiltrates (macrophages) were partially restored following WT bone marrow transplantation into Ccl2-/- mice (Lu, Huang, Ransohoff, *et al.*, 2011). Interestingly, myogenic cells also contribute towards CCL2 production and may directly respond to CCL2 signalling (Lu, Huang, Ransohoff, *et al.*, 2011). It has been shown that immune infiltration was also partially restored following Ccl2-/- bone marrow transplantation into WT mice, suggesting the importance of muscle-derived CCL2 (Lu, Huang, Ransohoff, *et al.*, 2011). Moreover, Myog-expressing cells (Warren *et al.*, 2005), express CCR2, suggesting differentiating myoblasts can sense and directly respond to CCL2 production.

TNF-α

TNF-α signals through two receptors, TNFR1 and TNFR2, the former facilitating the pro-inflammatory signals of TNF-α (Kondo and Sauder, 1997; Mori *et al.*, 2002). Following muscle injury, TNF-α signalling is upregulated, peaking by 24 hpi (Warren *et al.*, 2002). Mice lacking the TNF-α receptor fail to regenerate muscle, and present an increased immune infiltrate (Warren *et al.*, 2002; Chen *et al.*, 2005). Moreover, TNF-α receptor knock-out and animals treated with an anti-TNF-α antibody exhibit reduced *MyoD* expression with impaired muscle function (Warren *et al.*, 2002).

Additionally, TNF-α receptor mutation reduces p38, MEF-2C, Myogenin and p21 activation, and leads to increased cyclin D1 expression (Chen *et al.*, 2005). This suggests that TNF-α is important for the switch from a proliferative muscle cell state towards differentiation. Contrastingly, TNF-α induces MPC proliferation in a concentration dependent manner, with higher levels having a negative effect on MPC expansion *in vitro* (Li, 2003).

TNF-α activates p38 leading to the phosphorylation of EZH2 (reviwed by Tidball, 2017). EZH2 is the catalytic subunit of the Polycomb group 2 (POCG2) complex, responsible for the trimethylation of lysine 27 on histone 3 (H2K27me3) at the Polycomb-response element (PRE), inhibiting the promotion of target genes (reviwed by Tidball, 2017). Following injury, EZH2 supresses Pax7 expression to promote myogenic commitment and differentiation (Palacios *et al.*, 2010). Inhibition of TNF-α or p38 3 dpi (around when muSCs stop proliferating and begin to differentiate) leads to a downregulation of commitment and differentiation associated MRFs (Chen *et al.*, 2005; Zhan *et al.*, 2007). This results in impaired muscle repair. Another study examining the role of EZH2 during muSC activation shows that suppression of EZH2 function results in elevated expression of PAX7 (Palacios *et al.*, 2010). As EZH2 knockdown increased PAX7 expression, one would expect that inhibition of EZH2 would result in muSC exit from quiescence and increased proliferation. Contrastingly, muSC-specific Ezh2-/- mice have fewer muSCs in uninjured and injured muscle, associated with decreased myoblast proliferation (Juan *et al.*, 2011; Woodhouse *et al.*, 2013). Moreover, muSC-specific Ezh2-/- mice fail to regenerate muscle, whereas when Ezh2 was downregulated in MYOGENIN expressing cells only, mice displayed no proliferative or regenerative defects (Woodhouse *et al.*, 2013). TNF-α also increases EZH2-dependent methylation of the NOTCH1 promoter (Acharyya *et al.*, 2010) which could account for the loss of muSC expansion following muSC-specific Ezh2-/-.

IFN-γ

IFN-γ plays a dual role, promoting the pro-inflammatory environment and down-regulating myogenic differentiation (Cheng *et al.*, 2008; Villalta, Deng, *et al.*, 2011). Following CTX-induced injury, IFN-γ expression increases within the first 24 hpi,

peaking by 5 dpi coinciding with the increase in anti-inflammatory monocytes and MYOD expression (Cheng *et al.*, 2008).

Inhibition of IFN-γ in mice leads to impaired muscle regeneration and increased muscle fibrosis (Cheng *et al.*, 2008). Moreover, overactivation of INF-γ leads to muscle fibre damage *in vivo*, inhibiting proliferation and differentiation of C2C12 cells *in vitro* (Villalta, Deng, *et al.*, 2011); indicating, the importance of a balanced IFN-γ response. Inhibition of IFN-γ signalling skews macrophages towards an M2 phenotype, reducing expression of IRF1 and iNOS (Cheng *et al.*, 2008) and increasing expression of CD206, IL-4, arginase (Arg) 1, MGL2 and FIZZ1 (Villalta, Deng, *et al.*, 2011). IFN-γ activates the STAT1 and IFN regulatory factor 1 (IRF-1), which in turn leads to the expression of target genes, including the MHC class II transactivator (CIITA) (Morris *et al.*, 2002). CIITA binds to and inhibits Myogenin expression in C2C12 cells, moderately limiting proliferation and halting differentiation (Londhe and Davie, 2011). muSCs stimulated with IFN-γ do not express differentiation markers, disrupting the differentiation and fusion of muSCs later in regeneration (Londhe and Davie, 2013). IFN-γ stimulation leads to increased CIITA, which in turn increases the recruitment of PGC2 to the promoter region of differentiation specific genes (Londhe and Davie, 2011, 2013).

1.9 The larval zebrafish immune system

Despite the information on the role of the immune system during muscle repair in amniotes, the intricate network of leukocytes and cytokines has not been as heavily studied in the repair of muscle in larval zebrafish. The reason for this gap in knowledge is partly due to the lack of functional analysis on specific cell subtypes, (such as mast cells, basophils, and eosinophils) in addition to the temporal emergence of different cell populations. Regarding this point, the adaptive immunity is functional only from 4 weeks post-fertilisation (reviewed by Novoa and Figueras, 2012). Most analysis has been performed on early larval stages 2-4 days post fertilisation (dpf), stages at which macrophages and neutrophils are the predominant, if not the only functional immune cell responding to tissue damage and infection (reviewed by Chen and Zon, 2009; Renshaw and Trede, 2012). A functional complement system has also been described in larval zebrafish (reviewed by Zhang

and Cui, 2014). Therefore, in conjunction with *in vivo* live-imaging and the available genetic tools, zebrafish larvae provide us with the ideal platform to dissect the precise roles of macrophages and neutrophils during the process of tissue repair.

1.9.1 Zebrafish embryonic haematopoiesis

Zebrafish haematopoiesis occurs in two distinct waves: primitive haematopoiesis which occurs until 36 hpf, and definitive haematopoiesis which occurs from 36 hpf and throughout adulthood (reviewed by Chen and Zon, 2009; Fig. 1.11). Before the establishment of the blood circulation, haematopoietic stem cells are localised to the anterior lateral mesoderm (ALM; anterior to the yolk sac) and posterior lateral mesoderm (PLM; anterior to the gut; Detrich *et al.*, 1995). Myeloid progenitors emerge from the ALM 12-14 hpf in an Macrophage colony stimulating factor (M-CSF)-dependent manner (Herbomel *et al.*, 2001), migrating towards the yolk sac by 24 hpf (Bennett *et al.*, 2001). Zebrafish embryos possess competent L-plastin-expressing phagocytes by 24 hpf (Herbomel *et al.*, 2001), capable of engulfing microorganisms (Herbomel *et al.*, 1999) and injected carbon particles in the blood circulation (Lieschke *et al.*, 2001) by 29 hpf. Around this time (28 hpf) *l-plastin* transcript is also expressed in the posterior intermediate cell mass (ICM) and along the body axis (Bennett *et al.*, 2001). By 36 hpf, *l-plastin,* granulocyte-specific myeloperoxidase (*mpx), pu.1* and *gata2* transcripts are expressed in the posterior blood island (PBI) located in the tail (Rhodes *et al.*, 2005), the embryonic site of multipotent haematopoiesis (Bertrand *et al.*, 2008). From 36 hpf, the definitive wave of haematopoiesis takes over, and leukocytes are derived from the caudal hematopoietic tissue (CHT), liver and kidney (reviewed by Chen and Zon, 2009).

Although zebrafish eosinophils have been identified using the gata2 transgenic reporter line in adult zebrafish (Bennett *et al.*, 2001; Lieschke *et al.*, 2001; Balla *et al.*, 2010), description in the larvae is lacking. Similarly, mast cell progenitors (*cpa5*+) have been identified at 28 hpf (Dobson *et al.*, 2008) and FcεRI-like receptor+ mast cells in the adult (Da'as *et al.*, 2011), yet very little is known about the establishment and function of these cells.

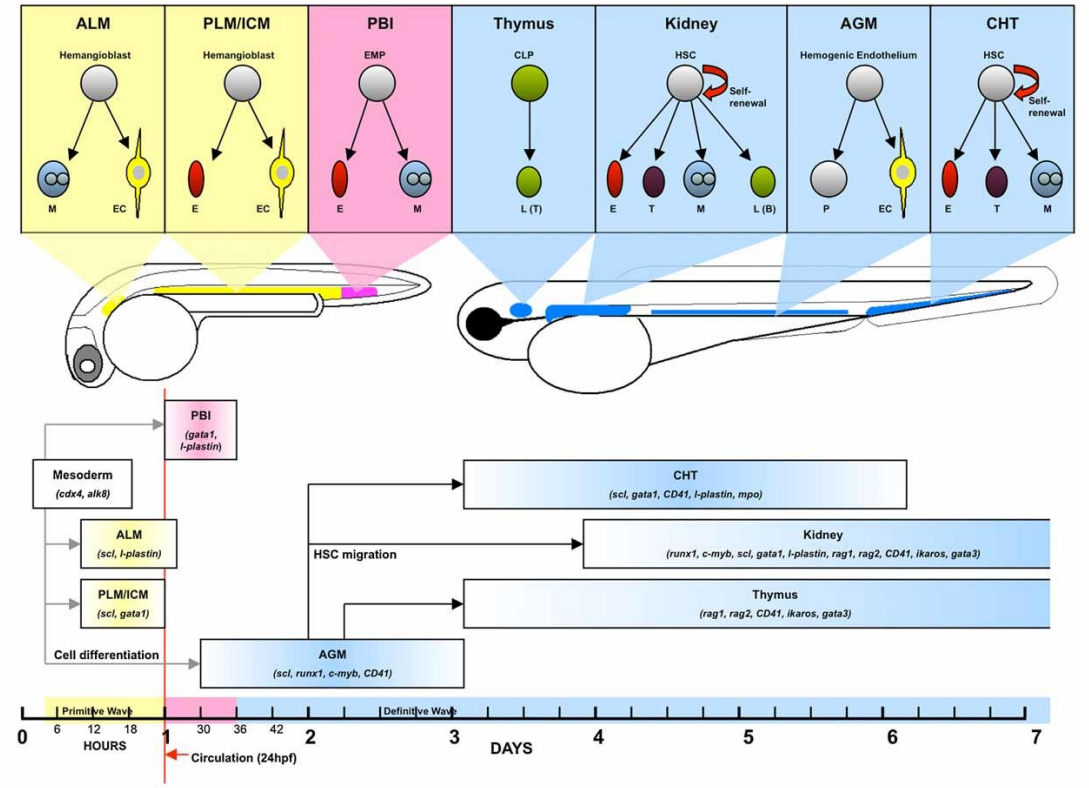

Figure 1.11. Zebrafish haematopoiesis.

Haematopoiesis in zebrafish occurs within two distanced phases. Primitive haematopoiesis occurs up until 36 hpf. Haematopoietic stem cells (HSCs) are initially found within the anterior lateral mesoderm (ALM) and posterior lateral mesoderm (PLM, which forms the intermediate cell mass [ICM]). Following blood circulation (24 hpf), erythromyeloid progenitors (EMPs) develop within the posterior blood island (PBI) and haemogenic endothelium develops in the aorta-gonad mesonephros (AGM). The subsequent definitive wave of haematopoiesis occurs from 36 hpf and throughout adulthood. HSCs migrate to the Caudal Hematopoetic Tissue (CHT), Thymus and pronepherous. From 3 dpf the primary site of haematopoiesis occurs within the Kidney, CHT and Thymus. It is possible to identify and trace individual cell population by their transcription factor expression patterns. Myeloid (M), erythroid (E), endothelial cells (EC), B-cell (L[B]), T-cell (L[T]), thromboid lineage (T), common lymphoid progenitor (CLP), hematopoietic progenitor (P; Chen and Zon, 2009).

1.9.2 Zebrafish neutrophil response to injury

Neutrophils are the most dominant leukocytes in zebrafish larvae from 2 dpf (Ellett *et al.*, 2011) identified by their expression of Mpx (Bennett *et al.*, 2001). Tissue damage leads to activation of dual oxidase, which results in H_2O_2 production (Niethammer *et al.*, 2009). This H_2O_2 gradient contributes to the recruitment of neutrophils to the site of injury (Niethammer *et al.*, 2009). Although in amniotes, neutrophils play a key phagocytic role during inflammation, there is a lack of clarity around their role in zebrafish, suggesting that macrophages are the major phagocytes. When bacteria are present in fluid environments (such as blood) they are exclusively phagocytosed by macrophages, whereas neutrophils contributed to the phagocytosis of bacteria presented on cell surfaces (Colucci-Guyon *et al.*, 2011). As with amniote tissue repair, a failure to resolve the pro-inflammatory environment is a key player in many inflammatory diseases. To abrogate the effects of neutrophilic damage during tissue repair, neutrophils exit the damaged area (Mathias *et al.*, 2006). Neutrophils can undergo a process of active (non-random) retrogradation, a 'backward' motion away from the site of inflammation during the resolution phase (Mathias *et al.*, 2006). One pathway important for the backward migration of neutrophils is the hypoxia induced factor (HIF) signalling pathway activated by the oxidative environment (Elks *et al.*, 2011). When zebrafish are treated with DMOG to inhibit the HIF signalling pathway, neutrophils display aberrant migratory behaviours and apoptosis leading to a prolonged inflammatory response (Elks *et al.*, 2011). Our knowledge of this process is being enhanced by the generation of photorecoverable fluorescent lines (Yoo *et al.*, 2010). Live-imaging data has highlighted PI3K activity at the leading edge of neutrophils during migration, regulating F-actin on RAC-induced membrane protrusions (Yoo *et al.*, 2010).

1.9.3 Zebrafish macrophage response to injury

Macrophages have been investigated using two macrophage-specific lines, Mpeg1:Gal4 (Ellett *et al.*, 2011) and Fms:Gal4 (Gray *et al.*, 2011). Mfap4 has been identified as a specific macrophage-marker, overlapping with Mpeg1:Gal4 reporter line by immunofluorescence (Walton *et al.*, 2015). The role of the pro- *versus* anti-inflammatory macrophages are being further dissected using a zebrafish reporter

line for TNF-α activity (Nguyen-Chi *et al.*, 2015, 2017). Currently, there is no way to distinguish between tissue macrophages and blood monocytes within larval zebrafish due to a lack of cell specific marks. However, the role of macrophages during larval tissue repair has been described during caudal fin regeneration (reviewed below).

Caudal fin amputation

Caudal fin regeneration relies on epimorphic regeneration. This type of repair forms a blastema, containing a mass of undifferentiated multi-potent stem cells. The multi-potent stem cells are able to differentiate into multiple tissue lineages for regeneration. Chemical (lipochlodronate) or pharmacogenetic (nitroreductase) ablation of macrophages has highlighted the key role of macrophages during caudal fin epimorphic regeneration at various time points following amputation, mediated through the production of paracrine factors (such as TNF-α ; Nguyen-Chi *et al.*, 2017). Following amputation, specific ablation of pro-inflammatory macrophages inhibits blastema cells proliferation. Additionally, ablation of 'non-inflammatory' (not pro-inflammatory) macrophages alters mesenchymal cell behaviour, perturbing regeneration (Nguyen-Chi *et al.*, 2017). Moreover, a pro-inflammatory response has been shown to enhance blastema cell expansion following tail-fin wounding (Miskolci *et al.*, 2019). Following caudal fin amputation, macrophages are initially pro-inflammatory observed at the site of injury 6 hours post amputation (hpa), expressing *tnfα*, *il-6* and *il-1β* transcripts, (Nguyen-Chi *et al.*, 2015). Macrophages sequentially switch to a non-inflammatory phenotype, accumulating from 24 hpa, expressing *tgfβ*, *ccr2* and *cxcr4b*, (Nguyen-Chi *et al.*, 2015).

In vivo live imaging has enhanced our understanding of macrophage migration and activity following zebrafish caudal fin amputation (Morales and Allende, 2019). Photoconvertible transgenic zebrafish lines (*mpeg1*:*dendra2*) have shown that peripheral macrophages are more readily recruited to injury followed by CHT-derived macrophages, responding to signals such as ROS production (Morales and Allende, 2019). Moreover, *Panther* (csf1ra−/−) larvae with fewer peripheral macrophages, exhibit reduced blastema cell proliferation 6-24 hpa, increased cell death, increased *il1β* expression 6 hpa, and reduced *tgfβ1α* expression 24 hpi at the site of injury

(Morales and Allende, 2019). Upon entry into the inflamed tissue, macrophages will phagocytose cell debris and apoptotic neutrophils (Ellett *et al.*, 2011). The process of cytoplasmic tethering and engulfment (phagocytosis) by macrophages was first shown in cancer using HRAS-G12V transformed cells by *in vivo* live imaging (Feng *et al.*, 2010). Moreover, the migration of macrophages towards HRAS-G12V cells is dependent on locally produced H_2O_2 (Feng *et al.*, 2010).

Following caudal fin amputation, proliferation and survival of blastemal cells are directly regulated by trophic factors produced by recruited immune cells. The *cloche* (*clo*) zebrafish mutant line has lost the hematopoietic compartment (Stainier *et al.*, 1995). Both *clo* mutants and larvae treated with *pu.*1 MO display increased blastemal cell susceptibility to apoptosis (Hasegawa *et al.*, 2015). The role of macrophages in the establishment of blastema has been further dissected, showing that, macrophage-derived TNF-α is important for proliferation of blastemal cells, as well as successful growth and regeneration of injured tissue (Nguyen-Chi *et al.*, 2017).

Summary

Taken together, studies investigating zebrafish immune cell development have shown that haematopoiesis occurs within two distinct waves. Primitive haematopoiesis occurs until 36 hpf, whereas definitive haematopoiesis occurs from 36 hpf. Zebrafish have competent phagocytes as early as 24 hpi. Studies investigating the immune response following caudal fin amputation have revealed that neutrophils followed by pro-inflammatory macrophages migrate to the site of injury. Subsequently, pro-inflammatory macrophages switch to an anti-inflammatory subtype, and neutrophils migrate away from the site of injury. Finally, the proliferation of blastemal cells has been associated with the duration of the pro-inflammatory response. Injury methods which induce a longer pro-inflammatory response leads to an increased blastemal cell proliferation.

1.10 The importance of macrophages during muscle repair

One common feature conserved between amniotes and teleost immune response towards tissue damage is the dynamic activation and plasticity of macrophages. The direct role of macrophages during muscle repair has been predominantly shown

through *in vitro* co-culture experiments, *in vivo* macrophage ablation, and phenotypic manipulations (reviewed below).

As previously mentioned, during the second wave of muscle injury-induced inflammation, $CD68^{high}CD163^{-}$ phagocytic pro-inflammatory macrophages are sequentially replaced by $CD68^{low}CD163^{+}$ anti-inflammatory macrophages (Arnold *et al.*, 2007; Villalta, Rinaldi, *et al.*, 2011; Deng *et al.*, 2012). This switch is mediated by IL-10 expression and mirrors the suppression activation of terminal differentiation associated genes in muscle cells (Villalta, Rinaldi, *et al.*, 2011; Deng *et al.*, 2012).

Pro- *versus* anti-inflammatory macrophages

Using *in vitro* culture systems, it has been demonstrated that macrophage conditioned medium promotes myoblast proliferation and differentiation (Cantini *et al.*, 1994, 2002). Moreover, *in vivo* following injury, rats injected with macrophage conditioned media display increased number and size of regenerating myofibers (Cantini *et al.*, 2002). It is now understood that pro-inflammatory macrophages promote proliferation whilst preventing differentiation of myoblasts, whereas anti-inflammatory macrophages promote differentiation and fusion into myotubes (Arnold *et al.*, 2007; Saclier, Cuvellier, *et al.*, 2013). Moreover, although MPC motility is unaffected by pro-inflammatory macrophage conditioned media, migration is reduced in the presence of anti-inflammatory macrophage conditioned media (Saclier, Cuvellier, *et al.*, 2013). The importance of macrophage phenotype has also been shown *in vivo* (Saclier, Cuvellier, *et al.*, 2013). It was shown for the first time that pro-inflammatory macrophages are proximal to proliferating muSCs, whereas anti-inflammatory macrophages were observed within the regenerating area, associated with differentiating myoblasts (Saclier, Cuvellier, *et al.*, 2013).

Anti-inflammatory macrophages

In vivo studies further dissected the roles of pro- and anti-inflammatory macrophages during muscle repair, largely through macrophage ablation models (Arnold *et al.*, 2007; Deng *et al.*, 2012; Mounier *et al.*, 2013; Akahori *et al.*, 2015). Following injury and intraperitoneal injections of anti-F4/80 (which bind to macrophage cell surface antigens, neutralising them), mice display normal numbers of macrophage by 2 dpi,

and reduced number by 4 dpi, therefore depleting macrophages during the pro- to anti-inflammatory switch (Tidball and Wehling-Henricks, 2007). Although anti-F4/80 treated mice display increased Pax7+ cells (1 dpi) and Myod+ cells (4 dpi), they display fewer newly regenerating centrally-nucleated myofibers (Tidball and Wehling-Henricks, 2007). This phenotype has been further characterised following tamoxifen induced depletion of CD11b+F4/80+ intramuscular macrophages during later stage of regeneration (5 dpi), highlighting a disruption in muscle regeneration (Arnold *et al.*, 2007). This result is supported by myeloid cell-specific AMPKα-/- and global IL-10-/- mouse knock-out models (Deng *et al.*, 2012; Mounier *et al.*, 2013). Myeloid cell-specific AMPKα-/- mice do not generate anti-inflammatory macrophages following CTX-induced injury, failing to repair muscle, leading to increased necrosis and reduced myofiber cross-section area (Mounier *et al.*, 2013). This phenotype can be rescued following transplantation of WT bone marrow-derived macrophages, revealing that these phenotypes are a direct result of perturbed macrophage function (Mounier *et al.*, 2013). IL-10-/- knock-out mutant mice express high levels of pro-inflammatory cytokines (IL-6 and CCL2) and reduced anti-inflammatory (CD163+, IL-10R1+, and Arg-1+) macrophage infiltrate (Deng *et al.*, 2012). Following re-loading-induced injury, IL-10-/- mice exhibited increased lesions, reduced centrally-nucleated myofibers and cross-section area (Deng *et al.*, 2012). Exogenous IL-10 treatment early in regeneration results in a supressed proliferative response by muSCs, reducing myofiber size 7 dpi following CTX-induced injury (Perdiguero *et al.*, 2011). Although IL-10 does not directly regulate myoblasts, it promotes the anti-inflammatory macrophage phenotype which favours myoblast differentiation (Deng *et al.*, 2012). Together, these studies suggest that anti-inflammatory macrophages improve muscle repair following injury. In contrast, investigations in CD136-/- knock-out mice show that anti-inflammatory macrophages limit ischemia-induced muscle repair (Akahori *et al.*, 2015). Following injury, CD136-/- mice display more proliferating PAX7+ muSCs (14 dpi), increased early MYOGENIN (14 dpi) and late MYHC (28 dpi) expression, and enhanced myofiber and capillary formation (Akahori *et al.*, 2015). The discrepancy, following CD163 mutation, may be due to the time frame muscle regeneration was investigated. During the earlier phases of muscle repair, the same study shows that CD163-/- mice display smaller myofiber area 14

dpi but not 28 dpi (Akahori *et al.*, 2015), similar to IL-10 (4 dpi; Deng *et al.*, 2012), CD11b+F4/80+ (10 dpi; Arnold *et al.*, 2007), and AMPKα (14 dpi; Mounier *et al.*, 2013) mutants. These data further highlight the importance of a temporal anti-inflammatory macrophage response during regenerative myogenesis.

Pro-inflammatory macrophages

Although anti-inflammatory macrophages are typically associated with tissue repair and growth, pro-inflammatory macrophages have been shown to be crucial for muscle repair (Arnold *et al.*, 2007). Depletion of the initial pro-inflammatory CD11b+ blood macrophage populations prevents muscle regeneration (Arnold *et al.*, 2007). Other studies have been conducted in mice deficient in CCR2 expression, essential for Ly6C^{high} monocyte recruitment to damaged muscle (Warren *et al.*, 2005; Contreras-Shannon *et al.*, 2007; Sun *et al.*, 2009; Martinez *et al.*, 2010). These mice display reduced monocyte infiltration, leading to impaired muscle regeneration (Warren *et al.*, 2005; Contreras-Shannon *et al.*, 2007; Sun *et al.*, 2009; Martinez *et al.*, 2010). In addition to a direct interaction between macrophages and muSC, this inability to repair muscle may also be attributed to insufficient clearance of necrotic tissue (Contreras-Shannon *et al.*, 2007; Martinez *et al.*, 2010) and prolonged pro-inflammatory neutrophilic response (Warren *et al.*, 2005; Contreras-Shannon *et al.*, 2007; Martinez *et al.*, 2010). Macrophage phagocytosis during muscle repair (reviewed by Tidball, 2017) results in the switch of macrophages to an anti-inflammatory phenotype, supressing TNF-α and inducing TGF-β synthesis to promote myoblast differentiation (Lu, Huang, Saederup, *et al.*, 2011; Mounier *et al.*, 2013). Ccr2-/- mice treated with Apolipoprotein E, to restore the phagocytic function in macrophage, successfully repaired muscle (Arnold *et al.*, 2015). Additionally, radiation-induced depletion of Pax7-expressing muSCs in mice delayed macrophage phenotypic transition following CTX-induced injury, demonstrating a regulatory feed-back loop between macrophages and resident muSCs (Patsalos *et al.*, 2017).

1.10.1 Macrophages regulate muSC activity

Macrophages play a key direct role on the activity of muscle cells during regeneration (Ratnayake *et al.*, 2021). This supportive role is partly mediated by macrophage-derived cytokines and growth factors, such as IL-6 (Zhang *et al.*, 2013), IL-1β (Luo *et al.*, 2003; Saclier, Yacoub-Youssef, *et al.*, 2013), TNF-α (Warren *et al.*, 2002; Li, 2003; Chen *et al.*, 2005), IFN-γ (Cheng *et al.*, 2008; Villalta, Deng, *et al.*, 2011), TGF-β (Saclier, Yacoub-Youssef, *et al.*, 2013), VEGF (Saclier, Yacoub-Youssef, *et al.*, 2013), and oncostatin M (Latroche *et al.*, 2017). These macrophage-derived cytokines and growth factors directly modulate myoblasts proliferation, differentiation, migration, and fusion (Li, 2003; Luo *et al.*, 2003; Warren *et al.*, 2002; Chen *et al.*, 2005; Cheng *et al.*, 2008; Villalta, Deng, *et al.*, 2011; Saclier, Yacoub-Youssef, *et al.*, 2013; Zhang *et al.*, 2013; Latroche *et al.*, 2017). Although there are far fewer examples, macrophages can directly interact with muSCs to modulate their activity (Ratnayake *et al.*, 2021; Chazaud *et al.*, 2003). *In vitro,* macrophages interact with muscle in an adhesion molecule-dependent manner to limit MPC apoptosis (Chazaud *et al.*, 2003). Although, not in muscle regeneration, macrophages make 'long-distant' direct contacts with xanthoblasts (pigment cells) in zebrafish (Eom and Parichy, 2017). In this system, macrophages recognize surface blebs expressing DeltaC Notch ligand (Eom and Parichy, 2017). These blebs are extended and 'pulled' by macrophages (Eom and Parichy, 2017). Moreover, in murine neo-angiogenesis, macrophages physically interact with damaged vasculature, a process conserved in zebrafish (Gurevich *et al.*, 2018).

Within zebrafish muscle regeneration, *in vivo* live imaging demonstrated that 'dwelling' (rounded anti-inflammatory macrophages which perdure in damaged muscle) mpeg1+ macrophages make direct contact with pax3+ expressing muSCs around 11 hpi, promoting muSC proliferation (Ratnayake *et al.*, 2021). Macrophages may signal to muSCs via Notch signalling to modulate their activity. It has been shown that following femoral ligation, CD163-/- mice, devoid of anti-inflammatory macrophages, express more NICD and DLL-4 within injured muscle relative to WT controls during the early stages of regeneration (14 dpi; Akahori *et al.*, 2015). Treating CD163-/- mice with DAPT (inhibitor of Notch) worsened the repair of muscle, reducing the percentage of regenerative myotubes and capillarisation

(Akahori *et al.*, 2015). Moreover, pro-inflammatory macrophages (Ly6C^{high}CD11b+F4/80+) secrete A Disintegrin-Like And Metalloproteinase With Thrombospondin Type 1 Motif (ADAMTS1) by 1 dpi (Du *et al.*, 2017). ADAMTS1 inhibits Notch signalling (reduced *Hes-1* and *Hey-1* gene expression) in murine muSCs (Du *et al.*, 2017). Although, ADAMTS-/- knock-out mice appear to regenerate muscle better than WT controls, displaying increased muSC proliferation and commitment resulting in larger myofibers, their muSC pool depletes with age (Du *et al.*, 2017). These studies suggest that pro- and anti-inflammatory macrophages can regulate muSCs via Notch signalling.

Summary

Taken together, both pro- and anti-inflammatory macrophages have been demonstrated to control muSC activity. In mammals, pro-inflammatory macrophages promote the proliferation of muSCs, whereas anti-inflammatory macrophages promote differentiation and fusion. Macrophages modulate muSC activity through the release of trophic factors. Moreover, it has been shown recently in zebrafish that anti-inflammatory macrophages make direct contacts with muSCs to promote proliferation. Finally, both pro- and anti-inflammatory macrophages have been shown to supress Notch signalling in muSCs following injury in mice. It is not currently known if macrophages can control Notch signalling in muSCs within zebrafish following injury.

1.11 Outstanding questions and rational

Is Notch signalling important for the control of muSCs in zebrafish?

Notch signalling is important for the amplification and self-renewal of MPCs during mammalian embryonic myogenesis. Furthermore, it has been shown in mouse that Notch signalling is important to limit differentiation and promote proliferation of Pax7-expressing cells *in vitro*, key for successful muscle repair *in vivo*. Currently, it is unknown how Notch activity is regulated in muSCs following injury *in vivo*, and if these cells contribute to muscle repair. Moreover, there are no description on the importance of Notch signalling for the control of muSCs in zebrafish.

Do macrophages control the muSC response to injury and is this Notch dependent?

Macrophages have been shown to regulate muSC behaviour via both trophic factors, and to a lesser extent, direct cell contact. *In vitro* and *in vivo* mouse studies have demonstrated that pro-inflammatory macrophages promote MPC proliferation, whereas anti-inflammatory macrophages promote MPC differentiation and fusion. Anti-inflammatory macrophages have also been shown to make direct contacts with pax3-expressing muSCs in zebrafish, promoting proliferation. Moreover, it has been shown in mouse that both pro- and anti-inflammatory macrophages limit Notch activity in muSCs following injury. Currently, it is unknown how the inflammatory microenvironment controls the response of muSCs to injury, and if macrophages can control muSCs which show Notch activity.

Rational for using the zebrafish

Humans are able to repair damaged muscle, but the entire process takes approximately 4 weeks, associated with fibrosis and reduced muscle functionality (reviewed by Laumonier and Menetrey, 2016). In spite of the vast research conducted using *in vitro*, *ex vivo*, and *in vivo* mammalian models, our understanding of the processes which govern muscle repair are lacking. Our understanding is largely limited by experiments which are conducted in mice that require sacrifice and examination of tissue post-mortem, or work carried out *ex vivo* following niche disruption (Reviewed by Relaix *et al.,* 2021). This means that studies carried out on mice are unable to characterise the process of muscle repair in live animals, often

losing spatial-temporal information (Reviewed by Relaix *et al.,* 2021). Contrastingly, zebrafish larvae have a remarkable ability to repair damaged tissue, completed within 3 days (Gurevich *et al.*, 2016). Moreover, zebrafish embryos are easily genetically modified and are transparent at larval stages (Ellett *et al.*, 2011; Gray *et al.*, 2011; Walton *et al.*, 2015; reviewed by Chen and Zon, 2009; Renshaw and Trede, 2012). Together, this makes the zebrafish a powerful tool to understand the entire process of muscle regeneration, visualising cells in live animals and conducting high throughput screens to understand the importance of different molecular pathways (reviewed by Chen and Zon, 2009; Renshaw and Trede, 2012). Therefore, in addition to providing a platform to further our knowledge on the mechanisms governing muscle regeneration in zebrafish and how this differs from mammals, this project aims to partially-replace and reduce the number of animals used to study muSC behaviour.

Together, this project will help us understand how zebrafish larvae efficiently repair muscle, allowing future work to develop targeted therapies to promote regeneration and circumvent muscle wasting associated with muscular dystrophy and aging.

1.12 Hypotheses

I hypothesise that

- Notch signalling is important for limiting muSC differentiation and promoting proliferation in zebrafish following injury.
- Macrophages control muSCs through regulating Notch activity.

1.13 Aims

1. Determine whether Notch signalling is important for limiting differentiation and promoting proliferation of muSCs in zebrafish following injury.
2. Determine the spatiotemporal activity of Notch in muscle during regeneration.
3. Test the importance of macrophages for the control of muSC function during muscle repair in zebrafish.

Chapter 2 Materials and methods

2.1 Methods

2.1.1 Fish lines maintenance

Adult zebrafish were maintained as previously described (Snider and Clegg, 1975; Westerfield, 2007), using in according to the Home office regulations. Collected embryos were raised in E3 medium (Table. 2.14) at 28.5 °C. 24 hours post fertilisation (hpf), larvae were transferred to E3 containing N-Phenylthiourea (E3 PTU; Table. 2.14) and raised at 28.5 °C to inhibit melanophore formation (Karlsson *et al.*, 2001). E3 PTU medium was replaced every two days to limit pigment formation at older stages (>5 dpf). Fish lines used have been described in Table 2.6.

2.1.2 Genotyping

Fin clips from adult zebrafish or dissected heads from larvae were incubated in an alkaline lysis buffer (Table. 2.14) for 2 hours at 90 °C in order to extract the DNA. Subsequently, the lysis was neutralised (Table 2.14) and the obtained DNA stored at -20 °C.

Polymerase chain reaction

Taq-polymerase (NEB) polymerase chain reaction (PCR) was used to genotype adult fish and larvae, conducted according to the standard protocol of the manufacturer (25 µl total volume). Primers used (Table. 2.7) and program run on Thermo Fisher thermocycler (Table. 2.1) have been listed.

Step	Temperature (°C)	Time (s)	Number of cycle
Hot start	94	120	1
Denaturation	94	20	35
Annealing	64	20	
Elongation	72	30	
Extension	72	420	1
Incubation	4	Hold	1

Table 2.1. PCR program

The PCR product was loaded mixed with 6x loading dye (1:6; NEB) allowing its precipitation into the well of a 1 % agarose gel containing gel red (1:10,000; Sigma), to visualise the PCR product after migration at 100 volts for 30 min. Product sizes (Table. 2.7) were estimated against a DNA ladder (1 kilobase or 100 base pair; NEB).

Tnfrsf1a KASP

KASP genotyping was conducted according to the protocol of the manufacturer (10 µl total volume; LGC) using 45 ng DNA. Primers were designed by LGC to detect *tnfrsf1a*^{Sa8496}. Known genotyped samples were used as a reference to ensure the auto-calling allelic discrimination on the BioRad CFX software was sufficient. If the segregation of genotypes were not resolved using the initial KASP program (Table. 2.2), the KASP assay was recycled for a further three cycles and re-assessed (Table. 2.3). The recycling protocol was repeated up to three times when appropriate.

Step	Temperature (°C)	Time (s)	Number of cycle
Activation	94	900	1
Denaturation	94	20	10
Annealing/ elongation	61-55 (-0.6 per cycle)	60	
Denature	94	20	
Annealing/ elongation	55	60	26
Read	37	60	1

Table 2.2. KASP genotyping program

Step	Temperature (°C)	Time (s)	Number of cycle
Denaturation	94	20	3
Annealing/ elongation	57	60	
Read	37	60	1

Table 2.3. KASP recycling program

2.1.3 Mechanical injury

Needle preparation

Tungsten wire was sharpened by electrolysis in a 5M potassium hydroxide solution. The tungsten wire was repetitively placed into the solution at a 45-degree angle to create a sharp edge, and the needle sharpness was assessed using a compound microscope.

3-7 dpf Larvae injury

Larvae were anesthetised in 0.004% Tricaine methanesulfonate (Tricaine; Sigma; Table. 2.14) in E3 PTU media and immobilised in 1.5 % low melting agarose (Sigma). Using a sharpened tungsten wire in a needle holder (small single myotome needlestick injury; Fig. 2.1A, A') or a 30g needle (large multiple myotome needlestab injury; Fig.2.1B, B') fixed to a micromanipulator, larvae were pierced at the 13th left ventral myotome. Injured larvae were then removed from agarose and incubated in multi-well dishes containing fresh E3 PTU media, allowing the effects of Tricaine to subside. A maximum of 10 larvae were incubated per well to reduce the occurrence of infection.

30 dpf larvae injury

Larvae were placed into a tank containing 0.013% Tricaine in system water. Once unresponsive, larvae were moved to a Petri dish which contained a damp paper towel soaked in 0.013% Tricaine. Using a 30g needle attached to a micromanipulator, larvae were injured on the left dorsal side above the pigment line and below the dorsal fin. Injuries were conducted horizontally to minimise bleeding.

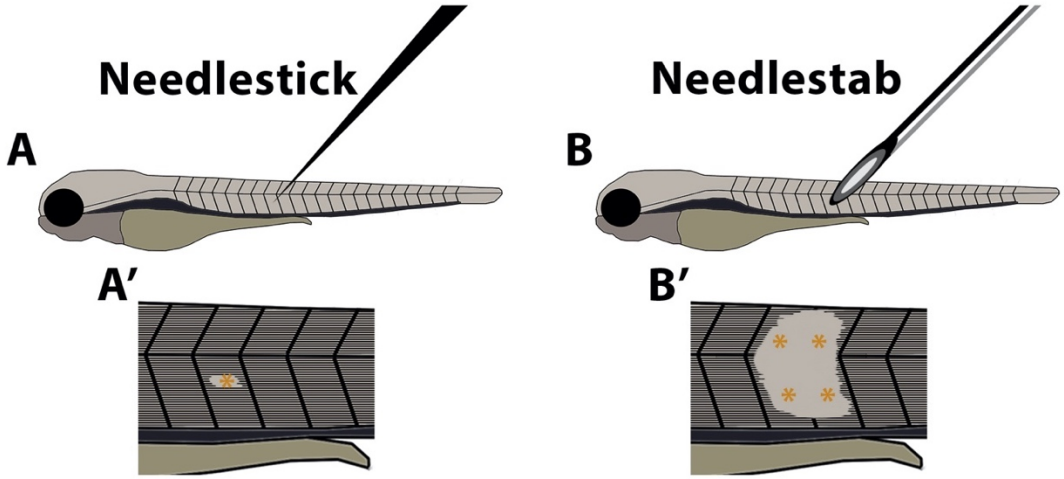

Figure 2.1. Schematic of injury techniques.
Zebrafish larvae were injured with the (**A**) needlestick or (**B**) needlestab method. Needle-stick injury was carried out using a sharpened tungsten wire to damage few myofibers (**A'**). Needle-stab injury was conducted using a 30g needle which damages multiple myotomes and surrounding vertical and horizontal myosepta (**B'**). Asterisk marks the damaged myotome(s).

2.1.3 Chemical treatments

Evans Blue

Evans Blue (Sigma; Table 2.13) staining was used to detect damaged muscle. Evans blue staining was performed by submerging larvae in 0.1 % volume per volume (v/v) Evans blue diluted in E3 PTU for 1 hour in the dark at room temperature then washed in E3, as previously described (Eliceiri *et al.*, 2011; Smith *et al.*, 2015). Larvae were then injured using the needlestick method, as previously described, and imaged 1 hpi to allow sufficient staining in the muscle.

DAPT

Notch signalling was inhibited using DAPT (Sigma; Table. 2.13; Dyer *et al.*, 2014). DAPT was reconstituted to a stock solution of 40 mM in 100 % Dimethyl sulfoxide (DMSO; Sigma), aliquoted and stored at -20 °C. The stock solution was then serially diluted to 10 mM in DMSO and then to 100 µM working concentration in E3 PTU. Larvae were treated at 25.8 °C in the absence of light, and the DAPT solution was refreshed every 24 hours.

Metronidazole

Macrophage ablation was achieved by treating Tg[*fms:Gal4;UAS:NfsB-mCherry*] larvae with 5 mM metronidazole (MTZ; Sigma; Table. 2.13; Gray *et al.*, 2011). Larvae were treated with 5 mM MTZ in E3 PTU medium 24 hours prior to injury. Following injury, larvae were placed into fresh 5 mM MTZ for the duration of the experiment. Larvae were treated at 25.8 °C in the absence of light, and the MTZ solution was refreshed every 12-14 hours. Fresh 5 mM MTZ was prepared for each 12-14 hour time window.

Dexamethasone

Dexamethasone (DEX; Sigma; Table. 2.13) is a steroid used to supress inflammatory processes (described by Hasegawa *et al.*, 2017). DEX was reconstituted to a stock solution of 100 mM in 100 % DMSO, aliquoted and stored at -20 °C. The stock solution was then diluted to 0.5 mM working concentration in E3 PTU medium. Larvae were treated 1 hour prior to injury and for the duration of the experiment. Larvae were treated at 25.8 °C in the absence of light, and the DEX was refreshed every 12-14 hours.

Bromodeoxyuridine

The Bromodeoxyuridine (BrdU; Sigma; Table. 2.13) incorporation assay was used to assess proliferation. BrdU was reconstituted to 1 M in 100 % DMSO and stored at -20 °C. Following injury, larvae were treated with 10 mM BrdU in E3 PTU medium for the duration of the experiment. Larvae were treated at 25.8 °C in the absence of light.

2.1.4 RT-PCR

TRIzol RNA extraction

In order to extract the RNA, tissue was suspended in 500 µm Tri-reagent (Sigma) and stored at -80 °C overnight. Samples were homogenised using sterile pestles or a series of needles (25g, 27g and 30g). A further 500 µm Tri-reagent was added and the sample was left at room temperature for 7 min. Following a 10 min spin at 11,000 rpm at 4 °C and the addition of 200 µl chloroform, homogenised samples were shaken vigorously for 15 sec and allowed to stand for 7 min. Samples were centrifuged once again for 10 min at 11,000 rpm at 4 °C and the addition of 500 µl 2-Propanol (Sigma) allowed for phase separation. As before, samples were shaken vigorously for 15 sec and allowed to stand for 7 min. Samples were then centrifuged for 15 min at 11,000 rpm 4 °C revealing the three phases. The aqueous phase (nucleic acid) was transferred to a new tube and 1 ml 70% ethanol (Thermo Fisher) was added. Following a 5 min spin at 7,000 rpm 4 °C the ethanol was removed. Finally, the pellet was set to air dry at room temperature and resuspended in 30 µl nuclease-

free water. The Ribonucleic acid (RNA) extracted was stored at -80 °C ready for complementary DNA (cDNA) synthesis.

cDNA synthesis

RNA concentration and purity was determined using Thermo Fisher nanodrop system. 500 ng RNA was used per cDNA synthesis reaction. RNA was primed using random primers (PROMEGA; Table. 2.8), heated to 70 °C for 5 min, followed by 5 min at 4 °C.

cDNA was synthesised using PROMEGA cDNA synthesis kit (Table. 2.9). Thermo Fisher thermocycler was used with the program listed in Table. 2.4.

Step	Temperature (°C)	Time (min)
Priming	25	10
Reverse transcription	45	60
Reverse transcription inactivation	95	3

Table 2.4. Thermocycler program used for cDNA synthesis

RT-PCR

To assess primer efficiency, 10 µl of synthesised 500 ng cDNA was taken from all samples tested to create a stock of neat cDNA. cDNA was then serially diluted 1:5 in RNase-free water to generate a 1, 1:5, 1:25, 1:125, 0 (non-template control) dilution series. Remaining experimental cDNA was diluted 1:2 in RNase-free water to minimize the effects amplification inhibitors. 10 µl reactions were prepared in 384 well PCR plates (Applied biosystems) using 4 ng cDNA as shown in Table. 2.10, using the primer sets in Table 2.11.

Gene expression was analysed using 2X SYBR Green (Applied Biosystems) on a ViiA-7 Real-Time PCR system (Applied Biosystems). 40 cycles were run, and the threshold cycles (Ct) to measure the expression of each gene (Table. 2.5). Concentration curves were assessed on the BioRad CFX software to calculate the primer efficiency. Primer efficiency was determined by the number of melt curves (greater than one indicates non-specific amplification). ΔCt values were calculated by normalising experimental Ct values against the Ct value of the housekeeping gene *elf1a*.

The ΔΔCt and fold changes were subsequently calculated:

$$\Delta\Delta Ct = \text{Experimental } \Delta Ct - \text{Control } \Delta Ct$$

$$\text{Fold change} = Primer\ efficiency^{-\Delta\Delta Ct}$$

Step	Temperature (°C)	Time (s)	Number of cycles
Hot start	95	600	1
Denaturation	95	30	40
Annealing	60	60	
Elongation	72	30	
Incubation	4	Hold	1

Table 2.5. qPCR program

2.1.5 Whole-mount immunolabelling

2.1.5.1 GFP, mCherry, dsRed, cNICD, Phalloidin, and BrdU

Larvae were culled by an overdose of 0.4 % Tricaine and fixed in 4 % paraformaldehyde (PFA; Table. 2.14) overnight at 4 °C or 2 hours at room temperature. Subsequently, larvae were washed four times in 0.1 % PBT (PBS: Thermo Fisher, Tween-20: Sigma; Table. 2.14) for 5 min each, followed by a methanol series (Thermo Fisher; Table. 2.14). Each methanol step was left for no less than 5 min and stored at -20 °C in 100 % methanol indefinitely.

GFP, mCherry, dsRed, cNICD, and Phalloidin

Fixed larvae were processed by a reverse methanol series, and permeabilized using 10 µg/ml proteinase K (3 dpf for 30 min, 5 dpf for 50 min and 7 dpf for 70 min; Sigma). The proteinase K was rinsed away with 0.1 % PBT. The samples were then blocked in 10 % new-born calf serum (NBCS; Thermo Fisher) for 1 hour at room temperature and incubated with primary antibody for 1-3 nights at 4 °C (Table. 2.12, 10 % NBCS). Samples were then washed in 0.1 % PBT (4 x 30 min), re-blocked in 10 % NBCS for 1 hour at room temperature and incubated with secondary antibody or phalloidin overnight at 4 °C (Table. 2.12, 10 % NBCS) in the dark. Subsequently, samples were washed in 0.1 % PBT (4 x 30 min) and post-fixed in 4 % PFA for 30 min at room temperature. Finally, the PFA was rinsed away, and the samples were processed through a glycerol series (Sigma; Table. 2.14).

BrdU

Fixed samples were processed through a reverse methanol series and washes in 1 % PBTx (3 x 5min; Triton X-100: BDH; Table. 2.14). Tissue was permeabilised with 10 µg/ml Proteinase K for 2 hours at room temperature, followed by a post-fixation in 4 % PFA for 20 min at room temperature. PFA was removed from the samples followed by 1 % PBTx washes (4 x 5 min), and then treated with 2 M Hydrochloric acid (HCl; Sigma) for 1 hour at room temperature, which was subsequently neutralised in 0.1 M borate buffer (Table. 2.14). Samples were subsequently washed in 1 % PBTx 1 % DMSO (3 x 5 min) and blocked in 5 % goat serum (Abcam) for 1 hour a room temperature. The samples were then incubated with primary antibody (Table. 2.12) in 2 % goat serum overnight at 4 °C. The following day samples were washed in 1 % PBTx 1 % DMSO (8 x 5 min), followed by a post fixation in 4 % PFA for 30 min at room temperature. The samples were then incubated with secondary antibody (Table. 2.12) in 2 % goat serum overnight at 4 °C in the dark. Samples were washed in 1 % PBTx 1 % DMSO (5 x 15 min), followed by a post fixation in 4 % PFA for 30 min at room temperature. Finally, samples were processed through a glycerol series.

2.1.5.2 Pax7 and Myogenin

Pre-absorption

Prior to immunolabeling the Myogenin primary antibody (1:10; Santa Cruz Biotechnology; Table. 2.12) was pre-absorbed as follows: stage matched fixed wildtype larvae (n = 10) were processed through a reverse methanol series and washed in 1 % PBT (3 x 5 min; Table. 2.14). The volume was adjusted to 40 µl in 1x PBS, and the larvae homogenised using sterile pestles or a series of needles (25g, 27g and 30g) before adding the Myogenin primary antibody (1:5). The sample was incubated with the antibody on a shaker at 4 °C for at least 2 days. Following incubation, larvae were spun down, the supernatant collected in a fresh tube, and the pellet re-suspended in 50 µl 1X PBS. The cellular debris were then spun down, and the supernatant collected. Final concentration of the Myogenin primary antibody was adjusted to 1:10.

Immunolabeling

Larvae were fixed in fresh 2 % PFA (Table. 2.14) for 30-45 min followed by 3 x 5 min 1% PBTx washes. Samples were then blocked in 5 % goat serum 1 h at room temperature. Primary antibody (Table 2.12) in 1 % PBTx 1 % DMSO supplemented with 2 % goat serum was incubated with the samples overnight at 4 °C (myogenin antibody; Table. 2.12) or 2 nights at room temperature on a rotary shaker (Pax7 antibody; Table. 2.12). Samples were washed in 1 % PBT x (4 x 20 min), and secondary antibody was added to 1 % PBTx 1 % DMSO supplemented with 5 % goat serum and this solution was incubated overnight at 4 °C in the dark with the samples. Excess secondary antibody was washed away in 1 % PBTx (4 x 20 min), and the samples put through a glycerol series.

2.1.5.3 L-plastin and MPX

Larvae were fixed in 4 % PFA in 0.4 % PBTx overnight at 4 °C or 2 hours at room temperature. Fixed larvae were washed in 0.1 % PBTx (4 x 5 min), blocked in 5 % goat serum for 2 hours at room temperature and incubated with primary antibody (Table 2.12) overnight at 4 °C. The following day, the samples were washed extensively in 0.1 % PBT (10 x 30 min) and then incubated with secondary antibody (Table 2.12) in 2 % goat serum overnight at 4 °C. Finally, the samples were washed in 0.1 % PBT (10 x 20 min) and processed through a glycerol series.

2.1.5 Imaging

Fixed sample imaging

Larvae were placed on a slide (Plain, 1.0-1.2 mm thick, 76 x 26 mm, Interleaved; Dixon Science), orientated to expose the 13th left ventral myotome and submerged in mounting solution (containing DAPI or Hoechst; Table 2.12). A Coverslip (20 X 20 mm thickness, No. 0; VWR International) was secured over the larvae using plasticine, ensuring the sample was not compressed. Larvae processed by immunolabelling were scanned on an inverted Leica SP5 microscope using a x20 air objective (NA = 0.7). Z-stacks (0.99 µm) were captured at a resolution of 512 x 512 (quantification or representative images) or 1080 x 1080 (representative images) pixels and each

channel was averaged 3-4 times. To limit the movement of sample in the mounting solution, the slide was inverted and stored at -20 °C in the dark for at least one night. All imaging were conducted within 3-weeks of immunostaining to avoid photobleaching.

Live imaging

For live imaging, larvae were anesthetised in 0.004 % w/v Tricaine and immobilised in 1.5% w/v low melt agarose in E3 PTU on a glass bottomed dish with size 0 glass (IBL). Larvae were pushed to the bottom to minimise movement of the larvae during imaging and injured using a sharpened tungsten wire, as previously described. Time-lapsed images were acquired on a 7MP multiphoton microscope (*Zeiss*) using a x20 water dipping objective (W Plan-Apochromat 20x/1.0 DIC VIS-IR M27 75mm). Z-stacks encompassing the total myotome (with 1 µm Z-slices) were captured every 5-15 minutes from 0.5-1 hour post injury (hpi).

Imaging 30 dpf larvae

A hole was created on opposite sides of a 60 mm dish to allow insertion of tubing (Masterflex peroxide-cured silicone tubing; Fig. 2.2A-B). With the tubing inserted, Polydimethylsiloxane (PDMS; Sylgard) and curing agent were mixed in a ratio of 10:1 and placed in the Petri dish. The Petri dish was incubated within a desiccator for 2 hours to remove bubbles before heating to 60 °C for 1 hour to facilitate the cross-linking. Once the PDMS has set, space for the tubing and imaging area were carved out with a scalpel. Some PDMS was left near the entrance of the tubing to ensure the chamber was waterproof. To image, larvae were anesthetised in 0.008% Tricaine and placed into the imaging chamber (Fig. 2.2B). The trunk and tail of the larvae were mounted in 2 % low melting agarose, ensuring the head and gills were free. The chamber was filled with E3 containing 0.008% Tricaine, and the tubing was attached to a peristaltic pump allowing water to pass over the gills (Fig. 2.2C). Images were acquired on a 7MP multiphoton microscope using a x20 water dipping objective (Fig. 2.2C).

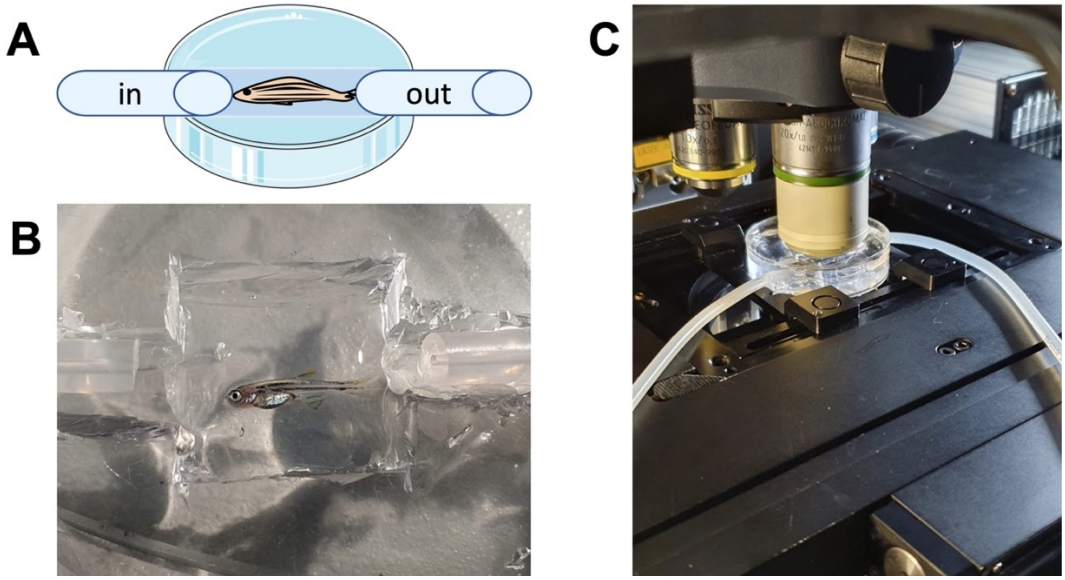

Figure 2.2. 30 dpf larvae imaging setup.
Schematic diagram (A) and photograph (B) showing 30 dpf larvae mounted in a 60 mm Petri dish within a PDMS chamber. Larvae were mounted in 2 % low melting agarose, ensuring the head and gills were free (B). Water passes over the gills of zebrafish which is mobilised through tubing connected to a peristaltic pump (A-B). Dish was mounted onto a 7MP multiphoton microscope using a x20 water dipping objective (C).

2.1.6 Image processing

Cell quantification

Images were processed using Fiji (Schindelin *et al.*, 2012) and all quantifications were conducted on the raw datasets. Cells were quantified within the myotome, injured region and myosepta (vertical and horizontal myosepta; Fig. 2.3). Images from time-lapsed movies were corrected for drift using the 'Correct 3D Drift' function (Parslow *et al.*, 2014).

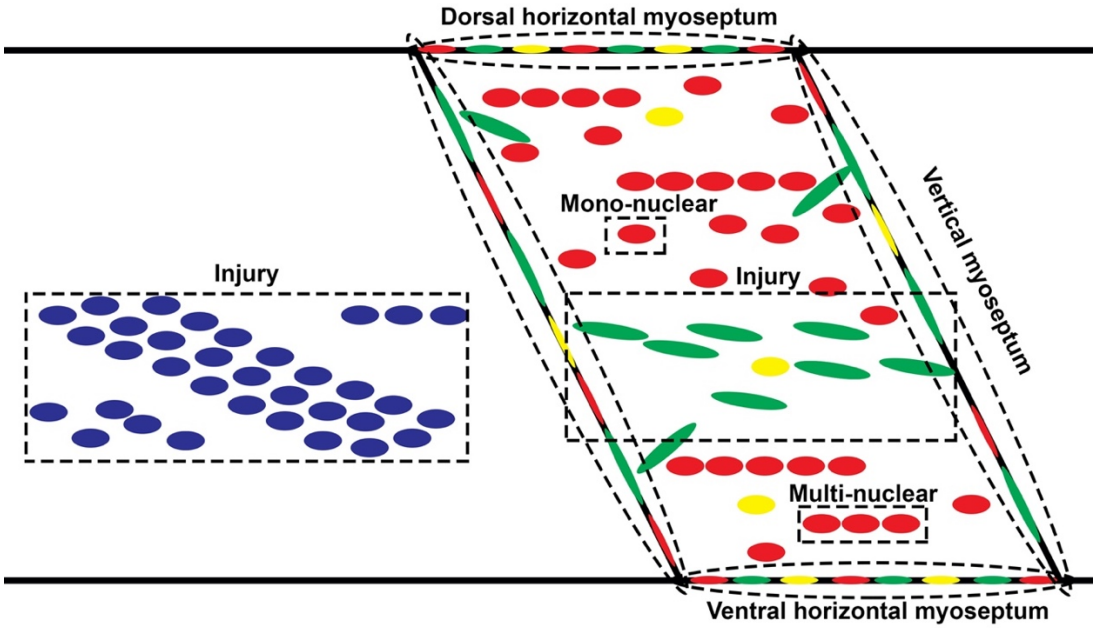

Figure 2.3. Schematic showing multi-colour quantification.
Fluorescent cells were quantified within uninjured and injured myotomes following injury. Cells were quantified in four discrete anatomical positions and the injured area (five quantifications per larvae). Cells were quantified in the myotome, vertical myosepta (VM; bilaterally located relative to the myotome of interest), ventral horizontal myoseptum (VHM; ventrally located relative to the myotome of interest) and dorsal horizontal myoseptum (DHM; dorsally located relative to the myotome of interest, medially located relative to the whole fish). For fixed sample imaging, the injured region was defined by brightfield imaging and the clustering of DAPI or Hoechst-33342 expressing cells at the site of injury. Within these locations, single, double and triple positive mono-nuclear and multi-nuclear cells were quantified.

Representatives

Brightness and contrast were adjusted to identify cells and the 'remove outlier' function utilised to remove non-specific signals by selecting bright spots which have a radius of 2-4 pixels at a threshold of 10-50. For staining which have non-specific binding at the point of injury, the image calculator function with the AND command in Fiji was used to only represent fluorescence signal which co-localises with a nuclear stain.

Volumetric quantification

Volume of injured muscle labelled with Evans Blue was quantified using Fiji (Schindelin *et al.*, 2012). Brightness and contrast were adjusted to visualise the injured region and remove non-specific background signals. The threshold and measure function on Fiji were used to measure the area labelled by Evans Blue for each Z-slice. The area for each slice was then used to calculate a slice volume (this is equivalent to the area as each Z–interval = 1 μm) and the total volume of the injury calculated from their summed values. In order to calculate the volume of the entire myotome, a transmitted image of the myotome at the lateral and medial extent were acquired and their area calculated (V1, V2). Intermediate areas of the myotome at each Z level were extrapolated from V1 and V2 and used to generate a volumetric measure of the total myotome.

2.2 Statistics

2.2.1 The experimental design

To detect statistically significant differences between samples, pairwise two-tailed tests were performed with an assumption of two independent samples in which the null hypothesis (H_0) states there is no difference between the means ($\mu 0, \mu 1$) and the alternative hypothesis (H_1) assumes a difference between the means:

$$H_0: \mu_0 = \mu_1$$

$$H_1: \mu_0 \neq \mu_1$$

The population has a unique distribution defined by mean and the variance (Σ^2):

$$(\mu_0, \Sigma_0^2)$$

$$(\mu_1, \Sigma_1^2)$$

2.2.2 Assessing normality and scedasticity

Before conducting pairwise and power analysis, normality and scedasticity (equal variance) was assessed. Normality was assessed using the Shapiro–Wilk test function. If the result of the Shapiro–Wilk test was greater than 0.05 (p>0.05) then normality was assumed. A density histogram was produced to visualise and assess the data for normality and variance confirming the Shapiro–Wilk test results. For datasets with more than two variables, if the dataset was parametric, the Bartlett test was used to determine scedasticity, whereas if the dataset was non-parametric the Fligner-Killeen test was used. Datasets which only have two variables the R: var.test function was used. If the result for the Bartlett, Fligner-Killeen test or var.test test was greater than 0.05 (p>0.05) then the assumption was that data have equal variance across the different conditions.

2.2.3.1 Calculating the probability of a type I error

Mono-parametric analysis

Student's t-test

A Student's t-test calculates a t- or z- statistic to assess differences in means from two samples. The assumption for this test is that the data are normally distributed with equal variance. The t-statistic can be defined as:

$$t = \frac{(\bar{x} - \mu)}{S_\sigma / \sqrt{n}}$$

(Lachin, 1981; Ogston *et al.*, 1991)

The sample mean (μ), sample standard deviation (S_σ) and sample size (n) of the test are used to calculate the t-value (t). Using a t-table, the calculated t-values are used to identify the associated p-value to the correct degrees of freedom ($n - 1$). Due to the low sample number in the datasets used for this study, a t-statistic was used instead of a z-statistic (t-approximation). Student's t-tests were performed using a t.test:

R: t.test(x, y, alternative = two.sided, var.equal= TRUE)

in which x and y define the two means. The same function was used to calculate the 95% Cis for each mean:

R: t.test(x/y, conf.level = 0.95).

The null hypothesis was rejected, and the alternative hypothesis is accepted if the p-value is below the alpha critical level ($p<0.05$).

Welch's t-test

Although the Student's t-test is a suitable analysis if the variance ratio is known, the large divergence in the sample variance may mask any significant changes between two sample means (Welch, 1938). Therefore, to account for differences in variance:

$$v = \frac{|\bar{x}_0 - \bar{x}_1|}{\sqrt{{\Sigma_0}/{n_0(n_0-1)} + {\Sigma_1}/{n_1(n_1-1)}}}$$

Welch (1938) also corrects the degrees of freedom. v is distributed as ct_f whereby c is a constant defined by Welch, and t_f denotes the Student's distribution with f degrees of freedom (Welch, 1938). Welch's t-tests were performed using a t.test:

R: t.test(x, y, alternative = two.sided, var.equal= FALSE)

in which x and y define the two means.

Wilcoxon Mann Whitney rank sum test

Data which were not normally distributed (non-parametric) were analysed using a Wilcoxon Mann-Whitney rank- sum (WMW) test. The WMW test ranks the changes in sample distributions in which m and n are the sample sizes for samples i and j respectively:

$$W = \Sigma_{i-1}^{m}\Sigma_{j-1}^{n} p(Y_j - X_i)$$

(Mollan *et al.*, 2019)

To detect any difference in the two distributions (i and j), the WMW test sequentially examines each data point from one distribution (Y_j) to the data points in the other distribution (X_i). If Y_j is greater than X_i, the W value is defined as 1 ($p(Y_j - X_i) = 1$). If this criteria is not met (Y_j is not greater than X_i), the W value is set to 0 (Mollan *et al.*, 2019). Therefore, the WMW test quantifies every instance Y_j is greater than X_i generating an overall W value (W-statistic). Using a W-table (also referred to as u-table), the W critical value and p-value at a specified alpha level and sample size are identified. If W< W critical value at an alpha level of 0.05, I reject the null hypothesis concluding there is a statistical difference in the distributions.

WMW tests were performed with an assumption of a 2-tailed distribution in which x and y define the means for the two populations:

R: wilcox.test(x, y, alternative = two.sided)

The same function was used to calculate the 90% confidence intervals (CIs) for each mean:

R: wilcox.test(x/y, conf.level = 0.90)

Due to the low sample size and ties within the data, a normal approximation was used on the ranked data with a maximum Ci of 90% (Hollander *et al.*, 2013).

Multi-parametric analysis

ANOVA

In order to assess the difference in means between two or more factors, an Analysis Of Variance (ANOVA) was conducted. An ANOVA measures the effects of multiple factors in addition to determining any interactions between factors. Data which were parametric were analysed using ANOVA (R: aov). Data which were non-parametric were analysed using a rank test. Aligned Rank Transformation (ART) aligns the data before determining the rank (Wobbrock *et al.*, 2011). Standard ranking techniques used to analyse non-parametric data lead to inaccuracies when determining interactions effects. Align Rank Transformation (ART) ANOVA eliminates this problem by first estimating the effect of factors (both main and interaction effects) as marginal means with all other effects removed (aligning) before ranking the data, accurately determining the effect of each factor (Wobbrock *et al.*, 2011). Data showing a non-parametric distribution with equal variance were transformed and ranked using the ARTool package (R: ART) then ranked data were analysed by ANOVA.

Multiple comparisons

When conducting sequential pairwise analysis between conditions on the same dataset, a correction for multiple comparisons was applied to minimise the occurrence of type I and II error. For parametric data, a one-way ANOVA with Tukey's honest significant difference (HSD) post-hoc test was applied, which is appropriate for test with small sample sizes (Barnette and McLean 1999).

Using the base R: aov to run an ANOVA, a Tukey's HSD multiple comparisons was conducted:

TukeyHSD(model, conf.level=0.95, alpha= 0.05)

The model defines the results from an ANOVA, and the Ci and alpha level are set to 0.95 and 0.05, respectively.

For non-parametric data, a Kruskal-Wallis one-way ANOVA with Dunn's post-hoc test was applied with the Benjamini and Hochberg (bh) correction. This test is suitable for non-parametric data (Dinno, 2015), accounting for multiple comparisons by assessing the false discovery rate (Benjamini and Hochberg, 1995). Using the dunn.test package (Dinno, 2017), the R: dunn.test function was used:

dunn.test(x , g, method = "bh", alpha = 0.05)

The cell population (x) and conditions (g) were defined and a Benjamini-Hochberg (bh) correction was applied. The alpha level was set to 0.05.

2.2.3.2 Calculating the probability of a type II error

Student's t-test

A Student's t-test was used to calculate power and ideal sample size for data showing a normal distribution and equal variance. Sample size (N) affects the power of the analysis as it dictates total variance (Σ^2) of the data in combination with the standard deviation (σ).

$$\mathrm{N}(\Sigma^2 = \frac{\sigma^2}{N}).$$

When using a t- or z-statistic to calculate significance, the ideal sample size avoids both type I and II errors and therefore simultaneously satisfies the following expressions:

$$P\left(Z > Z_{\alpha/2}\right) = \alpha \mid H_0 \; is \; true$$

$$P\left(Z > Z_{\alpha/2}\right) = 1 - \beta \mid H_1 \; is \; true$$

These expressions require that the probability (P) of a given value of Z (the t- or z-statistic) being greater than Z at a given alpha-level ($Z_{\alpha/2}$), is equivalent to alpha (α) when α=0.05, if the null hypothesis is true and the means are not significantly different. In addition, the probability of a given value of Z being greater than Z at a given alpha-level ($Z_{\alpha/2}$) is equivalent to 1- β where β is the probability of a type II

error, when the alternative hypothesis is true. This means that the ideal sample size is one which accepts the null hypothesis when it is true, reducing the probability of a type I error, or rejects the null hypothesis and accepts the alternative hypothesis when the null hypothesis is false, reducing the probability of a type II error. The Student's t-test can be used to calculate both sample size and power when the following conditions are met:

a) The proportion (Q) of samples in each group is defined as follows:

$$Q_{e(experimental)} + Q_{c(control)} = 1$$

b) Variance of individual samples (σ^2) is equal between groups:

$$\Sigma_0^2 = \Sigma_1^2 = {\sigma^2(Q_e^{-1} + Q_c^{-1})}/{N}$$

c) The experimental (v_e) and control (v_c) means $(v_e - v_c = \mu_1)$ are normally distributed.

Ideal sample size (N) and power (Z_β) can be calculated by the following expressions:

$$N = \frac{\sigma^2(Q_e^{-1} + Q_c^{-1})(Z_\alpha + Z_\beta)^2}{\mu_1^2}$$

$$Z_\beta = \frac{|\mu_1|\sqrt{N} - Z_\alpha\sigma\sqrt{(Q_e^{-1} + Q_c^{-1})}}{\sigma\sqrt{(Q_e^{-1} + Q_c^{-1})}}$$

(Lachin, 1981)

In the present study, I first aimed to calculate the retrospective power of our analysis at an alpha level of 0.05. Subsequently, I used the datasets produced to identify the ideal sample size needed to achieve a power of 80% for future experiments. Using a t-approximation (t-table and t-value) for the Z-value, the Z_α and Z_β values can be obtained for a two-tailed analysis at an α-level of 0.05 and power of 80% (probability of a type I error (p)=0.02) to the appropriate degrees of freedom $(n - 1)$. In order to calculate both power and ideal sample size, the R: power_t_test function was used (MESS package).

When calculating power, the known experimental sample size is included and the power is set to NULL. However, when calculating the ideal sample size at a power of 80%, power is set to 0.8 (80%) and samples size is set to NULL.

R: power_t_test(n = (NULL or sample size), delta = , sd = , sig.level = 0.05, power = (NULL or 0.8), ratio = , sd.ratio = , type= two.sample, alternative = two.sided, df.method = classical).

By setting one of these two parameters (power or sample size) to NULL, the R: power_t_test function will calculate the missing parameter.

Wilcoxon Mann Whitney (WMW) rank sum test

The WMW test was used when data were non-parametric to calculate the power and ideal sample size. The wmwpow package (Shieh *et al.*, 2006) was used to calculate power using the WMW rank-sum test assuming a two-tailed (sides = "two.sided") normal distribution (dist = "norm") with an α-level of 0.05 (alpha = 0.05). This assumes the sample size for both groups (n and m) and the probability of the two distributions are different (p; 1- the probability of a type I error)

R: shiehpow(n = , m = , p = , alpha = 0.05, dist = "norm", sides = "two.sided").

The WMWssp package (Happ *et al.*, 2019) was used to calculate the required sample size to achieve 80% power by running a simulation on the data provided. Sample size was calculated to achieve 80% power (power = 0.8) at an α-level of 0.05 (alpha = 0.05) in which x and y define the means of the two samples and t defines how the calculated ideal sample size (n) is allocated between conditions (set to 0.5 so evenly distribute samples between conditions; R: WMWssp(x, y, alpha = 0.05, power = 0.8, t = 0.5).

2.2.4 Calculating the effect size

The results of the test statistic are dependent on various conditions, one of which is the effect size. The effect size is the measure of the difference of sample means, thus the larger the effect size, the higher the power and significance of the statistical test (Cohen, 1988). To determine the relationship between effect size and power, the Cohen's d coefficient was calculated. This coefficient was calculated by dividing the difference in sample means ($\Delta\bar{\mu}$) by the standard deviation as follows:

$$Cohen's\ d = \frac{|\Delta\bar{\mu}|}{\bar{\sigma}}$$

In order to account for a difference in scedasticity of the two means, (σ) a pooled standard deviation (SD) was used which is calculated from the standard deviation of both samples.

$$Cohen's\ d = \frac{|\Delta\bar{\mu}|}{SD\text{pooled}}$$

Where $SD_{pooled} = \sqrt{((\sigma_1^2 + \sigma_2^2)/2)}$

2.2.5 Calculating linear regression

Initially the image was cropped around the site of injury so that all arbitrary co-ordinates are relative to the injured region. Each cells was selected suing the multi-point tool, and the measure plugin was used to get X, Y co-ordinates (in pixels). Using the Linest function on excel I was able to calculate the linear regression, the standard error of Y and the degrees of freedom. To calculate the 95% confidence intervals of the Y co-ordinates was calculated by:

$$\frac{T\ value\ X\ the\ standard\ error\ of\ Y}{\sqrt{N}}$$

Where the T value was calculated using the tinv function on excel, and N is equal to the degrees of freedom plus 2. The predicted X values were then calculated by:

$$m(slope)\ X\ x + b\ (intercept)$$

Where m and b were calculated using the Linest function on excel. Finally the uncertainty values for X calculated from the predicted Y was added and subtracted from the actual values.

2.3 Materials

Fish lines	Abbreviation	Reference
Tg[*pax7a:eGFP*]	-	(Mahalwar *et al.*, 2014)
pax7b$^{gSAIzGFFD164A;5xUAS:EGFP}$	*pax7b:GFP*	(Pipalia *et al.*, 2016)
Tg[*fms:Gal4;UAS:NfsB-mCherry*]	*fms:mCherry*	(Gray *et al.*, 2011)
Tg[*mpx:GFP*]	-	(Renshaw *et al.*, 2006)
Tg[*Tp1:H2BmCherry*]	-	(Parsons *et al.*, 2009; Ninov *et al.*, 2012)
Tg[*Tp1:VenusPEST*]	-	(Aulehla *et al.*, 2008; Ninov *et al.*, 2012)
Tg[*deltaD:Gal4;UAS:GFP]*	*DeltaD:GFP*	Scheer *et al.*, 2001)
Tg[*HS:dnsu(h)*]	-	(Latimer *et al.*, 2005)
Tg[*HS:Gal4*]/ Tg[*UAS:NICD*]	*HS:NICD*	(Scheer *et al.*, 2001)
tnfrsf1a^{Sa8496}	*tnfrsf1a*	Sanger Institute

Table 2.6. Zebrafish lines

Target	Forward primer sequence	Reverse primer sequence	Product size
Dnsu(h)	CGG GCA TTT ACT TTA TGT TCG	TGC ATT TCT TGC TCA CTG TTT C	1000 bp
Gal4	GGA ATC AAG GCT AGA AAG ACT GG	GAT CCG CTA CAT ATC CAG AGC G	500 bp
UAS:NICD	CGG AAT CGT TTA TTG GTG TCG	CATCGCGTCTCAGCCTCAC	500 bp

Table 2.7. PCR primers

Reagent	Volume
Random primers (PROMEGA)	2 µl
RNA	500 ng
Water	Top up to reach total volume
Total volume	**14 µl**

Table 2.8. Mix with random primers to prime reverse transcription throughout the transcript

Reagent	Volume
dNTPs (10mM)	1.25 µl
5X buffer	5 µl
M-MLV	1 µl
Water	3.75 µl
Total volume	**11 µl**

Table 2.9. cDNA PROMEGA synthesis mix

Reagent	Volume
SYBR Green buffer mix	5µl
Primer mix 2µM stock	0.4 µl
RNase free water	4.2 µl
Sample cDNA (4ng)	0.4 µl
Total volume	**10 µl**

Table 2.10. qRT-PCR reaction composition

Gene	Forward primer sequence	Reverse primer sequence
elf1a	TTC TGT TAC CTG GCA AAG GG	TTC AGT TTG TCC AAC ACC CA
her1	GAT CAA GGC GAT TCT AGC AAG G	TGG CGA GGT TAT GGG TTT GGA
her2	TTT ACC TTC TCT TTC CAG CTG AGG	GCT GAC TGG CCT TTA TTT CGG
her4.1	CTC CTG CAG ACC AGC ACA CAC G	ACA CGA CTA TTA AGT CTA CCA GGG TCT CCA
her6	CGT TAA TCT TGG ATG CTC TG	CTT CAC ATG TGG ACA GGA AC
her9	AAA AGC GCC GCA GAG CGA GAA T	CAG CTG ACA AGG CTG CGC TCA T

Table 2.11. Forward and reverse transcript primer sequences

Antibody	Concentration	Supplier	Cat No.
Chicken-anti-Rabbit 488	1:250	Life Technologies	A21441
Donkey-anti-mouse 488	1:250	Life Technologies	A21202
Goat-anti-mouse 488	1:250	Life Technologies	A11001
Goat-anti-chicken 488	1:250	Invitrogen	A11039
Goat-anti-chicken 488	1:250	Abcam	ab150169
Donkey-anti-rabbit 568	1:250	Invitrogen	A10042
Goat-anti-mouse 568	1:250	Abcam	ab175473
Goat-anti-mouse 633	1:250	Invitrogen	A21050
Goat-anti-chicken 633	1:250	Invitrogen	A21103
Goat-anti-rabbit 635	1:250	Life Technologies	A31576
Donkey-anti-rat 647	1:250	Jackson Laboratories	712-607-003
Chicken-anti-GFP	1:500	Millipore	AB16901
Rabbit-anti-GFP	1:500	Life Technologies	A6455
Rabbit-anti-GFP	1:500	AMS	210-PS-IGFP
Mouse-anti-GFP	1:500	DSHB	-
Rabbit-anti-L-Plastin	1:500	Paul Martin, University of Bristol	-
Chick-anti-L-Plastin	1:500	Paul Martin, University of Bristol	-
Rabbit-anti-Mpx	1:500	GeneTex	GTX128379
Rabbit-anti-dsRed	1:500	Living colours	632496
Mouse-anti-mCherry	1:500	DSHB	-
Rabbit-anti-activated Notch 1	1:500	Abcam	ab8925
Rat-anti-BrdU	1:500	Abcam	ab6326
Mouse-anti-Pax7-bioreactor	1:100	DSHB	-
Rabbit-anti-Myogenin	1:10	Santa Cruz	m-2250 sc-576

DAPI Vectorshield	-	Vector	H1200
Hoechst-33342	1:1000	Life Technologies	H3570
Phalloidin 633	1:300	PromoCell	PK-PF633P-7-01

Table 2.12. Antibodies and dyes used for immunostaining experiments

Name	Abbreviation	Concentration	Supplier	Cat No.
Bromodeoxyuridine	BrdU	10 mM	Sigma	B5002-1G
DAPT	DAPT	100 µM	Sigma	D5942-5MG
Dexamethasone	DEX	0.5 mM	Sigma	D2915-100MG
Evans Blue	-	0.1 % v/v	Sigma	E2129-10G
Metronidazole	MTZ	5 mM	Sigma	M3761-5G

Table 2.13. Chemical treatments

Name	Abbreviation	Constitution
E3 media	-	10X stock: 2.87 g NaCl, 0.13 g KCL, 0.48 g $CaCl_2.2H_2O$, 0.82 g $MgSO_4$, 1 L ddH_2O
N-Phenylthiourea	PTU	100X stock: 1.5 g PTU, 500 ml ddH_2O
Tricaine methanesulfonate	Tricaine	0.4 %: 0.4 g tricaine ethyl 3-aminobenzoate methanesulfonate, 2.1 ml Tris-HCl (pH 9), 100 ml ddH_2O. Adjusted to pH 7.0
Alkaline lysis buffer	-	50X stock: 7 g 1.25 mM KOH_2, 2 ml 10 mM EDTA, 100 ml ddH_2O
Neutralisation buffer	-	50X stock: 31.5g 2M Tris-HCL, 100 ml ddH_2O
Phosphate buffered saline with Tween 20	PBT	0.1%: 50 µl Tween 20 in 50 ml 1X PBS
Phosphate buffered saline with Triton X-100	PBTx	1%: 500 µl Tween 20 in 50 ml 1X PBS 0.4%: 20 µl Tween 20 in 50 ml 1X PBS
Paraformaldahyde	PFA	4 %: 8 g paraformaldehyde (prilled), 1 ml NaOH, 200ml ddH_2O Adjusted to pH 7. 2 %: 1 ml 4 % PFA, 1 ml PBS
Methanol series	-	25 %: 12.5 ml methanol, 37.5 ml PBS 50 %: 25 ml methanol, 25 ml PBS 75%: 37.5 ml methanol, 12.5 ml PBS
Glycerol series		25 %: 12.5 ml glycerol, 37.5 ml PBS 50 %: 25 ml glycerol, 25 ml PBS 75%: 37.5 ml glycerol, 12.5 ml PBS
Borate buffer	-	0.62 g Boric acid, 1.5 ml 75 mM NaCl, 100 ml ddH_2O

Table 2.14. General reagents

Chapter 3 Notch signalling regulates muscle stem cell homeostasis and regeneration in a teleost fish

3.1 Introduction

It has been shown that the size and type of injury influences the inflammatory response and subsequent tissue repair (Niethammer *et al.*, 2009; Knappe *et al.*, 2015; Weavers *et al.*, 2016). Currently, the standard methods to damage muscle in zebrafish include injection of myotoxic chemicals such as CTX (Seger *et al.*, 2011) or insertion of a sharp needle in the tissue (Gurevich *et al.*, 2016; Pipalia *et al.*, 2016; Nguyen *et al.*, 2017). Although these methods elicit a strong muSC response towards tissue repair, they lack precision and reproducibility, making it difficult to determine how muSC responses are dictated by defined variables. Therefore, I aimed to establish a reproducible injury model using a sharpened tungsten wire. Damaged myofibers in *pax7a:eGFP*-expressing larvae were identified using Evans blue, allowing me to accurately quantified the injury volume and the number of recruited eGFP+ muSC following injury.

During the early stages of larval development (3-7 dpf), the muscle undergoes drastic structural changes (Hollway *et al.*, 2007; Roy *et al.*, 2017). During these developmental changes, cells within the ECL migrate towards the horizontal and vertical myosepta, and muSCs begin to populate the deeper portion of the myotome (Seger *et al.*, 2011; Knappe *et al.*, 2015; Nguyen *et al.*, 2017). Moreover, following this cellular relocation, cells become less motile and proliferate less as the larval muscle develops (Seger *et al.*, 2011; Knappe *et al.*, 2015; Nguyen *et al.*, 2017). Many studies investigating muSC activity during growth and regeneration conduct investigations on zebrafish larvae younger than 5 dpf (Seger *et al.*, 2011; Gurevich *et al.*, 2016; Pipalia *et al.*, 2016; Ratnayake *et al.*, 2021). As the effect of developmental processes towards muscle regeneration is unknown, I aimed to investigate the influence of larval age (3 and 7 dpf) on the *pax7a:eGFP*-expressing muSC response to injury.

Notch signalling has been well characterised in amniotes, demonstrating a critical role in maintaining the quiescence and proliferative state of muSCs during muscle homeostasis and regeneration (Vasyutina *et al.*, 2007; Bjornson *et al.*, 2012;

Mourikis, Sambasivan, *et al.*, 2012; Picard and Marcelle, 2013; de Lima *et al.*, 2016; Yartseva *et al.*, 2020). There are no published reports demonstrating that Notch signalling regulates muSC activity during muscle homeostasis and regeneration in zebrafish. To elucidate the importance of Notch signalling in zebrafish muscle, I investigated how Notch inhibition and over activation influences the number of proliferating and differentiating muSCs.

In experiments investigating muSC biology in the myotome of larval stage zebrafish there are very few cells. This reflects a potential caveat for inferring statistically significant differences between conditions and highlights the need to develop a robust statistical methodology for determining whether muSC are affected by a specific variable. Therefore, I assessed the distribution of the data collected, the power of the analysis, and the sample size needed to achieve 80 % power when using zebrafish to investigate changes to muSC number in response to injury and Notch inhibition.

3.2 Results

3.2.1 Reproducible needlestick injury method

The type and size of wounding has been linked to the magnitude of the stem cell response in zebrafish (Niethammer *et al.*, 2009; Knappe *et al.*, 2015; Weavers *et al.*, 2016). Therefore, I investigated the relationship between the injury size and the recruitment of muSCs in zebrafish when using a sharpened tungsten wire to damage a discreet area of muscle in a precise and controlled manner.

Contrary to other studies where they damage multiple myotomes, I wanted to establish the needlestick injury method to damage a single zebrafish myotome. To visualise the injury volume in *pax7a:eGFP* expressing larvae I applied 0.1 % v/v Evans blue in E3 medium, which binds to damaged myofibers and fluoresces at far-red wavelengths (Hamer *et al.*, 2002). Following treatment, larvae were injured in the 13th left ventral myotome and imaged 1 hpi. To show that Evans blue marks the total area of damaged muscle, I captured Evans blue staining relative to second harmonic generation (SHG) signal, which labels all polarised structures such as myofibers (Plotnikov *et al.*, 2006). I observed that Evans blue stained all areas of damaged muscle (Fig. 3.1A; 83 Z-steps observed in Movie. 9.1) following 1 hour of treatment.

Next, I aimed to understand the reproducibility of the needlestick injury by injuring multiple zebrafish. To determine the injured volume, I acquired confocal stacks capturing Evans Blue and brightfield (Fig. 3.1B) from 5 independent injured zebrafish larvae. I measured the area of injured muscle at each Z-interval then used this to calculate an extrapolated volume (Fig. 3.1C). By comparing this relative to the total myotome volume (Fig. 3.1D) I estimated the injury extent (Fig. 3.1E). I found that the injury size varied between $2.4 \text{ and } 8.2 \times 10^4 \ \mu m^3$ with a majority (4/5) of injuries in a range between $2.4 \text{ and } 5.3 \times 10^4 \ \mu m^3$. To understand whether the overall size of the muscle introduces variability of tissue damage between larvae, I measured the total volume (Fig. 3.1D) of the injured myotome to calculate the relative proportion of muscle injured (Fig. 3.1E). I found that needlestick injury damaged approximately 7% of the myotome with low variability (±5%) between animals. These results highlight the reproducibility and low variability around the size of the injury when using a sharpened tungsten wire to damage the muscle.

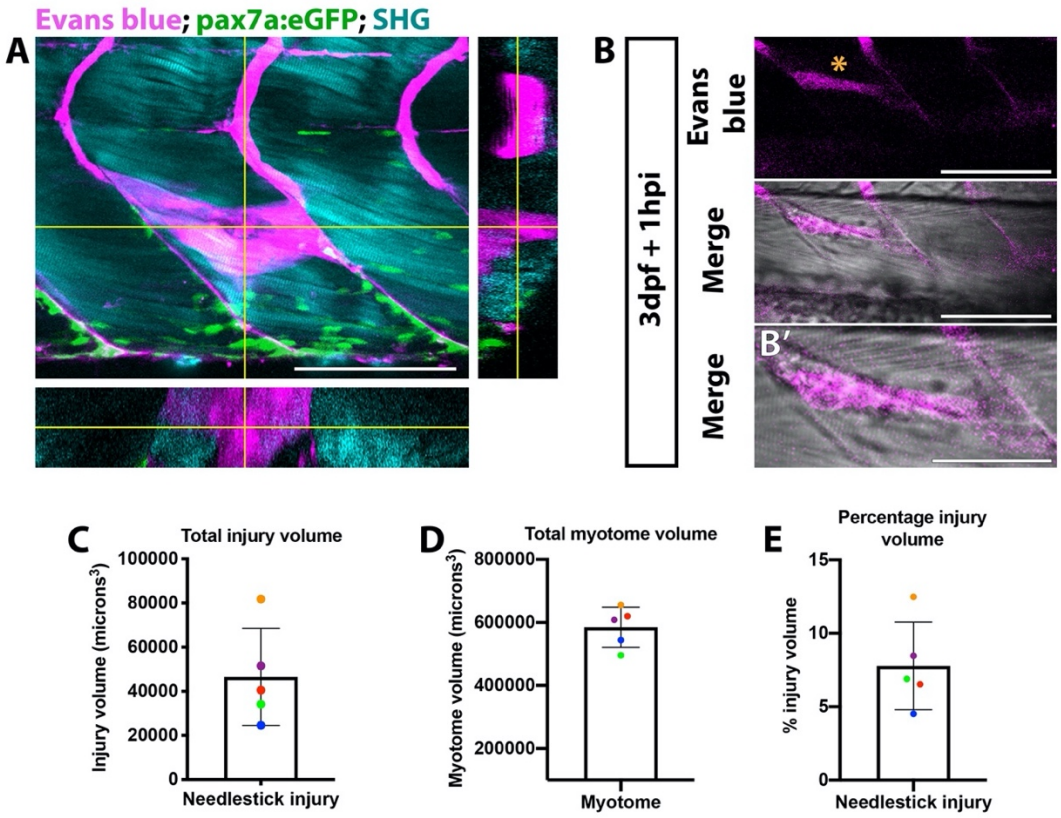

Figure 3.1. Visualisation of muscle injury using Evans blue reveals low variability of injury size caused by needlestick.

Evans blue labelling of damaged muscle (**A-B**) was visualised with a multiphoton microscope and localises with perturbed myofibre morphology (**B'**) at needlestick wounds (asterisk) in 3 dpf larvae at 1 hpi. Maximum projection (**A**) with orthogonal sections in planes YZ (right) and XZ (bottom) showing Evans blue staining relative to myofibers (visualised by second harmonic generation; SHG) and *pax7a:eGFP* expressing muSCs. Volumetric measures of the (**C**) total myotome and (**D**) injured region were calculated by measuring the injury size for each section. The percentage of injury volume (**E**) was calculated in function of the total myotome volume. Each larvae (n=5) has been colour coded to highlight the variance in myotome and injury size. Error bars display standard deviation.

Scale bars: 100 µm (**A-B**), 50 µm (**B'**).

3.2.2 The needlestick method is a reproducible muscle injury method

In order to understand whether the scaling of tissue damage affects the number of responding muSCs, I imaged the injured tissue by time-lapsed microscopy. The 5 injured larvae treated with Evans blue were imaged over a 16.83 hour time frame (Movie. 9.2). I aimed to determine the potential relationship between the initial injury volume and the subsequent muSC response by quantifying the number of eGFP+ muSCs responding towards the injury over time.

Following injury, the number of muSCs increased from 0.4 ± 0.9 to 4.2 ± 2.2 cells over the 16.83 hours (Fig. 3.2A, B). As expected, due to the low variability around the injury size, 4/5 larvae cluster around 3.3 ± 0.5 muSCs by 16.83 hours (Fig. 3.2C). Interestingly, when 12.5% of the muscle was damaged, I measured an increased number of muSCs responding to injury (8 cells), suggesting that larger injuries induce and increase in muSC response (Fig. 3.2C). Linear regression was calculated to determine the correlation between injury size and muSC number. I obtain an R^2 value of 0.74. Therefore, I showed that there is a strong correlation between the number of muSCs observed at 16.83 hpi with respect to the range of injury sizes examined. I note that as the data distribution was small, it was not possible to confidently state that there is a tight correlation between larger injury size and number of responding muSCs.

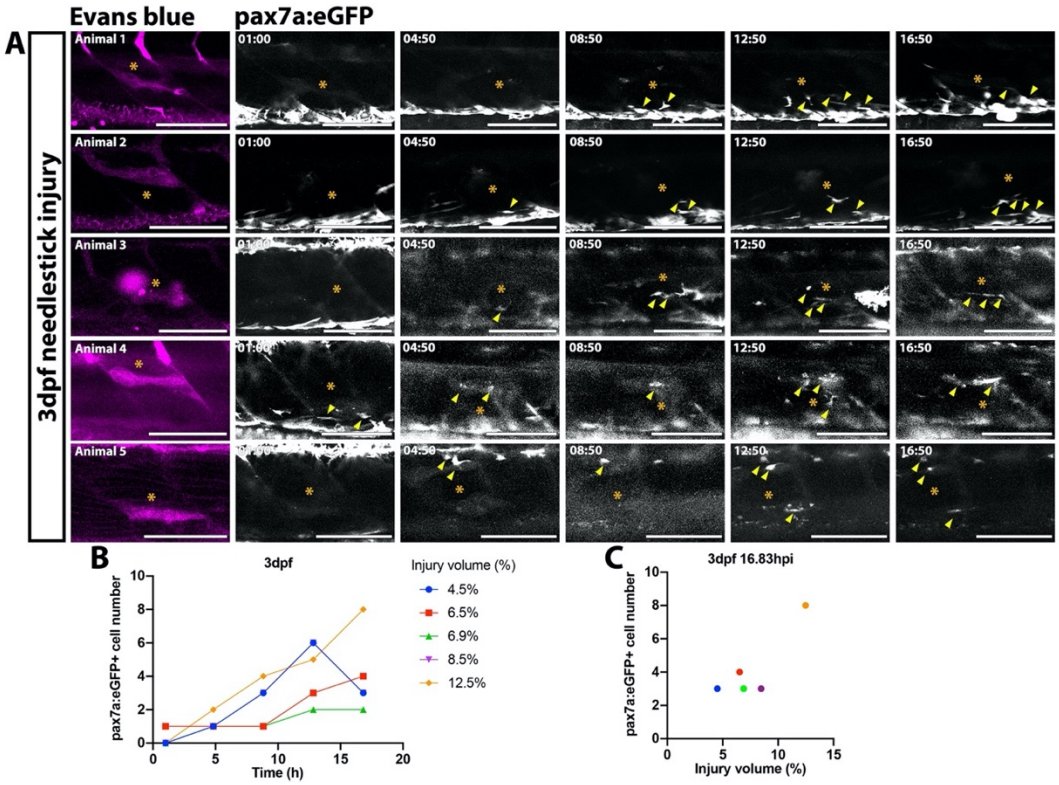

Figure 3.2. Similar muSC response observed when using the reproducible needlestick injury method.

Images from time-lapsed movies reveal *pax7a:eGFP*-expressing muSCs (arrowheads) response to injury (asterisk). The injury was labelled with Evans Blue (magenta) in the myotome of 5 representative 3 dpf larvae (**A**, animals 1-5). Images were acquired on a multiphoton microscope and maximum intensity projections generated. The number of *pax7a:eGFP*+ cells in the myotome was quantified and plotted against time (**B**) and injury volume (**C**). Each coloured line (**B**) or dot (**C**) represents a single animal.
Scale bars: 100 µm (**A**).

3.2.3 Expansion of the resident muSC population occurs in the myotome during larval development

Extensive structural changes occur to cell populations in the myotome during muscle development in zebrafish, with a marked change in the migration patterns and proliferation of muSCs between 3 dpf and 7 dpf larvae (Hollway *et al.*, 2007; Knappe *et al.*, 2015; Roy *et al.*, 2017). Previously, studies have used 3-4 dpf zebrafish larvae to investigate the muSC response to injury (Seger *et al.*, 2011; Gurevich *et al.*, 2016; Pipalia *et al.*, 2016; Ratnayake *et al.*, 2021). It is possible that muscle repair in zebrafish may be influenced by developmental programs.

To understand if the muSC response towards injury is different between larval stages, I injured the myotome of 3 and 7 dpf larvae, visualising eGFP+ muSCs at 24 hpi by confocal microscopy (Fig. 3.3). By using a confocal microscope, I could visualise all eGFP+ muSCs present, including those not easily detectable by multiphoton microscopy due to their dim fluorescence.

In the uninjured control larvae, I observed few eGFP+ cells within the myotome in 4 dpf (Fig. 3.3A') and 8 dpf (Fig. 3.3C') larvae (5.5 ± 1.5 at 4 dpf and 8.3 ± 4.6 at 8 dpf). At 24hpi, eGFP+ cells were observed at the site of injury, aligned with adjacent myofibers in both 4 dpf (Fig. 3.3C') and 8 dpf (Fig. 3.3D') larvae. To determine whether the number of muSCs in the myotome changes through development and in response to injury, I counted eGFP+ cells in the myotome of injured and uninjured control larvae. To test whether the number of muSCs is affected by the developmental stage I conducted a 2-way ANOVA. As expected, following injury, larvae have more muSCs relative to uninjured controls. I found that 8 dpf larvae have more muSCs compared to 4 dpf larvae. (Fig. 3.3E). Although both these variables independently influence muSC number, there was no interaction effect between the age of the larvae and the injury (Fig. 3.3E). Therefore, 8 dpf larvae did not elicited a greater muSC response towards muscle injury compared to 4 dpf larvae.

To understand how injury and age affected the number of muSCs, I performed a 1-way ANOVA. I found there was an increase in muSC number in the injured myotome at both 4 (Fig. 3.3F) and 8 (Fig. 3.3G) dpf relative to uninjured controls. I also found that there were significantly more muSCs in older larvae (17.2 ± 2.5) compared to younger larvae (11.7 ± 1.9) following injury (Fig. 3.3I). These results suggest that

although older larvae have more cells, the muSC response to injury is not affected by larval stage.

3.2.4 Expansion of the resident muSC population occurs in the myosepta during larval development

Descriptions of pax3a-expressing muSCs in zebrafish have highlighted the vertical and horizontal myosepta as a potential site for a stem cell niche for muSCs (Nguyen *et al.*, 2017). The vertical myoseptum and horizontal myoseptum are enriched with molecules associated to the ECM and with cell adhesion molecules, including Fibronectin and Laminin (Goody *et al.*, 2012). Characterisation of muSC response to injury in zebrafish has shown that *pax7a*-expressing cells detach from the VM (Knappe *et al.*, 2015) and HM (Movie. S2) and migrate towards damaged myofibers. Therefore, I quantified the number of muSC at the VM (bilaterally located relative to the myotome of interest; Fig. 2.3), ventral horizontal myoseptum (VHM; ventrally located relative to the myotome of interest; Fig. 2.3) and dorsal horizontal myoseptum (DHM; dorsally located relatively to the myotome of interest, medially located relative to the whole fish; Fig. 2.3). To understand if the developmental stage affects the number of muSCs at the myosepta, I conducted a 2-way ANOVA. I found an age dependent effect on the number of muSCs at the VM, VHM and DHM with an interaction effect between injury and age at the VHM (File. 9.1). To understand how injury and age affects the number of muSC at the myosepta, I conducted a 1-way ANOVA. I found that there was a significant increase in the number of muSC within the HM and VM in older larvae (8 dpf) relative to younger larvae (4 dpf) in the absence of injury (File. 9.1), substantiating my previous result. These results are also consistent with previously published work demonstrating an association between the age of the larvae and the enrichment of the ECL (VM and HM) with muSCs (3-7 dpf; Seger *et al.*, 2011). Moreover, I did not identify any changes to the number muSCs within the myosepta following injury in 4 dpf or 8 dpf larvae (File. 9.1).

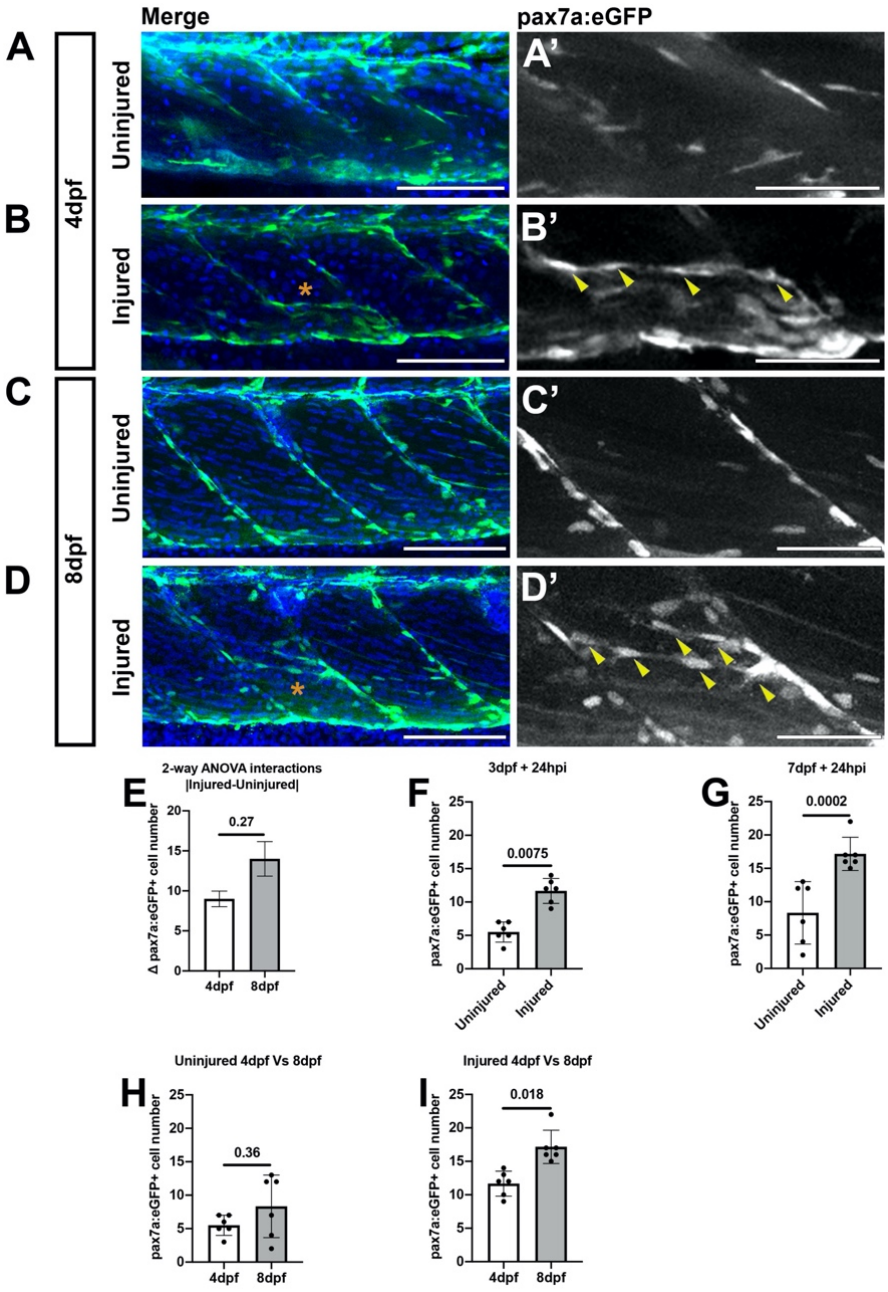

Figure 3.3. Muscle injury results in an increased number of *pax7a:eGFP*-expressing cells within the myotome at 4 and 8 dpf.

Projections of confocal z-stacks of the myotome in uninjured (**A, C**) and injured (**B, D**) 3 or 7 dpf *pax7a:eGFP* larvae at 24 hpi with nuclei labelled with DAPI. MuSCs (arrowheads) were recruited to the site of injury (asterisk) and aligned with myofibers at both stages (**A'-D'**). Quantification of *pax7a:eGFP*-expressing muSCs in uninjured and injured 3 and 7dpf larvae at 24 hpi. The magnitude of change to the number of muSCs responding to injury (Δ*pax7a:eGFP*+) was significantly different between 4 and 8 dpf larvae ($p>0.05$, **E**). Pairwise comparisons reveals a significant increase in the number of muSCs at both stages as a consequence of injury ($p<0.05$, **F, G**). There was no significant difference in the number of muSCs between uninjured animals at 4 and 8 dpf (**H**), but there were more muSCs in injured 8 dpf larvae relative to injured 4 dpf larvae ($p<0.05$, **I**). Significant differences were tested by 2-way ANOVA (n=47) with Tukey's HSD post-hoc test. Error bars represent standard deviation, and values above comparison bars represent significance (p-values).
Scale bars: 100 µm (**A-D**), 50 µm (**A'-D'**).

3.2.5 Notch regulates Pax7-expressing muSC response to injury in zebrafish larvae

Notch has been shown to be a critical regulator of muSC quiescence and proliferation in mouse and chick (Bjornson *et al.*, 2012; Mourikis, Sambasivan, *et al.*, 2012; Yartseva *et al.*, 2020). It is not known whether Notch signalling has a conserved role in regulating muSCs in zebrafish during regeneration. γ-secretase facilitates the second proteolytic cleavage of the Notch receptor following receptor-ligand binding, allowing the NICD to translocate into the nucleus (Geling *et al.*, 2002). Therefore, using DAPT, a well characterised pharmacological inhibitor of γ-secretase (Geling *et al.*, 2002), I investigated the importance of Notch signalling for zebrafish muscle homeostasis.

A loss of Notch signalling characteristically results in a depletion of the Pax7+ stem cell population (Vasyutina *et al.*, 2007; Picard and Marcelle, 2013; de Lima *et al.*, 2016). Therefore, using an antibody to detect Pax7+ cells in the presence and absence of DAPT, I examined whether there is a conserved role for Notch to maintain the Pax7+ stem cell population in zebrafish. I quantified the number of Pax7+ cells in the myotome of injured 3 dpf larvae at 24 hpi (Fig. 3.4). I observed fewer Pax7+ myoblasts in animals treated with 100 µM DAPT compared to control animals treated with a vehicle, DMSO (DMSO: 17.1 ± 4.7, DAPT: 11 ± 4; Fig. 3.4A', B', C). I also detected a reduction of Pax7+ cells at the VM (DMSO: 16 ± 2.7, DAPT: 13.8 ± 1.4; Fig. 3.4A'', B'', D) and no change to the number of Pax7+ cells within the VHM and DHM in animals exposed to DAPT (File. 9.1).

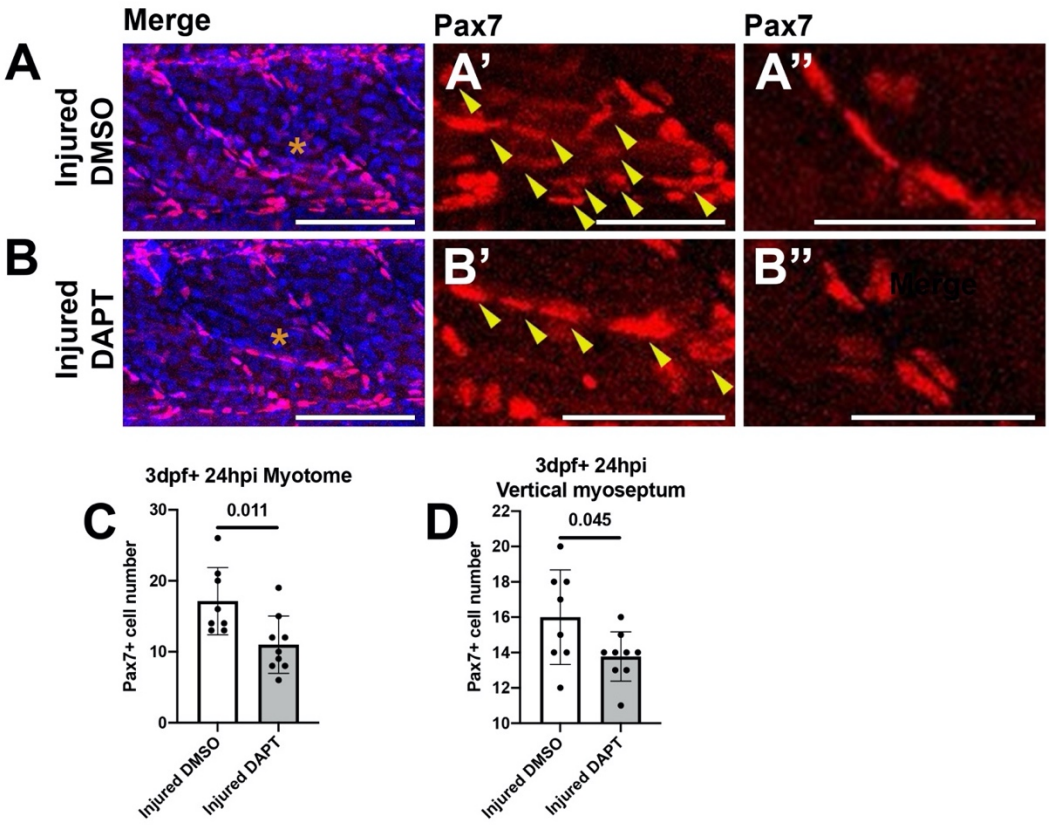

Figure 3.4. Notch inhibition by DAPT treatment results in fewer Pax7+ muSCs responding to muscle injury.

Projections of confocal stacks (**A-B**) of the myotome (**A'-B'**) and vertical myoseptum (**A''-B''**) of injured 3 dpf larvae. Larvae were treated with 1% v/v DMSO (**A**) or 100 µM DAPT (**B**) after injury, fixed at 24 hpi and labelled with anti-Pax7 antibody. MuSCs (yellow arrowheads) were recruited to the injury (asterisk) site (**A'-B'**). The number of cells expressing Pax7 was counted in the myotome (**C**) and vertical myoseptum (**D**) of animals treated with DMSO or DAPT. There were significantly fewer Pax7+ muSCs in the presence of DAPT compared to DMSO treated control animals in the myotome ($p<0.05$; **C**) and vertical myoseptum ($p<0.05$; **D**). Tests for significant differences were performed by Student's t-test (n=8-9 animals per condition). Error bars display standard deviation, and values above comparison bars indicate significance (p-values).

Scale bars: 100 µm (**A-B**), 50 µm (**A'-B', A''-B''**).

3.2.6 Notch regulates *pax7a*-expressing muSC response to injury in an age independent manner

To determine if the role of Notch signalling to maintain the Pax7+ population is affected by larval age, 3 and 7 dpf *pax7a:eGFP*-expressing larvae were injured and treated with 100 µM DAPT, and the number of *pax7a:eGFP*+ muSCs were quantified at 24 hpi (Fig. 3.5). By conducting a 3-way ANOVA I found that there was a 2-way interaction between injury and drug, but not age and DAPT (Fig. 3.5I). This may reflect differences in the relative injury size and therefore obscure any age-dependent difference. Moreover, there was no 3-way interaction between injury, age and DAPT (Fig. 3.5I). This reveals that that there was no stage-dependent difference in the response of the muSCs to injury when Notch is inhibited.

To understand how DAPT affects the number of muSCs relative to age and injury, I performed a 1-way ANOVA. DAPT treatment had no effect on the number of muSC within the myotome of uninjured larvae compared to DMSO treated control animals 4 dpf (Fig. 3.5A', C', J; File. 9.1) and 8 dpf (Fig. 3.5E', G', K; File. 9.1). Contrastingly, I found that in the context of injury, larvae treated with DAPT had fewer muSCs at the site of injury compared to larvae treated with DMSO at both 4 dpf (DMSO: 14 ± 2.6, DAPT: 7.8 ± 2.7; Fig. 3.5B', D', J) and 8dpf (DMSO: 17.3 ± 6.2, DAPT: 6.3 ± 1.8; Fig. 3.5F', H', K). When comparing between developmental stages, I found that Notch inhibition did not significantly change the number of muSCs in the presence (Fig. 3.5L) or absence (Fig. 3.5M) of injury (File. 9.1). This reveals that DAPT treatment does not affect the number muSCs within the myotome, but the loss of Notch signalling prevents the expansion of the muSC population in response to injury at both 4 and 8 dpf.

3.2.7 Notch differentially regulates *pax7a*-expressing cells at the myosepta in the presence and absence of injury

Pax7-expressing muSCs within 5 dpf larvae exhibit more extensive movements compared to 3 and 7 dpf larvae whilst more cells reside at the VM and HM at 3 and 7 dpf relative to larvae at 5 dpf (Knappe *et al.*, 2015). Additionally, I found that the number of muSCs within the myosepta was influenced by the age of the larvae (Fig. 3.3). To understand if there is an interaction between the age of the larvae and the inhibition of Notch signalling on the number of muSCs within in the myosepta I

conducted a 3-way ANOVA. I found that there was an interaction effect between injury and age with DAPT treatment on the number of muSCs at the VHM but not the VM or DHM (File. 9.1). To understand how DAPT treatment affects the number of *pax7a:eGFP*+ muSC at the myosepta, I conducted a 1-way ANOVA. Surprisingly, following DAPT treatment, in an absence of injury, there were fewer muSCs within the VHM compared to DMSO treated controls at 4 dpf (DMSO: 8 ± 2.1, DAPT: 5.2 ± 1.7; File. 9.1). Following DAPT treatment, there was also a decrease in the number of muSCs at the DHM following injury at 4 dpf (uninjured: 4.8 ± 1.2, injured: 3.2 ± 0.8; File. 9.1). Additionally, there were fewer muSCs within the DHM of injured larvae which were treated with DAPT relative to DMSO treated controls at 4 dpf (DMSO: 4.7 ± 0.8, DAPT: 3.2 ± 0.8; File. 9.1). My results demonstrate that, in the absence of injury, Notch signalling is important for the maintenance of *pax7a*-expressing muSCs within the VHM but not the DHM or VM. Moreover, following injury, Notch signalling maintains *pax7a*-expressing muSCs within the DHM. These changes were observed at 3 dpf and not 7 dpf, which also suggests a developmental influence.

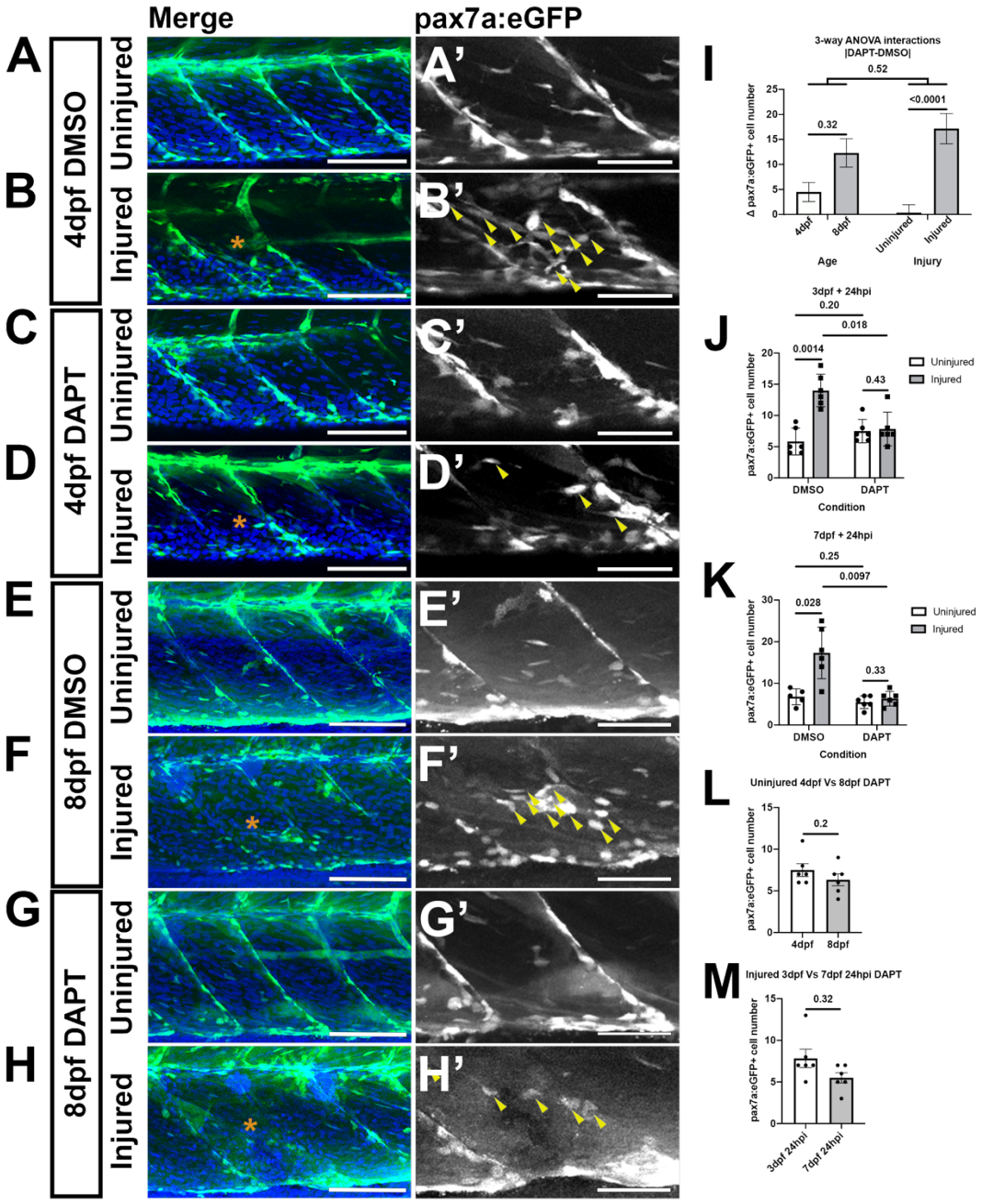
Merge
pax7a:eGFP
A
A'
4dpf DMSO
Uninjured
B
B'
Injured
C
C'
4dpf DAPT
Uninjured
D
D'
Injured
E
E'
8dpf DMSO
Uninjured
F
F'
Injured
G
G'
8dpf DAPT
Uninjured
H
H'
Injured
I
3-way ANOVA interactions
|DAPT-DMSO|
0.52
<0.0001
0.32
Δ pax7a:eGFP+ cell number
4dpf
8dpf
Uninjured
Injured
Age
Injury
J
3dpf + 24hpi
0.20
0.018
0.0014
0.43
pax7a:eGFP+ cell number
Uninjured
Injured
DMSO
DAPT
Condition
K
7dpf + 24hpi
0.25
0.0097
0.028
0.33
pax7a:eGFP+ cell number
Uninjured
Injured
DMSO
DAPT
Condition
L
Uninjured 4dpf Vs 8dpf DAPT
0.2
pax7a:eGFP+ cell number
4dpf
8dpf
M
Injured 3dpf Vs 7dpf 24hpi DAPT
0.32
pax7a:eGFP+ cell number
3dpf 24hpi
7dpf 24hpi

Figure 3.5. A loss of Notch activity attenuates the muSC response to injury.
Projections of confocal stacks of the myotome in uninjured (**A, C, E, G**) and injured (**B, D, F, H**) *pax7a:eGFP* larvae at 4 dpf (**A-D**) or 8 dpf (**E-H**). Animals were treated with 1% v/v DMSO (**A-B, E-F**) or 100 µM DAPT (**C-D, G-H**) prior to and after injury, fixed at 24 hpi and nuclei labelled with DAPI. There were more muSCs expressing eGFP (arrowheads) recruited to the injury (asterisk) in DMSO treated larvae (**B', F'**) compared to DAPT treated larvae (**D', H'**). Quantification of *pax7a:eGFP*-expressing muSCs in uninjured and injured 3 dpf and 7 dpf larvae treated with DMSO or DAPT. Tests for significant differences in muSC number due to injury, DAPT or age revealed that injury affected the number of muSCs present ($p<0.05$), but DAPT treatment nor developmental stage did ($p>0.05$, **I**). Pairwise comparisons revealed that injury-induced changes to the number of muSCs is attenuated by treatment with DAPT ($p<0.05$, **J, K**). There was no significant difference in the number of muSCs in the myotome of uninjured 4 and 8 dpf larvae treated with DAPT ($p>0.05$, **L**). Likewise, there was no difference of muSC number in the myotome of injured 4 and 8 dpf larvae treated with DAPT ($p>0.05$, **M**). Significant differences were tested by 3-way ANOVA following transformation by ART ($n=47$), and post-hoc tests performed using a Dunn's test with Benjamini and Hochberg correction. Error bars represent standard deviation, and values above comparison bars represent significance (p-values).
Scale bars: 100 µm (**A-H**), 50 µm (**A'-H'**).

3.2.8 Notch inhibition results in more *pax7a*-expressing muSCs in the absence of injury, earlier in the regeneration program

In mouse it has been shown that Notch signalling is supressed in Pax7-expressing cells shortly after injury (Bjornson *et al.*, 2012; Mourikis, Sambasivan, *et al.*, 2012). I wanted to understand if Notch signalling is important for the *pax7a*-expressing cell response to injury in zebrafish during the early stages of muscle repair. Therefore, I treated 7 dpf *pax7a:eGFP*+ larvae with DAPT and quantified the number of muSCs 8 hpi (Fig. 3.6). In order to identify if DAPT treatment affects the number of muSCs 8 hpi in the myotome or myosepta, I conducted a 2-way ANOVA. I found that DAPT treatment reduces the number of muSCs in the myotome following injury (File. 9.1). Moreover, I did not observe any affect to the number of muSCs in the myosepta following DAPT treatment. Post-hoc analysis revealed that there was no change to the number of muSCs in injured animals relative to uninjured animals in the presence of DMSO (Fig. 3.6A', B'; File. 9.1). I identified fewer muSCs in injured animals treated with DAPT compared to injured DMSO treated animals (DMSO: 10.8 ± 3.5, DAPT: 5.2 ± 2; Fig. 3.6B', D', E). In the absence of injury, I identified more muSCs within the myotome of DAPT treated animals (13.2 ± 2.4) relative to DMSO treated animals (Fig. 3.6A', C', D', E). I also detected no change to the number of muSCs at the VM, VHM or DHM by 8 hpi (File. 9.1). Altogether, these results reveals a temporal effect of Notch inhibition in the absence of injury. The number of cells were not significantly different between uninjured animals at 24 hpi within the myotome (Fig. 3.5), but were significantly different at 8 hpi (Fig. 3.6) when Notch is inhibited.

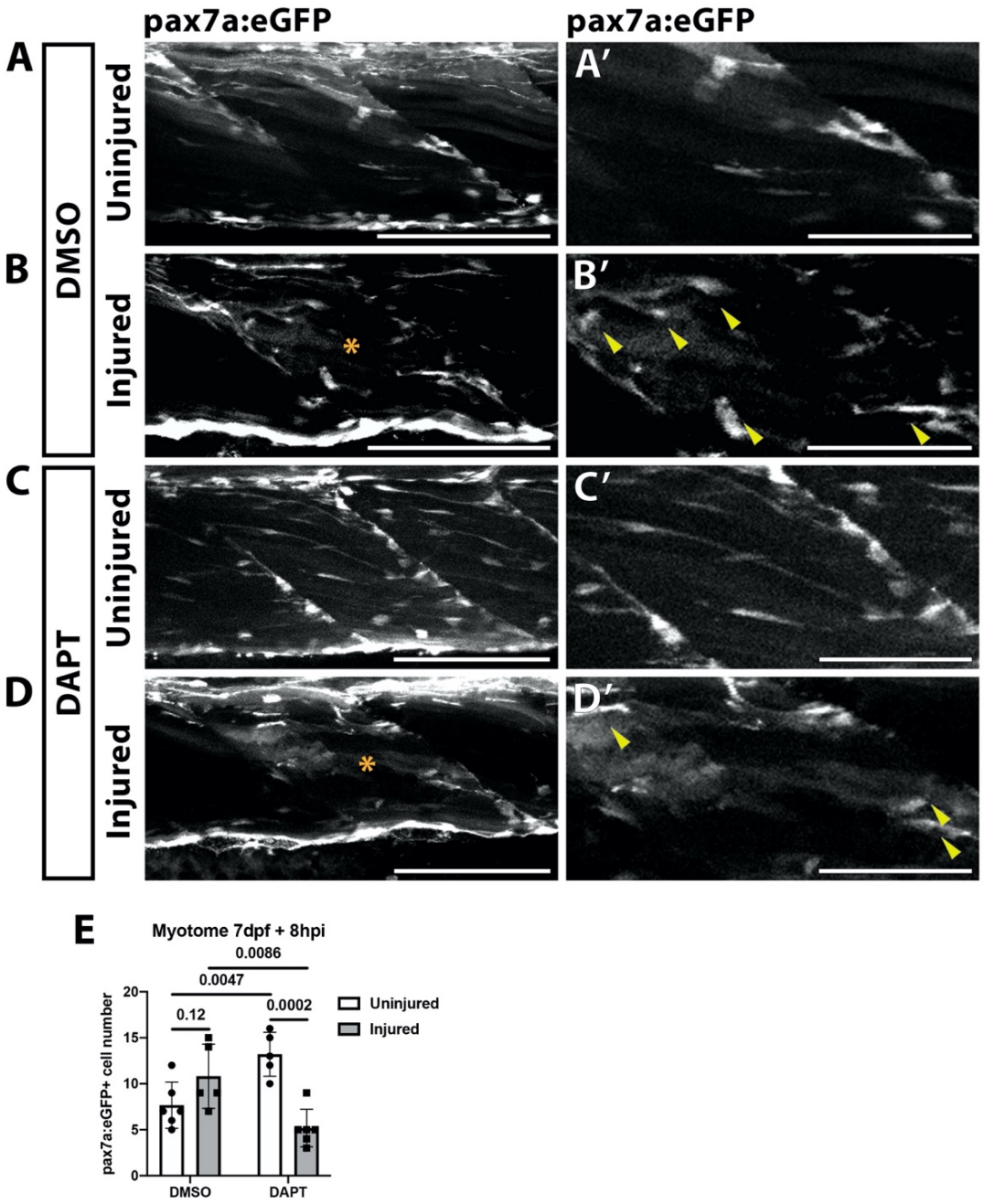

Figure 3.6. Short DAPT exposure results in more muSCs in an absence of injury.
7 dpf *pax7a:eGFP* larvae were injured in the 13th left ventral myotome and fixed 8 hpi. Projections acquired from confocal imaging of the myotome in uninjured (**A, C**) and injured (**B, D**) larvae treated with 1% v/v DMSO (**A, B**) or 100 µM DAPT (**C, D**) prior to and after injury. There were fewer eGFP+ muSCs (arrowheads) recruited to the injury (asterisk) following DAPT treatment (**D'**) compared to DMSO control animals (**B'**). Quantification of *pax7a:eGFP*-expressing muSCs in uninjured and injured larvae treated with DMSO or DAPT. Pairwise comparisons revealed that the injury-induced changes to the number of muSCs observed in control animals is lost following DAPT treatment by 8hpi ($p<0.05$, **E**). There was a significant increase in the number of muSCs in the myotome of uninjured larvae treated with DAPT compared to DMSO control animals ($p<0.05$, **E**). Significant differences were tested by post-hoc tests performed using a Dunn's test with Tukey's HSD post-hoc test. Error bars represent standard deviation, and values above comparison bars represent significance (p-values). Scale bars: 100 µm (**A-D**), 50 µm (**A'-D'**).

3.2.9 Dnsu(H) expression regulates *pax7a*-expressing muSC response to injury in zebrafish larvae

DAPT has been shown to inhibit Notch signalling (Geling *et al.*, 2002). To confirm that DAPT can inhibit Notch, I treated 3 dpf larvae with 100 µM DAPT for 18 hours. I then measured the expression of Notch target genes, *her*, in DAPT treated animals relative to DMSO treated controls by qPCR using RNA extracted from the whole larvae. I found that *her1, her2, her4.1, her6* and *her9* were downregulated following DAPT treatment of which *her2* and *her4.1* were significantly supressed within the whole zebrafish larvae (Fig. 9.2). These results suggests that DAPT partially inhibited the Notch signalling pathway. The failure to completely inhibit the expression of all Notch target genes may be due to the time of exposure. Ninov *et al.,* 2012 treated larvae with DAPT for 3 days before observing sufficient downregulation of the *Tp1*:VenusPEST transgene- a Notch reporter zebrafish line discussed in chapter 4 and 5 (Ninov *et al.*, 2012).

I have shown that treatment with DAPT results in fewer muSCs in an injury context (Fig. 3.5; Fig. 3.6). Therefore, to confirm that this phenotype results from DAPTs ability to specifically inhibit Notch, I evaluated the consequences of over-expressing a dominant negative version of the Suppressor of Hairless gene (dnSu(H); mammalian RBP-J orthologue Latimer *et al.*, 2005). A global over-expression of dnSu(H) was induced by heat-shock induction of the HS:dnSu(H) transgene in *pax7a:eGFP* larvae, and animals were injured (Fig. 3.7). To assess the effect of dnSu(H) expression on eGFP+ cell numbers I conducted a 2-way ANOVA. I found that there was an interaction effect between injury and dnsu(H) expression within the myotome and VM, and an effect of dnsu(H) expression on the number of muSCs within the VHM (File. 9.1). To understand how dnSu(H) expression affects the number of eGFP+ cell numbers I conducted a 1-way ANOVA. I found that dnsu(H) did not affect the number of *pax7a:eGFP*+ cells in the myotome of uninjured animals (Fig. 3.7A', C', E; File. 9.1), but did lead to a decrease of eGFP+ cells in injured animals compared to the wildtype siblings (WT: 14.2 ± 1.5, dnsu(H): 7.7 ± 2.8; Fig. 3.7B', D', E). I also note, there were no changes to the number of muSC within the HM (File. 9.1). Surprisingly, there was no change to the number of eGFP+ muSCs within the VM of uninjured dnsu(H) expressing larvae compared to the wildtype siblings (Fig. 3.7A'',

C’’, F; File. 9.1). This data suggest that the reduced number of eGFP+ cells observed following DAPT treatment in the injured myotome (Fig. 3.5) is a consequence of Notch signalling inhibition.

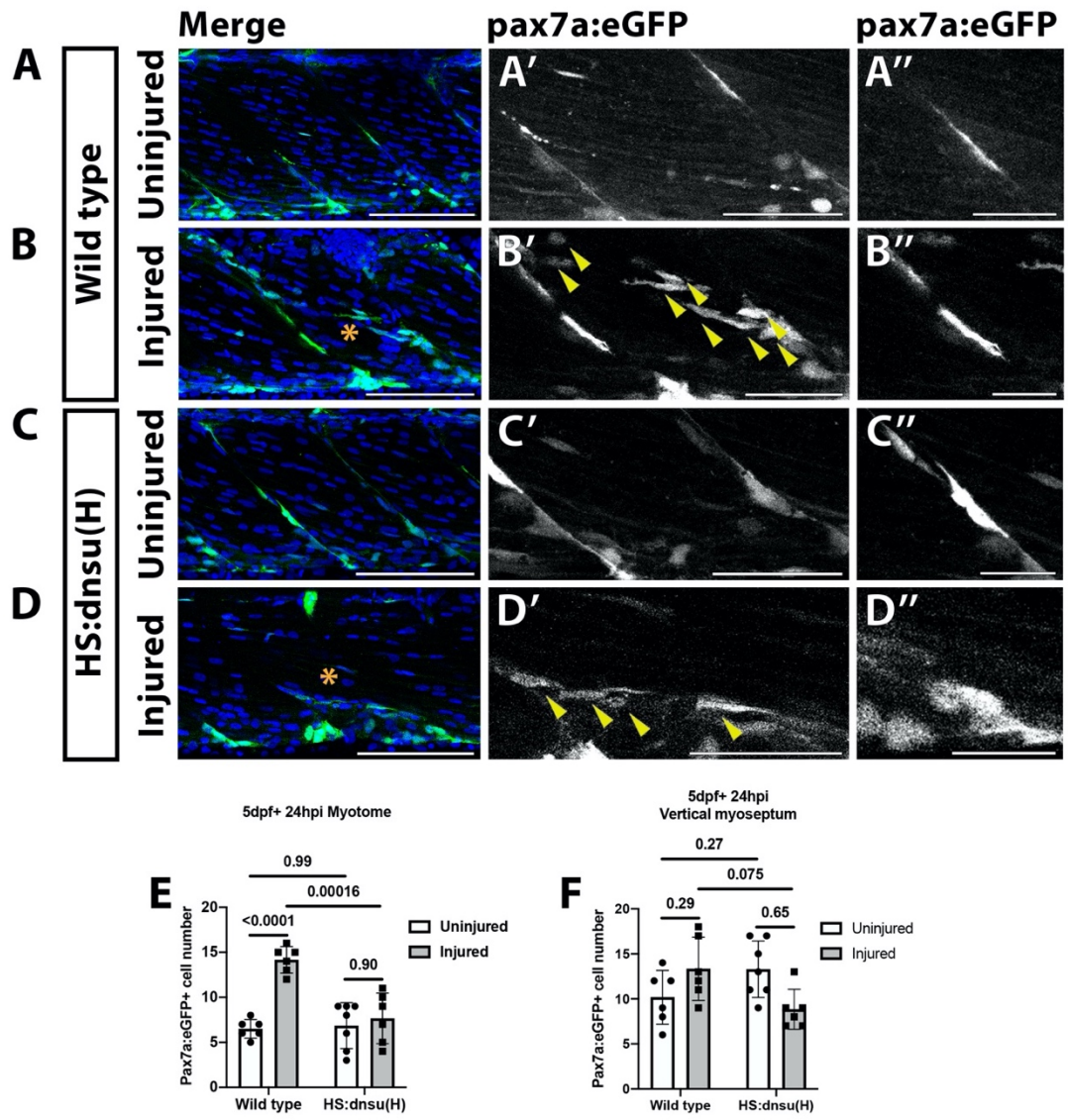

Figure 3.7. Expression of a dominant negative version of the suppressor of Hairless (dnsu[H]) results in fewer muSCs responding towards muscle injury.

Projections of confocal stacks (**A-D**) of the myotome (**A'-D'**) and vertical myoseptum (**A''-D''**) in injured 5 dpf larvae. Larvae were heat shocked for 1h, injured and fixed at 24 hpi. *pax7a:eGFP* expressing cells were detected in larvae which were wild type (**A-B**) or expressing HS:dnsu(H (**C-D**). MuSCs (yellow arrowheads) were recruited to the injury (asterisk) site (**B'-D'**). The number of cells expressing eGFP were counted in the myotome (**E**) and vertical myoseptum (**F**) of wild type and *HS:dnsu(h)* expressing larvae. Following injury, there were significantly fewer *pax7a:eGFP*+ muSCs in the presence of *dnsu(h)* compared to wild type control animals in the myotome ($p<0.05$; **E**). There were no significant changes to the number of *pax7a:eGFP* expressing cells in the vertical myoseptum ($p<0.05$; **F**). Significant differences were tested by 2-way ANOVA (n=25) with Tukey's HSD post-hoc test. Error bars display standard deviation, and values above comparison bars indicate significance (p-values).

Scale bars: 100 µm (**A-B**), 50 µm (**A'-B', A''-B''**).

3.2.10 NICD overexpression regulates *pax7a*-expressing muSC responses to injury in the vertical myoseptum of zebrafish larvae

I have shown that following the inhibition of the Notch signalling pathway by both pharmacological (DAPT; Fig. 3.5, 3.6) or genetic (HS:dnsu(H); Fig. 3.7) methods, there were fewer *pax7a:eGFP*+ muSCs within the myotome following injury 24 hpi. It has been demonstrated that the overexpression of NICD prevents myogenic cells from exiting quiescence by directly binding the promoter region of Pax7 (Yefei Wen *et al.*, 2012). Consequently, overexpression of NICD maintains proliferation (Yefei Wen *et al.*, 2012), and inhibits differentiation of MPCs (Kopan *et al.*, 1994). This suggests that that an over-activation of Notch signalling might induce elevated muSC proliferation. Therefore I aimed to examine the effects of Notch overexpression in zebrafish following muscle injury. I used a heat shock inducible expression of the Gal4 protein to globally promote the expression of the UAS:NICD transgene and therefore the overexpression of the NICD peptide (referred to as *HS:NICD*). To understand how *HS:NICD* effects the number of *pax7a:eGFP*+ muSCs 24 hpi (Fig. 3.8), I conducted a 2-way ANOVA, I observed an interaction effect between injury and NICD expression at the VM (File. 9.1). By conducting pair-wise analysis, I found that following injury there is an increase in the number of muSCs within the myotome compared to uninjured control animals, irrespective of NICD expression (wildtype [WT]- uninjured: 6.7 ± 0.8, injured: 11.7 ± 2.3; *HS:NICD*- uninjured: 6.5 ± 2, injured: 10 ± 2.5; Fig. 3.8A'-D', E). Within the VM, I detected an increase in the number of muSCs in WT animals following injury relative to control animals (uninjured: 9 ± 3, injured: 13.3 ± 2.8; Fig. 3.8A'', B'', F). Contrastingly there was no change to the number of *pax7a*-expressing muSCs in response to injury following NICD overexpression (Fig. 3.8C'', D'', F; File. 9.1). I found no change in the number of muSCs in the HM (File. 9.1). Overall, these data suggest that, although Notch inhibition results in the attenuation of the muSC response within the myotome following injury, the overexpression of the NICD peptide does not lead to more muSCs responding to injury.

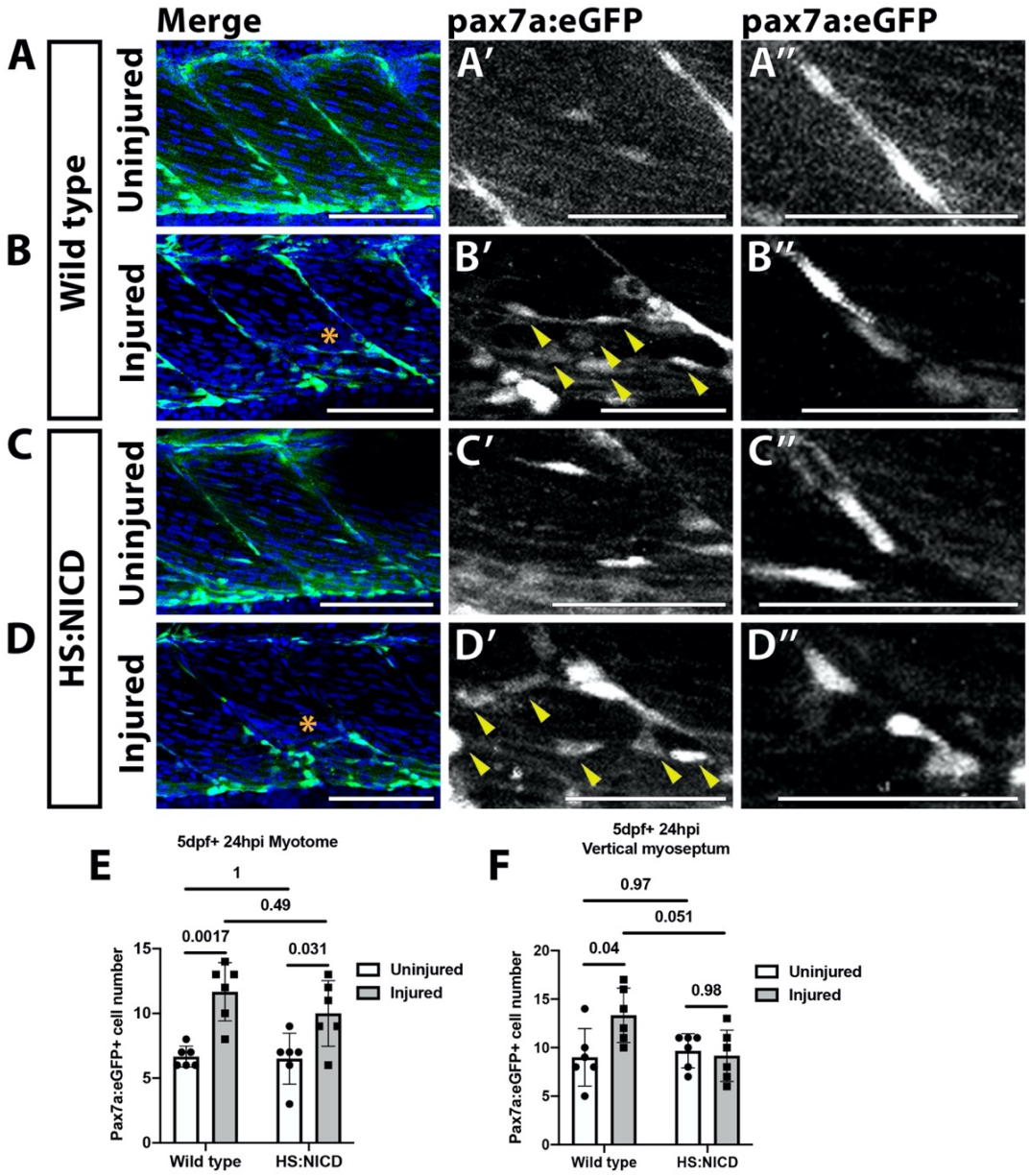

Figure 3.8. Overexpression of NICD result in fewer muSCs within the vertical myoseptum following injury.

Z-projections were generated from confocal stacks (**A-D**) of the myotome (**A'-D'**) and vertical myoseptum (**A''-D''**) in uninjured (**A, C**) and injured (**B, D**) 5 dpf larvae. Larvae were heat-shocked for 1 hour, injured and fixed 24 hpi. *pax7a:eGFP* expressing cells were detected in wild type larvae (WT; **A-B**) or larvae expressing heat shock Gal4 with UAS NICD (*HS:NICD*; **C-D**). Yellow arrowheads highlight recruited eGFP+ muSCs at the site of injury (asterisk; **B'-D'**). eGFP+ cells were counted in the myotome (**E**) and vertical myoseptum (**F**) of wild type and *HS:NICD* expressing larvae. Following injury, there were significantly more muSCs in the myotome of both *HS:NICD* expressing and WT larvae ($p<0.05$; **E**). In the vertical myoseptum, there was a significant increase in the number of *pax7a:eGFP*-expressing cells in WT larvae, but not in the *HS:NICD* expressing larvae ($p>0.05$; **F**). Significant differences were tested by post-hoc tests performed using a Dunn's test with Tukey's HSD post-hoc test. Error bars represent standard deviation, and values above comparison bars represent significance (p-values).

Scale bars: 100 µm (**A-B**), 50 µm (**A'-B', A''-B''**).

3.2.11 Notch inhibition reduces muSC proliferation in the myotome following injury

In mammals, the loss of the Pax7+ population has been associated with a loss of proliferation (Bjornson *et al.*, 2012; Mourikis, Sambasivan, *et al.*, 2012). Therefore, the failure of the muSC population to expand in response to injury in the presence of DAPT could reflect this requirement for Notch in regulating proliferation. To understand if proliferation is reduced in the absence of Notch in zebrafish, I measured BrdU incorporation in *pax7a:eGFP* expressing muSCs in the myotome 24 hpi in the presence of DAPT (Fig. 3.9). Following a 2-way ANOVA, I found that injury causes a significant increase in the number of proliferating muSCs as previously described (Knappe *et al.*, 2015; File. 9.1). In contrast, DAPT treatment significantly reduced the number of muSCs incorporating BrdU (File. 9.1). There was also a significant interaction effect between injury and DAPT treatment, suggesting that DAPT alters the proliferative muSC response to injury (File. 9.1).

To understand how DAPT affects the number of proliferating muSCs in response to injury, I conducted a 1-way ANOVA. I found that there were very few proliferating muSCs in uninjured larvae (DMSO: 2.5 ± 1.4; DAPT: 2.5 ± 1.6; Fig. 3.9A', C'). In injured larvae there was an increased number of proliferating muSCs compared to uninjured control larvae treated with either DMSO or DAPT (Fig. 3.9A'-D', G). There was a significant reduction in the number of proliferating muSCs in injured larvae treated with DAPT (5.2 ± 2.6) compared to those treated with DMSO (9.8 ± 3.5; Fig. 3.9B', D', G). However, this result did not reflect a change to the relative proportion of proliferating *pax7a:eGFP*-expressing cells within the myotome (Fig. 3.9H; File. 9.1), but is rather due to a decrease in the overall number of Pax7+ muSCs present (DMSO: 14.7 ± 4.5, DAPT: 7.2 ± 1.8; Fig. 3.9E).

3.2.12 Notch regulates muSC proliferation in the vertical myoseptum in an absence of injury

To determine whether Notch regulates muSCs at the myosepta I quantified *pax7a:eGFP*-expressing muSCs at the VM, conducting a 2-way ANOVA. I found that DAPT treatment affects the number of *pax7a:eGFP*+ muSCs at the VM relative to injury (File. 9.1). In order to understand the effects of Notch inhibition on this population of cells, I conducted a 1-way ANOVA. I identified few proliferating muSCs within the VM of uninjured animals treated with DMSO (2.8 ± 1.5; Fig. 3.9A''), which

did not change following injury (Fig. 3.9B'', K; File. 9.1). In the presence of DAPT, there was a significant increase in the number of proliferating muSCs in the myoseptum of uninjured larvae (6.5 ± 1.76) relative to DMSO treated animals (2.8 ± 1.5; Fig. 3.9 A'', C'', K). There was no significant difference of muSC proliferation at the vertical myosepta in injured animals in the presence of DAPT compared to DMSO treated control animals (Fig. 3.9B'', D'', K; File. 9.1). These data enforces the observation that Notch signalling plays a contextual role, promoting proliferation in the myotome following injury, and limiting proliferation in the VM in the absence of injury.

The HM has been described as the niche of low-cycling pax3a-expressing progenitor cells (Nguyen *et al.*, 2017). Therefore, I next assessed the proliferation of muSCs at the HM. Pair-wise comparisons reveal that only a few *pax7a:eGFP*-expressing cells with BrdU incorporation were detected at the HM (2 ± 1.1) which did not change following injury or DAPT treatment (File. 9.1). This may be a reflection of the low-cycling nature of the muSCs within the HM.

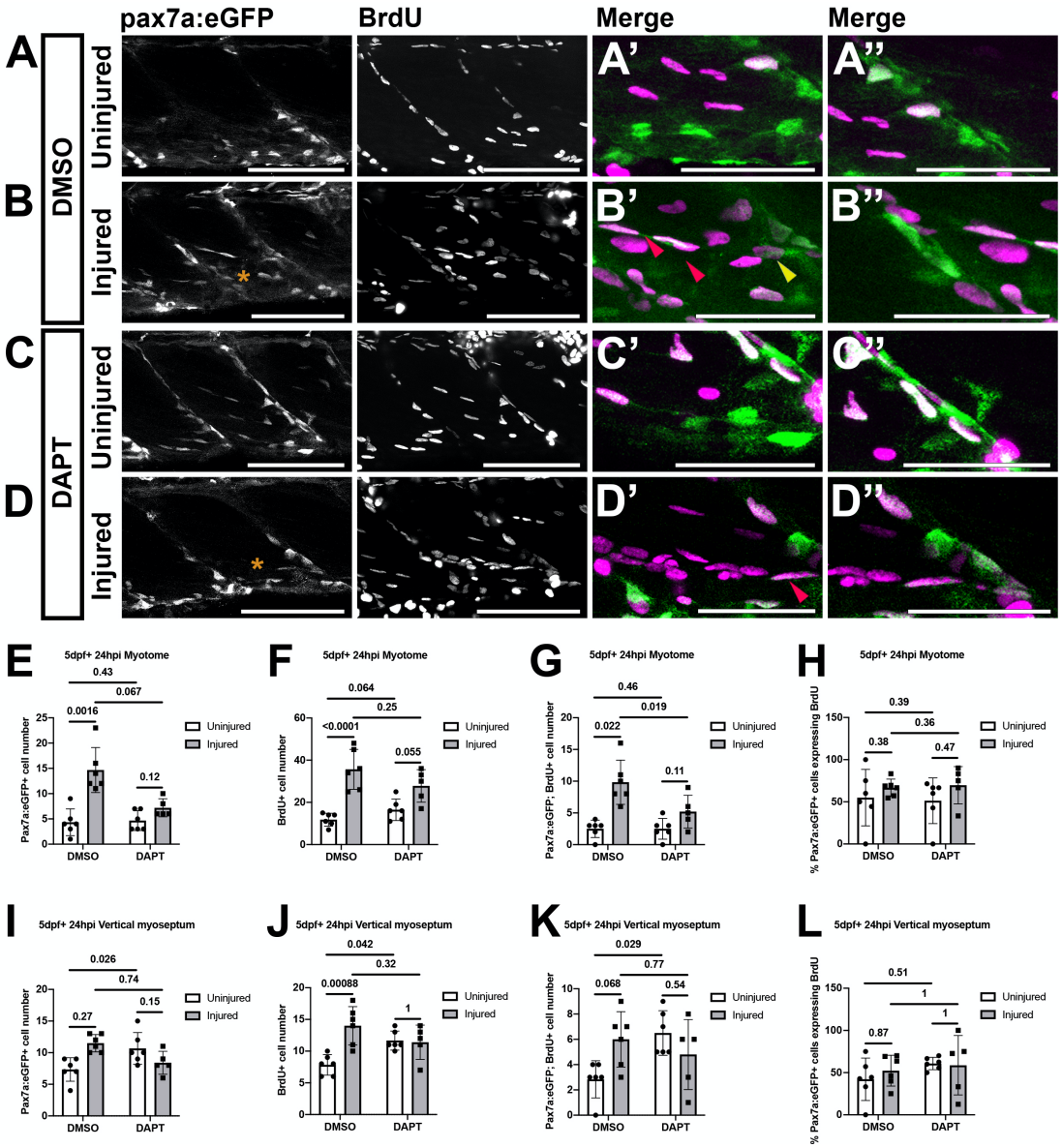
pax7a:eGFP
BrdU
Merge
Merge
A
B
C
D
DMSO
DAPT
Uninjured
Injured
A'
A''
B'
B''
C'
C''
D'
D''
E
5dpf+ 24hpi Myotome
Pax7a:eGFP+ cell number
0.43
0.067
0.0016
0.12
F
5dpf+ 24hpi Myotome
BrdU+ cell number
0.064
0.25
<0.0001
0.055
G
5dpf+ 24hpi Myotome
Pax7a:eGFP; BrdU+ cell number
0.46
0.019
0.022
0.11
H
5dpf+ 24hpi Myotome
% Pax7a:eGFP+ cells expressing BrdU
0.39
0.36
0.38
0.47
I
5dpf+ 24hpi Vertical myoseptum
Pax7a:eGFP+ cell number
0.026
0.74
0.27
0.15
J
5dpf+ 24hpi Vertical myoseptum
BrdU+ cell number
0.042
0.32
0.00088
1
K
5dpf+ 24hpi Vertical myoseptum
Pax7a:eGFP; BrdU+ cell number
0.029
0.77
0.068
0.54
L
5dpf+ 24hpi Vertical myoseptum
% Pax7a:eGFP+ cells expressing BrdU
0.51
1
0.87
1
Uninjured
Injured
DMSO
DAPT

Figure 3.9. Proliferation of muSCs during regeneration and homeostasis is Notch dependent.

Projections of confocal stacks (**A-D**) of the myotome (**A'-D'**) and vertical myoseptum (**A''-D''**) in uninjured (**A, C**) and injured (**B, D**) 5 dpf *pax7a:eGFP* larvae incubated with BrdU for 24 hours. Larvae were treated with 1% v/v DMSO (**A-B**) or 100 µM DAPT (**C-D**) after injury and detection of BrdU and eGFP was performed by immunolabelling. MuSCs with (red arrowheads) and without BrdU labelling (yellow arrowheads) were recruited to the injury (asterisk) site (**B', D'**). The number of cells expressing eGFP (**E, I**), incorporating BrdU (**F, J**) or both (**G, K**) were counted in the myotome (**E-G**) and vertical myoseptum (**I-K**) of animals treated with DMSO or DAPT. The proportion of eGFP+ muSCs incorporating BrdU was calculated for both myotome (**H**) and vertical myoseptum (**L**). There were significantly fewer GFP+ muSCs incorporating BrdU after injury in the presence of DAPT compared to DMSO treated control animals ($p<0.05$; **G**). There was no significant change to the number of GFP+ muSCs incorporating BrdU at the vertical myoseptum of injured animals in the presence of DAPT ($p>0.05$; **K**). In contrast, although there were only few cells present, there was a significant increase in the number of muSCs with BrdU labelling at the myoseptum in uninjured animals in the presence of DAPT ($p<0.05$; **K**). Significant differences were tested by 2-way ANOVA (n=23) with Tukey's HSD post-hoc test or by transforming data by ART and performing 2-way ANOVA followed by a Dunn's test with Benjamini and Hochberg correction. Error bars display standard deviation, and values above comparison bars indicate significance (p-values).

Scale bars: 100 µm (**A-D**), 50 µm (**A'-D', A''-D''**).

3.2.13 Notch inhibition results in an increase in the proportion of differentiating muSC in the myotome following injury

In mice, knockdown of Notch in muSCs results in them differentiating in a premature S-phase independent manner following muscle injury (Bjornson *et al.*, 2012; Mourikis, Sambasivan, *et al.*, 2012). To examine if Notch inhibition leads to premature differentiation of muSCs in zebrafish, I assessed the number of Myogenin (Myog) expressing muSCs in the myotome of larvae treated with DAPT 24hpi (Fig. 3.10). Results from a 2-way ANOVA highlight that injury and DAPT treatment did not alter the number of muSCs expressing Myogenin (Myog) (File. 9.1). However, when I tested for changes to the proportion of muSCs expressing Myog, I observed that there was a significant interaction effect between injury and DAPT (File. 9.1).

By comparing between uninjured *pax7a:eGFP*-expressing larvae treated with or without DAPT, I found that there were few Myog expressing muSCs within the myotome of uninjured larvae (3.7 ± 1.8) which did not change following Notch inhibition (3.2 ± 0.8; Fig. 3.10A', C', G). Although I detected an increase in the number of total Myog expressing cells following injury relative to uninjured controls (uninjured: 5.2 ± 1.7, injured: 9.3 ± 3.1; Fig. 3.10A', B', F), there was no change to the number of eGFP+ muSCs expressing Myog (Fig. 3.10G; File. 9.1). When comparing injured animals in the absence on Notch, I found that inhibition of Notch did not alter the number of muSCs expressing Myog after injury (Fig. 3.10C', D', G; File. 9.1). I noted that there are fewer *pax7a:eGFP* expressing muSCs in the myotome of injured animals when Notch is inhibited (DMSO: 21.3 ± 4.2, DAPT: 9 ± 1.9; Fig. 3.10B', D', G). Therefore, I examined whether the proportion of eGFP+ muSCs expressing Myog was altered by addition of DAPT. I found that the proportion of eGFP+ cells expressing Myog significantly increased in the absence of Notch signalling (DMSO: 15 ± 14.4%, DAPT: 47.4 ± 13.4%; Fig. 3.10H). This reveals that inhibition of Notch signalling both reduces the number of proliferating muSCs and results in a higher proportion of muSCs undergoing differentiation in the context of injury.

3.2.14 Notch inhibition regulates myogenic cell differentiation at the vertical myoseptum

Previously, I had shown that the proliferation of muSCs at the VM is regulated by Notch signalling in the absence of injury (Fig. 3.9). To determine if Notch inhibition

leads to a premature differentiation of muSCs within their niche, I quantified the number of muSCs expressing Myog at the VM of uninjured animals in the presence of DAPT (Fig. 3.10). Results from a 2-way ANOVA reveals an interaction between injury and DAPT treatment on eGFP+ and Myog+ cells but not eGFP+Myog+ cells at the VM (File. 9.1). I could not detect eGFP+Myog+ cells at the VM of uninjured animals. Following post-hoc tests, I found that the number of eGFP+Myog+ cells did not change in the presence of DAPT (Fig. 3.10A'', C'', K; File. 9.1). There was an increase in the total number of Myog+ cells at the VM in uninjured animals in response to DAPT treatment (DMSO: 0.5 ± 0.6, DAPT: 2 ± 1.1; Fig. 3.10J). This increased number of Myog+ cells resulting from DAPT treatment was not different between uninjured and injured animals (Fig. 3.10C'', D'', J; File. 9.1). I note there was no change to the number (Fig. 3.10K) or percentage (Fig. 310L) of eGFP+Myog+ in response to DAPT treatment (File. 9.1). This suggests there are other myogenic cells within the VM that undergo a premature differentiation in the absence of Notch activity in an injury-independent manner. I had shown that there was no change to the proliferation of the slow-cycling cells found within the HM. I now also observed very few cells showing Myog immunoreactivity at the HM in uninjured or injured animals and this did not change significantly in the presence of DAPT (File. 9.1).

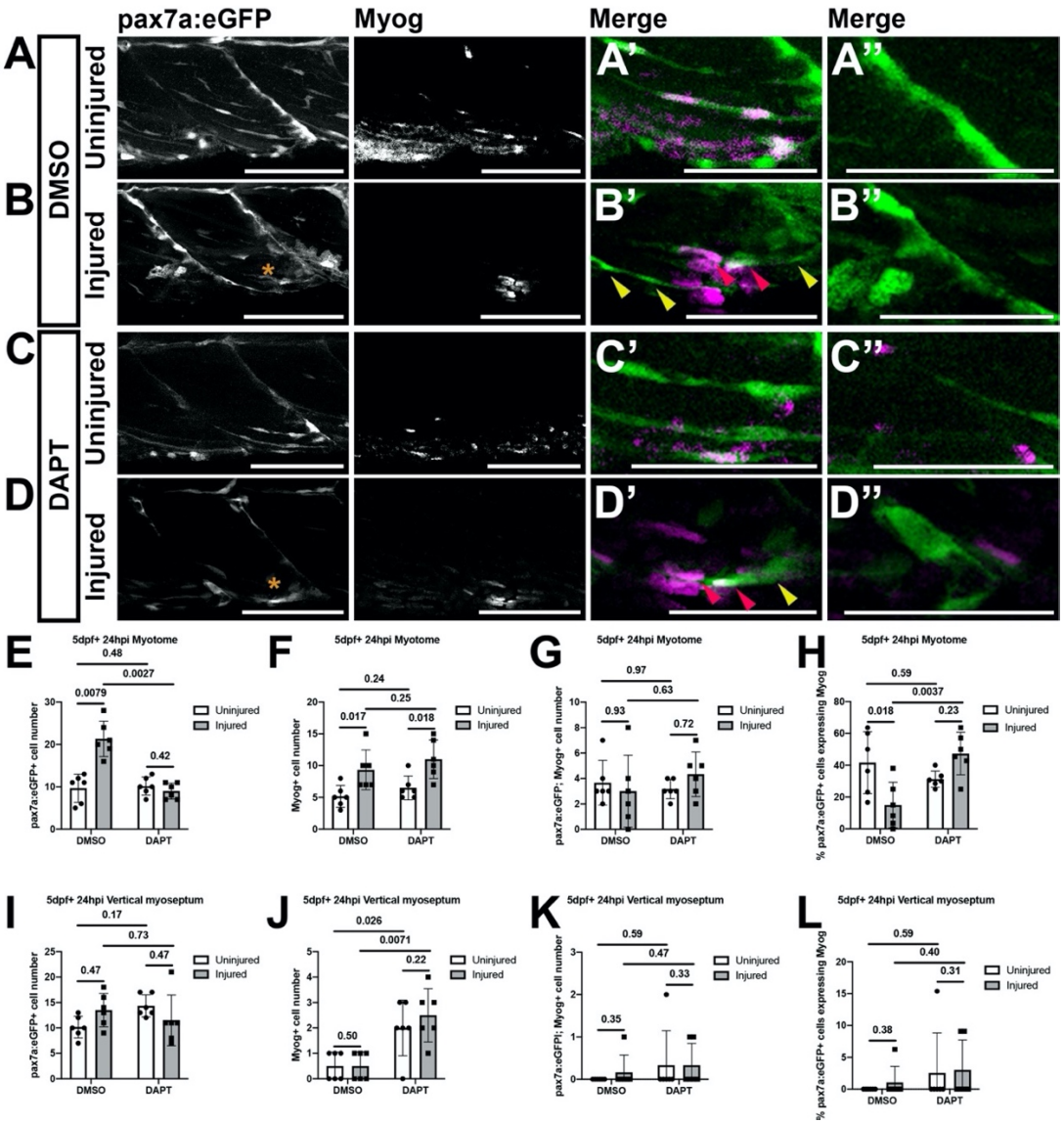

Figure 3.10. Inhibition of Notch signalling results in an increased differentiation of muSCs responding to injury.

Projections of confocal stacks (**A-D**) of the myotome (**A'-D'**) and vertical myoseptum (**A''-D''**) of 5 dpf *pax7a:eGFP* larvae treated with 1% v/v DMSO (**A-B**) or 100µM DAPT (**C-D**) prior to (**A, C**) and after injury (**B, D**), fixed at 24 hpi and labelled with anti-Myogenin. *pax7a:GFP* expressing muSCs with (red arrowheads) and without Myogenin labelling (yellow arrowheads) were recruited to the injury (asterisk) site (**B', D'**). Quantification of eGFP+ muSCs (**E, I**), Myogenin expressing cells (**F, J**) and co-labelled cells (**G, K**) in the myotome (**H-G**) and vertical myoseptum (**I-K**) revealed no significant difference in the number of muSCs expressing Myogenin in DAPT treated compared to DMSO treated animals ($p>0.05$, **G, K**). Examination of the proportion of eGFP+ muSCs expressing Myogenin in the myotome (**H**) and vertical myoseptum (**L**) revealed a significantly increase in those expressing Myogenin in the presence of DAPT following injury in the myotome ($p<0.05$, **H**). Significant differences were tested by 2-way ANOVA (n=24) with Tukey's HSD post-hoc test or by transforming data by ART and performing 2-way ANOVA followed by a Dunn's test with Benjamini and Hochberg correction. Errors bars display standard deviation and values above bars indicate significance (p-values).

Scale bars: 100µm (**A-D**), 50µm (**A'-D', A''-D''**).

3.2.15 High power when detecting changes to muSC number in response to injury in zebrafish

My results have shown that there are more *pax7a*-expressing muSCs in the myosepta in 8 dpf larvae compared to 4 dpf (File. 9.1). Although I have observed this increase, I fail to consistently detect significance differences between multiple datasets. Moreover, I do not detect significant changes when assessing the number of muSCs in the myotome between uninjured samples following drug treatment. It is possible that these discrepancies are due to low cell counts and the variability between animals lowering the power of analysis.

The power of the test and the ideal sample size needed to achieve 80% power is calculated with respect to the probability of a type I and type II error (Banerjee *et al.*, 2009). A type I error, also referred to as α, is the probability of rejecting the null hypothesis when the null hypothesis is true (false positive; Banerjee *et al.*, 2009). A type II error, also referred to as beta (β), is the probability of accepting the null hypothesis when the null hypothesis is false (false negative; Banerjee *et al.*, 2009). Therefore, as the power is the probability of rejecting the null hypothesis when the null hypothesis is false, the power can be defined as the probability of not making a type II error (1-β). I aimed to determine if variables such as injury, developmental stage, and inhibition of Notch affect the power of analysis when determining differences to muSC number within the myotome (Table. 3.1-3.3) and myosepta (Table. 3.4).

A comparison of data generated from the myotome of animals at different stages that were injured or uninjured showed a normal distribution with equal variance (Fig. 9.1). In contrast, when assessing the number of muSC in the myotome of animals exposed to DMSO or DAPT showed a non-normal distribution with equal variance (Fig. 9.1). The power is influenced by multiple factors, including the variability of the data, effect size, alpha (α) level and sample size. Therefore, I used the data generated (Table. 9.1) to calculate the effect size, CI, the probability of making a type I error (α, represented by the p-value) and, power (β). Additionally, I identify a sample size needed to achieve a power of 80% at an α level of 0.05.

When investigating the number of muSCs between uninjured and injured samples at 4 dpf and 8 dpf, I found that the power was 95.6-99.9%. This is reflected in the low p-value, non-overlapping CIs and large effect size (Table. 3.1). I also found that comparisons between injured samples at 4 dpf and 8 dpf achieved a higher power (97.4%). Contrastingly, when comparing uninjured 4 dpf to uninjured 8 dpf larvae, due to overlapping CIs and a high p-value, the power of analysis was only 24.9% (Table. 3.1). Although it may be possible to measure a significant difference between uninjured animals using 25 larvae, increasing the sample size would increase the probability of a type I error. The low power achieved when comparing uninjured datasets and the need to use many samples to discriminate differences between these stages suggests there is either considerable heterogeneity between samples or little difference in the number of muSCs between larval stages. I then evaluated the sample size needed for identifying differences in the presence of an injury. I found that using a sample size of n=4 is sufficient to discriminate differences (Table. 3.1).

Comparison	Statistical test	95% CI	Effect size	p-value	Power (%)	Ideal sample size (n)
4 dpf uninjured	Student's t-test	3.91, 7.09	3.63	0.00009	99.98	3
4 dpf injured		9.72, 13.62				
8 dpf uninjured	Student's t-test	3.43, 13.24	2.36	0.0022	95.64	5
8 dpf injured		14.6, 19.8				
4 dpf uninjured	Student's t-test	3.91, 7.09	0.82	0.19	24.86	25
8 dpf uninjured		3.43, 13.24				
4 dpf injured	Student's t-test	9.71, 13.62	2.51	0.0015	97.35	4
8 dpf injured		14.6, 19.8				

Table 3.1. Calculation of statistical power for comparing the number of muSCs in 4 and 8 dpf zebrafish larvae after muscle injury.

Power analysis comparing cell numbers obtained from uninjured and injured zebrafish larvae at 4 and 8 dpf. Data is parametric and homoscedastic, therefore a Student's t-test was used to calculate the 95% confidence interval (CI), p-value, power and ideal samples size (at 80% power). Effect size was calculated using Cohen's d. The sample size calculated has been rounded up to the nearest whole number and is per group (N*0.5).

3.2.16 High power when detecting changes to muSC number following Notch inhibition in response to injury in zebrafish

Next, I aimed to understand how DAPT treatment affects the power of analysis when determining differences to muSC number. I found that when comparing uninjured to injured larvae in the presence of DMSO at 4 dpf (Table. 3.2) or 8 dpf (Table. 3.3) I obtained a power >99.99%, a reflection of a low p-value, non-overlapping CIs and large effect size. I found that fewer muSCs were observed in the injured myotome following DAPT treatment, which increases the effect size. Therefore, when comparing injured 4 dpf (Table. 3.2) or 8 dpf (Table. 3.3) larvae treated with DMSO and DAPT, the power of analysis was >99.99%. Contrastingly, when comparing DMSO and DAPT treated animals in the absence of injury, the power of analysis was low (4dpf: 39.2%, 8dpf: 21.4%). To determine statistically significant differences to the number of muSCs between uninjured larvae treated with DMSO or DAPT at a power of 80%, 23 and 26 zebrafish larvae would need to be quantified at 4 dpf and 8 dpf, respectively. Contrastingly, to identify differences in the number of muSCs in DAPT treated compared to control animals in the presence of an injury, only n=5 and n=4 animals are needed at 4 dpf (Table. 3.2) and 8 dpf (Table. 3.3), respectively.

Comparison	Statistical test	90% CI	Effect size	p-value	Power (%)	Ideal sample size (n)
4 dpf uninjured DMSO	WMW test	4, 8	3.43	0.0049	>99.99	3
4 dpf injured DMSO		11, 18				
4 dpf uninjured DAPT	WMW test	6, 9	0.14	0.87	60.00	699
4 dpf injured DAPT		6, 10				
4 dpf uninjured DMSO	WMW test	4, 8	0.83	0.20	39.20	23
4 dpf uninjured DAPT		6, 9				
4 dpf injured DMSO	WMW test	11, 18	2.32	0.015	>99.99	5
4 dpf injured DAPT		6, 10				
4 dpf uninjured DMSO	WMW test	4, 8	0.82	0.25	26.10	29
4 dpf injured DAPT		6, 10				
4 dpf uninjured DAPT	WMW test	6, 9	2.86	0.0062	>99.99	3
4 dpf injured DMSO		11, 18				

Table 3.2. Calculation of statistical power for comparing the number of muSCs after muscle injury in 4 dpf zebrafish larvae in the presence of DAPT.

Power analysis comparing cell numbers obtained from uninjured and injured 4 dpf zebrafish larvae which were treated with DMSO or DAPT. Data is non-parametric and homoscedastic, therefore a Wilcoxon Mann Whitney U rank sum test was used to calculate the 90% confidence interval (CI), p-value, power and ideal samples size (at 80% power). Effect size was calculated using Cohen's d. The sample size calculated has been rounded up to the nearest whole number and is per group (N*0.5).

Comparison	Statistical test	90% CI	Effect size	p-value	Power (%)	Ideal sample size (n)
8 dpf uninjured DMSO	WMW test	4, 9	2.30	0.017	>99.99	5
8 dpf injured DMSO		8, 9				
8 dpf uninjured DAPT	WMW test	4, 7	0.51	0.51	5.3	77
8 dpf injured DAPT		5, 8				
8 dpf uninjured DMSO	WMW test	4, 9	0.75	0.27	21.40	26
8 dpf uninjured DAPT		4, 7				
8 dpf injured DMSO	WMW test	8, 25	2.42	0.0081	>99.99	4
8 dpf injured DAPT		5, 8				
8 dpf uninjured DMSO	WMW test	4, 9	0.25	0.71	18.20	181
8 dpf injured DAPT		5, 8				
8 dpf uninjured DAPT	WMW test	4, 7	2.63	0.0049	>99.99	3
8 dpf injured DMSO		8, 25				

Table 3.3. Calculation of statistical power for comparing the number of muSCs after muscle injury in 8 dpf zebrafish larvae in the presence of DAPT.

Power analysis comparing cell numbers obtained from uninjured and injured 8 dpf zebrafish larvae which were treated with DMSO or DAPT. Data is non-parametric and homoscedastic, therefore a Wilcoxon Mann Whitney U rank sum test was used to calculate the 90% confidence interval (CI), p-value, power and ideal samples size (at 80% power). Effect size was calculated using Cohen's d. The sample size calculated has been rounded up to the nearest whole number and is per group (N*0.5).

3.2.17 Variable power when detecting changes to muSC number in the myosepta

Relative to the myotome, the myosepta contains very few muSCs, often showing insignificant changes towards injury and DAPT treatment. Therefore, I aimed to understand how DAPT treatment affects the number of muSC at the VM, HVM, and DHM. I calculated the power and sample size needed to achieve 80% power at an alpha level of 0.05 across 3 different datasets (Table. 3.4). I observed large variability in the power of analysis between datasets when testing for differences in muSC number in response to injury and Notch inhibition at myosepta. Consequently, the number of animals needed to measure changes to muSC number in the myosepta, differs greatly between experiments. 18 ± 10 animals are needed to identify differences in muSC number in VM of uninjured and injured animals following DAPT treatment. Whereas in the DHM, 38 ± infinite (statistically indistinguishable) animals are needed (Table. 3.4). The variable power of analysis and animals needed to detect significant change in muSC number are a consequence of small cell number within the myosepta and effect sizes between conditions. This highlights the difficulties when detecting differences in *pax7a:eGFP*-expressing cell number at the myosepta.

Comparison	Power				Average power	Average Ideal sample size
	Dataset 1		Dataset 2	Dataset 3		
	3 dpf	7 dpf	5 dpf	5 dpf		
VM: Uninjured DMSO	36%	10%	29%	47%	31% ± 16%	44 ± 51
VM: Injured DMSO						
VM: Uninjured DAPT	64%	47%	82%	21%	54% ± 26%	18 ± 10
VM: Injured DAPT						
VM: Uninjured DMSO	34%	11%	98%	86%	57% ± 42%	20 ± 19
VM: Uninjured DAPT						
VM: Injured DMSO	11%	22%	12%	12%	14% ± 5%	50 ± 20
VM: Injured DAPT						
VHM: Uninjured DMSO	>99%	61%	15%	10%	46% ± 42%	39 ± 37
VHM: Injured DMSO						
VHM: Uninjured DAPT	90%	16%	22%	5%	33% ± 38%	632 ± 920
VHM: Injured DAPT						
VHM: Uninjured DMSO	95%	89%	7%	7%	50% ± 49%	527 ± 693
VHM: Uninjured DAPT						
VHM: Injured DMSO	39%	46%	7%	21%	28% ± 18%	159 ± 174
VHM: Injured DAPT						
DHM: Uninjured DMSO	12%	79%	7%	8%	27% ± 35%	398 ± 502
DHM: Injured DMSO						
DHM: Uninjured DAPT	>99%	16%	18%	55%	47% ± 39%	75 ± 94
DHM: Injured DAPT						
DHM: Uninjured DMSO	6%	>99%	5%	5%	29% ± 47%	2529 ± 2733
DHM: Uninjured DAPT						
DHM: Injured DMSO	>99%	>99%	9%	65%	68% ± 42%	38 ± Infinite
DHM: Injured DAPT						

Table 3.4. Variable power when assessing changes to *pax7a:eGFP*+ muSCs in response to injury and notch inhibition within the myosepta.

Power analysis comparing cell numbers obtained from uninjured and injured zebrafish larvae which were treated with DMSO or DAPT. *pax7a:eGFP*+ cell counts obtained in Fig. 3.3 (dataset 1), Fig. 3.9 (dataset 2) and Fig. 3.10 (dataset 3) from the vertical myoseptum (VM), ventral horizontal myoseptum (VHM) and dorsal horizontal myoseptum (DHM) were used to calculate power and sample size needed to obtain 80% power (ideal sample size). Average power and ideal samples size have been reported with standard deviation.

3.3 Discussion

Studies investigating muSC response towards muscle injury use blunt tools, such as CTX injection or 30g needle, to induce injuries spanning multiple myotome without accounting for the variability between injuries (Seger *et al.*, 2011; Gurevich *et al.*, 2016; Pipalia *et al.*, 2016; Nguyen *et al.*, 2017; Ratnayake *et al.*, 2021). It has been shown that the extent of the injury affects the activity of immune cells (Niethammer *et al.*, 2009) and muSCs (Knappe *et al.*, 2015) in zebrafish. Therefore, it is important to standardise a reproducible injury method to study the effect of defined variables on muSC activity. In this chapter I investigated the reproducibility of the needlestick injury as a method to conduct single myotome injuries in zebrafish larvae. By live imaging *pax7a:eGFP*-expressing larvae following injury I was able to quantify the number of responding muSCs over time. I found that more *pax7a:eGFP*-expressing muSCs were recruited to larger injuries. I note that it is difficult to extrapolate the correlation between injury size and muSC response to larger injuries, as 4/5 of the injuries were small. Overall, I found that the needlestick injury is highly reproducible showing little variability (7% ± 5%).

Between 3-7 dpf, zebrafish larval muscle undergoes substantial structural changes, during which muSCs populate the ECL and deeper myotome regions (Hollway *et al.*, 2007; Roy *et al.*, 2017), migrating and proliferating less as the larva develops (Seger *et al.*, 2011; Knappe *et al.*, 2015; Nguyen *et al.*, 2017). Moreover, it has been shown in mouse that Notch signalling is important for successful muscle repair (Kopan *et al.*, 1994; Bjornson *et al.*, 2012; Mourikis, Sambasivan, *et al.*, 2012; Yefei Wen *et al.*, 2012). Therefore, using the needlestick injury method, I investigated the effect of variables injury, age and Notch inhibition on the *pax7a:eGFP*-expressing muSC response in zebrafish. Moreover, I considered cells which are in the myotome and myosepta separately as these cells may be influenced by different molecular mechanisms (Nguyen *et al.*, 2017). I defined three separate myosepta compartments: VM, VHM and DHM.

3.3.1 Myotome

Initially, I wanted to understand whether the developmental stage of the zebrafish affects the muSC response to injury. By injuring 4 and 8 dpf larvae and fixing them 24

hpi, I found that there were more cells at the site of injury relative to uninjured control animals. Although there were no differences between uninjured animals, I found that following injury there are more muSCs in older (8 dpf) compared to younger (4 dpf) larvae. Knappe *et al.,* (2015) describes a failure to recruit muSCs towards small myotome injuries (Knappe *et al.*, 2015). As the injuries performed on animals at 3 and 7 dpf were of comparable size, the relative injury size is smaller in older animals and so, may not promote the same degree of response by the muSC population. The increase in the number of muSCs from 4 to 8 dpf larvae may be associated with the hypoplastic growth of the myotome and subsequent recruitment of muSC towards the injury (Hinits *et al.*, 2011).

I investigated the effect of Notch inhibition on the number on the muSC response to injury. To do so, I used 100 µM DAPT to inhibit Notch signalling (Geling *et al.*, 2002). I found that by 24hpi there are fewer Pax7+ muSCs within the injured myotome. To understand if this phenotype is influenced by the age of the zebrafish, I treated both 3 and 7 dpf *pax7a:eGFP* larvae with DAPT following injury, counting the number of muSCs 24hpi. I found that although DAPT attenuates the muSC response at 3 dpf and 7 dpf, this is not affected by larval age. I also observed fewer muSCs in larvae expressing dnSu(H) (Latimer *et al.*, 2005). Over-expression of the NICD-peptide did not affect the number of *pax7a:eGFP*-muSC 24 hpi. It is possible that the lack of observable changes following NICD overexpression is a result of the lateral inhibition of Notch signalling between adjacent cells (Bray, 2006).

To understand if the effect of Notch is temporarily regulated during muscle repair, I treated *pax7a:eGFP* larvae with DAPT for 8 hours, counting the number of muSCs. The attenuation of the muSC response to injury at 24 hpi was also observed at 8 hpi. Surprisingly, there were more cells in the absence of injury, suggesting a temporal effect of Notch inhibition in the absence of injury.

In mice, muSC specific inhibition of Notch results in S-phase-independent premature differentiation following muscle injury (Bjornson *et al.*, 2012; Mourikis, Sambasivan, *et al.*, 2012). Therefore, using a BrdU incorporation assay and an antibody specific for Myogenin (Myog), I investigated the consequences of Notch inhibition on both muSC proliferation and differentiation 24 hpi, respectively. I found that following injury there are fewer proliferating muSCs, and an increased proportion of

differentiating muSCs in DAPT treated animals compared to DMSO treated control animals.

Finally, I assessed the power and ideal sample size needed to achieve 80% power when investigating the effects of injury and Notch inhibition on the number of muSCs. I found that comparisons between uninjured samples have very low power and so, a high number of larvae are needed to detect any differences (n= 25-699). Contrastingly, when investigating differences in larvae following injury, there is a high power of analysis (95-99%). Therefore, few animals are needed to identify differences following injury in DAPT treated compared to DMSO treated control animals (n= 4-5).

3.3.2 Myosepta

Due to few cells, small effect sizes and large variability in the number of cells between larvae, the power of analysis drastically changes between datasets (5%- 99%; Table. 3.4). As a consequence many animals are needed to detect changes in muSC number in the myosepta in response to injury and Notch inhibition (18 ± 10 - 38 ± infinite). Therefore, as n= 5-6 larvae were used for each experiment, the variability in power makes it difficult to examine statistically significant results, masking the different phenotypes.

I found that there is an increase in the number of muSC at all the different myosepta in older (7 dpf) compared to younger (3dpf) larvae, which is consistent with published work demonstrating that the horizontal and vertical myosepta are populated with muSCs during muscle development (Seger *et al.*, 2011).

Following DAPT treatment I found there are fewer Pax7-expressing muSCs within the VM following injury. To understand if age influences this phenotype, I then looked at the number of *pax7a:eGFP*-expressing muSCs in younger and older larvae. I found that there was an interaction effect between DAPT treatment and age, observing changes at 3 dpf and not 7 dpf. There were fewer *pax7a:eGFP*+ cells at the VHM in an absence of injury following DAPT treatment. Additionally, there were fewer muSCs within the DHM of injured larvae which were treated with DAPT.

Finally, to understand if Notch inhibition effects the proliferation or differentiation of muSCs within their niche, I investigated changes in BrdU incorporation and Myog immunoreactivity, respectively. In an absence of injury, following DAPT treatment,

there are more proliferating muSCs in VM. Additionally, there are more differentiating myogenic cells (*pax7a*-Myog+) in the VM following drug treatment irrespective of injury. I did not observe any changes to the number of proliferating or differentiating muSC at the HM. The low number of cells detected and their presumably long cell cycle (Nguyen *et al.*, 2017), which would result in slow incorporation of BrdU, makes it difficult to draw definitive conclusions from this result as to whether resident muSCs at the HM are dependent on Notch signalling.

Finally, I wanted to understand if the overactivation of Notch signalling affects the muSC population within the myosepta. Following injury I measured an increase in the number of muSCs in the VM of WT animals. Following NICD over-expression, I observed no change to the number of *pax7a:eGFP*-expressing muSC number in response to injury in the VM.

3.4 Conclusion

I have shown that Notch signalling has a key role during muscle repair in zebrafish, limiting muSC differentiation and promoting proliferation. I have also found that in the absence of injury, Notch signalling limits muCS proliferation and myogenic cell differentiation at the vertical myosepta. This suggests that Notch is important to keep muSCs in a quiescent state within their niche. It is still not clear whether the response of muSCs are a direct consequence of Notch inhibition by DAPT. To investigate the direct consequence of Notch inhibition on muSC responses, future work should specifically express *dnsu(h)* in *pax7a*-expressing cells. I have also found that Notch inhibition by DAPT leads to less muSCs in both younger (3 dpf) and older (7dpf) larvae. Due to the variable number of muSCs at the myosepta between animals and conditions, there was low power when comparing the effect to injury, developmental stage and DAPT treatment. Therefore, in the next chapter, using a reporter of Notch activity (*Tp1*), I will investigate the effects of injury on the expression of Notch signalling on muSCs, focusing on the myotome of 5 dpf larvae.

Chapter 4 Identification of a Notch expressing population of muSCs following zebrafish muscle injury

4.1 Introduction

In mouse and chick, the regulation of Notch signalling to populate and maintain the quiescent post-natal muSC pool has been well characterised (Delfini *et al.*, 2000; Hirsinger *et al.*, 2001; Bröhl *et al.*, 2012; Mourikis, Gopalakrishnan, *et al.*, 2012; Fujimaki *et al.*, 2018). Notch signalling functions to maintain proliferation, limiting differentiation, and promoting the entrance into quiescence of muSCs (Delfini *et al.*, 2000; Hirsinger *et al.*, 2001; Bröhl *et al.*, 2012; Mourikis, Gopalakrishnan, *et al.*, 2012; Fujimaki *et al.*, 2018). Although the role of Notch signalling during the development of muscle is conserved across mouse (Bröhl *et al.*, 2012; Mourikis, Gopalakrishnan, *et al.*, 2012; Fujimaki *et al.*, 2018), chick (Delfini *et al.*, 2000; Hirsinger *et al.*, 2001) and zebrafish (Pascoal *et al.*, 2013; Lleras-Forero *et al.*, 2020), the role Notch signalling plays during post-natal muscle regeneration is less consistent. It was initially believed that Notch signalling was pivotal for the proliferation of muSCs following injury, subsequently downregulated to allow muSCs to differentiate and fuse into mature myofibers (Conboy and Rando, 2002; Sun et al., 2007; Brack et al., 2008). This model has been called to question by results demonstrating a loss of Notch target genes (*Hey1*, *Hey2*, *HeyL*, *Hes5* and *Hes1*) in proliferating muSCs following injury, which are then upregulated 4-5 dpi around the emergence of Myog-expressing cells (Bjornson *et al.*, 2012; Mourikis, Sambasivan, *et al.*, 2012). These findings are further complicated by discrepancies observed when using Pax7-expressing muSC specific Rbp-jk homozygote knockout model (Bjornson *et al.*, 2012; Mourikis, Sambasivan, *et al.*, 2012). Although SCs show precarious differentiation in an S-phase-independent manner following injury (EdU-; Myog+ cells; Bjornson *et al.*, 2012; Mourikis, Sambasivan, *et al.*, 2012), the contribution of Rbp-jk null SCs towards successful muscle regeneration is poorly understood. Mourikis, Sambasivan *et al.,* (2012) suggest that Rbpj-/- SCs contribute towards normal muscle repair albeit with smaller myofibers, retaining a proliferative state in culture, amplifying before differentiating (Mourikis, Sambasivan, *et al.*, 2012). Contrastingly, Bjornson *et al.,*

(2012) highlights a failure to repair muscle in the presence of Rbpj-/- SCs, with a loss of proliferative capacity (Bjornson *et al.*, 2012).

During regeneration, muSCs interact with different cell types, including infiltrating inflammatory cells (Ratnayake *et al.*, 2021). These interactions may be, in part, facilitated by Notch signalling. Moreover, cross-talk between Notch signalling and other pathways such as Wnt (Brack *et al.*, 2008), VEGF (Verma *et al.*, 2018), and YAP (de Lima *et al.*, 2016) signalling have been discussed in the maintenance of the muSC population. Therefore, it is not known if the phenotypes observed following Notch signalling manipulations are a direct result of Notch activity within the muSC or an indirect effect on supporting cells or secondary molecular pathways.

I have shown that the inhibition of Notch signalling using DAPT results in fewer proliferating *pax7a:eGFP*+ cells in response to injury with an increase in the proportion of differentiating muSCs. The expression of Notch signalling in muSCs during muscle repair in zebrafish has not been characterised. Therefore, using the *Tp1* zebrafish reporter line as a readout of Notch activity (Aulehla *et al.*, 2008; Parsons *et al.*, 2009; Ninov *et al.*, 2012), I aimed to understand if *pax7a:eGFP*+ muSCs express Notch in a cell specific manner in zebrafish, and if Notch signalling is temporally regulated following muscle injury.

4.2 Results

4.2.1 *Tp1* zebrafish reporter lines can be used to identify Notch expressing cells

To understand the regulation of Notch following muscle injury, it was first necessary to characterise a system to visualise the expression of Notch in zebrafish. The *TP1* module is an Epstein-Barr virus derived Notch responsive element with multiple rbp-jk binding sites (Grossman *et al.*, 1994; Henkel *et al.*, 1994; Kato *et al.*, 1997; Kohyama *et al.*, 2005). Therefore, using the *Tp1* promoter to drive nuclear localised mCherry (*Tp1:H2BmCherry*- Parsons *et al.*, 2009; Ninov *et al.*, 2012) or destabilised Venus (*Tp1*:VenusPEST- Aulehla *et al.*, 2008; Ninov *et al.*, 2012), I was able to identify both cells which have expressed and actively express Notch, respectively.

To confirm the Notch activity described using the *Tp1:H2BmCherry* and *Tp1*:VenusPEST reporter lines (Ninov *et al.*, 2012), I used an antibody specific to the cleaved NICD (Garcia-Concejo *et al.*, 2018). Notch plays an important role in the

development of the central nervous system of the zebrafish (Geling *et al.*, 2004; Chung *et al.*, 2011; Dyer *et al.*, 2014; Hadjivasiliou *et al.*, 2019; Sharma *et al.*, 2019). Therefore, I conducted an immunofluorescence antibody staining specific for cleaved NICD on 24 hours hpf *Tp1:H2BmCherry*; *Tp1*:VenusPEST-expressing embryos (Fig. 9.3). The *Tp1:H2BmCherry* and *Tp1*:VenusPEST reporters are expressed within the prosencephalic regions and midbrain structures of the zebrafish brain, and co-expressed with Hoechst+ cells within neuronal structures (Fig. 9.3A). Moreover, the population of cells expressing *Tp1:H2BmCherry* was larger than the population of cells expressing *Tp1*:VenusPEST. Although the *Tp1:H2BmCherry*+ nuclei could be observed throughout the zebrafish brain, the *Tp1*:VenusPEST-expressing cell population appeared restricted to a smaller neuronal population within the prosencephalic regions and midbrain structures (Fig. 9.3A). This partial co-expression is likely a consequence of H2BmCherry stability and perdurance. Contrastingly, cleaved NICD-expressing nuclei constituted a much larger population, expressed throughout the prosencephalic regions, midbrain and hindbrain (Fig. 9.3A). Moreover, many cells which expressed cleaved NICD did not express the *Tp1:H2BmCherry* or *Tp1*:VenusPEST transgenes (Fig. 9.3A).

Next, I investigated the response of cells expressing the *Tp1:H2BmCherry* and *Tp1*:VenusPEST transgenes towards muscle injury. By live imaging *Tp1:H2BmCherry*; *Tp1*:VenusPEST- expressing zebrafish on a multi-photon system (Fig. 4.1; Movie. 9.3), I identified a population of migratory Venus+ cells which also express mCherry (~5 hpi; Fig. 4.1A). These Venus+mCherry+ cells could be observed migrating from the VM and HM, reaching the site of injury by 18.75 hpi (Fig. 4.1). Although there were only 2.3 ± 1.2 Venus+mCherry+ cells identified, it was possible to observe Venus+mCherry+ cells downregulating Venus expression (~11 hpi; Fig. 4.1A; Fig. 4.1). Moreover, I found that there were fewer mCherry+ (3 hpi: 60.6 ± 6.7, 19 hpi: 29.3 ± 14.8; Fig. 4.1B), Venus+ (3 hpi: 5.7 ± 2.1, 19 hpi: 1 ± 1; Fig. 4.1C) and Venus+mCherry+ (3 hpi: 4 ± 1.7, 19 hpi: 1 ± 1; Fig. 4.1D) cells over time.

My results highlight a population of cells which have active Notch signalling in response to muscle injury expressing both *Tp1:H2BmCherry* and *Tp1*:VenusPEST. These cells then de-activate supressed Notch signalling, downregulating the expression of the *Tp1*:VenusPEST transgene. Moreover, these cells maintain

Tp1:H2BmCherry expression which is likely due to the stability and perdurance of fluorophores which have been tagged with a nuclear localisation domain (H2B; Brennand *et al.*, 2007).

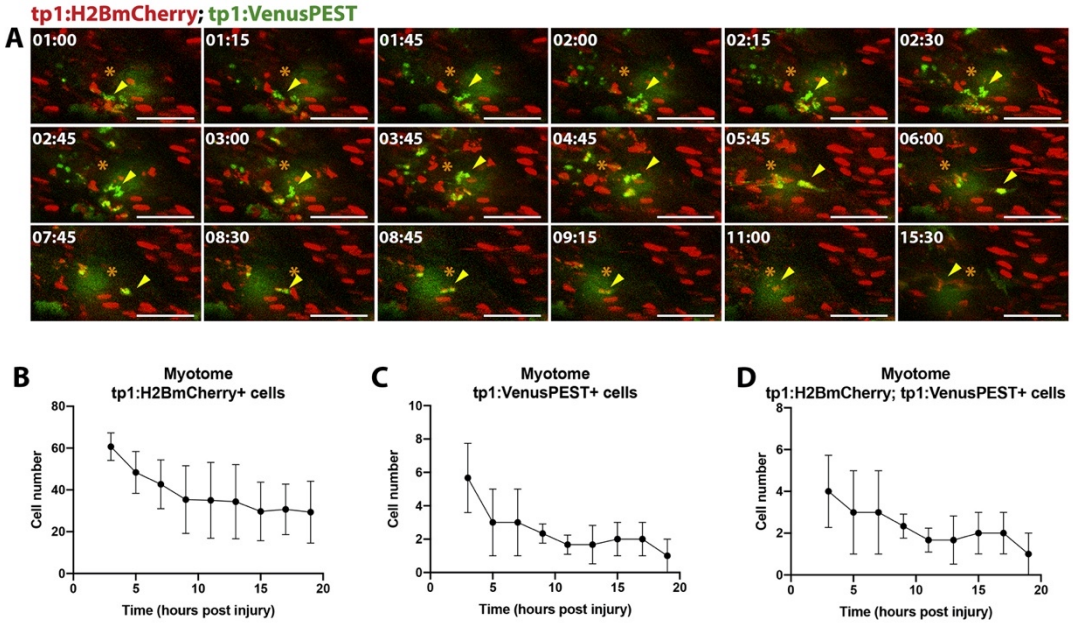

Figure 4.1. Cells expressing *Tp1:H2BmCherry* an *Tp1*:VenusPEST respond to muscle injury.
5 dpf *Tp1:H2BmCherry*; *Tp1*:VenusPEST+ larvae were injured and live imaged on a multi-photon system over a 17.75 hour time period. Representative z-projections (**A**) show migratory mCherry;Venus+ cells responding to injury (asterisk). Venus+ cells migrate towards the site of injury, upregulating mCherry expression before supressing Venus expression (yellow arrowhead). The number of mCherry+ (**B**), Venus+ (**C**), or mCherry+Venus+ (**D**) cells were quantified, highlighting a reduction in cell number over time.
Scale bars: 50 µm

4.2.2 Few *pax7a:eGFP* cells express the *Tp1:H2BmCherry* reporter 24 hpi

Investigations in mouse have revealed an important role of Notch signalling for the maintenance of muSCs during muscle regeneration (Bjornson *et al.*, 2012; Mourikis, Sambasivan, *et al.*, 2012) . Moreover, I have shown a conserved role for Notch signalling in zebrafish. Next I investigated how Notch signalling (*Tp1*) is regulated in *pax7a:eGFP*-expressing muSCs following muscle injury in zebrafish.

I used the *Tp1:H2BmCherry* zebrafish reporter line in conjunction with the *pax7a:eGFP* zebrafish reporter line, injuring 5 dpf *pax7a:eGFP*; *Tp1:H2BmCherry*+ larvae and counted the number of *pax7a*-expressing muSCs and *Tp1*-expressing cells 24 hpi (Fig. 4.2A, B). I found that in an absence of injury, there were many mCherry+ cells within the myotome (33.8 ± 11.8; Fig. 4.2D). I also found very few GFP+ cells (4.2 ± 1.5) expressing mCherry (1.2 ± 0.8; Fig. 4.2E). Following injury, I found that although the number of GFP+ cells increases (11 ± 2.6; Fig. 4.2C), there is no change to the number of mCherry+ cells (Fig. 4.2D; File. 9.2) and GFP+mCherry+ cells (Fig. 4.2E; File. 9.2).

My data showed that *Tp1:H2BmCherry*+ myonuclei are aligned within myofibers, and following injury, *Tp1:H2BmCherry*-expressing nuclei are not expressed within *pax7a:eGFP*-expressing cells.

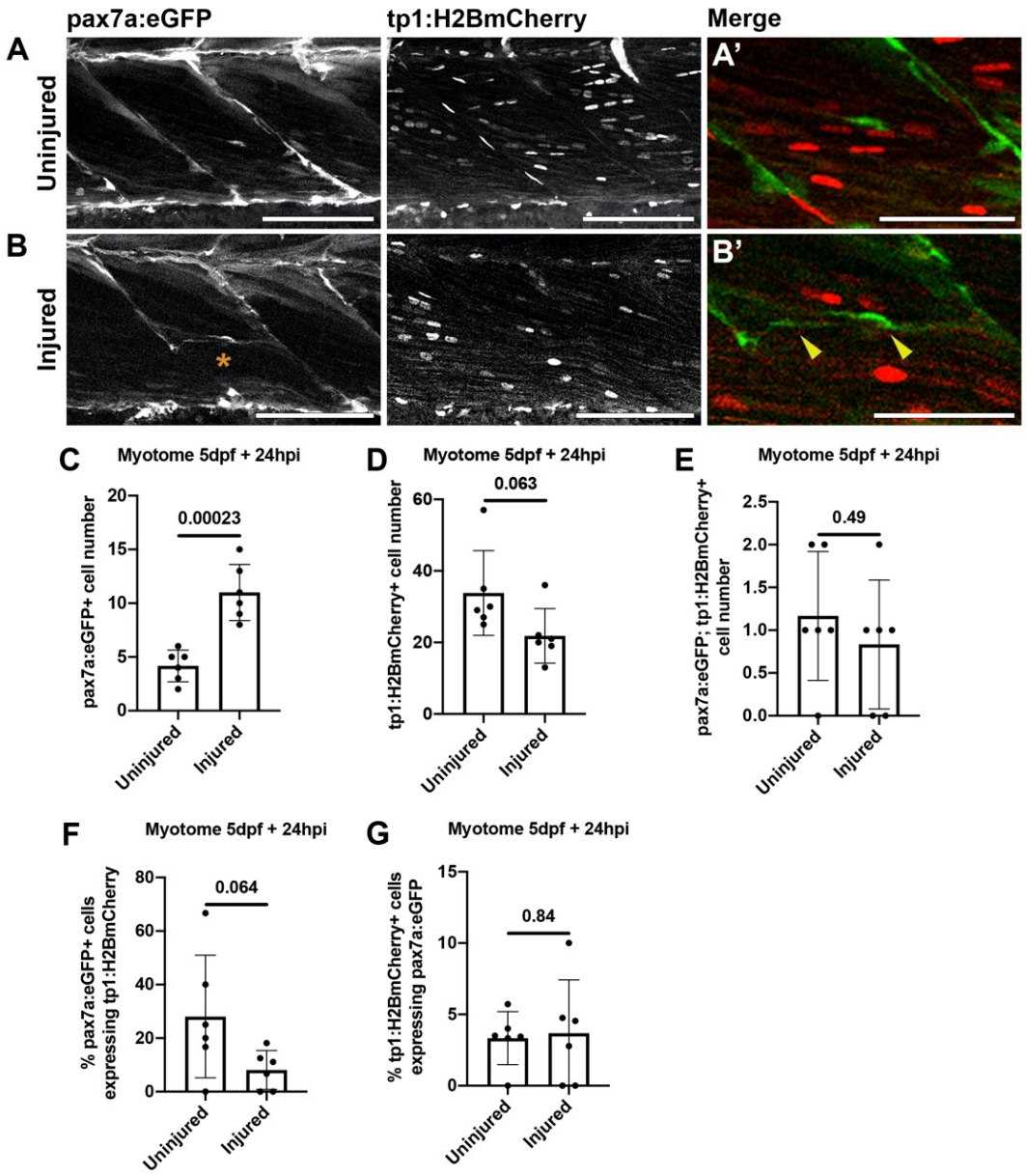

Figure 4.2. *pax7a:eGFP*+ cells do not express *Tp1:H2BmCherry* in response to injury 24 hpi.

Representative projections from confocal z-stacks of the myotome in uninjured (**A**) and injured (**B**) 5 dpf *pax7a:eGFP*; *Tp1:H2BmCherry*-expressing larvae 24 hpi. *pax7a:eGFP*-expressing muSCs (yellow arrowheads) were recruited to the site of injury (asterisk). Many *Tp1:H2BmCherry*+ cells were observed within the myotome of uninjured (**A'**) larvae but they did not appear to align at the site of injury (**B'**). The number of cells were quantified. There were significantly more eGFP+ cells ($p<0.05$; **C**) and no change to the number mCherry+ cells ($p>0.05$; **D**) following injury. There were few eGFP+mCherry+ cells within the uninjured myotome which did not change following injury ($p>0.05$; **E**). The proportion of double positive cells of the total eGFP+ (**F**) and mCherry+ (**G**) populations was calculated. There was no change to the proportion of eGFP+ cells expressing mCherry or the proportion of mCherry+ cells expressing eGFP ($p>0.05$). Significant differences were tested by Student's t-test or Wilcoxon Mann Whitney U rank sum test for normal and non-normal comparisons, respectively. Error bars represent standard deviation, and values above comparison bars represent significance (p-values).

Scale bars: 100 µm (**A-B**), 50 µm (**A'-B'**).

4.2.3 *Tp1:H2BmCherry*-expressing muSCs do not respond towards muscle injury

In the uninjured myotome, I have identified many *Tp1:H2BmCherry*-expressing cells, of which very few expressed *pax7a:eGFP* (Fig. 4.2). Although the number of mCherry+ cells did not significantly change following injury, mCherry+ cells were observed migrating towards the site of injury (Fig. 4.1). Therefore, I assessed whether these migratory mCherry+ cells also expressed eGFP following injury (Fig. 4.3A; Movie. 9.4).

I observed many mCherry+ cells within the myotome (2.7 hpi: 26.7 ± 6.8, 11 hpi: 23 ± 3.6; Fig. 4.3C). Additionally, these mCherry+ cells were mostly a static population, with a few cells migrating around the site of injury (Movie. 9.4). I also found a small population of eGFP+mCherry+ cells, which did not expand following injury (2.7 hpi: 2 ± 2, 11 hpi: 2.7 ± 1.5; Fig. 4.3D). Moreover, these eGFP+mCherry+ cells were not observed at the site of injury, nor did they migrate towards the site of injury (Movie. 9.4).

Although I was not able to observe any eGFP+ cells expressing the *Tp1:H2BmCherry* transgene over time, my previous results suggests that it takes ~5 hours for *Tp1*:VenusPEST-expressing cells to express the *Tp1:H2BmCherry* reporter following injury (Fig. 4.1). Therefore, it is possible that *pax7a:eGFP*-expressing muSCs express *Tp1:H2BmCherry* at a later time point.

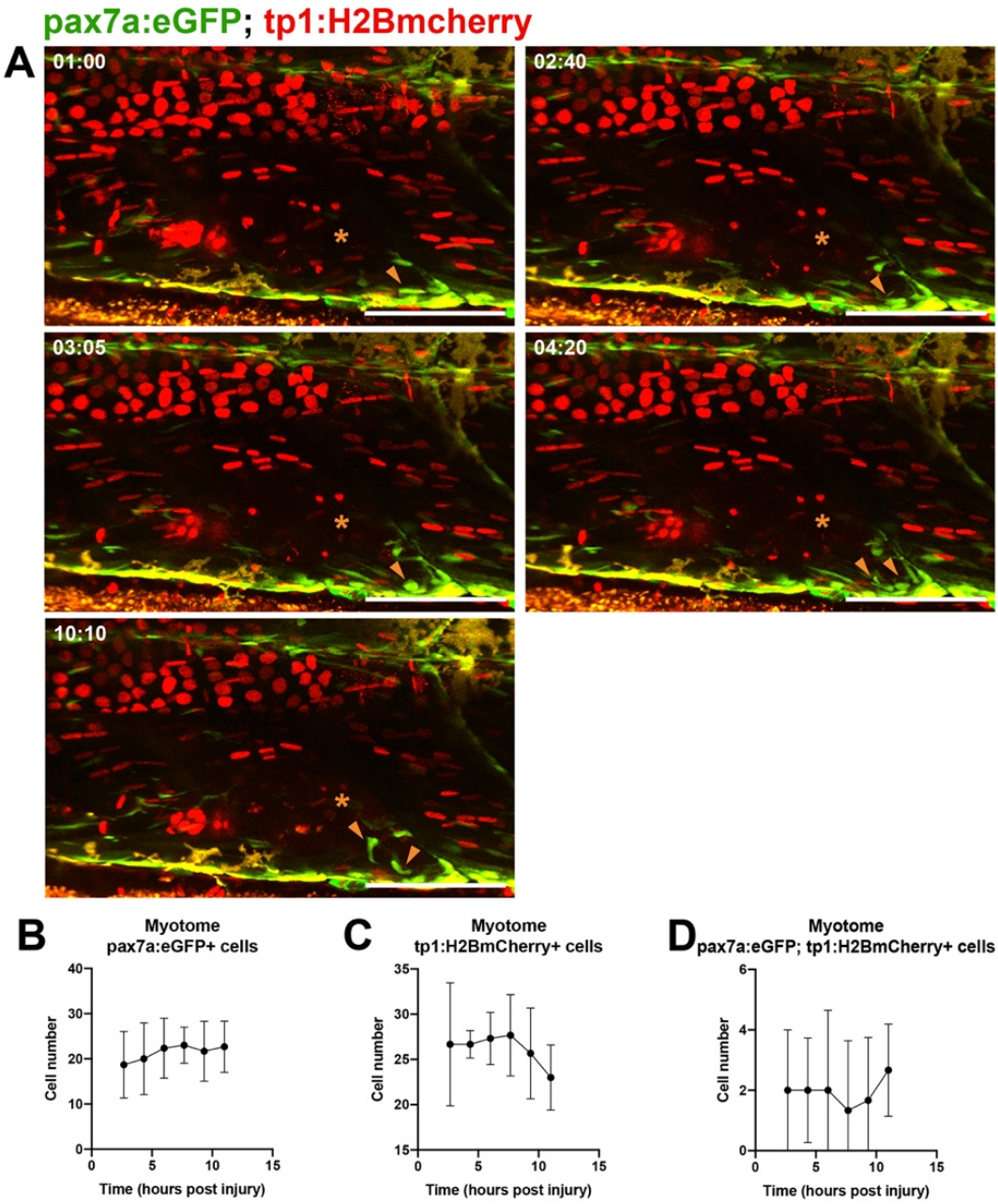

Figure 4.3. *Tp1:H2BmCherry*-expressing muSCs do not respond to injury.
7 dpf *pax7a:eGFP*; *Tp1:H2BmCherry*- expressing larvae were injured and live imaged for 9.17 hours on a multiphoton system. Representative z-projections (**A**) showing migratory eGFP+ (orange arrow heads) and mCherry+ cells responding to injury (asterisk). The number of eGFP+ (**B**), mCherry+ (**C**), or eGFP+mCherry+ (**D**) cells were quantified, highlighting an increase in the number of eGFP+ cells, a decrease in the number of mCherry+ cells, and no change to the number of eGFP+mCherry+ cells over time.
Scale bars: 100 µm

4.2.4 proliferating *pax7a*-expressing muSCs express *Tp1*:VenusPEST following injury

In mouse, Notch target genes are weakly expressed in proliferating myoblasts following injury (Mourikis and Tajbakhsh, 2014). I have demonstrated using DAPT that a similar requirement for Notch exists to maintain the Pax7-expressing muSC population in zebrafish (Fig. 3.9). Therefore, I examined whether *pax7a:eGFP*-expressing myoblasts also show Notch activity in zebrafish. In contrast to the stable H2BmCherry fluorophore (*Tp1:H2BmCherry*), the *Tp1*:VenusPEST zebrafish line expresses destabilised VenusPEST and therefore is an accurate representation of cells which are actively expressing Notch signalling (Ninov *et al.*, 2012). To understand if Notch signalling is expressed in proliferating muSCs, I live imaged *pax7a:eGFP*; *Tp1*:VenusPEST-expressing larvae following injury (Fig. 4.4A, B; Movie. 9.5). The excitation and emission spectra for eGFP and Venus are largely overlapping. Therefore exciting eGFP at the optimal 850 nm would also excite Venus. In order to image both eGFP and Venus in tandem, I optimised an imaging strategy to avoid bleed-through between eGFP and Venus acquisition. Venus has a second emission peak at ~1400nm. Therefore, to acquire both eGFP and Venus signals, eGFP was excited at a lower wavelength (830 nm) to avoid exciting Venus, and the Venus was excited at 1050 nm avoiding any overlap with eGFP excitation. Both fluorophores were subsequently detected sequentially at 490-507 nm. By imaging neuronal cells within the zebrafish midbrain, I demonstrated that with this imaging strategy, no Venus signal was detected when eGFP was excited, and no eGFP signal was detected when (Fig. 9.4).

Following injury, I found that although only 19.7% ± 12.7% eGFP+ cells expressed Venus (3.6 hpi: 11.7 ± 7, 18.3 hpi: 14 ± 7.2; Fig. 4.4C), both proliferating (Fig. 4.4A; Movie. 9.5-9.6), and migratory (Fig. 4.4B; Movie. 9.5) eGFP+ cells expressed Venus. Interestingly, although there were very few Venus+ cells shortly after injury (3.6 hpi: 5.7 ± 3.8, 18.3 hpi: 5.3 ± 1.2; Fig. 4.4D), there were more eGFP+Venus+ muSCs over time (3.6 hpi: 1.7 ± 1.5, 18.3 hpi: 3 ± 1; Fig. 4.4E). It is possible that this is a consequence of the proliferation of *pax7a:eGFP*+ cells. I noted that with the current time-lapse it was not possible to capture when *pax7a:eGFP*+ cells expressed *Tp1*:VenusPEST following injury. Moreover, it was difficult to understand if all proliferating *pax7a:eGFP*+ muSCs expressed *Tp1*:VenusPEST (n= 2 proliferating cells

in 1/3 animals) and if the two daughter cells continued to express *Tp1*:VenusPEST following division. My data were consistent with the low level of Notch signalling observed within proliferating muSCs in mouse following injury.

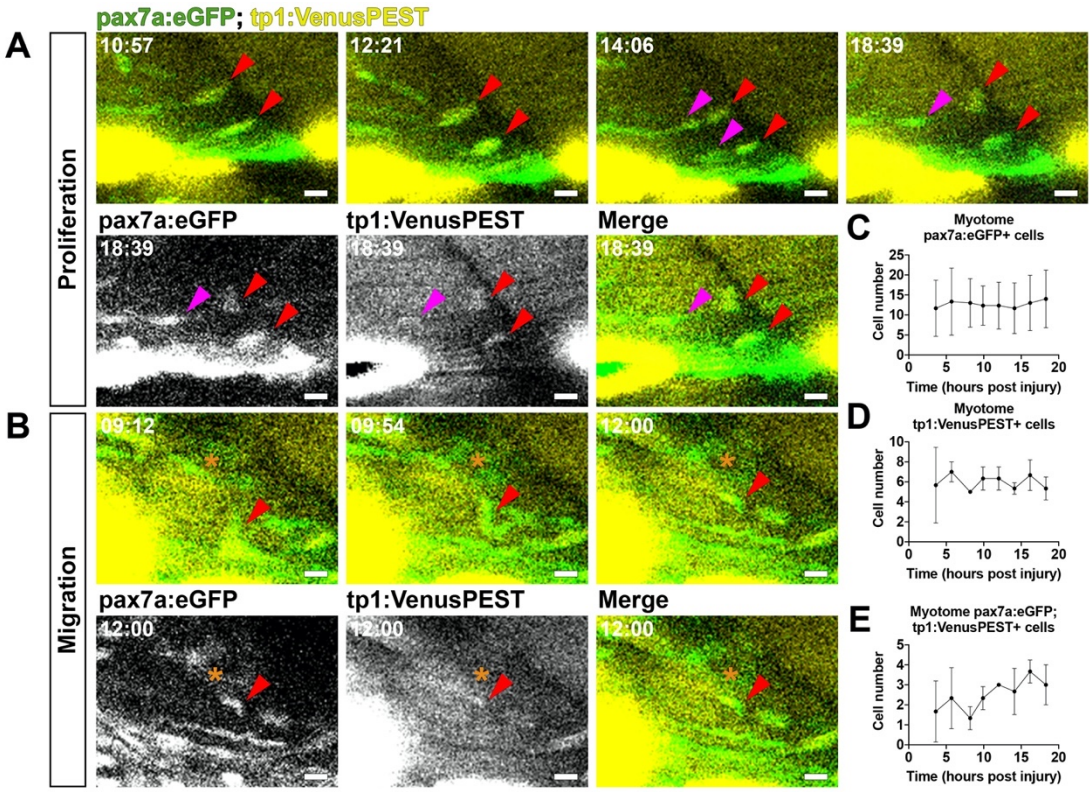

Figure 4.4. Activated muSCs express *Tp1*:VenusPEST following injury.
5 dpf *pax7a:eGFP*; *Tp1*:VenusPEST-expressing larvae were injured and imaged on a multiphoton system over 16.8 hours. Representative z-projections of proliferating (**A**) and migrating (**B**) eGFP+Venus+ cells (cells: red arrow head; daughter cells: magenta arrow heads) in response to injury (asterisk). The number of eGFP+ (**C**), Venus+ (**D**) and eGFP+Venus+ (**E**) cells were quantified over time. There was an increase in the number of eGFP+ and eGFP+Venus+ muSCs, and no change to the number of Venus+ cells over time. Scale bars: 10 µm

4.2.5 The number of *pax7a:eGFP*+ cells expressing *Tp1:H2BmCherry* temporally increases following injury

I have shown that, following injury, proliferating *pax7a*-expressing cells expressed *Tp1*:VenusPEST+ (Fig. 4.4) and that it takes ~5 hours for *Tp1*:VenusPEST+ cells to express *Tp1:H2BmCherry* following injury (Fig. 4.1). Therefore, I asked whether there might be an increase in *pax7a:eGFP*+ cells expressing the *Tp1:H2BmCherry* transgene later during muscle repair. By injuring *pax7a:eGFP*; *Tp1:H2BmCherry*-expressing larvae, I counted the number of muSCs expressing the *Tp1:H2BmCherry* reporter 48 hpi (Fig. 4.5A, B). I found that although there was no change to the number of mCherry+ cells in the myotome following injury (Fig. 4.5D; File. 9.2), there was an increase in the number of eGFP+ cells (uninjured: 7.3 ± 2.5, injured 13.2 ± 3.8; Fig. 4.5C) and eGFP+mCherry+ cells (uninjured 0.3 ± 0.5, injured: 2.2 ± 1; Fig. 4.5E). This represents an increased proportion of eGFP+ cells initiating the expression of the *Tp1:H2BmCherry* transgene (uninjured: 1.5% ± 2.9%, injured: 7.5% ± 4.6%; Fig. 4.5G). I also noted that, although there was an increase in the number of eGFP+mCherry+ cells (Fig. 4.5E), this represented small population relative to the total mCherry+ population (Fig. 4.5D).

Phenotypically, the completion of muscle repair following a small, single myotome injury is associated with the elongation and fusion of muSCs, and the innovation of NMJ, which takes approximately 3 days (Knappe *et al.*, 2015; Gurevich *et al.*, 2016; Pipalia *et al.*, 2016). Therefore, I aim to understand if the relatively small number of eGFP+mCherry+ cells observed at 24 hpi and 48 hpi, could contribute to nascent muscle fibre formation at the site of injury. Therefore, I injured *pax7a:eGFP*; *Tp1:H2BmCherry*-expressing larvae and counted the number of cells 72hpi (Fig. 4.6A, B). Similar to the samples collected at 48 hpi, I detected an increased number of eGFP+ muSCs (uninjured: 8 ± 2.1, injured 21.3 ± 5.5; Fig. 4.6C) and eGFP+mCherry+ cells (uninjured 0.33 ± 0.52, injured: 2.17 ± 0.98; Fig. 4.6E) following injury. By 72 hpi I also found significantly more eGFP+mCherry+ cells following injury (uninjured 37.3 ± 16.3, injured: 30 ± 11.3; Fig. 4.6D), a consequence of an increased proportion of mCherry+ cells expressing eGFP (uninjured: 4.3% ± 2.9%, injured: 18.8% ± 8%; Fig. 4.6G).

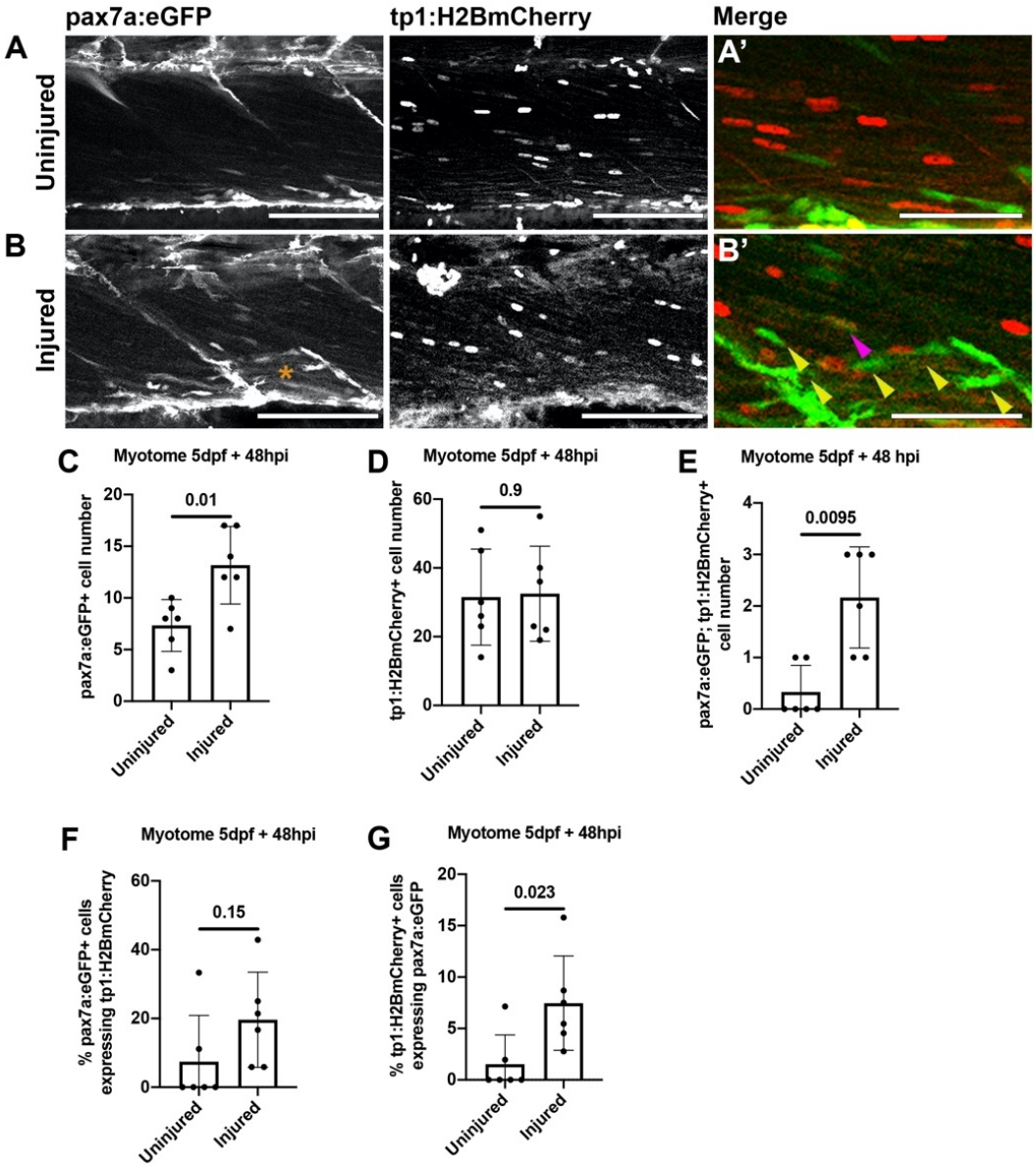

Figure 4.5. *Tp1:H2BmCherry*-expressing cells progressively express the *pax7a:eGFP* reporter 48 hpi.

Representative projections from confocal z-stacks of the myotome in uninjured (**A**) and injured (**B**) 5 dpf *pax7a:eGFP*; *Tp1:H2BmCherry*-expressing larvae 48 hpi. eGFP+ (yellow arrowheads) and eGFP+mCherry+ (magenta arrowheads) muSCs were recruited to the site of injury (asterisk). Very few eGFP+mCherry+ cells were observed within the myotome of uninjured (**A'**) larvae. By 48 hpi there were more eGFP+mCherry+ cells within the myotome, but very few aligned at the site of injury (**B'**). The number of cells were quantified. There were significantly more eGFP+ cells ($p<0.05$; **C**) and no change to the number mCherry+ cells ($p>0.05$; **D**) following injury. There were few eGFP+mCherry+ cells within the uninjured myotome which increased following injury ($p<0.05$; **E**). The proportion of double positive cells of the total eGFP+ (**F**) and mCherry+ (**G**) cells were calculated. The proportion of GFP+ cells expressing mCherry ($p>0.05$) did not change, and the proportion of mCherry+ cells expressing eGFP increased ($p<0.05$) following injury. Significant differences were tested by Student's t-test or Wilcoxon Mann Whitney U rank sum test for normal and non-normal comparisons, respectively. Error bars represent standard deviation, and values above comparison bars represent significance (p-values).

Scale bars: 100 µm (**A-B**), 50 µm (**A'-B'**).

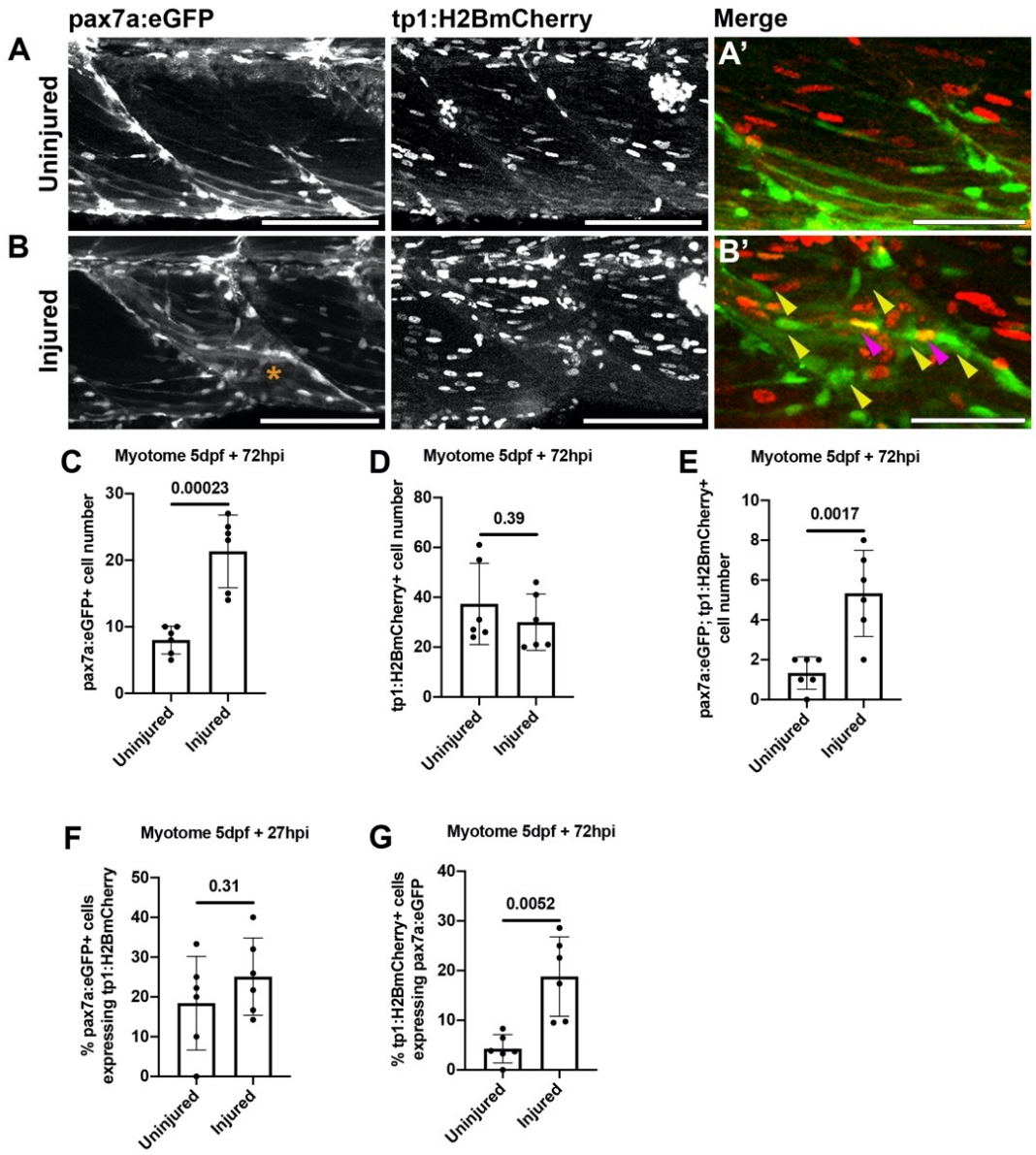

Figure 4.6. *Tp1:H2BmCherry*-expressing cells progressively express the *pax7a:eGFP* reporter 72 hpi.

Representative projections from confocal z-stacks of the myotome in uninjured (**A**) and injured (**B**) 5 dpf *pax7a:eGFP*; *Tp1:H2BmCherry*-expressing larvae 72 hpi. eGFP+ (yellow arrowheads) and eGFP+mCherry+ (magenta arrowheads) muSCs were recruited to the site of injury (asterisk). Very few eGFP+mCherry+ cells were observed within the myotome of uninjured (**A'**) larvae. By 72 hpi there were more eGFP+mCherry+ cells aligned at the site of injury (**B'**). The number of cells were quantified. There were significantly more eGFP+ cells ($p<0.05$; **C**) and eGFP+mCherry+ cells following injury relative to uninjured control animals ($p<0.05$; **E**). There was no change to the number mCherry+ cells ($p>0.05$; **D**) following injury. The proportion of double positive cells of the total eGFP+ (**F**) and mCherry+ (**G**) cells were calculated. The proportion of eGFP+ cells expressing mCherry did not change ($p>0.05$), and the proportion of mCherry+ cells expressing eGFP increased ($p<0.05$) following injury. Significant differences were tested by Student's t-test. Error bars represent standard deviation, and values above comparison bars represent significance (p-values).
Scale bars: 100 µm (**A-B**), 50 µm (**A'-B'**).

4.2.6 Temporal increase in the number of *pax7b:GFP*+ cells expressing *Tp1:H2BmCherry* following injury

Due to a whole genome duplication, the zebrafish has two Pax7 paralogues- *pax7a* and *pax7b* (Seo *et al.*, 1998; Relaix *et al.*, 2004). While both these transcription factors are markers of zebrafish muSCs, Pipalia *et al.,* (2016) reports that these cells have the capacity to respond differently towards muscle injury (Pipalia *et al.*, 2016). Therefore, as it has become evident that the majority of *Tp1:H2BmCherry*-expressing cells do not express *pax7a:eGFP*, I next examined if *Tp1:H2BmCherry*+ cells express *pax7b*. To visualise *pax7b*-expressing cells, I used the *pax7b:gal4;UAS:GFP* (*pax7b:GFP*) reporter line which utilizes the gal4-UAS system (Pipalia *et al.*, 2016). This line expresses gal4 under the control of the *pax7b* promoter, which binds the upstream activator sequence (UAS) resulting in GFP expression (Fig. 4.7). *pax7b:GFP*; *Tp1:H2BmCherry*-expressing larvae were injured using the adjacent uninjured myotome as the uninjured control, and the number of cells were quantified at 24 hpi (Fig. 4.7A) and 48 hpi (Fig. 4.7B).

I found that there was an increase in the number of GFP+ cells following injury at 24 hpi (uninjured: 2.6 ± 1.8, injured 14.3 ± 2.6; Fig. 4.7C) and 48 hpi (uninjured: 1.3 ± 1.2, injured 8.3 ± 3.2; Fig. 4.7H). Moreover, as with the *pax7a* reporter, there were few GFP+ cells that expressed the *Tp1:H2BmCherry* transgene, which did not change by 24 hpi (Fig. 4.7E; File. 9.2) and increased by 48 hpi (uninjured: 0 ± 0, injured: 1.6 ± 1.2; Fig. 4.7J). By 48 hpi there was also an increase in the proportion of mCherry+ cells expressing GFP (uninjured: 0% ± 0%, injured: 7.3% ± 5.6%; Fig. 4.7L). There was no change to the number of mCherry+ cells (Fig. 4.7I; File. 9.2). By 48 hpi, I also observed an increase in the proportion of GFP+ cells expressing mCherry (uninjured: 0% ± 0%, injured: 18.8% ± 14.2%; Fig. 4.7K).

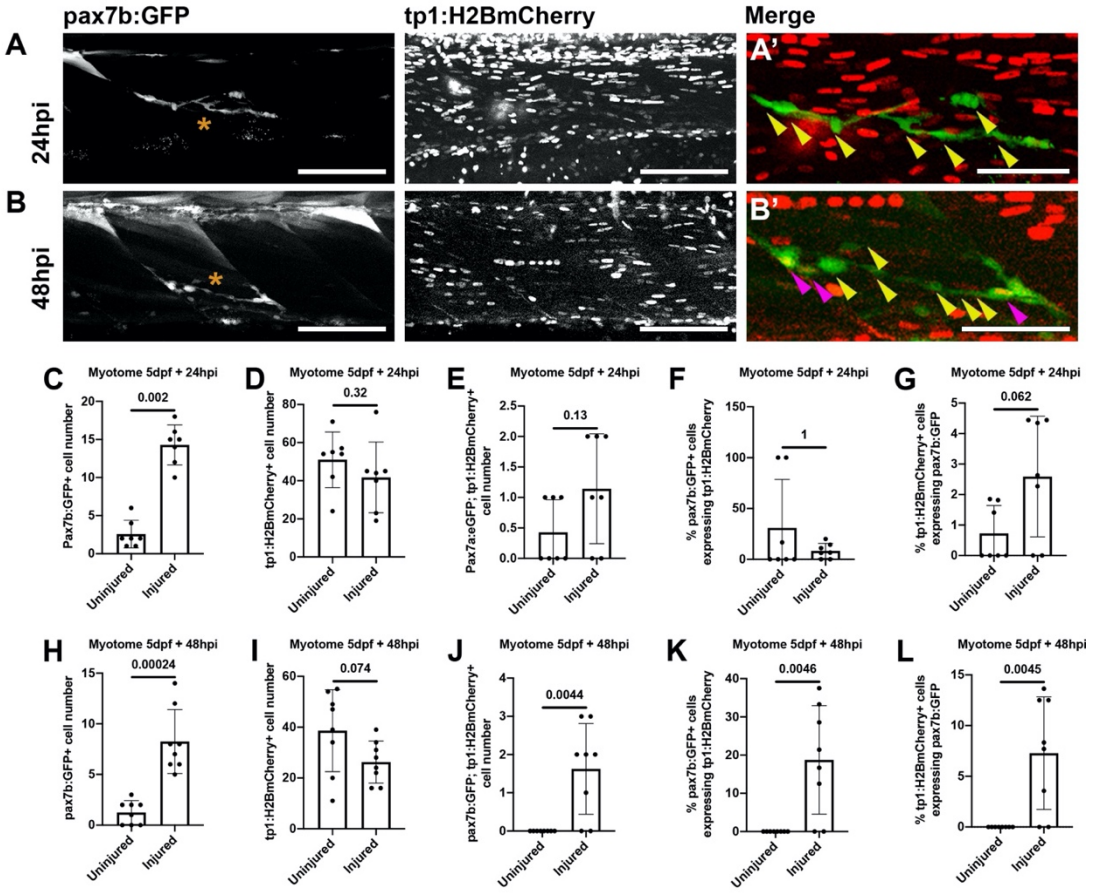

Figure 4.7. The number of *pax7b:GFP*; *Tp1:H2BmCherry*+ cells temporally increases following injury.

Representative projections from confocal z-stacks of the myotome in injured 7 dpf *pax7b:GFP*; *Tp1:H2BmCherry*-expressing larvae 24 hpi (**A**) and 48 hpi (**B**). GFP+ (yellow arrowheads) and GFP+mCherry+ (magenta arrowheads) muSCs were recruited to the site of injury (asterisk). Assessing the adjacent uninjured myotome, very few GFP+mCherry+ cells could be observed within the myotome of uninjured muscle. There were more GFP+mCherry+ cells within the injured myotome by 24 hpi (**A'**), aligning at the site of injury by 48 hpi (**B'**). The number of cells were quantified. There were significantly more GFP+ cells ($p<0.05$; **C**) and no change to the number of mCherry+ cells ($p>0.05$; **D**) 24 hpi. There was no change to the number of GFP+mCherry+ cells 24 hpi ($p>0.05$; **E**). The proportion of double positive cells of the total GFP+ (**F**) and mCherry+ (**G**) cells were calculated. The proportion of GFP+ cells expressing mCherry and the proportion of mCherry+ cells expressing GFP did not change ($p>0.05$) 24 hpi. By 48 hpi, there were significantly more GFP+ cells ($p<0.05$; **H**), no change to the number of mCherry+ cells ($p>0.05$; **I**) and significantly more GFP+mCherry+ cells ($p<0.05$; **J**). By 48 hpi, the proportion of GFP+ cells expressing mCherry and the proportion of mCherry+ cells expressing GFP increased ($p<0.05$). Significant differences were tested by Student's t-test, Welch's t-test or Wilcoxon Mann Whitney U rank sum test. Error bars represent standard deviation, and values above comparison bars represent significance (p-values).

Scale bars: 100 μm (**A-B**), 50 μm (**A'-B'**).

4.2.7 Few Pax7+ cells express the *Tp1:H2BmCherry* reporter 24 hpi

So far, I have used the zebrafish reporter lines for *pax7a* and *pax7b* to understand if Pax7-expressing muSC demonstrate activated Notch signalling in response to injury. I concluded that few Pax7-expressing cells expressed *Tp1:H2BmCherry*, and the majority of the *Tp1:H2BmCherry*-expressing cells did not express *pax7a* or *pax7b*. Although the *pax7* reporter lines are a useful tool to track existing pax7-expressing populations, the long half-life of the GFP means that information on activation state of the muSC is lost (Knappe *et al.*, 2015). Therefore, I used an antibody specific for Pax7, which has been described to detect approximately 92% of all *pax7a:eGFP* positive cells (Knappe *et al.*, 2015). I aimed to understand if these *Tp1:H2BmCherry*-expressing cells express the Pax7 protein, a marker of muSC activation (Fig. 4.8A, B; Knappe *et al.*, 2015).

Tp1:H2BmCherry+ larvae were injured and a Pax7 immunofluorescent antibody staining was conducted at 24 hpi. I found that there was an increase in the number of Pax7+ cells following injury (uninjured: 26.3 ± 10.5, injured 48.6 ± 4.1; Fig. 4.8C). Moreover, there was no change to the number of Pax7+mCherry+ cells following injury (Fig. 4.8E; File. 9.2) and a decrease in the number of mCherry + cells (uninjured: 131.7 ± 15.1, injured: 106.2 ± 5.2; Fig. 4.8D). I also identified a decrease in the proportion of Pax7 cells expressing mCherry (uninjured: 65.2% ± 9.8%, injured 31.2% ± 12.7%; Fig. 4.8F). This data shows that the number of *Tp1:H2BmCherry*+ cells expressing Pax7 does not change following injury, phenocopying the data seen in both the *pax7a* and *pax7b* reporter lines 24 hours after injury.

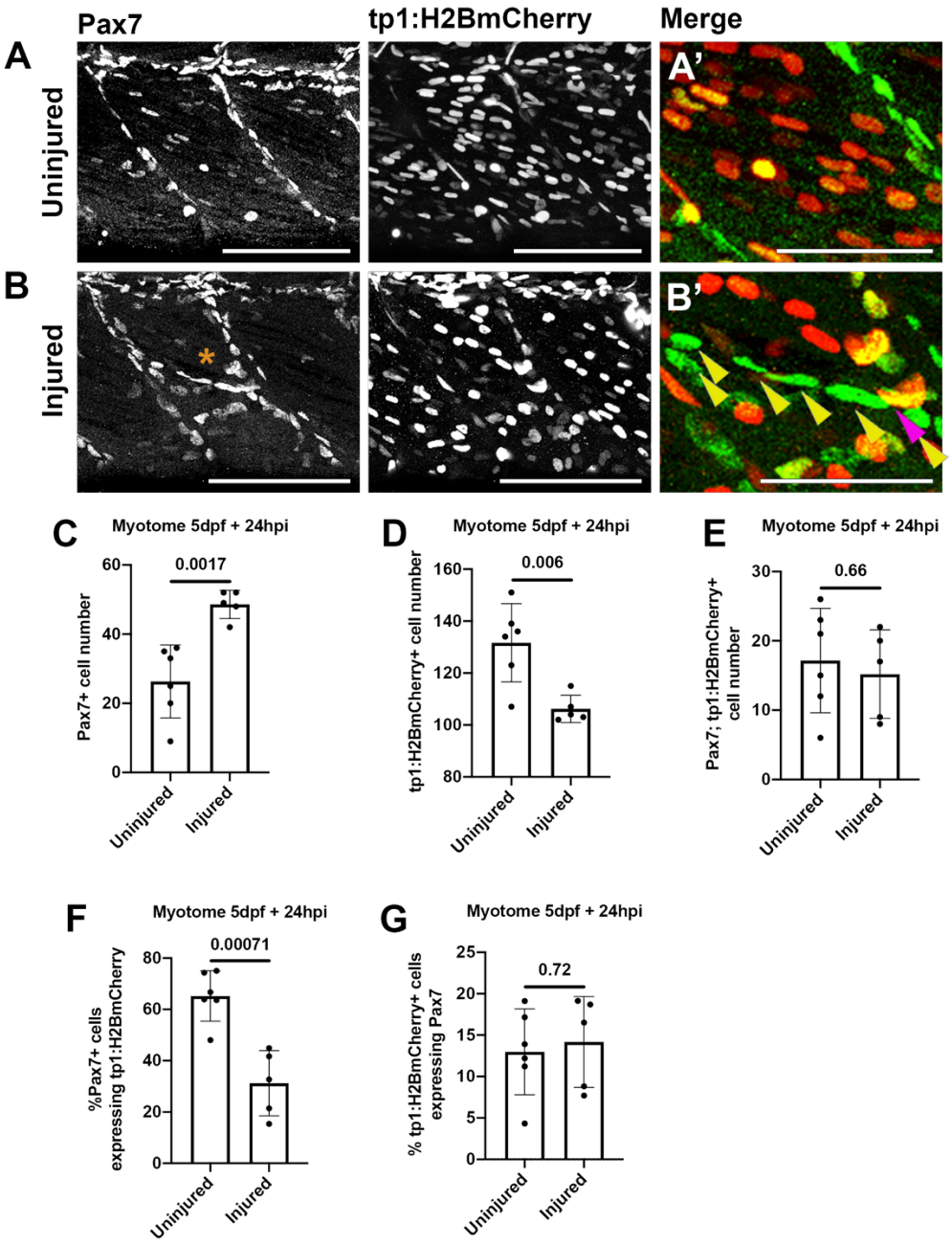

Figure 4.8. Pax7+ cells do not express *Tp1:H2BmCherry* in response to injury 24 hours post injury.

Confocal z-projections of the myotome in uninjured (**A**) and injured (**B**) 5 dpf *Tp1:H2BmCherry*-expressing larvae processed with an antibody specific for Pax7 24 hpi. Pax7-expressing (yellow arrowheads) and Pax7+mCherry+ (magenta arrowheads) muSCs were recruited to the site of injury (asterisk). The number of cells were quantified. There were significantly more Pax7+ cells ($p<0.05$; **C**) and significantly less mCherry+ cells ($p<0.05$; **D**) following injury. There were few Pax7+mCherry+ cells within the uninjured myotome which did not change following injury ($p>0.05$; **E**). The proportion of double positive cells of the total Pax7+ (**F**) and mCherry+ (**G**) cells were calculated. The proportion of Pax7+ cells expressing mCherry was significantly reduced following injury ($p<0.05$). There was no change to the proportion of mCherry+ cells expressing Pax7. Significant differences were tested by Student's t-test. Error bars represent standard deviation, and values above comparison bars represent significance (p-values).

Scale bars: 100 µm (**A-B**), 50 µm (**A'-B'**).

4.2.8 *Tp1:H2BmCherry*-expressing myonuclei perdure during early muscle development

My results show that the majority of the *Tp1:H2BmCherry*+ cells are not responding to muscle injury, and even fewer are expressing Pax7. This is because most *Tp1:H2BmCherry*+ nuclei are located within myofibers. Notch is important for the development of muscle and subsequent establishment of the muSCs niche (Delfini *et al.*, 2000; Hirsinger *et al.*, 2001; Bröhl *et al.*, 2012; Mourikis, Gopalakrishnan, *et al.*, 2012; Fujimaki *et al.*, 2018). It is possible that these *Tp1:H2BmCherry*-expressing myonuclei perdure throughout development. Therefore, I aimed to understand if mCherry+ nuclei found within myofibers are derived from a developmental population. I assessed the endogenous fluorescence within the uninjured myotome of 24 hpf and 48 hpf embryos (Fig. 4.9A, B, C, D). I found that at 24 hpf both *Tp1:H2BmCherry* and *Tp1*:VenusPEST were strongly expressed within the zebrafish myotome (Fig. 4.9A, C). In contrast, at 48 hpf, *Tp1:H2BmCherry* expression was maintained (Fig. 4.9B) whilst *Tp1*:VenusPEST expression was lost (Fig. 4.9D). Next, I evaluated the muscle of 30 dpf juvenile zebrafish (Fig. 4.9E, F). The muscular architecture of juvenile zebrafish was similar to the muscle of adult zebrafish (Alexander, 1969; Devoto *et al.*, 1996; Van Leeuwen *et al.*, 2008). Assessing the epaxial sloping portion of the *pax7a:eGFP*; *Tp1:H2BmCherry*-expressing larvae muscle at 30 dpf, I found that there were few eGFP+ cells adjacent to myofibers (Fig. 4.9E). Interestingly, I did not observe any single positive mCherry+ cells within the muscle, all mCherry+ cells co-localised with eGFP+ cells (Fig. 4.9F).

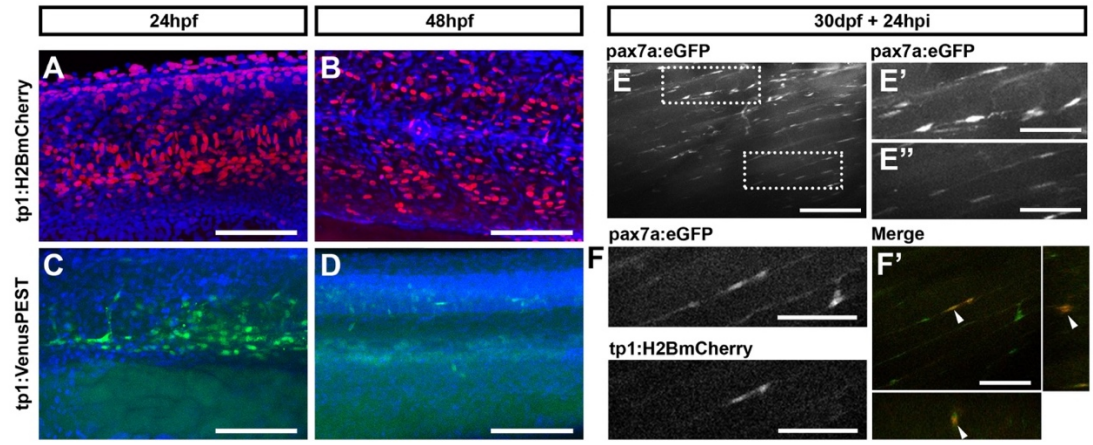

Figure 4.9. *Tp1:H2BmCherry+ pax7a:eGFP*- cells are expressed in larval but not juvenile zebrafish.

Endogenous *Tp1:H2BmCherry* (**A-B**) and *Tp1*:VenusPEST (**C-D**) signal was captured by confocal microscopy at 24 hpf (**A, C**) and 48 hpf (**B, D**). The *Tp1:H2BmCherry* and *Tp1*:VenusPEST signals were expressed at 24 hpf. By 48 hpf only the *Tp1:H2BmCherry* signal was expressed. 30 dpf *pax7a:eGFP*; *Tp1:H2BmCherry*+ juvenile zebrafish were injured and imaged on a multiphoton system 24 hpi. eGFP+ cells were observed aligned along myofibers (**E, E', E''**), some of which expressed mCherry (**F**). Orthogonal view of a eGFP+mCherry+ cell (white arrowhead) aligned on a myofiber (**F'**). No eGFP-mCherry+ cells were detected in juvenile 30 dpf zebrafish (**E-F**).

Scale bars: 100 µm (**A-F**), 50 µm (**E'-F', E''**).

4.2.9 Notch inhibition results in more proliferating *Tp1:H2BmCherry* cells in response to injury

Previously I have shown that Notch signalling plays a key role in regulating the activity of *pax7a:eGFP*+ muSCs. I found that Notch promotes proliferation and limits differentiation of *pax7a:eGFP*-expressing cells within the myotome in response to injury. Contrastingly, Notch supresses proliferation at the VM in the absence of injury. I have also identified a novel injury responsive *Tp1:H2BmCherry*+ cell population in the zebrafish muscle. Therefore, I aimed to understand if *Tp1:H2BmCherry*-expressing muSCs are regulated by Notch signalling. I injured and treated *pax7a:eGFP*; *Tp1:H2BmCherry*-expressing larvae with DMSO (Fig. 4.10A, B) or DAPT (Fig. 4.10C, D) and assessed proliferation with a BrdU incorporation assay, counting the number of cells 24 hpi.

To test whether injury or DAPT treatment affected proliferation of *Tp1:H2BmCherry*-expressing cells, I conducted a 2-way ANOVA. I found that injury and DAPT treatment affected the number and proportion of proliferating mCherry+ cells, and injury affects the proportion of proliferating mCherry+ cells expressing eGFP (File. 9.2). I also identified an interaction effect between Injury and DAPT treatment on the proportion of proliferating mCherry+ cells (File. 9.2). Therefore, Notch inhibition affected the proportion of proliferating mCherry+ cells following injury.

To understand how the number of proliferating mCherry+ cells is affected by injury and DAPT treatment, I conducted a 1-way ANOVA. Following injury, there were more proliferating mCherry+ cells in DAPT treated animals compared to DMSO treated control animals (DMSO: 7.6 ± 1.5, DAPT: 10.8 ± 2.5; Fig. 4.10I). This was not a consequence of a change to the number of mCherry+ cells (Fig. 4.10F; File. 9.2), or proportion of proliferating mCherry+ cells (Fig. 4.11B; File. 9.2). Contrastingly, in the absence of injury, Notch inhibition did not affect the number of mCherry+ cells (Fig. 4.10F; File. 9.2), the number of proliferating mCherry+ cells (Fig. 4.10I; File. 9.2), or the proportion of proliferating mCherry+ cells (Fig. 4.11B; File. 9.2).

Relative to the mCherry+ cells, there were far fewer eGFP+mCherry+ cells within the myotome. The number of eGFP+mCherry+ cells (Fig. 4.10J; File. 9.2), the proportion of eGFP+ cells expressing mCherry (Fig. 4.11C; File. 9.2), or the proportion of mCherry+ cells expressing eGFP (Fig. 4.11D; File. 9.2) did not change following DAPT

treatment in uninjured or injured larvae. Assessing BrdU incorporation, I found that there was no change to the number of proliferating eGFP+mCherry+ cells in the absence or presence of injury (Fig. 4.10K; File. 9.2). There was also no change to the proportion of proliferating eGFP+ cells expressing mCherry+ (Fig. 4.11E), or the proportion of proliferating mCherry+ cells expressing eGFP in uninjured and injured larvae (Fig. 4.11F; File. 9.2).

My results have revealed that a large proportion of the total *Tp1:H2BmCherry*-expressing nuclei resided in myofibers within the zebrafish muscle did not respond towards injury. It is possible that these cells lower the effect size and the power of analysis, masking significant changes in cell number. Therefore, I next quantified the number of cells within the injured region (Fig. 2.2; Ratnayake *et al.*, 2021). I found that within the injured region, DAPT treatment resulted in more mCherry+ cells (DMSO: 6.8 ± 1.8, DAPT: 12.7 ± 3.1; Fig. 4.10M). Moreover, this was associated with an increase in the number of proliferating mCherry+ cells (DMSO: 3.6 ± 0.9, DAPT: 7.5 ± 2.9; Fig. 4.10P). This increase in cell number was not a consequence of a change to the proportion of mCherry+ cells incorporating BrdU (Fig. 4.11H; File. 9.2). Therefore, there are more proliferating mCherry+ cells, but the rate of proliferation is unaffected by DAPT treatment.

Assessing the number of eGFP+mCherry+ cells, I found that DAPT treatment did not affect the number of eGFP+mCherry+ cells (Fig. 4.10Q; File. 9.2), the proportion of eGFP+ cells expressing mCherry (Fig. 4.11I; File. 9.2), or the proportion of mCherry+ cells expressing eGFP (Fig. 4.11J; File. 9.2). This was associated with no change to the number of proliferating eGFP+mCherry+ cells (Fig. 4.10R; File. 9.2), the proportion of proliferating eGFP+ cells expressing mCherry (Fig. 4.11K; File. 9.2), or the proportion of proliferating mCherry+ cells expressing eGFP (Fig. 9.31L; File. 9.2).

Together my data demonstrates that although the number of proliferating *Tp1:H2BmCherry*-expressing cell population increases in the absence of Notch following injury, the number of *pax7a:eGFP*; *Tp1:H2BmCherry*-expressing cell population is unaffected.

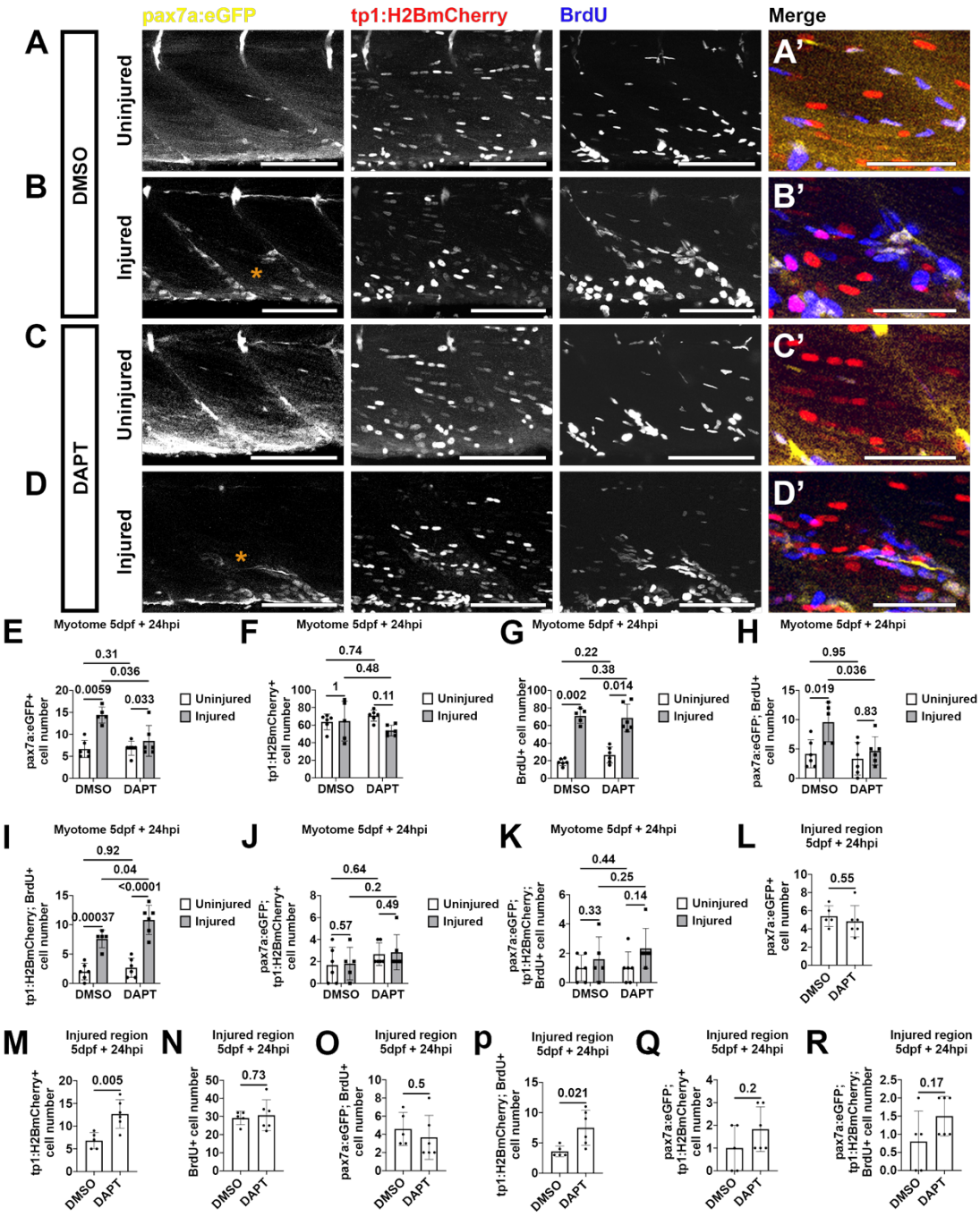
pax7a:eGFP
tp1:H2BmCherry
BrdU
Merge
A
B
C
D
DMSO
DAPT
Uninjured
Injured
A'
B'
C'
D'
E
F
G
H
I
J
K
L
M
N
O
P
Q
R
Myotome 5dpf + 24hpi
Injured region 5dpf + 24hpi
pax7a:eGFP+ cell number
tp1:H2BmCherry+ cell number
BrdU+ cell number
tp1:H2BmCherry; BrdU+ cell number
pax7a:eGFP; tp1:H2BmCherry+ cell number
pax7a:eGFP; tp1:H2BmCherry; BrdU+ cell number
pax7a:eGFP+ cell number
pax7a:eGFP; BrdU+ cell number
0.31
0.036
0.0059
0.033
0.74
0.48
1
0.11
0.22
0.38
0.002
0.014
0.95
0.036
0.019
0.83
0.92
0.04
<0.0001
0.00037
0.64
0.2
0.57
0.49
0.44
0.25
0.33
0.14
0.55
0.005
0.73
0.5
0.021
0.2
0.17

Figure 4.10. Proliferation of *Tp1:H2BmCherry*-expressing myoblasts is limited by Notch expression.

Projections of confocal stacks (**A-D**) of the myotome (**A'-D'**) in uninjured (**A, C**) and injured (**B, D**) 5 dpf *pax7a:eGFP*; *Tp1:H2BmCherry*-expressing larvae incubated with BrdU for 24 hours. Larvae were treated with 1% v/v DMSO (**A-B**) or 100 µM DAPT (**C-D**) after injury and detection of BrdU, eGFP and mCherry was performed by immunolabelling. Asterisk marks injured myotomes and cyan arrowheads highlights proliferating cells. Yellow eGFP+ cells expressing BrdU (appear green), mCherry+ (appear orange) or BrdU and mCherry (appear white) were observed (**A'-D'**). Red mCherry+ cells expressing BrdU (appear magenta) were identified (**A'-D'**). The number of eGFP+ cells (**E, L**), mCherry+ cells (**F, M**), BrdU+ (**G, N**), eGFP+BrdU+ cells (**H, O**), mCherry+BrdU+ cells (**I, P**), eGFP+mCherry+ cells (**J, Q**), and eGFP+mCherry+BrdU+ cells (**K, R**) were quantified. Cells were counted in the myotome (**E-K**) and injured region (**L-R**) of animals treated with DMSO or DAPT. Although there was no change to the number of mCherry+ cells following injury or DAPT treatment ($p>0.05$; **F**), there were more proliferating mCherry+ cells following injury in the presence or absence of Notch signalling ($p<0.05$; **I**) in the myotome. There was no change to the number of eGFP+mCherry+ cells (**J**) or eGFP+mCherry+BrdU+ cells following DAPT treatment ($p>0.05$; **K**) in the myotome. Contrastingly, there were more mCherry+ cells (**M**) and mCherry+BrdU+ cells (**P**) in the injured region following DAPT treatment. Significant differences in the myotome were tested by 2-way ANOVA (n=23) with Tukey's HSD post-hoc test or by transforming data by ART and performing 2-way ANOVA followed by a Dunn's test with Benjamini and Hochberg correction. Significant differences in the injured region were tested by Student's t-test or Wilcoxon Mann Whitney U rank sum test. Errors bars display standard deviation and values above bars indicate significance (p-values).

Scale bars: 100 µm (**A-D**), 50 µm (**A'-D'**).

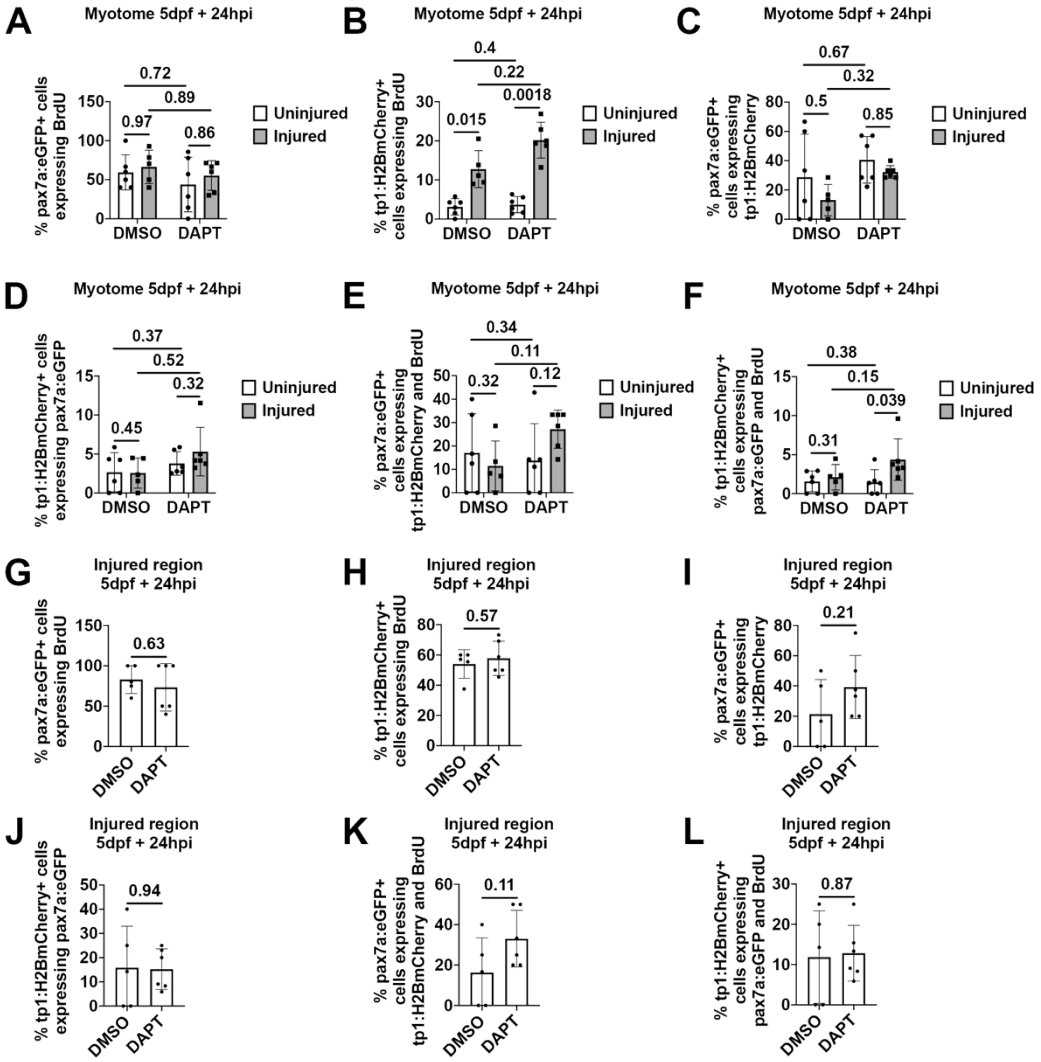

Figure 4.11. Notch inhibition does not affect the proportion of proliferating *Tp1:H2BmCherry*-expressing myoblasts.

The proportion of proliferating eGFP+ cells (**A, G**), mCherry+ cells (**B, H**), eGFP+ cells expressing mCherry (**C, I**), mCherry+ cells expressing eGFP (**D, J**), eGFP+BrdU+ cells expressing mCherry (**E, K**), and mCherry+BrdU+ cells expressing eGFP (**F, L**) was calculated from cell quantifications. DAPT treatment did not affect the proportion of proliferating mCherry+ cells. Significant differences in the myotome were tested by 2-way ANOVA (n=23) with Tukey's HSD post-hoc test or by transforming data by ART and performing 2-way ANOVA followed by a Dunn's test with Benjamini and Hochberg correction. Significant differences in the injured region were tested by Student's t-test, Welch's t-test or Wilcoxon Mann Whitney U rank sum test. Errors bars display standard deviation and values above bars indicate significance (p-values).

4.3 Discussion

Before elucidating the expression pattern of Notch signalling in muSCs following injury, I first investigated the usefulness of the *Tp1* reporter lines to measure Notch activity (Aulehla *et al.*, 2008; Parsons *et al.*, 2009; Ninov *et al.*, 2012). By using an antibody specific for cleaved NICD (Garcia-Concejo *et al.*, 2018), I could detect cleaved NICD immunoreactivity in all *Tp1:H2BmCherry*- and *Tp1*:VenusPEST-expressing cells in the developing zebrafish mid-brain. Therefore, I concluded that the *Tp1* reporter gene expression reflected Notch activation, in accordance with published work (Ninov *et al.*, 2012). The *Tp1:H2BmCherry* reporter line expresses a nuclear localised mCherry with a long half-life (Parsons *et al.*, 2009; Ninov *et al.*, 2012), whereas the *Tp1*:VenusPEST reporter line expresses a PEST-tagged Venus which has a shorter half-life (Aulehla *et al.*, 2008; Ninov *et al.*, 2012). Therefore, to understand if 1) cells expressing the *Tp1* transgenes respond to injury and 2) the dynamics of the two fluorophores, I performed live imaging on *Tp1:H2BmCherry*; *Tp1*:VenusPEST-expressing larvae. This allowed me to identify if cells which are actively expressing Notch (*Tp1*:VenusPEST) or cells which have expressed Notch (*Tp1:H2BmCherry*) respond to muscle injury, and if these populations overlap. I found that *Tp1*:VenusPEST-expressing cells respond to injury. Moreover, these cells began to express *Tp1:H2BmCherry* around 5 hpi before subsequently loosing *Tp1*:VenusPEST expression by approximately 11 hpi. By live imaging *pax7a:eGFP*; *Tp1:H2BmCherry*-expressing larvae, I found that these responding *Tp1:H2BmCherry*+ cells were not *pax7a:eGFP*+. Contrastingly, by live imaging *pax7a:eGFP*; *Tp1*:VenusPEST-expressing larvae following injury, I found that some proliferating and migrating muSCs express the *Tp1*:VenusPEST reporter. This is consistent with published work, suggesting that a low level of Notch signalling is maintained in proliferating muSCs following injury (Bjornson *et al.*, 2012; Mourikis, Sambasivan, *et al.*, 2012; Mourikis and Tajbakhsh, 2014).

The lack of *Tp1:H2BmCherry* expression in responding *pax7a:eGFP*-expressing cells in response to injury may be a result of the H2BmCherry maturation time. Therefore, I injured *pax7a:eGFP*; *Tp1:H2BmCherry*-expressing zebrafish, quantifying the number of cells 24 hpi, 48 hpi and 72 hpi. I found that although there was no change to the number of *Tp1:H2BmCherry*+ cells, there was a temporal increase in the number of

pax7a:eGFP+*Tp1:H2BmCherry*+ muSCs following injury. I noted that although there was an increase in the number of *Tp1:H2BmCherry*+ muSCs, this was a very small population relative to the total *Tp1:H2BmCherry*+ cell population, contributing little to fibre formation by 72 hpi. These findings were phenocopied when using the *pax7b* reporter line and Pax7 antibody. I recognised that the majority of *Tp1*+ nuclei are found within myofibers, which do not respond to muscle injury. Additionally, there is a smaller population of *Tp1*+ cells which respond to muscle injury.

The importance of Notch signalling during the development of zebrafish fin muscle has been previously described (Pascoal *et al.*, 2013; Lleras-Forero *et al.*, 2020). Therefore, to understand if the *Tp1:H2BmCherry*+ nuclei, which reside in myofibers are derived from a developmental cell population, I imaged *Tp1:H2BmCherry*+ and *Tp1*:VenusPEST+ larvae at 24 hpf and 48 hpf. I found that although mCherry persists until 48 hpf, Venus did not. Additionally, by fixing injured 30 dpf *pax7a:eGFP*;*Tp1:H2BmCherry*-expressing larvae 24 hpi, I found that all mCherry+ cells were eGFP+. In mouse, it has been shown that Notch signalling is important for the quiescent state of Pax7-expressing muSCs in mice (Kopan *et al.*, 1994; Bjornson *et al.*, 2012; Mourikis, Sambasivan, *et al.*, 2012; Yefei Wen *et al.*, 2012). Therefore, I have found that during the early developmental stage of zebrafish muscle development, eGFP+ muSCs did not have active Notch signalling. Contrastingly, in the 30 dpf juvenile zebrafish, eGFP+ muSCs displayed active Notch signalling, which may be important for their quiescence and maintenance, similarly to what happens in mouse.

Finally, to understand if Notch signalling was important for the proliferation of the *Tp1:H2BmCherry*+ cell population, I conducted a BrdU incorporation assay on *pax7a:eGFP*; *Tp1:H2BmCherry*-expressing larvae in the presence of DAPT or DMSO vehicle control. I found that although there were more proliferating mCherry+ cells after injury, this was unaffected by Notch inhibition. Assessing the number of cells at the site of injury (Ratnayake *et al.*, 2021), I found that the number of proliferating mCherry+ increased following DAPT treatment. Injury and DAPT treatment did not affect the number of proliferating eGFP+mCherry+ cells within the myotome or injured region.

4.4 Conclusion

Taken together, I have identified a novel *Tp1*-expressing cell population which responds to muscle injury in zebrafish. My data suggest that although muSCs express *Tp1*:VenusPEST following muscle injury, the *pax7a:eGFP*+ muSC and *Tp1:H2BmCherry*+ cells are largely two independent cell populations. Moreover, these cells appear to differentially respond to injury and Notch inhibition. In the absence of Notch signalling, *pax7a:eGFP*-expressing cells fail to proliferate in response to injury. Contrastingly, following injury, *Tp1:H2BmCherry*-expressing cells hyper-proliferate in the absence of Notch signalling. My results also highlight the presence of two *Tp1*+ myonuclei populations. Most *Tp1*+ nuclei reside in myofibers and do not respond to injury. Contrastingly, *Tp1:H2BmCherry*-expressing muSCs temporally increases following injury at the site of injury by 48 hpi. It is possible that the temporal increase in the number of *Tp1:H2BmCherry*-expressing muSCs is a result of the slow maturation of H2BmCherry, expressed in myoblasts which originally expressed *Tp1*:VenusPEST following injury.

Chapter 5 Macrophages are important for the regulation of muSCs following zebrafish muscle injury

5.1 Introduction

The process of post-natal myogenesis in response to sterile injury is a multi-cellular process (reviewed by Pedersen, 2011). Following injury, tissue resident macrophages, migratory neutrophils and then migratory macrophages respond to muscle-derived cytokines and chemoattractant cytokines, termed myokines (reviewed by Pedersen, 2011). Although the widely accepted model is that anti-inflammatory macrophages drive the regenerative process, promoting repair and reducing scarring, evidence suggest that a balance between pro- and anti-inflammatory signals are required for successful wound healing (Thornton, 1949; Mathew *et al.*, 2007). Early experiments in Xenopus have shown that beryllium treatment (inflammatory agent) results in failure to regenerate tissue (Thornton, 1949). Furthermore, this inability to repair tissue has also been observed when zebrafish were treated with beclomethasone (anti-inflammatory agent) following caudal fin amputation (Mathew *et al.*, 2007), demonstrating that pro-inflammatory signals are required for successful tissue repair.

The importance of macrophage function during the process of muscle repair has been demonstrated using murine macrophage depletion models (Arnold *et al.*, 2007; Segawa *et al.*, 2008). The loss of macrophages results in impaired myoblast proliferation and delayed differentiation, resulting in smaller myofibers (Arnold *et al.*, 2007; Segawa *et al.*, 2008). This demonstrates a key requirement of macrophages for the growth and repair of muscle (Dumont and Frenette, 2010). It has also been shown by *in vitro* co-culture systems and *in vivo* that pro-inflammatory macrophages promote myogenic precursor cell proliferation whereas anti-inflammatory macrophages promote migration and fusion (Mounier *et al.*, 2013; Saclier, Yacoub-Youssef, *et al.*, 2013). Whether there are distinct macrophage subtypes in zebrafish, is still undetermined. Zebrafish transgenic reporter lines used to visualize macrophage function in response to wounding and infection (Fan *et al.*, 2012; Nguyen-Chi *et al.*, 2015, 2017; Sanderson *et al.*, 2015), it has been shown that pro-inflammatory macrophages migrate towards injury (Mathias *et al.*, 2006; Ratnayake

et al., 2021). These pro-inflammatory macrophages express TNF-α (Nguyen-Chi *et al.*, 2015), subsequently switching to an anti-inflammatory phenotype associated with a decrease in pro-inflammatory cytokines (TNF-α, IL-1β, and IL-6; Nguyen-Chi *et al.*, 2015). Moreover, non-inflammatory macrophages have been shown to directly promote mesenchymal cell remodelling during muscle regeneration (Nguyen-Chi *et al.*, 2017). Vimentin is a type III intermediate filament protein expressed within blastemal cells following tail-fin amputation in zebrafish (LeBert *et al.*, 2018). Vimentin expression within cells at the wounded edge is important for collagen production and tissue reconstruction (LeBert *et al.*, 2018). Miskolci *et al.,* (2019) have demonstrated that tail fin amputations in zebrafish infected with *L. monocytogenes* displayed a protracted pro-inflammatory (TNF-α +) macrophage response (Miskolci *et al.*, 2019). This results in fewer vimentin-expressing cells, and a failure to regenerate damaged fin (Miskolci *et al.*, 2019).

How macrophages modulate muSC activity is not well understood, particularly in zebrafish. Evidence suggests that monocytes directly interact with myogenic precursor cells via adhesion molecules (Chazaud *et al.*, 2003). Recent work in zebrafish has also demonstrated that macrophages make contacts with muSCs following muscle injury (Ratnayake *et al.*, 2021). Although macrophages have been observed making long distance contacts with xanthoblasts (pigment cells) via DeltaC expressing protrusions in zebrafish (Eom and Parichy, 2017), it is not known if macrophages can regulate Notch signalling in muSCs. Therefore, in this chapter I utilise the nitroreductase metronidazole (MTZ) method to ablate macrophages in zebrafish (Gray *et al.*, 2011; Ratnayake *et al.*, 2021), to understand if macrophages are able to regulate Notch active cells (*Tp1*). Moreover, using dexamethasone (DEX) and TNF-α receptor mutant fish, I investigated the effect of an anti-inflammatory microenvironment on the activity of macrophages and neutrophils, and the consequences this has on the activity of Pax7- and *Tp1*-expressing cells following injury. Finally, by concomitantly treating larvae with MTZ and DAPT to ablate macrophages and inhibit Notch signalling, respectively, I aimed to understand if macrophages regulate Pax7- and *Tp1*-expressing cells in a Notch dependent manner.

5.2 Results

5.2.1 Fms:mCherry+ macrophage ablation in *fms:Gal4;UAS:NfsB-mCherry* zebrafish larvae using 5 mM Metronidazole

In order to understand the regulatory role of macrophages on the activity of muSCs following injury, I first optimised a system to ablate macrophages in zebrafish. A study by Gray *et al.,* (2011) has demonstrated that treating *fms:Gal4;UAS:NfsB-mCherry* (referred to as *fms:mCherry*) larvae with 5mM MTZ specifically ablates macrophages in whole larvae (Gray *et al.*, 2011). Moreover, recent work has demonstrated that 5 mM MTZ is sufficient to deplete 77.94% of anti-inflammatory macrophages in zebrafish (*mmp9; mpeg1*-expressing; Ratnayake *et al.*, 2021). To confirm that MTZ depletes *fms*+ macrophages without affecting the recruitment of *mpx*+ neutrophils in injured muscle of older larvae, I treated 4 dpf *fms:mCherry*; *mpx:GFP*-expressing larvae with 5 mM MTZ for 24 hours, before injuring the 13th left ventral myotome. Following injury, I continued to treat larvae with 5 mM MTZ. I then live-imaged both injured MTZ-treated and DMSO control animals on a 2-photon microscope, quantifying the number of recruited mCherry+ macrophages and GFP+ neutrophils (Fig. 9.5A, C; Movie. 9.7, 9.9). Following injury, I found that both macrophages (Fig. 9.5D) and neutrophils (Fig. 9.5E) are recruited to the site of injury in DMSO control animals. Furthermore, 5 mM MTZ treatment results in a total loss of macrophage recruitment (Fig. 9.5D) and a reduction in the number of recruited neutrophils (Fig. 9.5E). I observed that the number of neutrophils begins to decline in DMSO control animals by 3 hpi. Contrastingly, in MTZ-treated animals, the number of neutrophils continues to increase throughout the duration of the time-lapse imaging (Fig. 9.5E). This data confirms previous findings that no macrophages were observed at the injury site after 5 mM MTZ treatment.

5.2.2 Macrophage ablation results in more Pax7-expressing and Myog-expressing cells 24 hpi

In mouse, macrophage ablation results in reduced myoblast proliferation and premature differentiation, leading to smaller myofibers (Arnold *et al.*, 2007; Segawa *et al.*, 2008). Moreover, it has been shown in zebrafish that macrophage ablation results in fewer *pax3*-expressing and *pax7b*-expressing muSCs following injury (Ratnayake *et al.*, 2021). Ratnayake *et al.,* (2021) utilises the *mpeg* reporter line to ablate macrophages and induces large injuries using a 30g needle. Therefore, I aimed to investigate how *fms+* macrophage ablation affects the number of Pax7-expressing muSC following needlestick muscle injury in zebrafish. I treated 4 dpf *fms:mCherry*+ larvae with MTZ 24 hours before injury and continued the MTZ treatment following injury. Larvae were injured at 5 dpf. Pax7 and Myog expression marks activated and differentiating muSCs, respectively. Therefore, I examined the number of cells expressing Pax7 and Myog 24 hpi by immunolabelling relative to untreated control larvae (E3; Fig. 5.1A-B). I found that following macrophage ablation there were more Pax7+ (E3: 15.3 ± 8.6, MTZ: 26.5 ± 5.7; Fig. 5.1C) and Myog+ (E3: 12.5 ± 3.6, MTZ: 16.8 ± 1.7; Fig. 5.1D) cells in the injured myotome relative to untreated control animals. There was no change to the number of differentiating Pax7+ cells (Fig. 5.1E; File. 9.3). Interestingly, Pax7+ (Fig. 5.1A') and Myog+ (Fig. 5.1B') cells do not appear to align at the site of injury following macrophage ablation, compared to untreated animals. Therefore, I aimed to quantify the distribution of Pax7+ and Myog+ cells with respect to the injury. To do so, I assigned each Pax7+ and Myog+ cell an arbitrary co-ordinate, plotting each value and calculating the linear regression. I found that following macrophage ablation, both Pax7+ (E3: R^2 = 0.13, MTZ: R^2 = 0.059; Fig. 5.1L) and Myog+ (E3: R^2 = 0.16, MTZ: R^2 = 0.056; Fig. 5.1N) cells were less aligned at the site of injury compared to untreated animals (Fig. 5.1K, M).

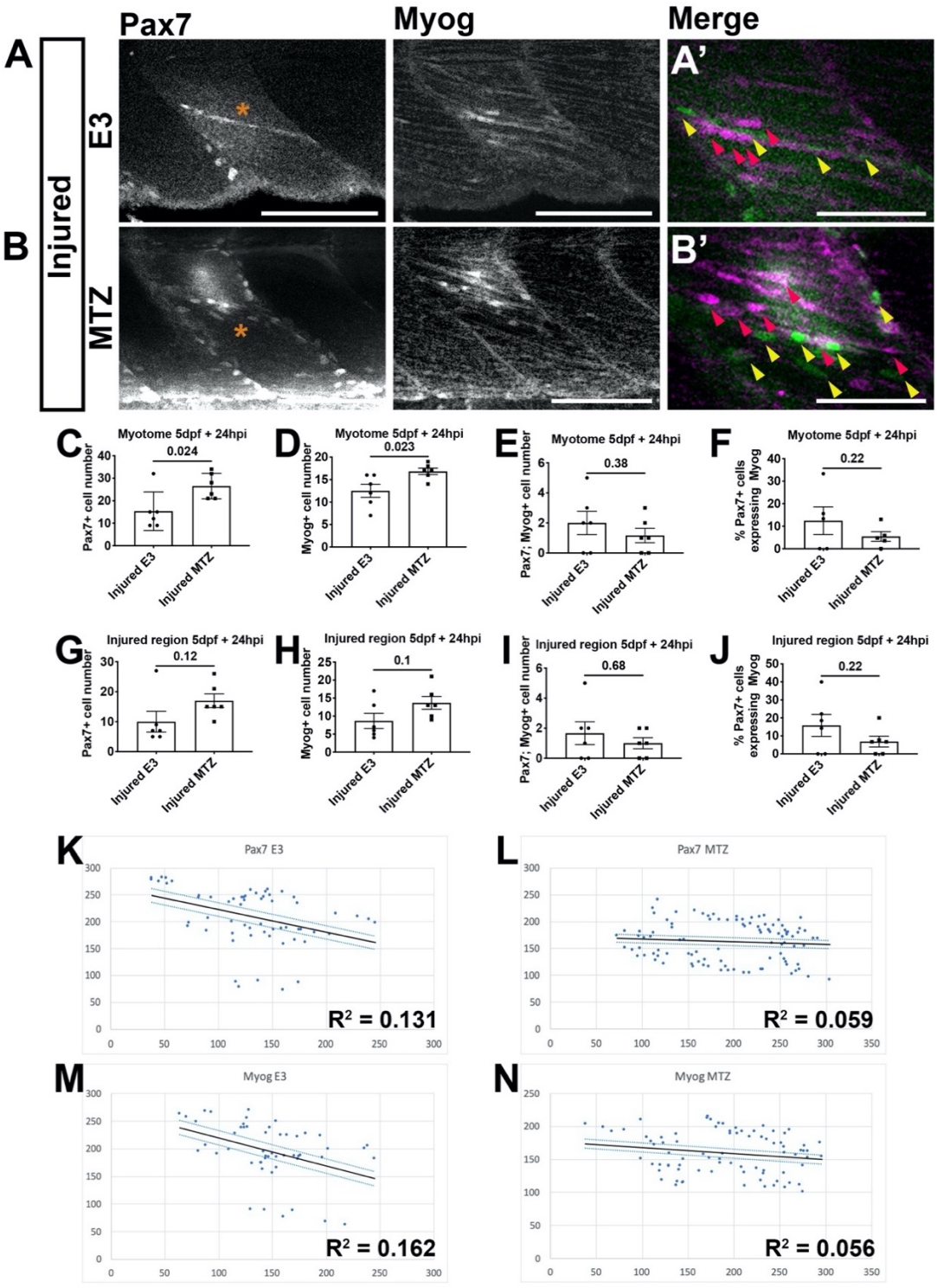
Pax7
Myog
Merge
A
B
Injured
E3
MTZ
A'
B'
C
Myotome 5dpf + 24hpi
0.024
Pax7+ cell number
D
Myotome 5dpf + 24hpi
0.023
Myog+ cell number
E
Myotome 5dpf + 24hpi
0.38
Pax7; Myog+ cell number
F
Myotome 5dpf + 24hpi
0.22
% Pax7+ cells expressing Myog
Injured E3
Injured MTZ
G
Injured region 5dpf + 24hpi
0.12
Pax7+ cell number
H
Injured region 5dpf + 24hpi
0.1
Myog+ cell number
I
Injured region 5dpf + 24hpi
0.68
Pax7; Myog+ cell number
J
Injured region 5dpf + 24hpi
0.22
% Pax7+ cells expressing Myog
K
Pax7 E3
R² = 0.131
L
Pax7 MTZ
R² = 0.059
M
Myog E3
R² = 0.162
N
Myog MTZ
R² = 0.056

Figure 5.1. Macrophages regulate Pax7 and Myog expressing muSCs following injury.
Representative projections from confocal z-stacks of the injured myotome in untreated (**A**) and MTZ-treated (**B**) 5 dpf *fms:mCherry*+ larvae 24 hpi. Cells expressing Pax7 (yellow arrowheads) and Myog (red arrowheads) immunoreactivity were detected by immunolabelling (**A'-B'**), and the number of cells were quantified in the injured myotome (asterisk; **C-F**) and injured region (**G-J**). Following MTZ treatment, there were more Pax7+ and Myog+ cells within the injured myotome (**C-D**), but not the injured region ($p > 0.05$; **G-H**). There was no change to the number or percentage of differentiating Pax7+ cells ($p > 0.05$; **E-F, I-J**). To assess the organisation of Pax7+ and Myog+ cells, the position of each cell was calculated relative to the site of injury, and the linear regression was calculated with Cis. Following macrophage ablation, both Pax7+ (**K-L**) and Myog+ (**M-N**) cells were less organised. Injury denoted with an asterisk. Significant differences were tested by Student's t-test or Wilcoxon Mann Whitney U rank sum test for normal and non-normal comparisons, respectively. Error bars represent standard deviation, and values above comparison bars represent significance (p-values). Linear regression represented by R^2 values.
Scale bars: 100 μm (**A-B**), 50 μm (**A'-B'**).

5.2.3 Macrophage ablation results in an increasing number of *pax7a*-expressing myofibers 72 hpi

In the absence of macrophages, there were more Pax7+ and Myog+ cells which were disorganised relative to the site of injury. I examined if this disorganization leads to the formation of ectopic fibres within the injured myotome. I treated 4 dpf *fms:mCherry*+ larvae with MTZ 24 hours before injury, continuing MTZ treatment after injury. I subsequently quantified the number of *pax7a:eGFP*-expressing muSCS cells 72 hpi relative to untreated control animals (Fig. 5.2A-B). I found that there were more *pax7a:eGFP*-expressing cells in the absence of macrophages within the injured myotome (E3: 11 ± 3.1, MTZ: 19.5 ± 6.5; Fig. 5.2A). Subsequently, I counted the number of eGFP+ myofibers and assessed the fusion index of muSCs. To calculate the fusion index of *pax7a:eGFP*-expressing muSCs, I quantified eGFP+ cells with two or more Hoechst+ nuclei. I found that, although there were more eGFP+ myofibers (E3: 2.7 ± 1, MTZ: 5.2 ± 2; Fig. 5.2D) in the absence of macrophages compared to untreated larvae, there was no change to the average fusion index (E3: 1.5 ± 1, MTZ: 1.9 ± 0.9; Fig. 5.2E) of *pax7a:eGFP*-expressing cells. This demonstrates that although there are more *pax7a:eGFP*-expressing muSCs fusing into more myofibers following injury in the absence of macrophages, the proportional fusion rate is unchanged. Using phalloidin to stain f-actin-enriched myofibers, I observed comparable muscle architecture between untreated (Fig. 5.2A) and MTZ-treated larvae (Fig. 5.2B), suggesting that the repair of muscle was not perturbed.

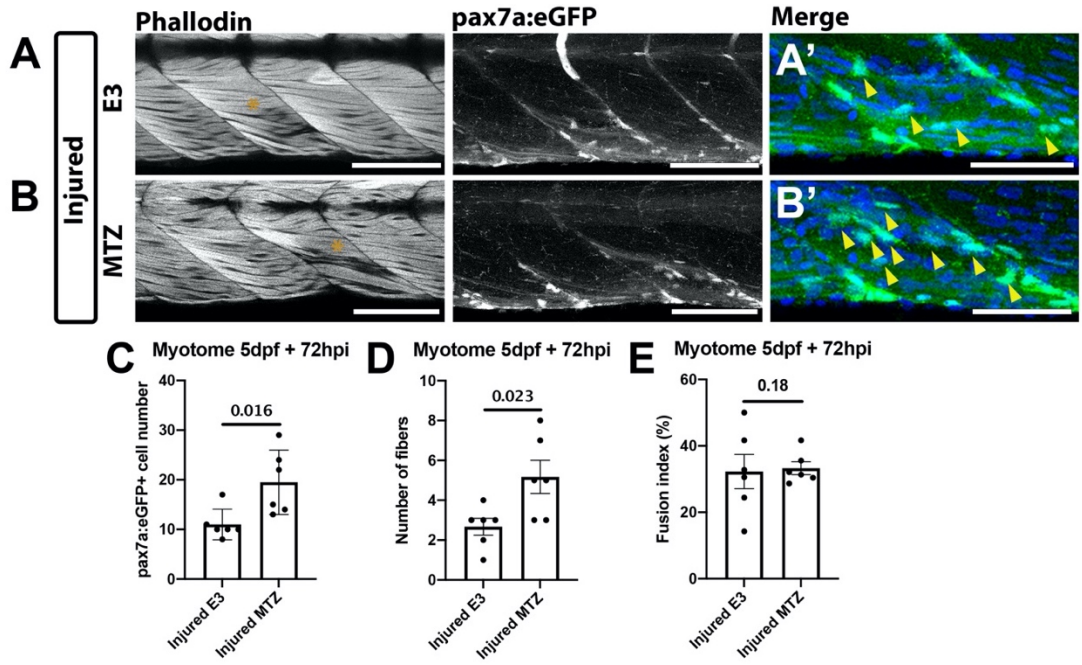

Figure 5.2. Macrophage ablation does not affect the fusion of *pax7a*-expressing muSCs.
Representative projections from confocal z-stacks of the injured myotome in untreated (**A**) and MTZ-treated (**B**) 5 dpf *pax7a:eGFP*; *fms:mCherry*+ larvae 72 hpi. eGFP+ cells (yellow arrowheads) were detected (**A'-B'**), and the number of cells were quantified in the injured myotome (**C**). Myofibers were detected by phalloidin staining, relative to the site of injury (asterisk). Following MTZ treatment, there were more eGFP+ cells (**C**). To assess fusion, the number of eGFP+ cells with two or more Hoechst+ nuclei were quantified. Although there were more myofibers (**D**), the fusion index of eGFP+ cells was no altered by the absence of macrophages ($p > 0.05$; **E**). Significant differences were tested by Student's t-test or Wilcoxon Mann Whitney U rank sum test for normal and non-normal comparisons, respectively. Error bars represent standard deviation, and values above comparison bars represent significance (p-values).
Scale bars: 100 µm (**A-B**), 50 µm (**A'-B'**).

5.2.4 Injury size modulates the effects of macrophage ablation on the number of Pax7-expressing cells

Recent work has demonstrated the importance of macrophage function on the regulation of pax3-expressing muSC proliferation in zebrafish (Ratnayake *et al.*, 2021). The ablation of macrophages results in fewer proliferating muSCs following needlestab injuries (Ratnayake *et al.*, 2021). This finding contradicts my own data which I predicted was a consequence of the injury size. Larger needlestab injuries disrupts the myosepta (Fig. 2.1), which has been described as the muSC niche in zebrafish (Nguyen-Chi *et al.*, 2017). Therefore, I aimed to understand if the size of the injury affects the muSC response towards injury following macrophage ablation. I treated 4 dpf *fms:mCherry*+ larvae with MTZ 24 hours. Subsequently, I injured the larvae using the needlestick or needlestab method (Fig. 2.1), refreshing the MTZ after injury. I then assessed the number of cells expressing Pax7 by immunolabelling 24 hpi and 48 hpi relative to untreated controls (24 hpi: Fig. 5.3A-D, 48 hpi: Fig. 5.4A-D). I found that smaller needlestick injuries resulted in more Pax7-expressing muSCs within the injured myotome following MTZ treatment by 24 hpi (E3: 15 ± 5.9, MTZ: 38.2 ± 13.6; Fig. 5.3E) and 48 hpi (E3: 9.8 ± 3, MTZ: 18.4 ± 4; Fig. 5.4E). Contrastingly, when damaging 4-6 myotomes with the larger needlestab method, there were less Pax7 cells within the injured myotome following MTZ treatment by 24 hpi (E3: 143.8 ± 35.7, MTZ: 100 ± 31.3; Fig. 5.3E) and 48 hpi (E3: 173.2 ± 64.3, MTZ: 78.4 ± 27.3; Fig. 5.4E). I have shown that injury size affects how muSCs respond to macrophage ablation after injury.

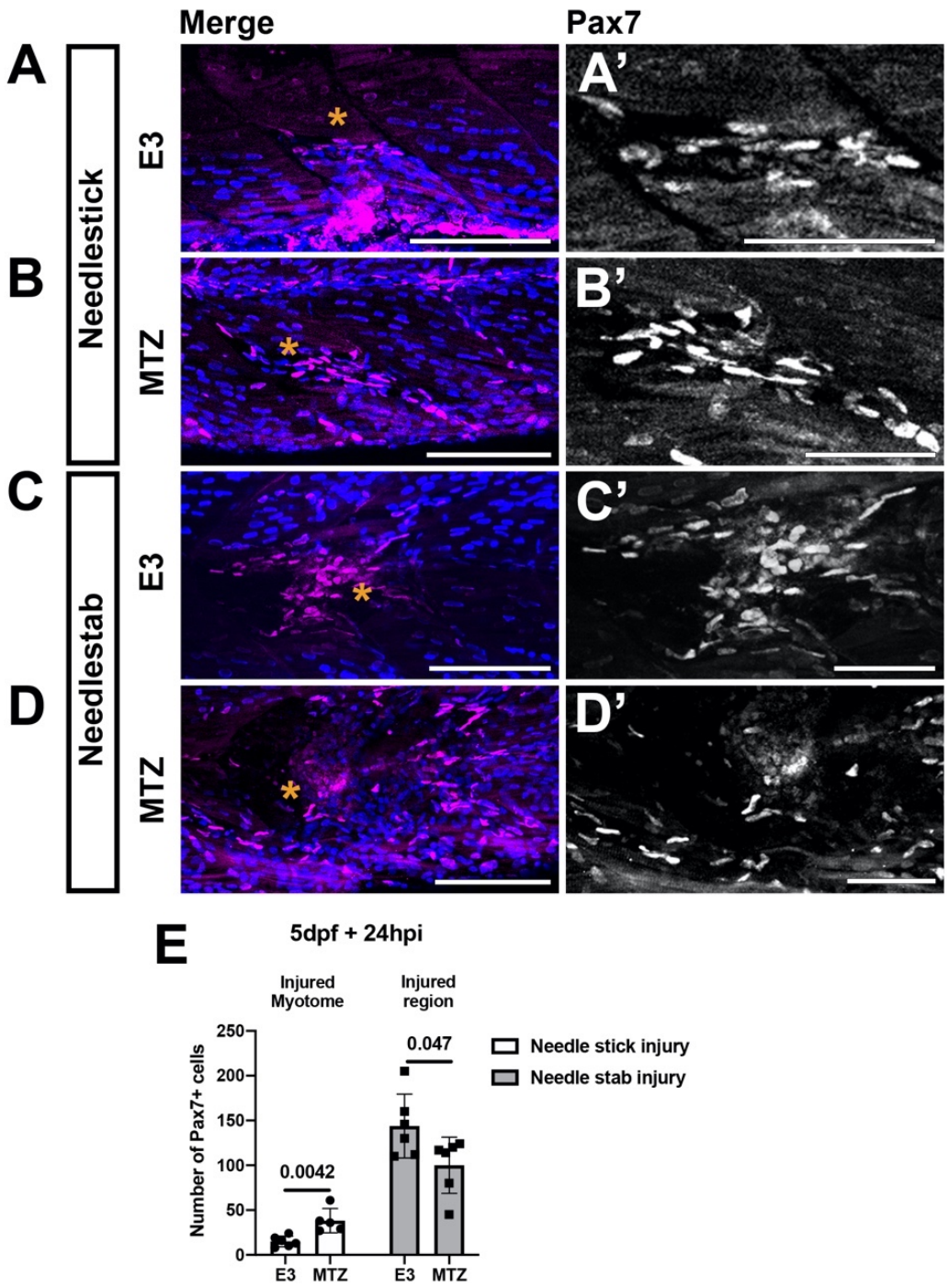

Figure 5.3. Larger myotome injures results in fewer Pax7 expressing cells 24 hpi.
5dpf *fms:mCherry*+ larvae were injured using a tungsten wire (A-B) or 30g needle (C-D). Representative projections from confocal z-stacks of the injured myotome in untreated (**A, C**) and MTZ-treated (**B, D**) larvae 24 hpi. Cells expressing Pax7 immunoreactivity were detected by immunolabelling (**A'-D'**), and the number of cells were quantified in the injured myotome (asterisk; **A-B**) or injured region (asterisk; **C-D**). Following macrophage ablation, there were more Pax7+ cells within the injured myotome when using the needlestick method. There were less Pax7+ cells within the injured region when using the needlestab method. Significant differences were tested by Student's t-test. Error bars represent standard deviation, and values above comparison bars represent significance (p-values).
Scale bars: 100 µm (**A-D**), 50 µm (**A'-D'**).

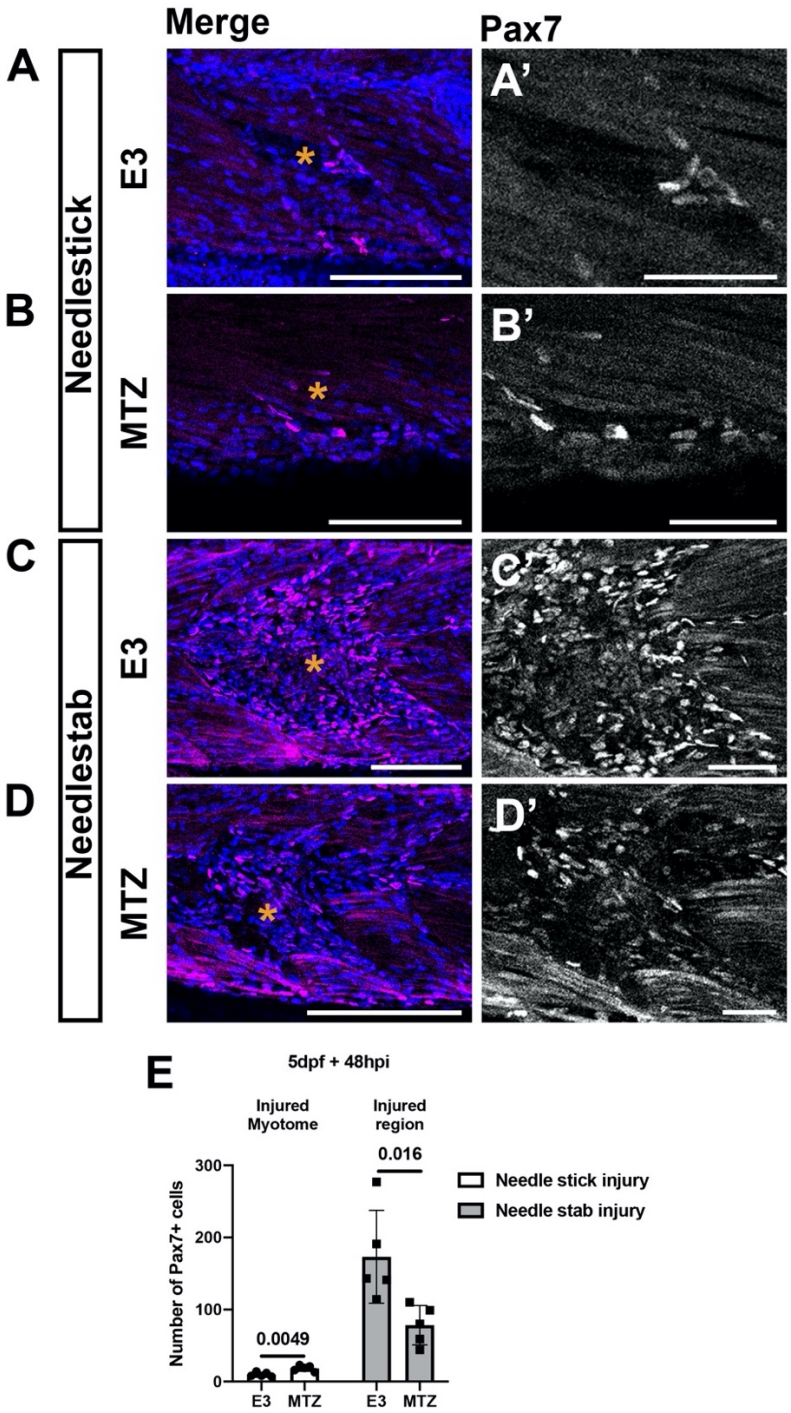

Figure 5.4. Larger myotome injures results in fewer Pax7 expressing cells 48 hpi.
5dpf *fms:mCherry*+ larvae were injured using a tungsten wire (A-B) or 30g needle (C-D). Representative projections from confocal z-stacks of the injured myotome in untreated (**A, C**) and MTZ-treated (**B, D**) larvae 48 hpi. Cells expressing Pax7 immunoreactivity were detected by immunolabelling (**A'-D'**), and the number of cells were quantified in the injured myotome (asterisk; **A-B**) or injured region (asterisk; **C-D**). Following macrophage ablation there were more Pax7+ cells within the injured myotome when using the needlestick method (**E**). There were less Pax7+ cells within the injured region when using the needlestab method (**E**). Significant differences were tested by Student's t-test. Error bars represent standard deviation, and values above comparison bars represent significance (p-values).
Scale bars: 100 µm (**A-D**), 50 µm (**A'-D'**).

5.2.5 Increased number of *Tp1:H2BmCherry*-expressing cells following injury in the absence of macrophages

I have previously identified a novel population of injury responsive *Tp1:H2BmCherry*+ cells. To understand the importance of macrophages on the activity of *Tp1:H2BmCherry*-expressing cells following injury, I treated 4 dpf *Tp1:H2BmCherry*; *fms:mCherry*-expressing larvae with MTZ for 24 hours before injuring the 13th left ventral myotome (Fig. 5.5A-B). Following injury, I continued to treat larvae with MTZ. I found that following injury there were more mCherry+ cells within the injured region in the absence of macrophages (E3: 0 ± 0, MTZ: 8 ± 1.8; Fig. 5.5C).

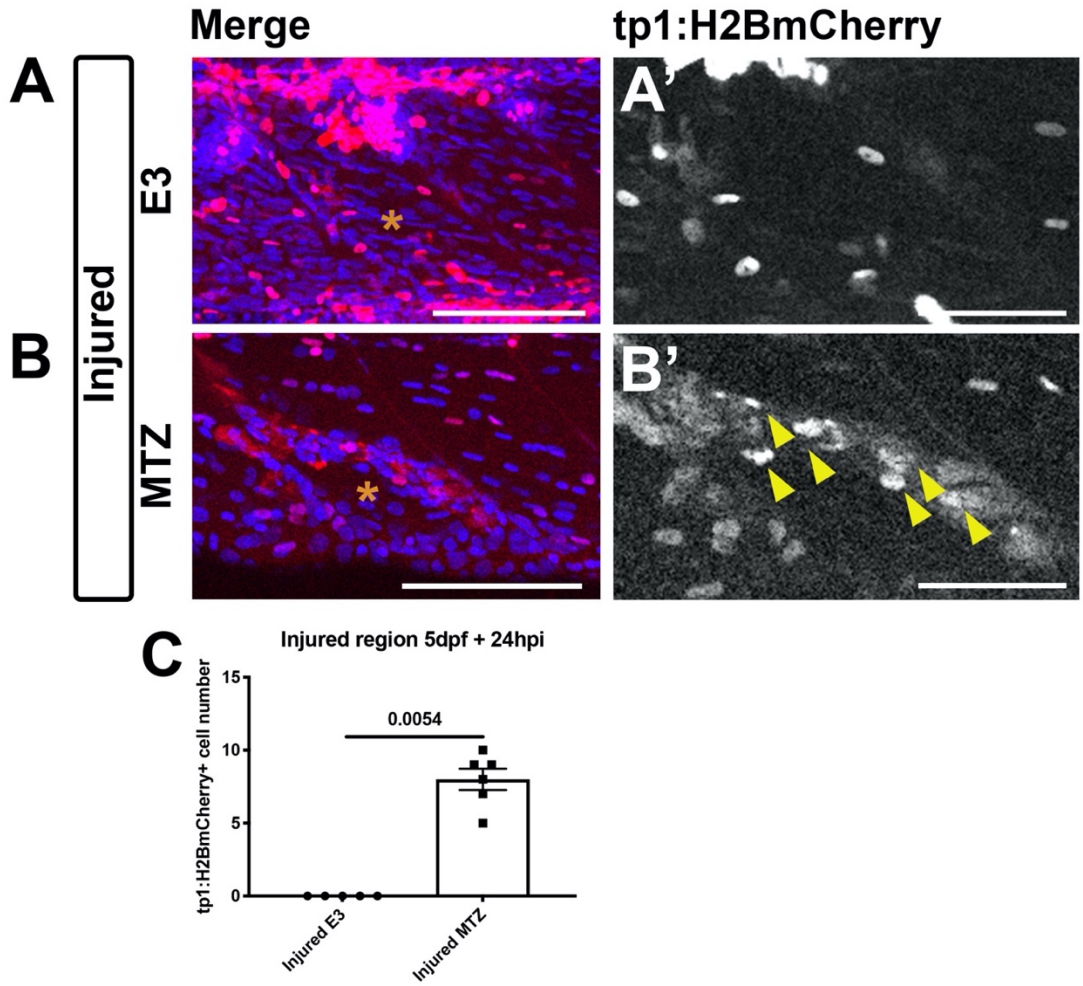

Figure 5.5. Macrophages regulate *Tp1* expressing myoblasts following injury.
Representative projections from confocal z-stacks of the injured myotome in untreated (**A**) and MTZ-treated (**B**) 5 dpf *Tp1:H2BmCherry*; *fms:mCherry*+ larvae 24 hpi. mCherry+ cells (yellow arrowheads) were detected (**A'-B'**), and the number of cells were quantified in the injured region (asterisk; **C**). Following macrophage ablation there were more mCherry+ cells within the injured region. Significant difference was tested by Wilcoxon Mann Whitney U rank sum test. Error bars represent standard deviation, and values above comparison bars represent significance (p-values).
Scale bars: 100 µm (**A-B**), 50 µm (**A'-B'**).

5.2.6 Macrophage ablation leads to more proliferating *Tp1:H2BmCherry*-expressing cells following injury

Next, I aimed to understand if the increased number of *Tp1:H2BmCherry*- expressing cells observed following injury in the absence of macrophages is a consequence of increased proliferation. I treated 4 dpf *Tp1:H2BmCherry*; *fms:mCherry*-expressing larvae with MTZ for 24 hours before injury. Following injury, I treated larvae with MTZ and BrdU. I subsequently counted the number of mCherry+, BrdU+ and mCherry+BrdU+ cells relative to untreated controls (Fig. 5.6A-D). To determine if macrophage ablation affects mCherry+ cell proliferation, I assessed the number of cells within the injured region. I found that there were more mCherry+BrdU+ cells in the absence of macrophages, relative to untreated larvae (E3: 3.2 ± 0.8, MTZ: 5 ± 1.6; Fig. 5.6G). This did not result from a change in the proportion of proliferating mCherry+ cells (Fig. 5.6H; File. 9.3). This suggests that although there are more proliferative *Tp1*+ cells following injury in the absence of macrophages, the rate of proliferation does not change.

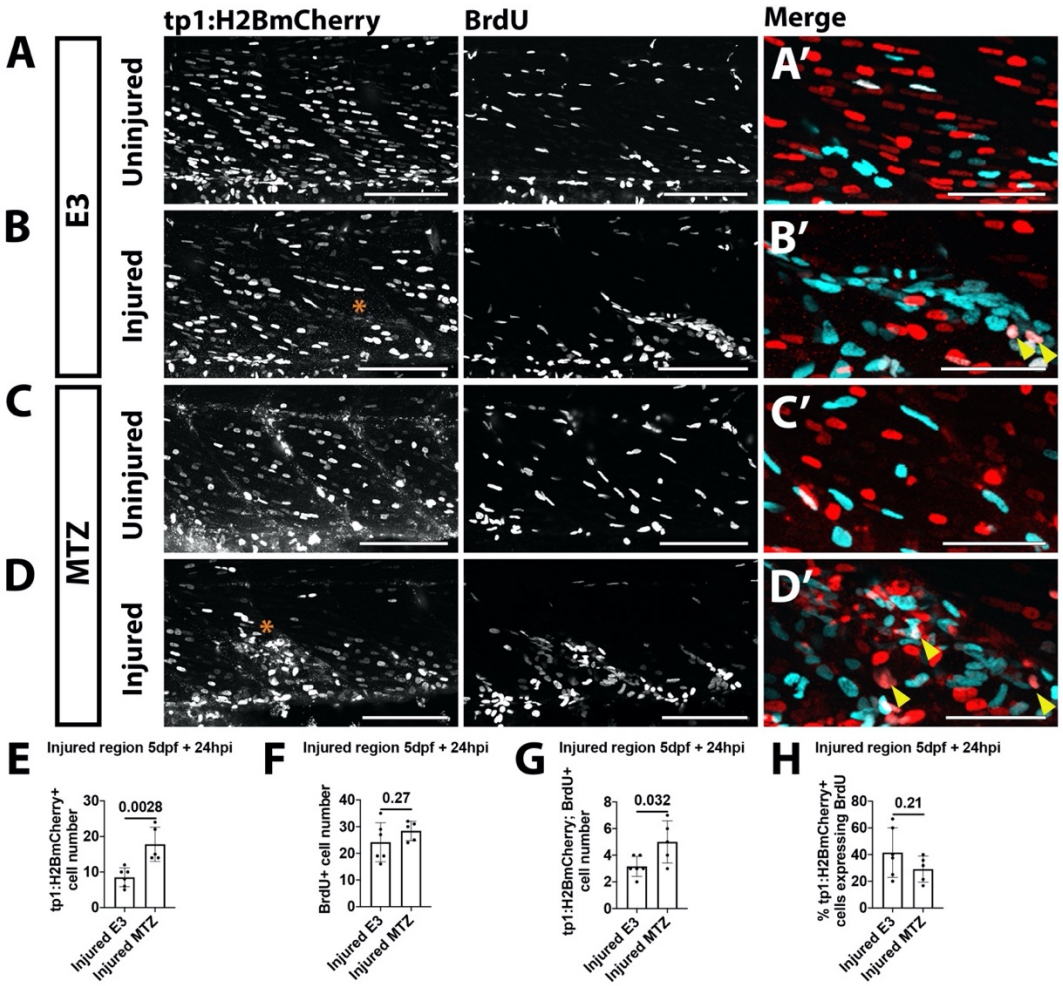

Figure 5.6. Macrophage ablation results in more proliferating *Tp1* expressing cells following injury.

Representative projections from confocal z-stacks of the myotome (asterisks) in uninjured (**A, C**) and injured (**B, D**) 5 dpf *Tp1:H2BmCherry*; *fms:mCherry*+ larvae incubated with BrdU for 24 hours. Larvae were untreated (**A-B**) or treated with MTZ (**C-D**). mCherry+ cells which had incorporated BrdU (yellow arrowheads) were detected by immunolabelling (**A'-D'**) and quantified in the injured region (**E-H**). Following injury, MTZ treatment results in more mCherry+ cells within the injured region (**G**), which are proliferating (**H**). There was no change to the proportion of proliferating mCherry+ cells (**L**). Significant differences were tested by Student's t-test. Errors bars display standard deviation and values above bars indicate significance (p-values).

Scale bars: 100 µm (**A-D**), 50 µm (**A'-D'**).

5.2.7 Macrophage ablation results in an increased number of *Tp1:H2BmCherry*-expressing Pax7 positive cells 24 hpi

I have previously observed an increase in the number of Pax7+ and *Tp1:H2BmCherry*+ cells following injury in an absence of macrophages. To determine if the change to the number of *Tp1:H2BmCherry*-expressing cells represents a change in the resident Pax7+*Tp1*+ population, I compared mCherry to Pax7 expression. I pre-treated 4 dpf *Tp1:H2BmCherry*; *fms:mCherry*+ larvae with MTZ for 24 hours before injury. Following injury, I refreshed the MTZ treatment. At 24 hpi, I quantified the number of Pax7+ and mCherry+ cells by immunolabeling (Fig. 5.7A-B). I detected more Pax7+mCherry+ cells within the injured myotome (E3: 2 ± 1.7, MTZ: 4.4 ± 1.7; Fig. 5.7E) and injured region (E3: 0.8 ± 0.9, MTZ: 3 ± 0.8; Fig. 5.7J) following macrophage ablation. This was not due to a change in the proportion of Pax7+ cells expressing mCherry (Fig. 5.7F, K) or mCherry+ cells expressing Pax7 (Fig. 5.7G, L; File. 9.3).

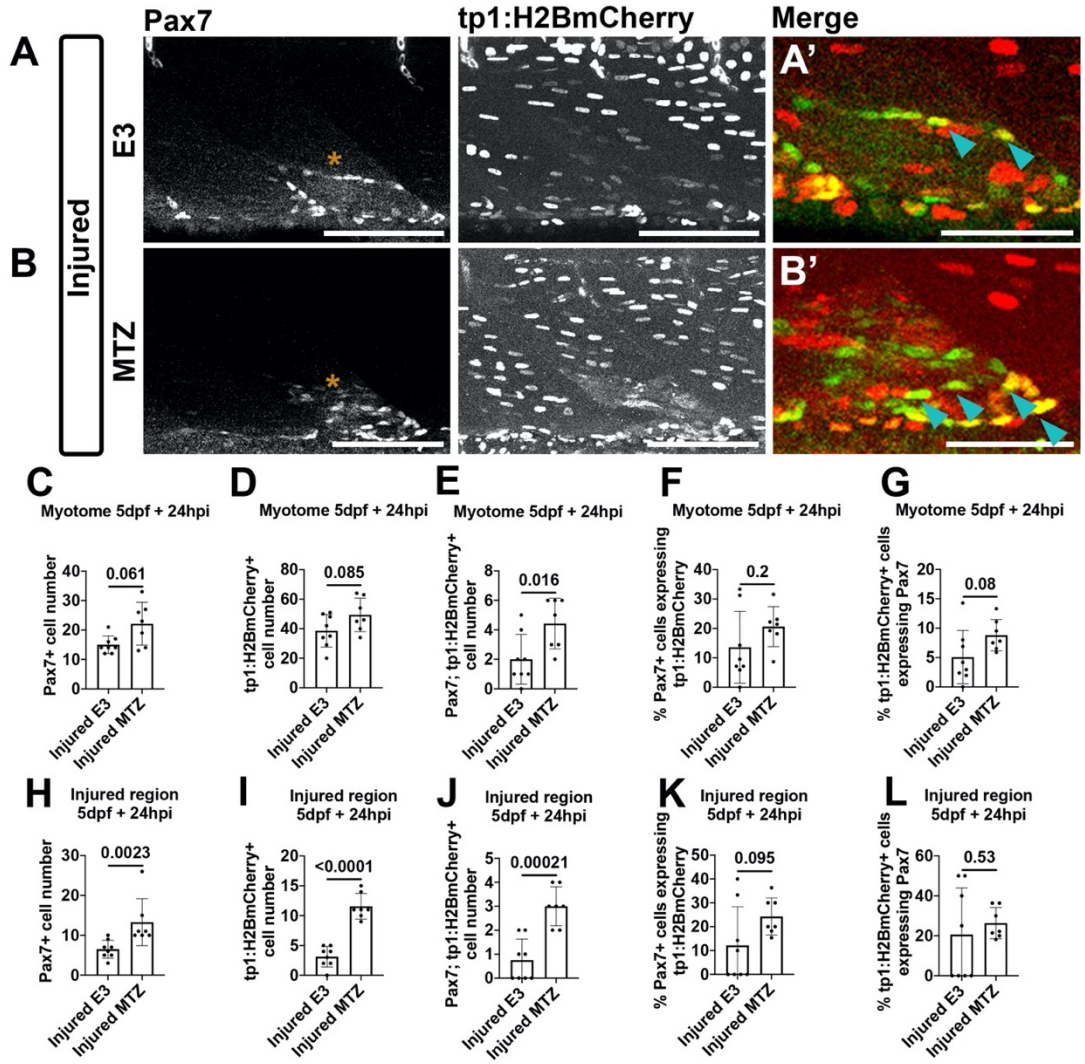

Figure 5.7. Macrophages regulate Pax7; *Tp1:H2BmCherry* expressing cells following injury.

Representative projections from confocal z-stacks of the injured myotome in untreated (**A**) and MTZ treated (**B**) 5 dpf *Tp1:H2BmCherry*; *fms:mCherry*+ larvae 24 hpi. Cells expressing Pax7 immunoreactivity were detected by immunolabelling (**A'-B'**), and the number of cells were quantified in the injured myotome (**C-G**) and injured region (**H-L**). Following macrophage ablation there were more Pax7+mCherry+ cells (cyan arrowheads) within the injured myotome (**E**) and injured region (**J**). This did not result from a proportional change ($p > 0.05$; **F-G, K-L**). Injury denoted with an asterisk. Significant differences were tested by Student's t-test or Wilcoxon Mann Whitney U rank sum test for normal and non-normal comparisons, respectively. Error bars represent standard deviation, and values above comparison bars represent significance (p-values).

Scale bars: 100 µm (**A-B**), 50 µm (**A'-B'**).

5.2.8 Macrophage ablation does not affect the *pax7a:eGFP*-expressing cell response to injury 24 hpi

I subsequently determined if the expansion of the Pax7; *Tp1:H2BmCherry* positive cell population following injury in the absence of macrophages are derived from the existing *pax7a* population. To determine if *Tp1*+ myoblasts expressing Pax7 are derived from *pax7a:eGFP*-expressing myoblasts, I compared mCherry and eGFP expression in *pax7a:eGFP*; *Tp1:H2BmCherry*-expressing animals. I treated 4 dpf *pax7a:eGFP*; *Tp1:H2BmCherry*; *fms:mCherry*+ larvae with MTZ for 24 hours. Following MTZ treatment, larvae were injured and continuously treated with MTZ (Fig. 5.8A-D). To understand if macrophage ablation affects the number of eGFP+, mCherry+, and eGFP+mCherry+ cells, I conducted a 2-way ANOVA. I found that macrophage ablation did not affect the number or percentage of eGFP+mCherry+ cells in response to injury (File. 9.3).

To determine changes in the number of eGFP+ cells in the myotome following injury and macrophage ablation, I conducted a 1-way ANOVA. I found that the number of eGFP+ cells increased following injury of untreated (uninjured: 7 ± 1.1, injured: 15 ± 5.4; Fig. 5.8E) and MTZ treated larvae (uninjured: 7.2 ± 1.7, injured: 12.8 ± 2.6; Fig. 5.8E). I found no change in the number of eGFP+mCherry+ cells (Fig. 5.8G; File. 9.3) or the proportion of eGFP+ cells expressing mCherry (Fig. 5.8H; File. 9.3). I also identified an increase in the proportion of mCherry+ cells expressing eGFP in injured muscle absent of macrophages (uninjured: 0.6% ± 1%, injured: 10.9% ± 16.5%; Fig. 5.8I).

To understand if the increase in mCherry+ cells (Fig. 5.8K; File. 9.3) within the injured region is reflected by a change in the number of eGFP+mCherry+ cells, I assessed the number of cells at the site of injury. I found no change in the number of eGFP+ (Fig. 5.8J; File. 9.3), or eGFP+mCherry+ (Fig. 5.8L; File. 9.3) cells. There was also no change in the proportion of eGFP+mCherry+ cells (Fig. 5.8M-N; File. 9.3). This suggests that although there is an increase in the number of *Tp1*+ cells in the absence of macrophages, these cells are not part of the *pax7a:eGFP*+ population of muSCs.

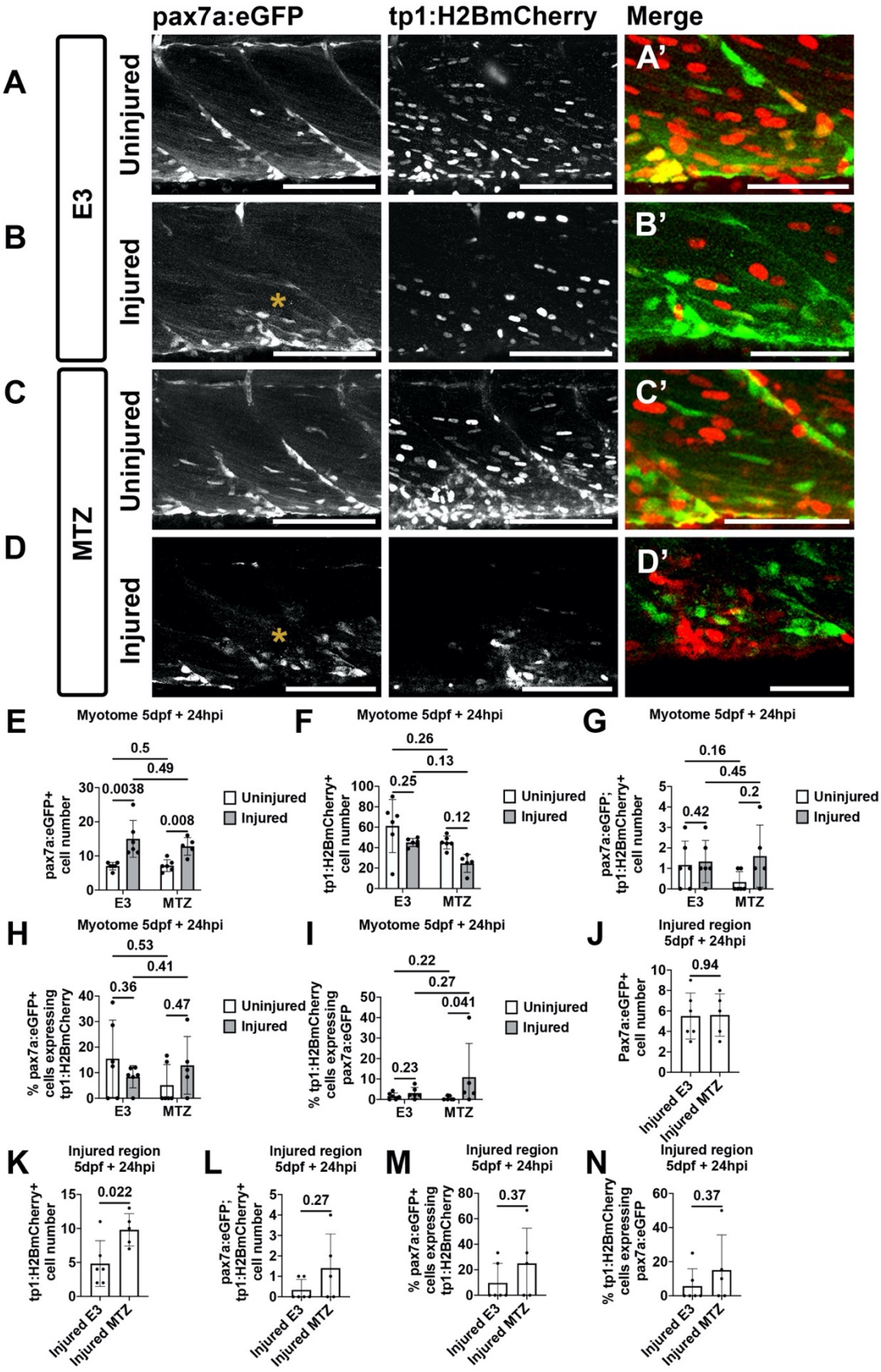
pax7a:eGFP
tp1:H2BmCherry
Merge
A
B
C
D
E3
MTZ
Uninjured
Injured
A'
B'
C'
D'
E
Myotome 5dpf + 24hpi
pax7a:eGFP+ cell number
0.5
0.49
0.0038
0.008
F
tp1:H2BmCherry+ cell number
0.26
0.13
0.25
0.12
G
pax7a:eGFP; tp1:H2BmCherry+ cell number
0.16
0.45
0.2
0.42
H
% pax7a:eGFP+ cells expressing tp1:H2BmCherry
0.53
0.41
0.36
0.47
I
% tp1:H2BmCherry cells expressing pax7a:eGFP
0.22
0.27
0.041
0.23
J
Injured region 5dpf + 24hpi
Pax7a:eGFP+ cell number
0.94
Injured E3
Injured MTZ
K
tp1:H2BmCherry+ cell number
0.022
L
pax7a:eGFP; tp1:H2BmCherry+ cell number
0.27
M
% pax7a:eGFP+ cells expressing tp1:H2BmCherry
0.37
N
% tp1:H2BmCherry cells expressing pax7a:eGFP
0.37

Figure 5.8. Macrophage ablation does not affect the *pax7a* expressing muSC response to injury 24 hpi.
Representative projections from confocal z-stacks of the myotome (asterisks) in uninjured (**A, C**) and injured (**B, D**) 5 dpf *pax7a:eGFP*; *Tp1:H2BmCherry*; *fms:mCherry*+ larvae 24 hpi. Larvae were untreated (**A-B**) or treated with MTZ (**C-D**). eGFP+ and mCherry+ cells were detected (**A'-D'**), and the number of cells were quantified in the injured myotome (**E-I**) and injured region (**J-N**). Macrophage ablation did not affect the number of eGFP+ ($p > 0.05$; **E, J**) or eGFP+mCherry+ ($p > 0.05$; **G, L**) muSCs following injury. Significant differences in the myotome were tested by 2-way ANOVA (n=22) with Tukey's HSD post-hoc test or by transforming data by ART and performing 2-way ANOVA followed by a Dunn's test with Benjamini and Hochberg correction. Significant differences in the injured region were tested by Student's t-test or Wilcoxon Mann Whitney U rank sum test. Error bars represent standard deviation, and values above comparison bars represent significance (p-values).
Scale bars: 100 μm (**A-D**), 50 μm (**A'-D'**).

5.2.9 A higher proportion of *Tp1:H2BmCherry*+ cells express *pax7a:eGFP* in the absence of macrophages 48 hpi

I have previously demonstrated that by 72 hpi there are more *pax7a:eGFP*+ muSCs following macrophage ablation relative to untreated control animals (Fig. 5.2). Subsequently, I aimed to understand if there is a temporal increase in the number of *pax7a:eGFP*; *Tp1:H2BmCherry*-expressing cells following injury at 48 hpi. I treated 4 dpf *pax7a:eGFP*; *Tp1:H2BmCherry*; *fms:mCherry*-expressing larvae with MTZ for 24 hours before injury. Following injury, I refreshed the MTZ treatment. I then quantified the number of eGFP+, mCherry+ and eGFP+mCherry+ cells relative to untreated larvae 48 hpi (Fig. 5.9A-D). To understand if macrophage ablation affects the number of mCherry+ cells expressing eGFP within the myotome, I conducted a 2-way ANOVA. I found that MTZ treatment affected the number of eGFP+ and mCherry+ cells (File. 9.3). Furthermore, the relative proportion of cells expressing both transgenes increased in injured animals when macrophages were ablated (File. 9.3). I also found that the increased number of eGFP+ and mCherry+ cells following injury was higher following macrophage ablation (File. 9.3). Macrophage ablation did not affect the eGFP+mCherry+ response to injury (File. 9.3). I also found that macrophage ablation increases the proportion of mCherry+ cells expressing eGFP in response to injury (File. 9.3), suggesting that *Tp1:H2BmCherry*-expressing cells temporally express *pax7a:eGFP*.

Within the injured myotome, I compared cell number by 1-way ANOVA. This revealed that there were more eGFP+ cells in the injured myotome of untreated larvae, which increased following macrophage ablation (E3: 13.2 ± 2.8, MTZ: 19.8 ± 3.2; Fig. 5.9E). I also observed more mCherry+ cells in the injured myotome of MTZ-treated relative to untreated control larvae (E3: 22.5 ± 7.4, MTZ: 33.2 ± 2.6; Fig. 5.9F).

Following the quantification of *pax7a:eGFP*; *Tp1:H2BmCherry*-expressing cells within the injured myotome, I found there were more eGFP+mCherry+ cells with the myotome of untreated larvae following injury (uninjured: 1 ± 0.9, injured: 4.8 ± 1.6; Fig. 5.9G). This increase in eGFP+mCherry+ number is a reflection of an increased proportion of cells co-expressing both transgenes (Fig. 5.9H-I; File. 9.3). In the absence of macrophages, there were more eGFP+mCherry+ cells following injury within the myotome (uninjured: 0.7 ± 0.8, injured: 4.3 ± 1.8; Fig. 5.9G). Following

macrophage ablation, I did not observe a change in the proportion of eGFP+ cells expressing mCherry after injury (Fig. 5.9H; File. 9.3). Contrastingly, there was an increase in the proportion of mCherry+ cells expressing eGFP following injury in the absence of macrophages (uninjured: 2.4% ± 3.2%, injured: 13% ± 5.1%; Fig. 5.9I). This suggests that mCherry+ cells are temporally expressing eGFP, but eGFP+ cells are not upregulating mCherry.

To test if the increased proportion of eGFP+mCherry+ cells is a consequence of cell fusion, I quantified the number of multinucleate eGFP+mCherry+ cells in the absence of macrophages. I found that there were no multinucleate eGFP+mCherry+ cells in uninjured larvae (0 ± 0; Fig. 5.9A', C'), which did not change following injury (0 ± 0; Fig. 5.9B', D'). This shows that the increased proportion of eGFP+mCherry+ cells following macrophage ablation is a consequence of mCherry+ cells upregulating eGFP after injury and not cell fusion.

I identified an increase in the number of *Tp1:H2BmCherry* cells within the injured region (E3: 4.8 ± 2.2, MTZ: 12.2 ± 2.1; Fig. 5.9K). Although I did not detect a change in the number of eGFP+mCherry+ cells following macrophage ablation (E3: 3 ± 1.5, MTZ: 3.2 ± 2; Fig. 5.9L), there was a decrease in the proportion of mCherry+ cells expressing eGFP (E3: 59.5% ± 33.9%, MTZ: 25.4% ± 13.3%; Fig. 5.9N). This proportional decrease is likely due to the drastic increase in the number of mCherry+eGFP- cells within the injured region following macrophage ablation. There was no change in the proportion of eGFP+ cells expressing mCherry in the absence of macrophages (Fig. 5.9M; File. 9.3).

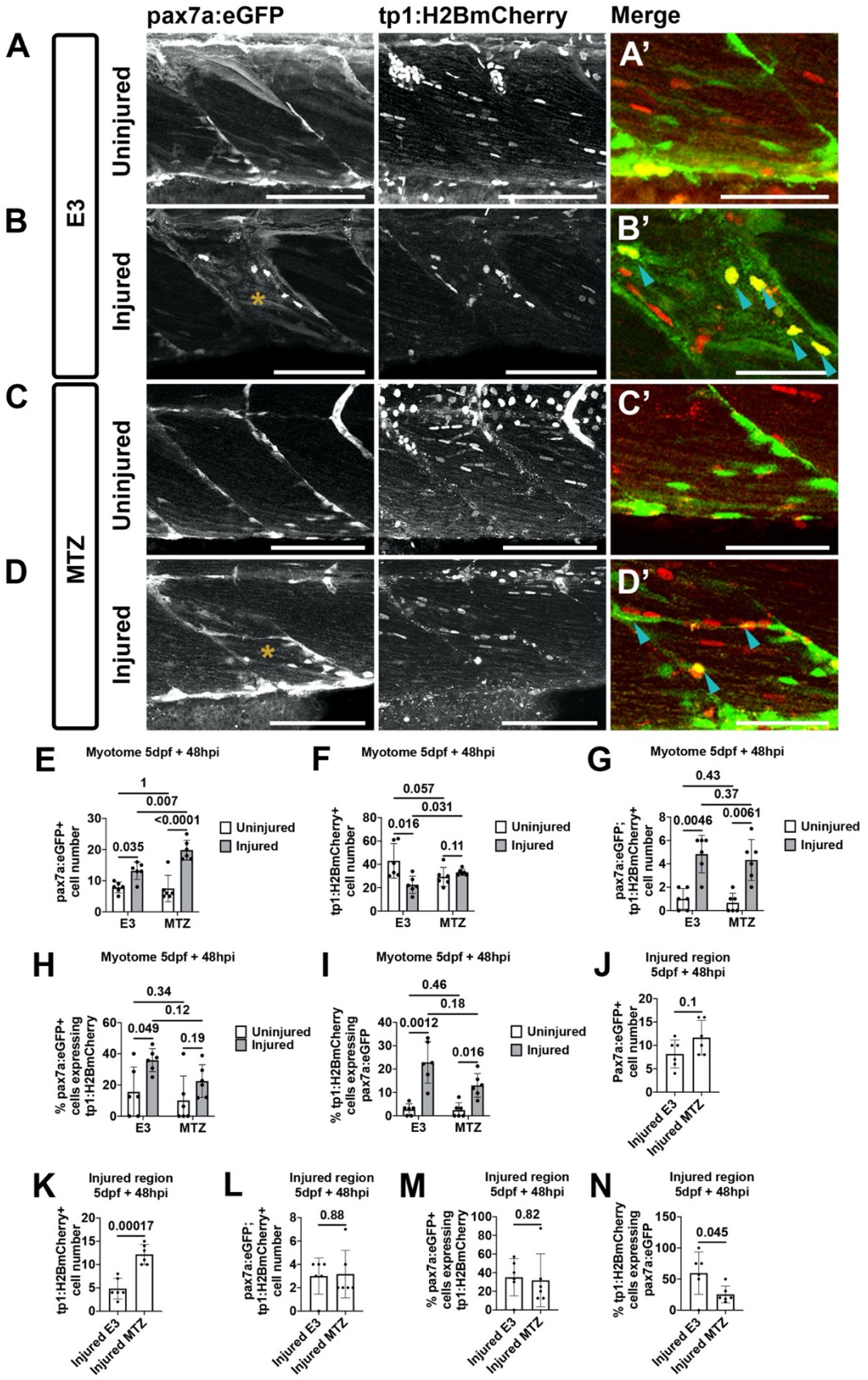
pax7a:eGFP
tp1:H2BmCherry
Merge
A
B
C
D
E3
MTZ
Uninjured
Injured
A'
B'
C'
D'
E
Myotome 5dpf + 48hpi
pax7a:eGFP+ cell number
1
0.007
<0.0001
0.035
F
tp1:H2BmCherry+ cell number
0.057
0.031
0.016
0.11
G
pax7a:eGFP; tp1:H2BmCherry+ cell number
0.43
0.37
0.0061
0.0046
H
% pax7a:eGFP+ cells expressing tp1:H2BmCherry
0.34
0.12
0.049
0.19
I
% tp1:H2BmCherry cells expressing pax7a:eGFP
0.46
0.18
0.0012
0.016
J
Injured region
5dpf + 48hpi
Pax7a:eGFP+ cell number
0.1
Injured E3
Injured MTZ
K
tp1:H2BmCherry+ cell number
0.00017
L
pax7a:eGFP; tp1:H2BmCherry+ cell number
0.88
M
% pax7a:eGFP+ cells expressing tp1:H2BmCherry
0.82
N
% tp1:H2BmCherry cells expressing pax7a:eGFP
0.045

Figure 5.9. Macrophage ablation results in more *pax7a*-expressing muSCs following injury 48 hpi.

A, C) and injured (**B, D**) 5 dpf *pax7a:eGFP*; *Tp1:H2BmCherry*; *fms:mCherry*+ larvae 48 hpi. Larvae were untreated (**A-B**) or treated with MTZ (**C-D**). eGFP+, mCherry+, and eGFP+mCherry+ (cyan arrowheads) cells were detected (**A'-D'**), and the number of cells were quantified in the injured myotome (**E-I**) and injured region (**J-N**). Macrophage ablation resulted in more eGFP+ cells within the injured myotome (**E**) but not the injured region (**J**). This did not reflect a change to the number of eGFP+mCherry+ cell number (**G**). Significant differences in the myotome were tested by 2-way ANOVA (n=24) with Tukey's HSD post-hoc test or by transforming data by ART and performing 2-way ANOVA followed by a Dunn's test with Benjamini and Hochberg correction. Significant differences in the injured region were tested by Student's t-test. Error bars represent standard deviation, and values above comparison bars represent significance (p-values).

Scale bars: 100 µm (**A-D**), 50 µm (**A'-D'**).

5.2.10 Macrophage ablation does not affect the proliferation of *pax7a*-expressing muSCs following injury 24hpi

I have identified a temporal increase in the number of *pax7a*-expressing myoblasts following macrophage ablation. I subsequently investigated how macrophage ablation effects *pax7a:eGFP*-expressing cell proliferation. I treated 4 dpf *pax7a:eGFP*; *Tp1:H2BmCherry*; *fms:mCherry*-expressing larvae with MTZ for 24 hours before injury. Following injury, I treated larvae with MTZ and BrdU. I then quantified the number of eGFP+ cells, mCherry+ cells, and cells which have incorporated BrdU 24 hpi (Fig. 5.10A-D). To understand if macrophage ablation affects the proliferation of eGFP+ and mCherry+ cells following injury within the myotome, I conducted a 2-way ANOVA. I found that macrophage ablation affected the number and proportion of proliferating eGFP+ cells (File. 9.3). I found that macrophage ablation also affected the proportion of proliferating eGFP+ cells expressing mCherry after injury (File. 9.3). To understand the consequence of macrophage ablation on the number of proliferating eGFP+ and mCherry+ cells within the injured myotome, I conducted a 1-way ANOVA. I identified more proliferating eGFP+ cells in untreated larvae following injury relative to uninjured larvae (uninjured: 1.3 ± 0.5, injured: 4.3 ± 2.2; Fig. 5.10H). Although MTZ results in an overall increase in the number of proliferating eGFP+ cells (results from 2-way ANOVA; File. 9.3), MTZ treatment did not result in significantly more proliferating eGFP+ cells relative to untreated controls (Fig. 5.10H; File. 9.3). I found that injury and MTZ treatment did not affect the number of proliferating eGFP+mCherry+ cells (Fig. 5.10K; File. 9.3). I detected no change in the proportion of proliferating eGFP+ cells (Fig. 5.11A; File. 9.3), eGFP+ cells expressing mCherry (Fig. 5.11E; File. 9.3), or proliferating mCherry+ cells expressing eGFP (Fig. 5.11F; File. 9.3).

I investigated if macrophages ablation has an effect on the number of proliferating eGFP+ and mCherry+ cells within the injured region. I found that there was no change in the number of proliferating eGFP+ cells (Fig. 5.10O; File. 9.3) or eGFP+mCherry cells (Fig. 5.10R; File. 9.3). There was also no change in the proportion of proliferating eGFP+mCherry+ cells expressing either transgene (Fig. 5.11I-L; File. 9.3).

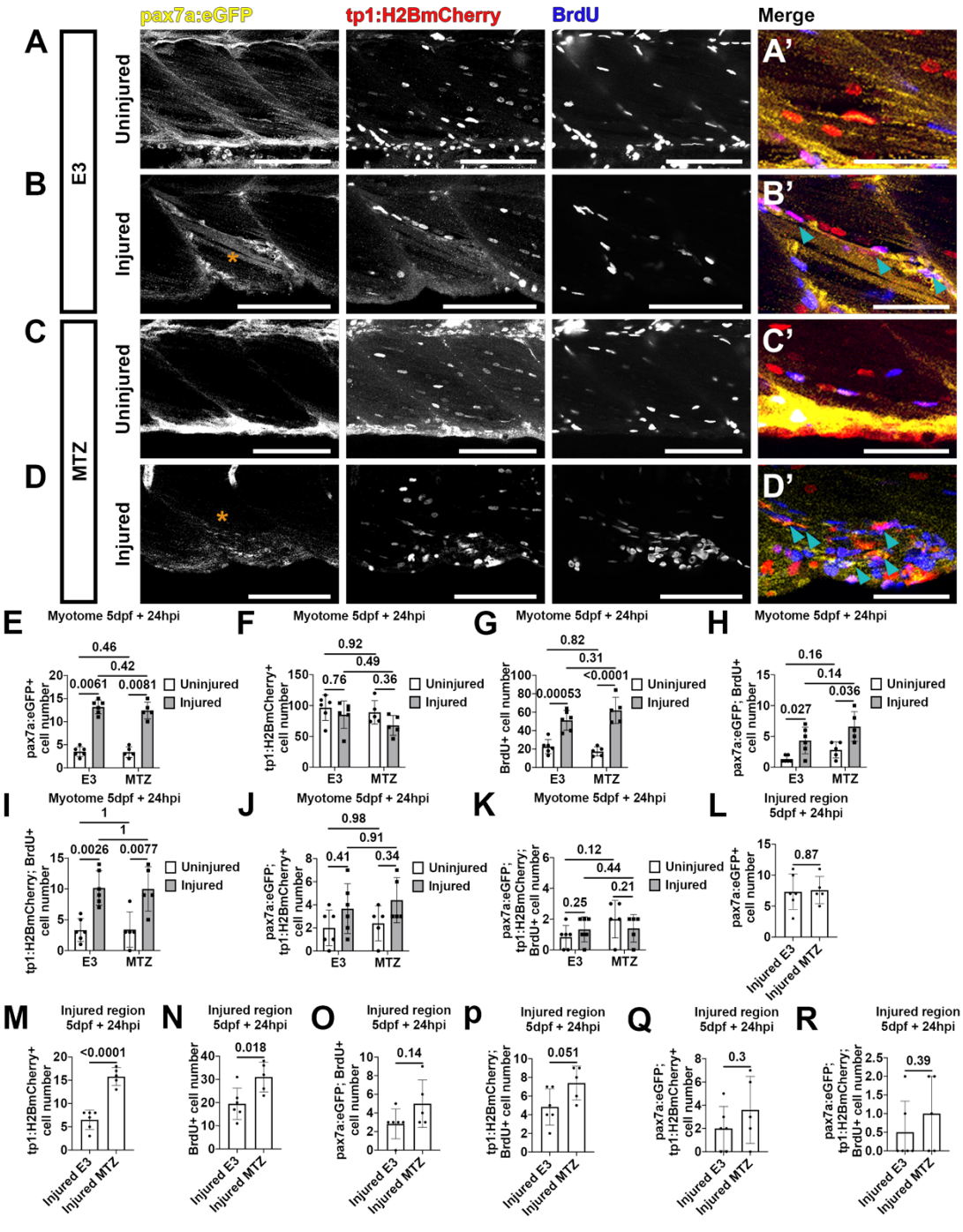
pax7a:eGFP
tp1:H2BmCherry
BrdU
Merge
A
B
C
D
E3
MTZ
Uninjured
Injured
A'
B'
C'
D'
E
F
G
H
I
J
K
L
M
N
O
p
Q
R
Myotome 5dpf + 24hpi
Injured region 5dpf + 24hpi
pax7a:eGFP+ cell number
tp1:H2BmCherry+ cell number
BrdU+ cell number
pax7a:eGFP; BrdU+ cell number
tp1:H2BmCherry; BrdU+ cell number
pax7a:eGFP; tp1:H2BmCherry+ cell number
pax7a:eGFP; tp1:H2BmCherry; BrdU+ cell number
Injured E3
Injured MTZ

Figure 5.10. Macrophage ablation does not perturb the proliferation of *pax7a*-expressing muSCs following injury 24 hpi.
Representative projections from confocal z-stacks of the myotome (asterisks) in uninjured (**A, C**) and injured (**B, D**) 5 dpf *pax7a:eGFP*; *Tp1:H2BmCherry*; *fms:mCherry*+ larvae incubated with BrdU for 24 hours. Larvae were untreated (**A-B**) or treated with MTZ (**C-D**). *pax7a*- and *Tp1*-expressing cells which had incorporated BrdU were detected by immunolabelling (**A'-D'**) and quantified in the injured myotome (**E-K**) and injured region (**L-R**). Following injury, MTZ treatment did not affect the proliferation of *pax7a:eGFP*+ (**H, O**) or *pax7a:eGFP*; *Tp1:H2BmCherry*+ (**K, R**) cells following injury. Significant differences in the myotome were tested by 2-way ANOVA (n=22) with Tukey's HSD post-hoc test or by transforming data by ART and performing 2-way ANOVA followed by a Dunn's test with Benjamini and Hochberg correction. Significant differences in the injured region were tested by Student's t-test or Wilcoxon Mann Whitney U rank sum test. Errors bars display standard deviation and values above bars indicate significance (p-values).
Scale bars: 100 µm (**A-D**), 50 µm (**A'-D'**)

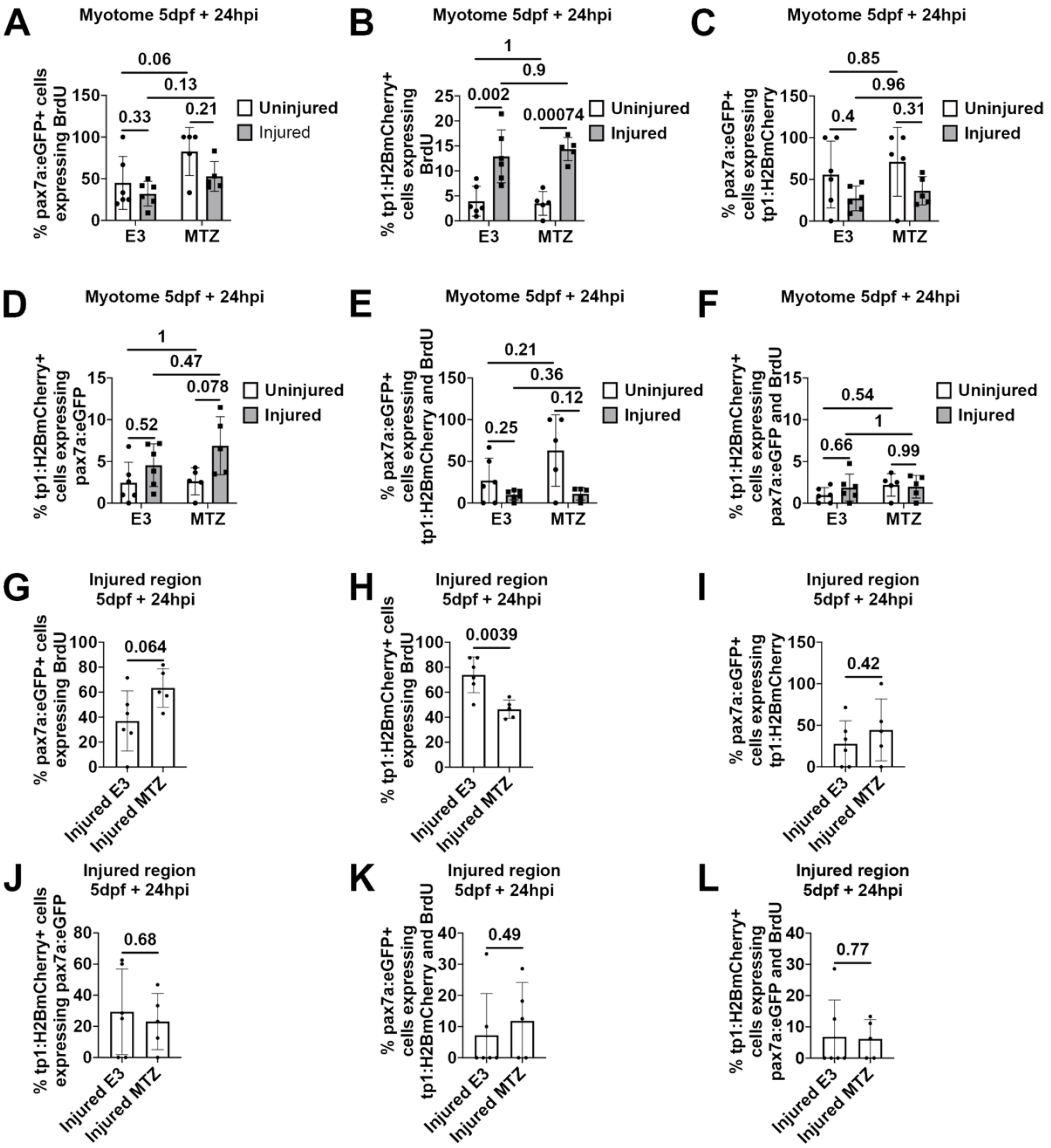

Figure 5.11. Macrophage ablation does not affect the proportion of proliferating *pax7a*-expressing muSCs 24 hpi.

The proportion of proliferating *pax7a:eGFP*+ cells (**A, G**), proliferating *Tp1:H2BmCherry*+ cells (**B, H**), *pax7a:eGFP*+ cells expressing *Tp1:H2BmCherry* (**C, I**), *Tp1:H2BmCherry*+ cells expressing *pax7a:eGFP* (**D, J**), proliferating *pax7a:eGFP*+ cells expressing *Tp1:H2BmCherry* (**E, K**), and proliferating *Tp1:H2BmCherry*+ cells expressing *pax7a:eGFP* (**F, L**) were calculated from cell quantifications. MTZ treatment did not affect the proportion of proliferating *pax7a:eGFP*+ or *pax7a:eGFP*; *Tp1:H2BmCherry*+ cells. Significant differences in the myotome were tested by 2-way ANOVA (n=22) with Tukey's HSD post-hoc test or by transforming data by ART and performing 2-way ANOVA followed by a Dunn's test with Benjamini and Hochberg correction. Significant differences in the injured region were tested by Student's t-test, Welch's t-test or Wilcoxon Mann Whitney U rank sum test. Errors bars display standard deviation and values above bars indicate significance (p-values).

5.2.11 The number of Myog-expressing *Tp1:H2BmCherry*+ cells increases following macrophage ablation 24 hpi

Following macrophage ablation, I found that there were more *Tp1:H2BmCherry*-expressing cells within the injured myotome and injured region relative to E3 treated control animals (Fig. 5.5). I also found that more Pax7-expressing *Tp1*:H2mCherry+ cells respond to injury (Fig. 5.7). To understand if *Tp1:H2BmCherry*+ cells can differentiate into muscle, I detected cells which have Myog immunoreactivity by immunolabeling. I treated 4 dpf *Tp1:H2BmCherry*; *fms:mCherry*-expressing larvae with MTZ for 24 before injury. Following injury, I continued to treat larvae with MTZ. I then quantified the number of mCherry+, Myog+ and mCherry+Myog+ cells relative to untreated control larvae 24 hpi (Fig. 5.12A-D). To understand if macrophage ablation affects the differentiation of mCherry+ cells within the myotome, I conducted a 2-way ANOVA. I found that MTZ treatment affected the number and proportion of differentiating mCherry+ cells in the injured myotome (File. 9.3). Moreover, macrophage ablation enhanced the increased number and proportion of differentiating mCherry+ cells following injury (File. 9.3).

To understand how macrophage ablation affects the differentiation of mCherry+ cells within the myotome, I conducted a 1-way ANOVA. I identified more mCherry+Myog+ cells following injury in untreated animals (uninjured: 1.3 ± 1.2, injured: 4.3 ± 2.2; Fig. 5.12G). I also observed an increase in mCherry+Myog+ cells following macrophage ablation after injury (MTZ; uninjured: 8.3 ± 1.4, injured: 21.7 ± 10.3; Fig. 5.12G). I found an increase in the proportion of mCherry+Myog+ cells following injury in both untreated (uninjured: 2.7% ± 2.3%, injured: 10.2% ± 4.8%; Fig. 5.12H) and MTZ-treated (uninjured: 2.8% ± 1.4%, injured: 19.3% ± 8.4%; Fig. 5.12H) animals.

Assessing the number of cells at the site of injury, I found that there were more Myog+ cells (E3: 1.5 ± 1.8, MTZ: 7.7 ± 2.9; Fig. 5.12J) and mCherry+Myog+ cells (E3: 6.3 ± 3.8, MTZ: 12 ± 4.5; Fig. 5.12K) following macrophage ablation. This could not be explained by a relative increase in the proportion of mCherry+ cells expressing Myog as it did not change (Fig. 5.12L; File. 9.3). Therefore, following macrophage ablation, mCherry+ cells proliferate more after injury, relative to untreated controls. These

mCherry+ cells then begin to express Myog, and therefore have the capacity to contribute to new myofibers.

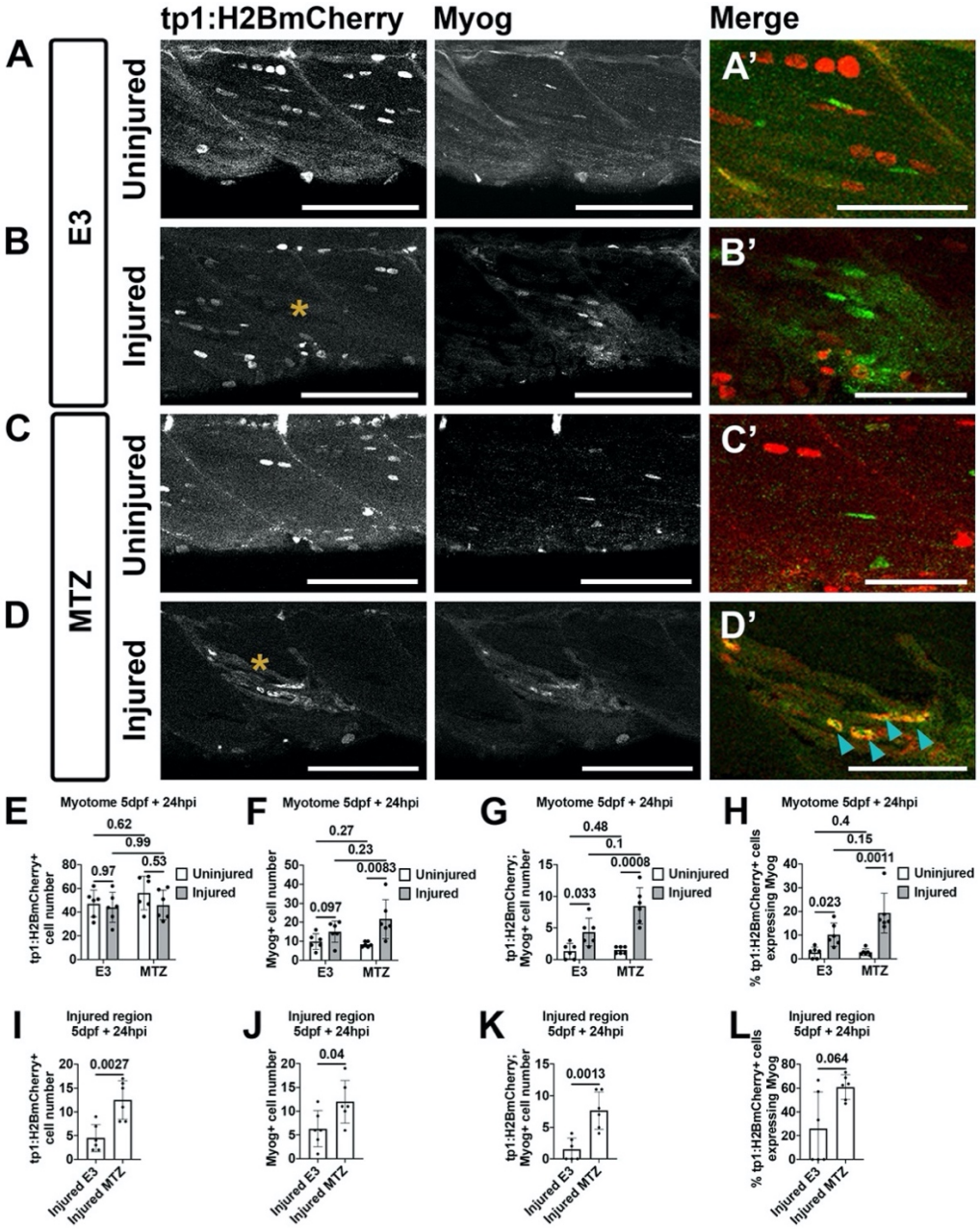

Figure 5.12. Increased number of differentiating *Tp1*-expressing myoblasts following macrophage ablation in response to injury 24 hpi.

Representative projections from confocal z-stacks of the myotome (asterisks) in uninjured (**A, C**) and injured (**B, D**) 5 dpf *Tp1:H2BmCherry*; *fms:mCherry*+ larvae 24 hpi. Larvae were untreated (**A-B**) or treated with MTZ (**C-D**). mCherry+ cells expressing Myog immunoreactivity (cyan arrowheads) were detected by immunolabelling (**A'-D'**), and the number of cells were quantified in the injured myotome (**E-H**) and injured region (**I-L**). Following MTZ treatment, there were more Myog+ (**J**) and mCherry+Myog+ (**K**) cells within the injured region. This was not a consequence of a proportional change (**L**). This difference was not observed in the total injure myotome (**F-G**). Significant differences in the myotome were tested by 2-way ANOVA (n=24) with Tukey's HSD post-hoc test or by transforming data by ART and performing 2-way ANOVA followed by a Dunn's test with Benjamini and Hochberg correction. Significant differences in the injured region were tested by Student's t-test or Wilcoxon Mann Whitney U rank sum test. Error bars represent standard deviation, and values above comparison bars represent significance (p-values).
Scale bars: 100 µm (**A-D**), 50 µm (**A'-D'**).

5.2.12 Macrophages express *DeltaD:GFP* following muscle injury

I aimed to elucidate if migratory macrophages can interact with muSCs by regulating Notch signalling following injury in zebrafish. To examine DeltaD expression on macrophages, I labelled macrophages with L-Plastin (pan-leukocyte marker) in DeltaD:eGFP-expressing larvae (Fig. 5.13). Macrophages could be identified by their morphology (Mathias *et al.*, 2006; Ratnayake *et al.*, 2021). I found that macrophages express DeltaD:eGFP at both 8 hpi (Fig. 5.13A) and 24 hpi (Fig. 5.13B) within the injured myotome. This data reveals that macrophages hold the capacity to signal via the Notch ligand DeltaD.

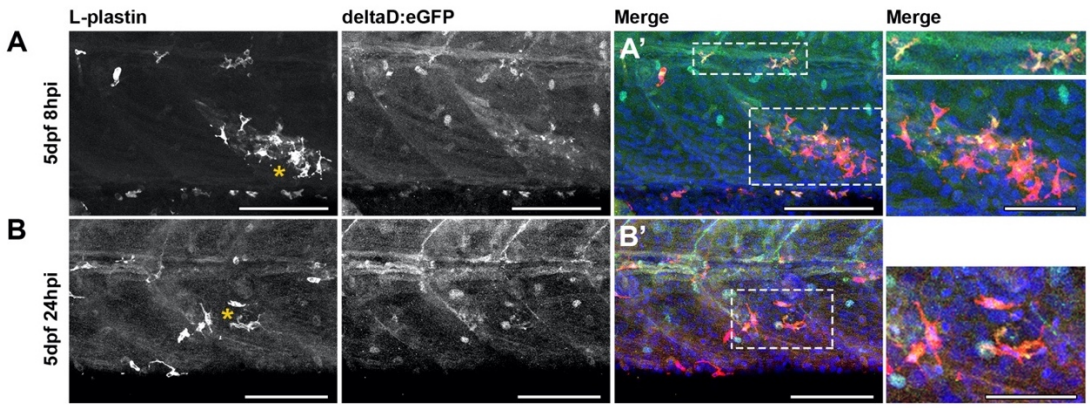

Figure 5.13. Macrophages express DeltD following injury.
Representative projections from confocal z-stacks of the injured myotome (asterisks) of 5 dpf deltaD:eGFP+ larvae 8 hpi (A) and 24 hpi (B). Immune cells were detected by L-plastin immunostaining (A'-B'). Macrophages could be identified by their morphology. Macrophages express DeltaD following injury at 8 hpi and 24 hpi.
Scale bars: 100 µm (**A-B**), 50 µm (**A'-B'; cropped merge panels**).

5.2.13 Concurrent macrophage ablation and Notch inhibition did not have a cumulative effect on the number of *Tp1:H2BmCherry*-expressing cells 24 hpi

I have previously shown that there were more *Tp1*-expressing cells following injury in the absence of Notch signalling (Fig. 4.10). I have also shown that macrophages expressed DeltaD (Fig. 5.13). Therefore, I investigated if macrophages are able to regulate cells expressing Notch activity (*Tp1*+). I treated 4 dpf *Tp1:H2BmCherry*; *fms:mCherry*-expressing larvae with MTZ for 24 hours before injury. After injury, I treated larvae with MTZ and DAPT. I subsequently quantified the number of mCherry+ cells at the site of injury 24 hpi (Fig. 5.14A-D). Evaluating the number of *Tp1:H2BmCherry*+ cells within the injured region, I found that both DAPT and MTZ treatment results in more mCherry+ cells relative to DMSO-treated controls (DMSO: 2.7 ± 2, DAPT: 11.7 ± 3.4, MTZ DMSO: 7.2 ± 2.4; Fig. 5.14E). DAPT also had a stronger effect on the increased number of mCherry+ cells at the site of injury relative to MTZ treatment (Fig. 5.14F). Furthermore, in the absence of macrophages, Notch inhibition did not result in an increase in mCherry+ cells (MTZ DMSO: 7.2 ± 2.4, MTZ DAPT: 9.4 ± 2.2; $p > 0.05$ Fig. 5.14E).

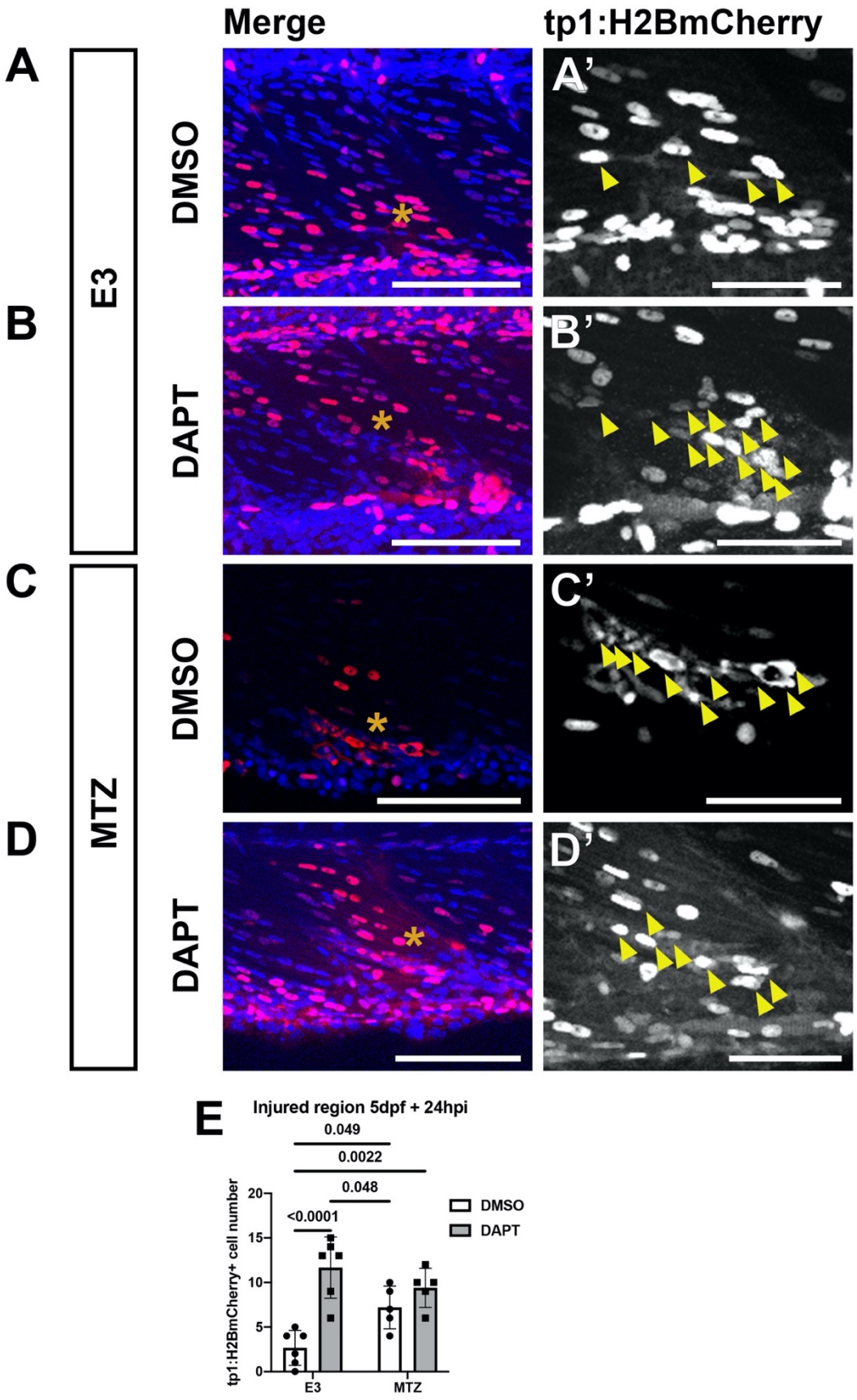
Merge
tp1:H2BmCherry
A
A'
B
B'
C
C'
D
D'
E3
MTZ
DMSO
DAPT
DMSO
DAPT
E
Injured region 5dpf + 24hpi
0.049
0.0022
0.048
<0.0001
tp1:H2BmCherry+ cell number
20
15
10
5
0
DMSO
DAPT
E3
MTZ

Figure 5.14. DAPT and MTZ co-treatment did not show a cumulative effect on the number of *Tp1* expressing cells following injury 24 hpi.
Representative projections from confocal z-stacks of the injured myotome (asterisks) in DMSO treated (**A**), DAPT treated (**B**), MTZ treated (**C**) and DAPT and MTZ co-treated (**D**) 5 dpf *Tp1:H2BmCherry*; *fms:mCherry*+ larvae 24 hpi. mCherry+ cells (yellow arrowheads) were detected by immunolabelling (**A'-D'**), and the number of cells were quantified in the injured region (**E**). There were more mCherry+ cells following DAPT treatment in the injured region (**E**). There were also more mCherry+ cells in the injure region following MTZ treatment (**E**). In the injured region (**E**), MTZ and DAPT co-treatment reduced the number of mCherry+ cells relative to DAPT treated animals. Significant differences were tested by 2-way ANOVA (n=22) with Tukey's HSD post-hoc test. Error bars represent standard deviation, and values above comparison bars represent significant differences only (p-values).
Scale bars: 100 µm (**A-D**), 50 µm (**A'-D'**).

5.2.14 Macrophage ablation and DAPT treatment have antagonistic effects on the response of Pax7+ muSCs to injury

To understand the effects of concurrent macrophage ablation and Notch inhibition on the number of Pax7-expressing muSCs following injury, I treated 4 dpf *Tp1:H2BmCherry*; *fms:mCherry*-expressing larvae with MTZ for 24 hours before injury. Following injury, I continuously treated larvae with MTZ and DAPT. I then assessed the number of Pax7+ and mCherry+ cells relative to untreated controls 24 hpi (Fig. 5.14A-D). To detect if concurrent macrophage ablation and Notch inhibition affects the number of Pax7+ and mCherry+ cells, I conducted a 2-way ANOVA. I found that DAPT and MTZ co-treatment affected the number of mCherry+ cells, and proportion of Pax7+mCherry+ cells within the injured region (File. 9.3).

To determine how DAPT and MTZ co-treatment affects the number of Pax7+ and mCherry+ cells within the myotome, I conducted a 1-way ANOVA. I identified fewer Pax7+ cells within the following DAPT treatment relative to DMSO-treated larvae (DMSO: 9.7 ± 3.1, DAPT: 5.7 ± 1.6; Fig. 5.14E). Following concurrent DAPT and MTZ treatment, the number of Pax7+ cells did not change relative to MTZ-treated animals (Fig. 5.14E; File. 9.3). This suggests that Notch signalling regulates Pax7-expressing cells independently macrophages. DAPT, MTZ or concurrent DAPT and MTZ treatment did not affect the number of Pax7+mCherry+ cells relative to DMSO-treated controls (DMSO: 2 ± 1.3; Fig. 5.14G). I also did not detect any change in the proportion of Pax7+ cells expressing mCherry, or the proportion of mCherry+ cells expressing Pax7 (Fig. 5.14H-I; File. 9.3).

To understand if the increased number of mCherry+ cells observed following concurrent DAPT and MTZ treatment within the injured region (Fig. 5.14) reflects a change to the number of Pax7+ cells, I assessed the number of mCherry+ and Pax7+ cells within the injured region. I found that MTZ treatment leads to more Pax7+ cells relative to DAPT treated animals (DAPT: 3.8 ± 0.8, MTZ DMSO: 10.4 ± 5.3; Fig. 5.15J). This increase in Pax7+ cells was not observed when larvae were co-treated with both MTZ and DAPT, relative to MTZ-treated animals (Fig. 5.15J; File. 9.3). I observed no change in the number of Pax7+mCherry+ cells (Fig. 5.15L; File. 9.3) or the proportion of Pax7+ cells expressing mCherry following DAPT, MTZ, or concurrent DAPT and MTZ treatment relative to DMSO-treated larvae (Fig. 5.14M; File. 9.3). I note that

following DAPT treatment, the proportion of mCherry+ cells expressing Pax7 is reduced relative to DMSO-treated animals (DMSO: 69.4% ± 40%, DAPT: 9.8% ± 12.2%; Fig. 5.15N) implying that DAPT treatment prevents mCherry+ cells from expressing Pax7.

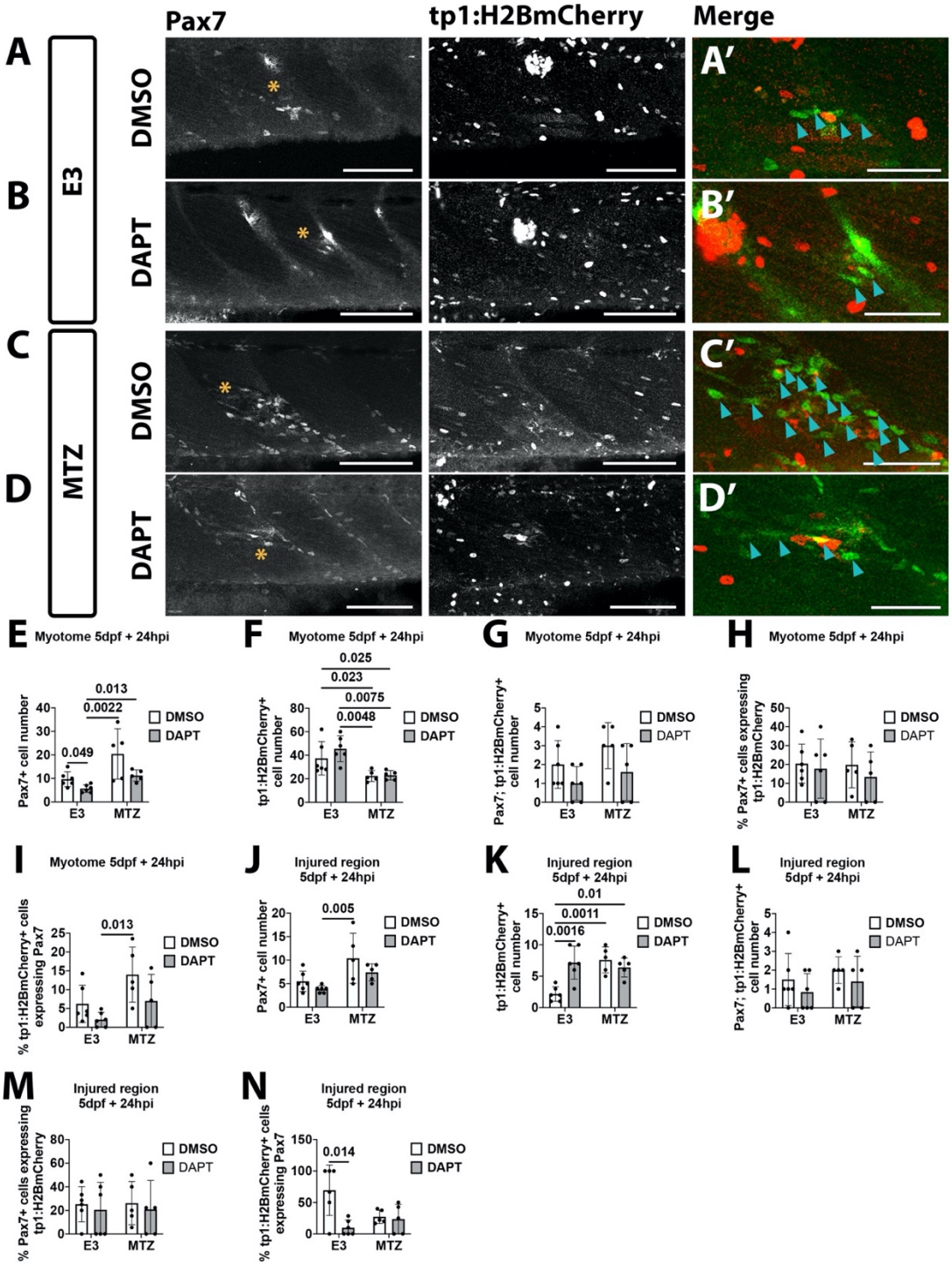
Pax7
tp1:H2BmCherry
Merge
A
B
C
D
E3
MTZ
DMSO
DAPT
A′
B′
C′
D′
E Myotome 5dpf + 24hpi
Pax7+ cell number
0.013
0.0022
0.049
F Myotome 5dpf + 24hpi
tp1:H2BmCherry+ cell number
0.025
0.023
0.0075
0.0048
G Myotome 5dpf + 24hpi
Pax7; tp1:H2BmCherry+ cell number
H Myotome 5dpf + 24hpi
% Pax7+ cells expressing tp1:H2BmCherry
I Myotome 5dpf + 24hpi
% tp1:H2BmCherry+ cells expressing Pax7
0.013
J Injured region 5dpf + 24hpi
Pax7+ cell number
0.005
K Injured region 5dpf + 24hpi
tp1:H2BmCherry+ cell number
0.01
0.0011
0.0016
L Injured region 5dpf + 24hpi
Pax7; tp1:H2BmCherry+ cell number
M Injured region 5dpf + 24hpi
% Pax7+ cells expressing tp1:H2BmCherry
N Injured region 5dpf + 24hpi
% tp1:H2BmCherry+ cells expressing Pax7
0.014

Figure 5.15. Notch inhibition and macrophage ablation antagonistically affect the number of Pax7+ cells.

Representative projections from confocal z-stacks of the injured myotome (asterisks) in DMSO-treated (**A**), DAPT-treated (**B**), MTZ-treated (**C**) and DAPT and MTZ co-treated (**D**) 5 dpf *Tp1:H2BmCherry*; *fms:mCherry*+ larvae 24 hpi. mCherry+ cells and cells expressing Pax7 immunoreactivity (cyan arrowheads) were detected by immunolabelling (**A'-D'**), and the number of cells were quantified in the injured myotome (**E-I**) and injured region (**J-N**). Following DAPT treatment there was a decrease in the number of Pax7+ cells in the myotome (**E**). DAPT and MTZ co-treatment reduces the number of Pax7+ cells relative to DAPT or MTZ-treated animals (**E**). These changes were not reflected within the injured region (**J**), nor was there an effect on the number of Pax7+mCherry+ cells (**G, L**). Significant differences in the myotome were tested by 2-way ANOVA (n=24) with Tukey's HSD post-hoc test or by transforming data by ART and performing 2-way ANOVA followed by a Dunn's test with Benjamini and Hochberg correction. Error bars represent standard deviation, and values above comparison bars represent significant differences only (p-values).
Scale bars: 100 μm (**A-D**), 50 μm (**A'-D'**).

5.2.15 Neutrophils express *Tp1:H2BmCherry* following injury

I have shown that macrophage ablation leads to more Pax7+ muSCs in the absence of Notch signalling, suggesting that macrophages can also regulate muSC activity via a Notch-independent mechanism. Live time-lapse imaging reveals a population of *Tp1:H2BmCherry* cells migrate towards and around the site of injury (Movie. 9.10). These cells are round, and do not morphologically appear to be muSCs (Movie. 9.10). In the absence of CCR2-expressing macrophages in mouse, it has been demonstrated that there is a prolonged neutrophilic response after muscle injury (Contreras-Shannon *et al.*, 2007). Therefore, I aimed to understand if the neutrophilic response to muscle injury is affected following macrophage ablation. Moreover, I investigated if recruited neutrophils express the *Tp1:H2BmCherry* transgene.

First, I assessed if the recruited *Tp1:H2BmCherry*-expressing cells observed in my time-lapse imaging following macrophage ablation are neutrophils. I treated *mpx:GFP*; *Tp1:H2BmCherry*; *fms:mCherry*-expressing larvae for 24 hours before injury. Following injury, I continued to treat larvae with MTZ, live imaging *mpx:GFP*+ and *Tp1:H2BmCherry*+ cells (Movie. 9.11). I found that in an absence of macrophages, migratory *mpx*+ neutrophils are mCherry+.

To understand if neutrophils express the *Tp1*:H2BCherry transgene following injury, I injured 5 dpf *Tp1:H2BmCherry* larvae, assessing cells for Mpx immunoreactivity at 5 hpi (Fig. 5.16A-B). I found that there were no Mpx+ cells in the uninjured myotome (Fig. 5.16C). Following injury, Mpx+ neutrophils were recruited to the site of injury (uninjured: 0 ± 0, injured 7.5 ± 4.3; Fig. 5.16C), 100 % of which were expressing *Tp1:H2BmCherry* (uninjured: 0 ± 0, injured 7.5 ± 4.3; Fig. 5.16D). This suggests that the *Tp1:H2BmCherry*+ cell population which are recruited to the site of injury is a multi-cellular population, consisting of both muSCs (Pax7+) and immune cells (Mpx+).

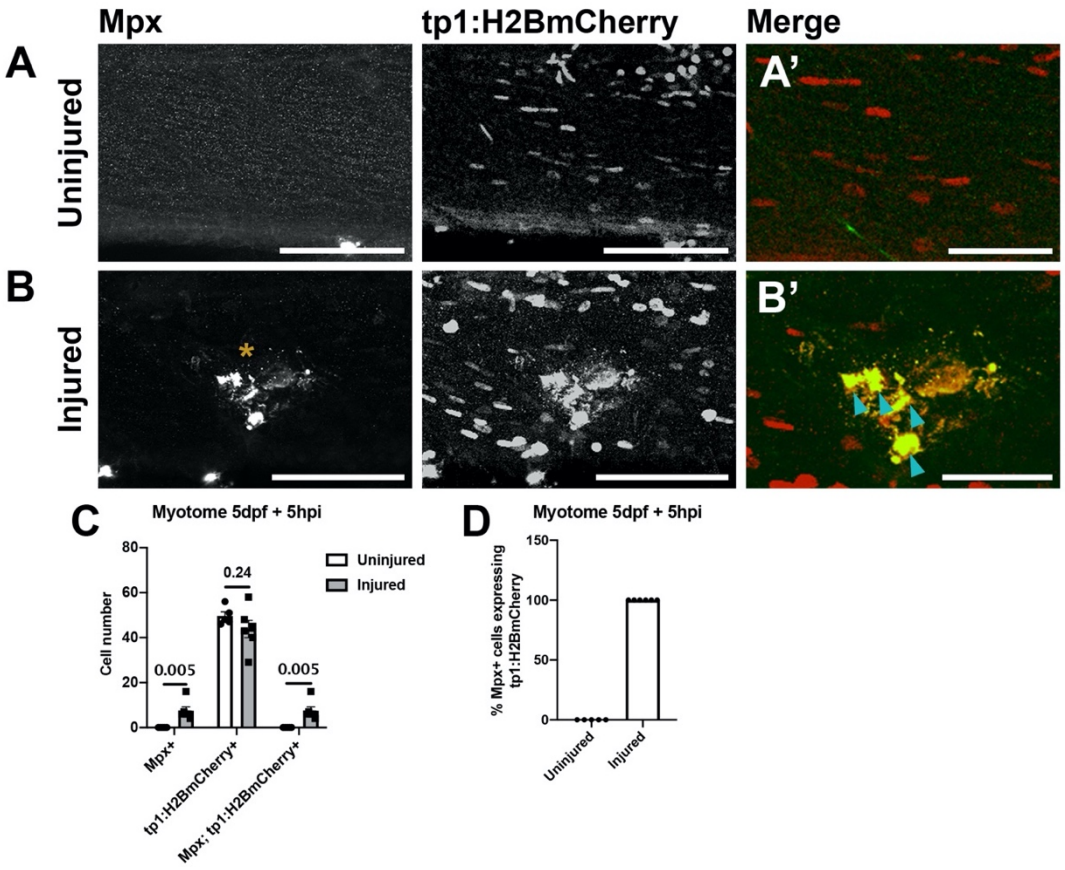

Figure 5.16. Neutrophils express *Tp1:H2BmCherry* following injury.
Representative projections from confocal z-stacks of the myotome of uninjured (**A**) and injured (**B**) 5 dpf *Tp1:H2BmCherry* larvae 5 hpi. mCherry+ cells and neutrophils expressing Mpx immunoreactivity (yellow arrowheads) were detected by immunolabelling (**A'-B'**), and the number of cells were quantified within the myotome (**C-D**). Following injury there were more Mpx+ neutrophils (**C**), all of which express mCherry (100%; **D**). Injury denoted with an asterisk. Significant differences were tested by Student's t-test or Wilcoxon Mann Whitney U rank sum test for normal and non-normal comparisons, respectively. Error bars represent standard deviation, and values above comparison bars represent significance (p-values). Scale bars: 100 µm (**A-B**), 50 µm (**A'-B'**).

5.2.16 *Tp1:H2BmCherry*-expressing neutrophils perdure within the injured myotome following macrophage ablation

Macrophages facilitate the exit of neutrophils from injured tissue during the resolution of the immune response towards injury (Mathias *et al.*, 2006). Mouse macrophage depletion models have demonstrated an extended neutrophilic response following injury (Segawa *et al.*, 2008). I measured the effects of macrophage ablation on the perdurance of neutrophils following muscle injury in zebrafish. I treated *mpx:GFP*; *fms:mCherry*-expressing larvae with MTZ for 24 hours before injury. Following injury, I continued the MTZ treatment, assessing the number of GFP+ neutrophils relative to untreated control larvae 24 hpi (Fig. 5.17A-B). I found that there were very few GFP+ cells within the injured muscle of untreated larvae, whilst the number of GFP+ cells was increased in the injured muscle following MTZ treatment (E3: 2.2 ± 1.2, MTZ: 6.2 ± 2.1; Fig. 5.17C).

To confirm that neutrophils which have remained within the injured myotome 24 hpi are expressing the *Tp1:H2BmCherry* transgene, I treated *Tp1:H2BmCherry*; *fms:mCherry*-expressing larvae for 24 hours before injury. Following injury, I continued MTZ treatment, detecting cells with Mpx immunoreactivity relative to untreated control larvae 24 hpi (Fig. 5.18A-B). I found that there were more Mpx+ cells within the injured myotome following macrophage ablation 24 hpi relative to untreated control animals (E3: 0.6 ± 0.9, MTZ: 3.4 ± 1.7; Fig. 5.18C). These Mpx-expressing neutrophils are positive for the *Tp1:H2BmCherry* reporter (E3: 0.6 ± 0.9, MTZ: 3 ± 1; Fig. 5.18C-D).

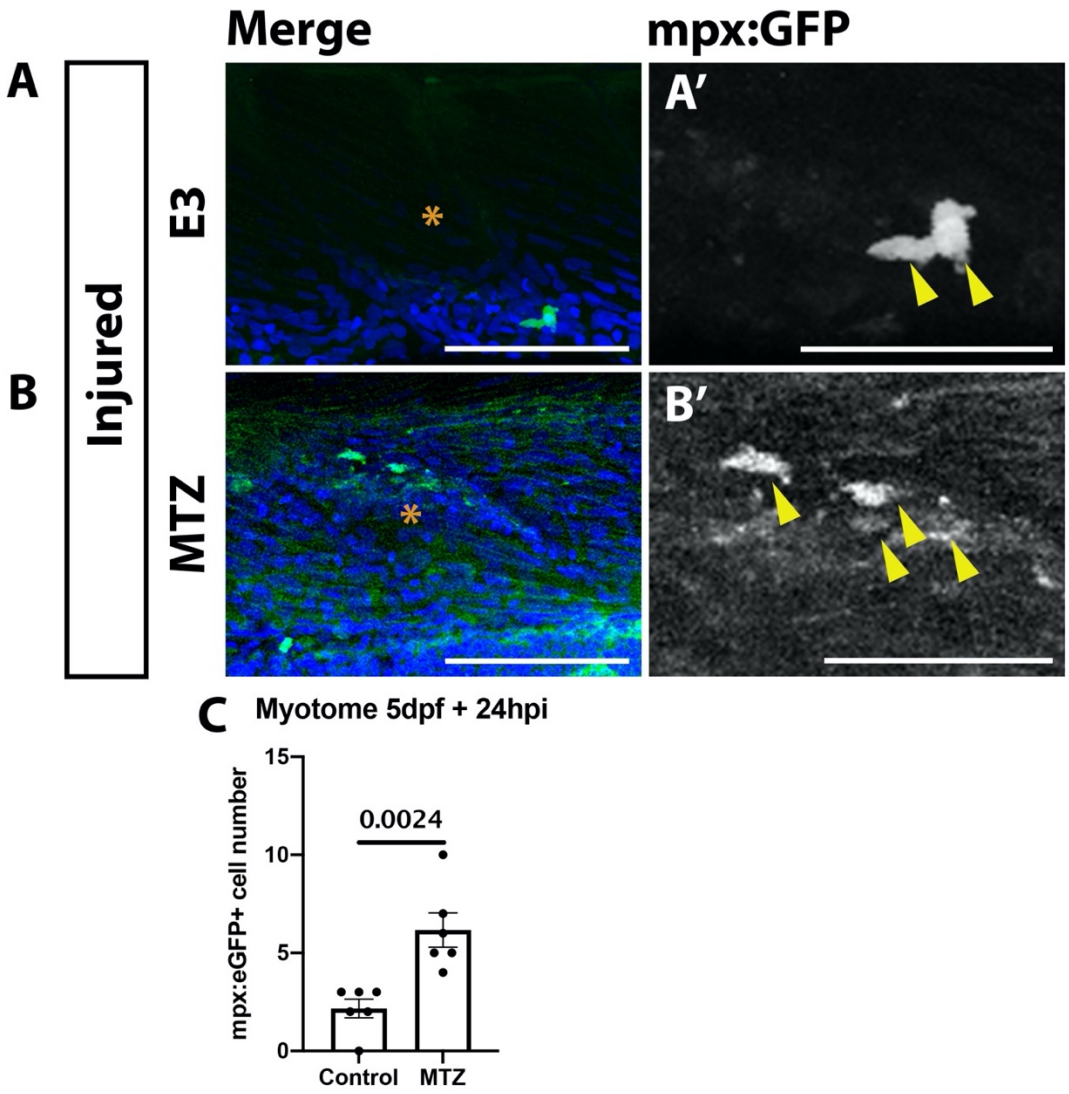

Figure 5.17. Neutrophils perdure within the injured myotome 24 hpi following macrophage ablation.

Representative projections from confocal z-stacks of the injured myotome (asterisk) in untreated (**A**) and MTZ treated (**B**) 5 dpf *mpx:GFP* larvae 24 hpi. GFP+ neutrophils (yellow arrowheads) were detected by immunolabelling (**A'-B'**), and the number of cells were quantified within the myotome (**C**). Following macrophage ablation there were more neutrophils within the injured myotome (**C**). Significant difference was tested by Student's t-test. Error bar represents standard deviation, and the value above the comparison bar represents significance (p-values).

Scale bars: 100 µm (**A-B**), 50 µm (**A'-B'**).

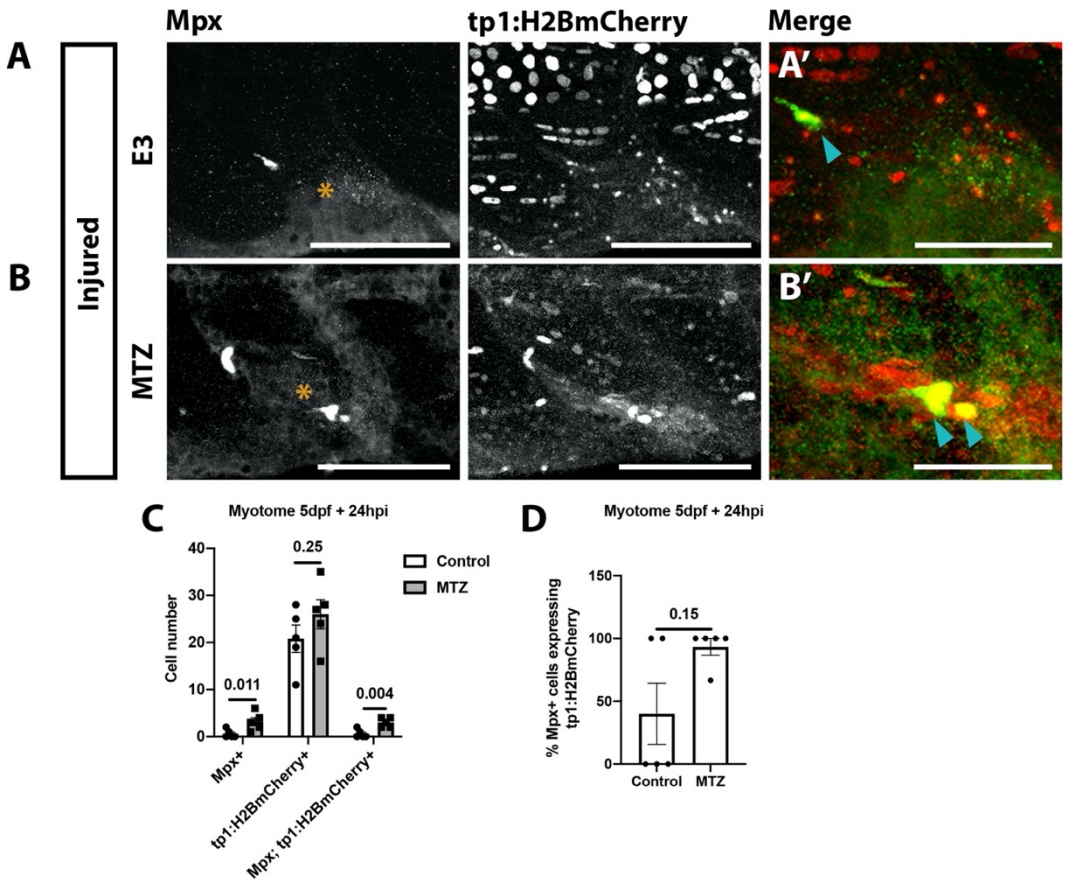

Figure 5.18. Neutrophils which have perdured following macrophage ablation express *Tp1:H2BmCherry*.

Representative projections from confocal z-stacks of the injured myotome (asterisk) in untreated (**A**) and MTZ treated (**B**) 5 dpf *Tp1:H2BmCherry*+ larvae 24 hpi. mCherry+ cells and neutrophils expressing Mpx immunoreactivity (cycan arrowheads) were detected by immunolabelling (**A'-B'**), and the number of cells were quantified within the myotome (**C-D**). Following macrophage ablation there were more Mpx+mCherry+ neutophils within the injured myotome (**C**). Significant differences were tested by Student's t-test or Wilcoxon Mann Whitney U rank sum test for normal and non-normal comparisons, respectively. Error bars represent standard deviation, and values above comparison bars represent significance (p-values).

Scale bars: 100 µm (**A-B**), 50 µm (**A'-B'**).

5.2.17 Macrophage recruitment towards injury is regulated by Notch signalling

Notch signalling is important for the polarisation of macrophages, skewing macrophages towards a pro-inflammatory phenotype (Lin *et al.*, 2018). Therefore, Notch inhibition may perturb macrophage recruitment and activity in response to muscle injury. To understand the importance of Notch signalling on the recruitment of macrophages towards muscle injury, I live-imaged injured 5dpf *fms:mCherry*-expressing treated with DMSO or DAPT. I then quantified the number of recruited *fms*-expressing macrophages over time (Fig. 5.19A-B; Movie. 9.12-9.13). Macrophages were recruited to the injured myotome in both DMSO and DAPT-treated animals (1.7 hpi- DMSO: 3.3 ± 0.6, DAPT: 3 ± 0; Fig. 5.19C). Although there is a temporal increase in the number of *fms*+ macrophages in both DAPT and DMSO treated control larvae, there are fewer macrophages recruited in DAPT-treated larvae (3.7 hpi- DMSO: 10 ± 1, DAPT: 6.3 ± 0.6; Fig. 5.19C). This suggests that macrophage recruitment following muscle injury in the zebrafish is controlled by Notch signalling.

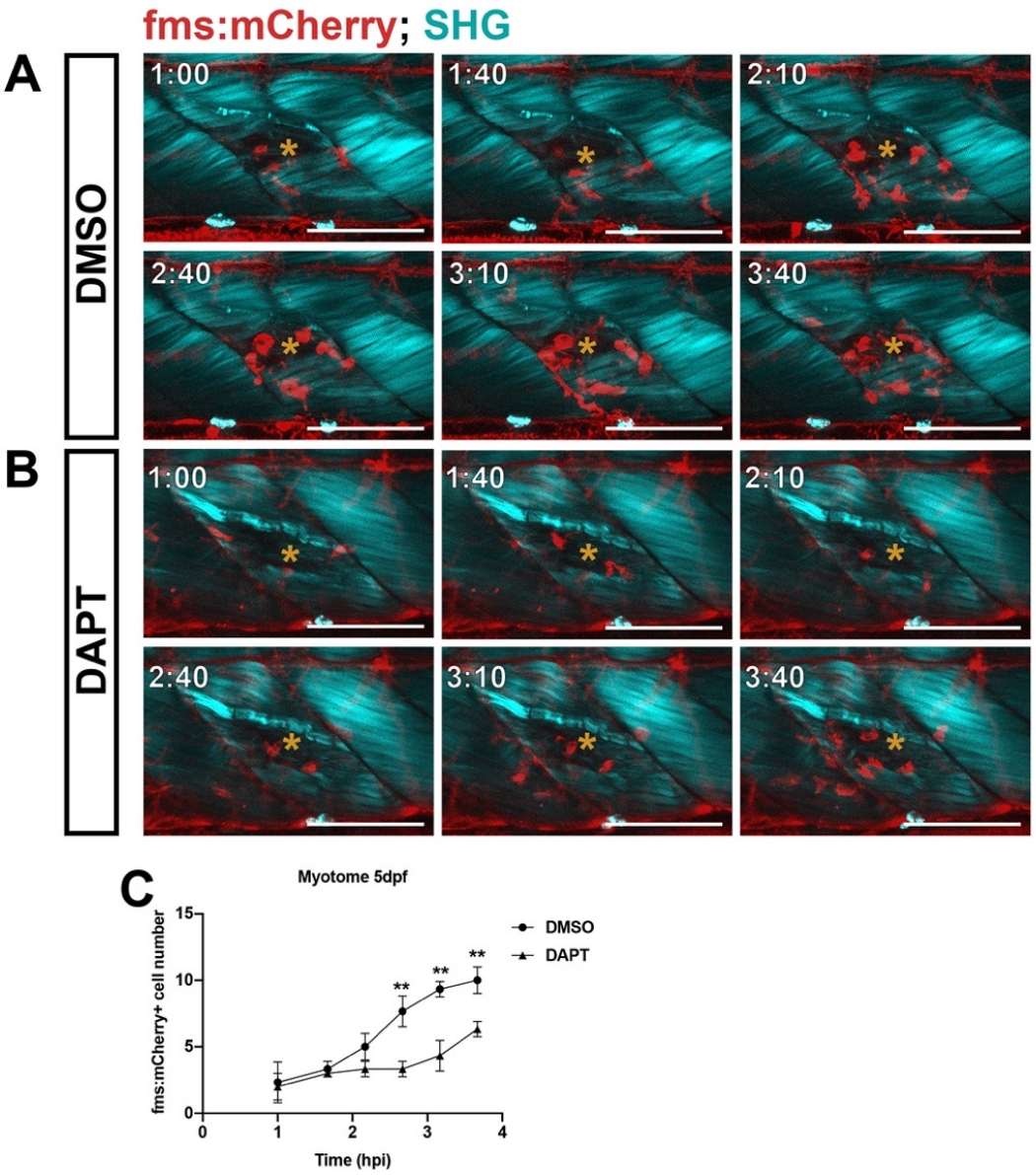

Figure 5.19. Macrophage recruitment following injury is regulated by Notch signalling.
5 dpf *fms:mCherry*+ larvae (n=6) were injured and treated with DMSO (**A**) or DAPT (**B**). Larvae were then live-imaged on a multi-photon system over 3.7 hours. Representative z-projections (**A-B**) show migratory mCherry+ cells responding to injury (asterisk; SHG signal). The number of mCherry+ cells were quantified (**C**). Over time, there were fewer mCherry+ macrophages following DAPT treatment (**C**). Significant differences were tested by Student's t-test (** $p < 0.01$). Error bars represent standard deviation, and values above comparison bars represent significance (p-values).
Scale bars: 100 µm

5.2.18 Less neutrophils and macrophages are recruited towards injury following dexamethasone treatment

The inhibition of Notch signalling results in less macrophages which may induce an anti-inflammatory microenvironment. Contrastingly, the loss of macrophages results in a prolonged neutrophilic response which may generate a protracted pro-inflammatory response. The regulation of the immune microenvironment is important for tissue repair (Thornton, 1949; Mathew *et al.*, 2007). Therefore, to examine the effect of an anti-inflammatory microenvironment on muSC response to injury, I used the glucocorticoid DEX. To optimise the use of DEX, I aimed to replicate published data demonstrating a reduction in the number of neutrophils and macrophages recruited to the tail fin amputated region (Sharif *et al.*, 2015; Hasegawa *et al.*, 2017; Xie *et al.*, 2019). I treated 2 dpf *mpx:GFP*; *fms:mCherry*-expressing larvae with 0.5 mM DEX 1 hour before caudal fin amputation. Following caudal fin amputation, I continued treating the larvae with DEX. I subsequently quantified the number of neutrophils and macrophages in a 100µm injured region (Fig. 9.6A-D). I found that using 0.5mM DEX leads to fewer macrophages (DMSO: 17.2 ± 12.1, DEX: 8.6 ± 3.9; $p > 0.05$; Fig. 9.6E) and neutrophils (DMSO: 2.6 ± 2.1, DEX: 0.4 ± 0.5; Fig. 9.6F) 5 hpa relative to DMSO treated controls. Next, I assessed if DEX treatment effectively supresses pro-inflammatory signals and therefore the recruitment of immune cells towards muscle damage in older larval stages. I treated 5 dpf *mpx:GFP*; *fms:mCherry*-expressing larvae with 0.5 mM DEX 1 hour before muscle injury. Following injury, I live-imaged DEX- and DMSO-treated larvae. I then quantified the number of neutrophils and macrophages recruited to the site of injury over time (Fig. 9.5B; Movie. 9.8). I found that 0.5mM DEX resulted in fewer macrophages (DMSO: 10 ± 2.6, DEX: 5.7 ± 0.6; Fig. 9.5D) and neutrophils (DMSO: 12.3 ± 3.5, DEX: 4 ± 1.2; Fig. 9.5E) relative to DMSO-treated animals at 3 hpi.

To examine the effect of DEX treatment on the neutrophils which perdure following macrophage ablation, I treated 4dpf *mpx:GFP*; *fms:mCherry*-expressing larvae with MTZ 24 hours before injury and DEX 1 hour before injury. Following injury, I continued both MTZ and DEX treatment. I then quantified the number of GFP+ cells within the injured myotome 24 hpi (Fig. 9.7A-B). I found that there were fewer GFP+ neutrophils following DEX and MTZ co-treatment relative to MTZ-only treated

controls (MTZ DMSO: 8.2 ± 3.7, MTZ DEX: 2.3 ± 1; Fig. 9.7C). This reveals that DEX reduces the number of neutrophils and macrophages recruited to muscle injury, abrogating the prolonged neutrophilic response.

5.2.19 Dexamethasone leads to an increase in *Tp1:H2BmCherry*-expressing Pax7+ cells at the site of injury 24 hpi

To understand the effects of an anti-inflammatory microenvironment on Pax7-expressing cells following injury, I treated 5 dpf *Tp1:H2BmCherry*-expressing larvae with DEX for 1 hour before injury. Following injury, I refreshed the DEX treatment. At 24 hpi, I assessed the number of Pax7+, mCherry+ and Pax7+mCherry+ cells by immunolabeling relative to DMSO-treated animals (Fig. 5.20A-D). To evaluate if DEX treatment affects the number of Pax7+ and mCherry+ cells within the myotome, I conducted a 2-way ANOVA. I found that DEX treatment affected the number of Pax7+ and Pax7+mCherry+ cells following injury (File. 9.3). Moreover, DEX treatment affected the proportion of mCherry+ cells expressing Pax7 in response to injury (File. 9.3).

To understand how DEX treatment affects the number of Pax7+ and mCherry+ cells in the injured myotome, I conducted a 1-way ANOVA. I found that the number of Pax7+ cells increased in DMSO (uninjured: 4.7 ± 1.4, injured: 12.7 ± 5; Fig. 5.20E) and DEX (uninjured: 4.3 ± 1.4, injured: 32.8 ± 8.1; Fig. 5.20E) treated larvae following injured relative to uninjured animals. Moreover, there were more Pax7+ cells post-injury, following DEX treatment relative to DMSO-treated animals (Fig. 5.20E). I found an increase in Pax7+mCherry+ cells within the injured myotome relative to uninjured controls following DMSO (uninjured: 2.7 ± 0.8, injured: 3.8 ± 3.5; Fig. 5.20G) or DEX (uninjured: 2.5 ± 1.4, injured: 8.3 ± 2.7; Fig. 5.20G) treatment. Moreover, there were more Pax7+mCherry+ cells following DEX treatment relative to DMSO controls (Fig. 5.20G). I found no change in the proportion of Pax7+ cells expressing mCherry in DMSO or DEX-treated larvae (Fig. 5.20H; File. 9.3). Following injury, DEX-treated animals had an increased proportion of mCherry+ cells expressing Pax7 relative to DMSO control larvae (DMSO: 4.8% ± 3.4%, DEX: 9.2% ± 2.1%; Fig. 5.20I).

Previously, I have shown that most *Tp1*+ myonuclei were found within myofibers and do not contribute towards injury. Therefore, to understand the effect of DEX treatment on the injury responsive *Tp1*+ cells, I quantified the number of cells at the injured region. I found that DEX treatment resulted in more Pax7+ (DMSO: 7.2 ± 3.4, DEX: 19.8 ± 6.8; Fig. 5.20J), mCherry+ (DMSO: 8.3 ± 6.3, DEX: 21.3 ± 6; Fig. 5.20K),

and Pax7+mCherry+ cells (DMSO: 1.7 ± 1.5, DEX: 6.3 ± 2; Fig. 5.20L). Moreover, this was not a consequence of a change in the proportion of Pax7+ cells expressing mCherry (DMSO: 24.3% ± 20.5%, DEX: 36% ± 19%; Fig. 5.20M) or proportion of mCherry+ cells expressing Pax7 (DMSO: 16.8% ± 16%, DEX: 31% ± 9.7%; Fig. 5.20N). This suggests that DEX treatment causes elevated proliferation of Pax7+ and *Tp1*+ cells.

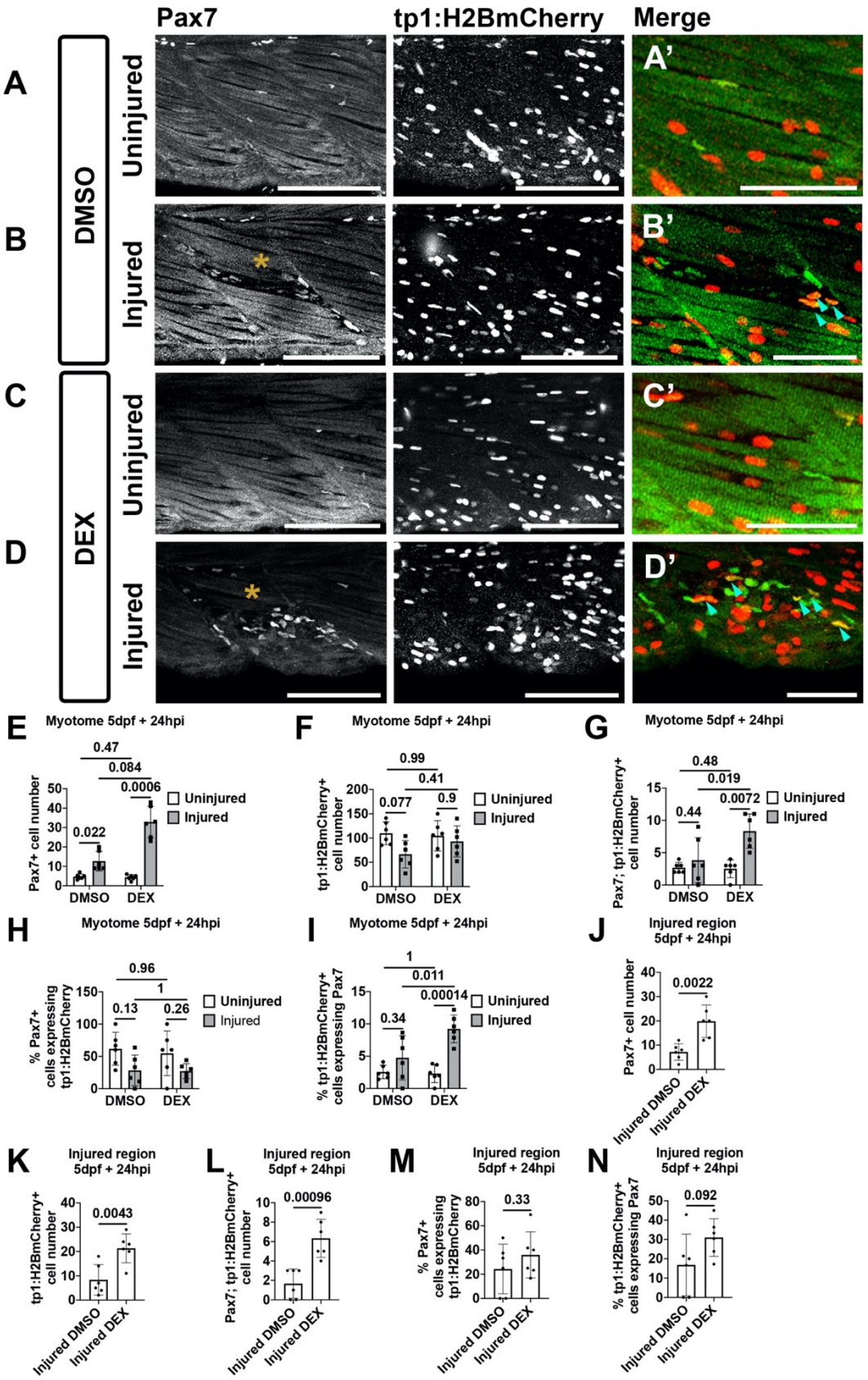
Pax7
tp1:H2BmCherry
Merge
A
B
C
D
DMSO
DEX
Uninjured
Injured
A'
B'
C'
D'
E Myotome 5dpf + 24hpi
Pax7+ cell number
0.47
0.084
0.0006
0.022
F Myotome 5dpf + 24hpi
tp1:H2BmCherry+ cell number
0.99
0.41
0.077
0.9
G Myotome 5dpf + 24hpi
Pax7; tp1:H2BmCherry+ cell number
0.48
0.019
0.0072
0.44
H Myotome 5dpf + 24hpi
% Pax7+ cells expressing tp1:H2BmCherry
0.96
1
0.13
0.26
I Myotome 5dpf + 24hpi
% tp1:H2BmCherry+ cells expressing Pax7
1
0.011
0.00014
0.34
J Injured region 5dpf + 24hpi
Pax7+ cell number
0.0022
Injured DMSO
Injured DEX
K Injured region 5dpf + 24hpi
tp1:H2BmCherry+ cell number
0.0043
L Injured region 5dpf + 24hpi
Pax7; tp1:H2BmCherry+ cell number
0.00096
M Injured region 5dpf + 24hpi
% Pax7+ cells expressing tp1:H2BmCherry
0.33
N Injured region 5dpf + 24hpi
% tp1:H2BmCherry+ cells expressing Pax7
0.092

Figure 5.20. Dexamethasone treatment results in more Pax7; *Tp1:H2BmCherry*+ cells following injury 24 hpi.

Representative projections from confocal z-stacks of the myotome (asterisks) in uninjured (**A, C**) and injured (**B, D**) 5 dpf *Tp1:H2BmCherry* + larvae 24 hpi. Larvae were treated with DMSO (**A-B**) or DEX (**C-D**). Pax7+, mCherry+, and Pax7+mCherry+ (cyan arrowheads) were detected by immunostaining (**A'-D'**), and the number of cells were quantified in the injured myotome (**E-I**) and injured region (**J-N**). There were more Pax7+mCherry+ cells within the injured myotome following DEX treatment (**G**). This change is associated with an increase in the proportion of mCherry+ cells expressing Pax7 (**I**). There were also more Pax7+ (**J**), mCherry+ (**K**) and Pax7+mCherry+ (**L**) cells within the injured region following DEX treatment. This was not due to a proportional change (**M-N**). Significant differences in the myotome were tested by 2-way ANOVA (n=22) with Tukey's HSD post-hoc test or by transforming data by ART and performing 2-way ANOVA followed by a Dunn's test with Benjamini and Hochberg correction. Significant differences in the injured region were tested by Student's t-test. Error bars represent standard deviation, and values above comparison bars represent significance (p-values).

Scale bars: 100 μm (**A-D**), 50 μm (**A'-D'**).

5.2.20 Macrophage ablation and dexamethasone treatment do not have a cumulative effect on the Pax7+ and *Tp1*+ myoblast populations in the injured region 24 hpi

To understand if the induction of an anti-inflammatory microenvironment, using DEX, modulates the elevated Pax7+ and *Tp1*+ cell number observed following macrophage ablation, I pre-treated 4dpf *Tp1:H2BmCherry*; *fms:mCherry*-expressing larvae with MTZ and DEX 24 and 1 hour before injury, respectively. Following injury, I continued MTZ and DEX treatment. I then detected and quantified the number of Pax7+, mCherry+, and Pax7+mCherry+ cells by immunolabelling at 24 hpi (Fig. 5.21A-D). To understand if DEX and MTZ co-treatment affects the number of Pax7+ and mCherry+ cells within the myotome and injured region, I conducted a 2-way ANOVA. I found that concurrent DEX and MTZ treatment affects the number of Pax7+ and Pax7+mCherry+ cells and the proportion of mCherry+ cells expressing Pax7 within the injured myotome (File. 9.3). Additionally, concurrent DEX and MTZ treatment affected the number of Pax7+ and Pax7+mCherry+ cells within the injured region (File. 9.3).

To understand how DEX and MTZ co-treatment affects the number of Pax7+ and mCherry+ cells, I conducted a 1-way ANOVA. I found that within the injured myotome, DEX treatment resulted in more Pax7+ cells following injury relative to DMSO treated controls (DMSO: 15.8 ± 4.4, DEX: 36.3 ± 10.1; Fig. 5.21E). This was unaffected by MTZ treatment (Fig. 5.21E; File. 9.3). DEX treatment did not affect the number of mCherry+ cells, which was unchanged by MTZ treatment (Fig. 5.21F; File. 9.3). DEX treatment resulted in more Pax7+mCherry+ cells relative to DMSO-treated larvae (DMSO: 5.2 ± 2.1, DEX: 15.8 ± 7.7; Fig. 5.21G), which was unaffected by MTZ co-treatment (Fig. 5.21G; File. 9.3). Interestingly, DEX-treated animals had more Pax7+mCherry+ cells than MTZ-treated animals (DEX: 15.8 ± 7.7, MTZ DMSO: 6.7 ± 2.9; Fig. 5.21G). This was a result of an increase in the proportion of mCherry+ cells expressing Pax7 (MTZ DMSO: 8.7% ± 3.2%, DEX: 16.6% ± 4%; Fig. 5.21I), and not a change in the proportion of Pax7+ cells expressing *Tp1:H2BmCherry* (Fig. 5.21H; File. 9.3).

Next I assessed changes to the number of Pax7+ and mCherry+ cells within the injured region. I found that both DEX and MTZ treatment resulted in more Pax7+ cells

relative to DMSO-treated controls (DMSO: 7.2 ± 2.2, DEX: 21.2 ± 7.2; MTZ DMSO: 18.2 ± 9.5; Fig. 5.21J). Although the number of Pax7+ cells increased with both DEX and MTZ treatment, surprisingly the number of Pax7+ cells did not significantly change when larvae were co-treated with both DEX and MTZ relative to DEX-only treatment (Fig. 5.21J; File. 9.3). Consequently, I did not find the expected increase in the number of Pax7+ cells following DEX and MTZ co-treatment relative to DMSO controls. Due to the high variability in mCherry+ cell counts, I was unable to detect a significant change in the number of mCherry+ cells following DEX treatment (Fig. 5.21K; File. 9.3). This was unchanged by MTZ co-treatment (Fig. 5.21K; File. 9.3). I also found that there was an increase in the number or Pax7+mCherry+ cells following DEX and DEX and MTZ co-treatment (DMSO: 3.3 ± 1, DEX: 9.5 ± 4.3, MTZ DEX: 6 ± 1.7; Fig. 5.21L). Interestingly, the number of Pax7+mCherry+ cells was higher in larvae which have been treated with DEX relative to MTZ treatment (DEX: 9.5 ± 4.3, MTZ DMSO: 5 ± 2.4; Fig. 5.21L). This was not a consequence of a change in the proportion of Pax7+ cells expressing mCherry (Fig. 5.21M) or proportion of mCherry+ cells expressing Pax7 (Fig. 5.21N). This reveals that inhibition of inflammation by DEX results in more Pax7+ cells and an increased number of *Tp1*+ cells showing Pax7 expression.

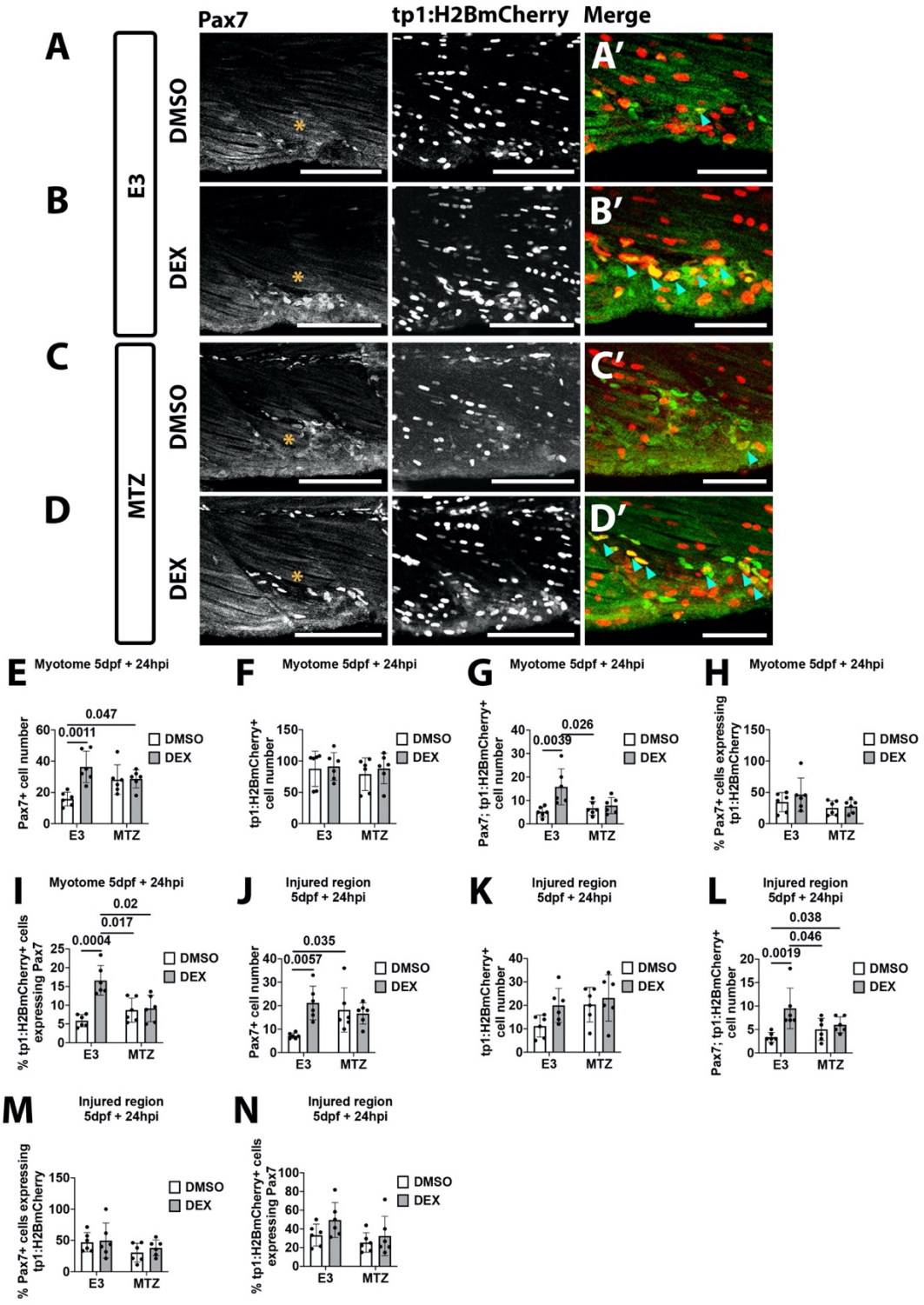
Pax7
tp1:H2BmCherry
Merge
A
B
C
D
E3
MTZ
DMSO
DEX
A′
B′
C′
D′
E Myotome 5dpf + 24hpi
Pax7+ cell number
F Myotome 5dpf + 24hpi
tp1:H2BmCherry+ cell number
G Myotome 5dpf + 24hpi
Pax7; tp1:H2BmCherry+ cell number
H Myotome 5dpf + 24hpi
% Pax7+ cells expressing tp1:H2BmCherry
I Myotome 5dpf + 24hpi
% tp1:H2BmCherry+ cells expressing Pax7
J Injured region 5dpf + 24hpi
Pax7+ cell number
K Injured region 5dpf + 24hpi
tp1:H2BmCherry+ cell number
L Injured region 5dpf + 24hpi
Pax7; tp1:H2BmCherry+ cell number
M Injured region 5dpf + 24hpi
% Pax7+ cells expressing tp1:H2BmCherry
N Injured region 5dpf + 24hpi
% tp1:H2BmCherry+ cells expressing Pax7

Figure 5.21. There is no cumulative effect of DEX and MTZ treatment on the number of Pax7; *Tp1:H2BmCherry*+ cells following injury 24 hpi.
Representative projections from confocal z-stacks of the injured myotome (asterisks) in DMSO-treated (**A**), DEX-treated (**B**), MTZ-treated (**C**) and DEX and MTZ co-treated (**D**) 5 dpf *Tp1:H2BmCherry*; *fms:mCherry*+ larvae 24 hpi. Pax7+, mCherry+, and Pax7mCherry+ (cyan arrowheads) were detected by immunolabelling (**A'-D'**), and the number of cells were quantified in the injured myotome (**E-I**) and injured region (**J-N**). Although both DEX and MTZ treatment resulted in more Pax7+ cells (**E, J**), only DEX treatment leads to more Pax7+mCherry+ cells within the injured myotome and injured region (**G, L**). This was caused by an increase in the proportion of mCherry+ cells expressing Pax7 within the injured myotome (**I**). There was no cumulative effect of DEX and MTZ treatment on the number of Pax7+ (**E, J**) and Pax7+mCherry+ cells (**G, L**). Significant differences in the myotome were tested by 2-way ANOVA (n=24) with Tukey's HSD post-hoc test or by transforming data by ART and performing 2-way ANOVA followed by a Dunn's test with Benjamini and Hochberg correction. Error bars represent standard deviation, and values above comparison bars represent significant differences only (p-values).
Scale bars: 100 μm (**A-D**), 50 μm (**A'-D'**).

5.2.21 Tnfrsf1a results in more *pax7a*-expressing cells following injury 24 hpi

I have demonstrated that Notch signalling and macrophages are important for the regulation of Pax7-expressing myoblast. Although the Notch pathway can independently influence myogenesis (Delfini *et al.*, 2000; Hirsinger *et al.*, 2001; Bröhl *et al.*, 2012; Mourikis, Gopalakrishnan, *et al.*, 2012; Fujimaki *et al.*, 2018), there is also evidence suggesting a cross talk between Notch and pathways such as, the NF-κB/ TNF-α pathway (Kondoh *et al.*, 2007; Acharyya *et al.*, 2010). Therefore, I aimed to understand if the increase in Pax7-expressing muSCs, observed following macrophage ablation or DEX treatment, is a consequence of perturbed TNF-α signalling.

I utilised a zebrafish line which harbours a single nucleotide polymorphism (SNP) in the third exon of the *tnfrsf1a* gene (*tnfrsf1a*^{Sa8496}). This leads to a frame shift within the cysteine-rich region of the TNF-α receptor 1. I injured 5 dpf *pax7a:eGFP*; *tnfrsf1a* mutants and *pax7a:eGFP*; WT siblings, quantifying the number of *pax7a*-expressing cells 24 hpi (Fig. 5.22A-B). I found that there were more *pax7a:eGFP*+ cells in the *tnfrsf1a* mutants compared to WT siblings in the myotome (WT: 13.5 ± 1.6, *tnfrsf1a*: 20.2 ± 1.2; Fig. 5.22C) and injured region (WT: 6.2 ± 1.2, *tnfrsf1a*: 10.8 ± 3.5; Fig. 5.22D).

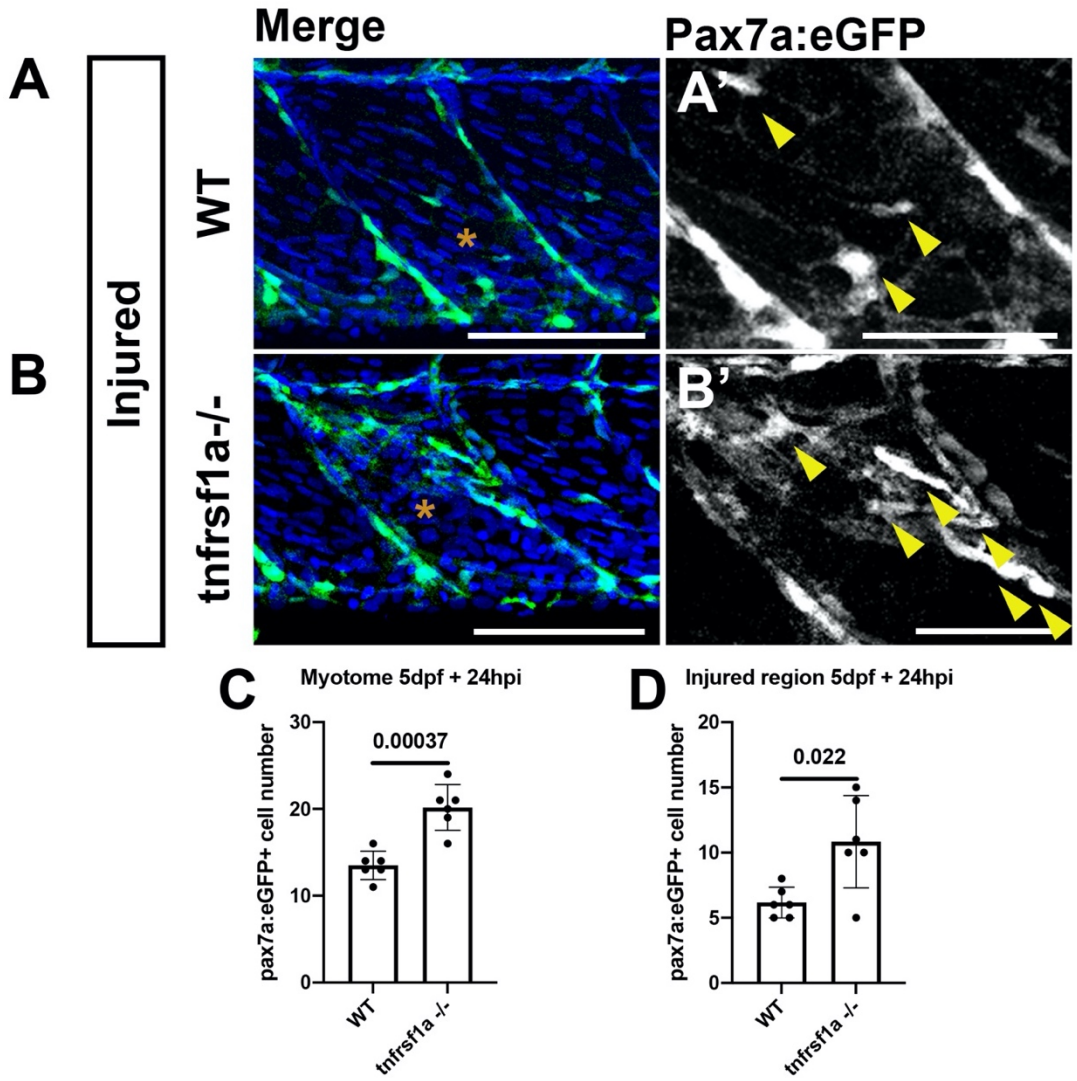

Figure 5.22. TNF-α regulates *pax7a*-expressing muSC activity following injury.
Representative projections from confocal z-stacks of the injured myotome in 5dpf WT (**A**) and *tnfrsf1a* mutants (*tnfrsf1a-/-*; **B**) *pax7a:eGFP*-expressing larvae 24 hpi. eGFP+ cells were detected (**A'-B'**), and the number of cells were was quantified in the injured myotome (**C**) and injured region (**D**). Injury denoted by an asterisk. There were more eGFP+ muSCS in the myotome (**C**) and injured region (**D**) of *tnfrsf1a-/-* mutants relative to WT siblings. Significant differences were tested by Student's or Welch's t-test for comparisons with equal and unequal variance, respectively. Error bars represent standard deviation, and values above comparison bars represent significance (p-values).
Scale bars: 100 µm (**A-B**), 50 µm (**A'-B'**).

5.3 Discussion

I have previously shown that Notch signalling is important for the activity of Pax7-expressing and *Tp1*-expressing muSCs following injury in zebrafish. Co-culture studies have found that macrophages can make contacts with myogenic precursor cells via adhesion molecules (Chazaud *et al.*, 2003). The ability for macrophages to make direct contacts with pax3-expressing cells has also been shown recently in zebrafish (Ratnayake *et al.*, 2021). Moreover, it has been demonstrated in mouse that anti- and pro-inflammatory macrophages can control Notch signalling in muSCs (Akahori *et al.*, 2015; Du *et al.*, 2017). In this chapter, I aimed to understand if macrophages can regulate cells displaying Notch activity in zebrafish following injury. Initially, I found that macrophage ablation resulted in more Pax7-expressing, Myog-expressing and proliferating *Tp1*-expressing muSCs following injury, relative to untreated animals. I also found that there were more Pax7+*Tp1:H2BmCherry*+ cells. Using the *pax7a:eGFP* zebrafish line, I found that these Pax7+*Tp1:H2BmCherry*+ cells were not derived from the resident *pax7a* muSC population. Contrastingly, it appears that these Pax7+*Tp1:H2BmCherry*+ cells were a consequence of an increase in the proportion of *Tp1:H2BmCherry*+ cells upregulating *pax7a* by 24 hpi, suggesting that new Pax7+ myoblasts arise from macrophage ablation. Myog is expressed in committed myogenic cells, preceding differentiation and fusion (reviewed by Bentzinger *et al.*, 2012). I have found that these novel proliferating *Tp1:H2BmCherry*+ population expressed Myog following injury, and so, can contribute to myogenesis. Moreover, the number of *Tp1*:H2BmCerry+Myog+ cells increased following macrophage ablation.

Using a zebrafish reporter line for DeltaD, I found that L-plastin+ macrophages expressed DeltaD following injury, suggesting that macrophages hold the capacity to signal to adjacent cells in a DeltaD-dependent manner. Therefore, I wanted to understand if macrophages regulate muSCs in an absence of Notch signalling. Interestingly, I found that concurrent DAPT and MTZ treatment acted differently on Pax7-expressing and *Tp1*-expressing cells following injury. I found there were more *Tp1*-expressing myoblasts in response to injury when larvae were treated with either DAPT or MTZ, but fewer cells when larvae were treated with both. Contrastingly, macrophage ablation counter-acted the loss of Pax7-expressing cells observed

following DAPT treatment. This suggests that Notch signalling is important for the proliferation of Pax7-expressing cells independently of macrophages. Although my data does not address if macrophages can signal to muscle cells via DeltaD, I propose that a Notch-dependent macrophage-muSC axis exists following muscle injury in zebrafish.

Notch signalling is a key player during the process of haematopoiesis (He *et al.*, 2015), associated with the polarisation of macrophages. Notch signalling promotes a pro-inflammatory macrophage phenotype, important for the recruitment of macrophages following skin wounding (Hamilton Outtz *et al.*, 2010; Lin *et al.*, 2018). Therefore, I investigated the effects of Notch inhibition and macrophage ablation on the immune response. I found that Notch inhibition resulted in a suppressed macrophage response as fewer macrophages were recruited to the site of injury. Moreover, I found that *Tp1:H2BmCherry*-epressing neutrophils perdure within the injured myotome in the absence of macrophages (Fig 5.16-5.17). To understand if the phenotype observed following MTZ treatment was a consequence of a loss of pro-inflammatory macrophages, I used the steroid DEX. DEX treatment reduced the number of macrophages and neutrophils recruited to the injury site in zebrafish (Sharif *et al.*, 2015; Hasegawa *et al.*, 2017; Xie *et al.*, 2019), perturbing the inflammatory microenvironment. Following DEX treatment, there were more Pax7+, *Tp1*+ and Pax7+*Tp1*+ cells, phenocopying the results observed following MTZ treatment. Although macrophage ablation and DEX treatment did not have an additive effect of the number of Pax7+ and *Tp1*+ cells, these data highlight the importance of a balanced immune response for the activity of muscle cells in response to injury.

I have shown that the Notch pathway has a conserved role in the maintenance of muSCs during myogenesis (Delfini *et al.*, 2000; Hirsinger *et al.*, 2001; Bröhl *et al.*, 2012; Mourikis, Gopalakrishnan, *et al.*, 2012; Fujimaki *et al.*, 2018). Evidences suggest that there is an interaction between the Notch and the TNF-α pathway in the regulation on myogenic precursor cells (Kondoh *et al.*, 2007; Acharyya *et al.*, 2010). Therefore, using a TNF-α receptor 1 mutant line, I aimed to understand if the increased number of Pax7-expressing cells, following macrophage ablation or induction of an anti-inflammatory microenvironment, is a consequence of disturbed

pro-inflammatory (TNF-α) signals. I found that perturbed TNF-α signalling resulted in more Pax7-expressing cells following injury. Together my data suggest that the loss of pro-inflammatory macrophages generates an anti-inflammatory microenvironment promoting muSC activation.

5.4 Conclusion

In this chapter, I have shown that following macrophage ablation, a new population of *Tp1:H2BmCherry*-expressing cells expands following injury. These cells are Pax7+ and express *pax7a:eGFP* by 24 hpi. Moreover, I found that later in regeneration, there is an increase in *pax7a*-expressing fibres, which may arise from these novel *Tp1:H2BmCherry*-expressing cells which express Myog. I also found that macrophages regulate Pax7-expressing and *Tp1*-expressing muSCs following injury. Subsequently, by treating larvae with DEX or using *tnfrsf1a* mutant larvae, I found that induction of an anti-inflammatory microenvironment also leads to more Pax7- and *Tp1*-expressing cells following injury. This suggests that the increased Pax7- and *Tp1*-expressing cells observed following injury is a consequence of a loss of pro-inflammatory macrophages. As I have shown that macrophages express DeltaD, I propose that pro-inflammatory macrophages regulate Pax7- and *Tp1*-expressing cell proliferation in a DeltaD-dependent manner. Moreover, as macrophage ablation and Notch inhibition have apposing effects on the number of Pax7-expresing cells, Notch is also important for the proliferation of Pax7-expressing cells.

Chapter 6 General discussion

In mouse, Notch signalling is important to limit differentiation and promote proliferation of Pax7-expressing cells following injury (Bjornson *et al.*, 2012; Mourikis, Sambasivan, *et al.*, 2012). A recent study has demonstrated the importance of macrophages during zebrafish muscle repair (Ratnayake *et al.*, 2021). They found that macrophages make direct contacts with pax3-expressing cells, promoting proliferation (Ratnayake *et al.*, 2021). Moreover, in mouse, pro- and anti-inflammatory macrophages control Notch signalling in myoblasts following injury (Akahori *et al.*, 2015; Du *et al.*, 2017). Some key questions remain unexplored such as, 1) whether zebrafish muSCs are controlled by Notch signalling during homeostasis and regeneration, 2) how the inflammatory microenvironment controls the response of muSCs to injury, and 3) if macrophages control muSCs which show Notch activity. Therefore, I aimed to understand whether Notch signalling is important for the recruitment of Pax7+ muSCs following injury, evaluating cells which display Notch activity (*Tp1*+). I then aimed to understand if inhibiting the recruitment of pro-inflammatory immune cells affects Pax7+ and *Tp1*+ cell activity following injury. Finally, I explored the effects of Notch inhibition and macrophage ablation on Pax7+ and *Tp1*+ cell response to injury.

6.1 The inflammatory microenvironment controls muSC activity

The immune response towards tissue damage in zebrafish has been predominantly characterised following tail fin amputation (Mathias *et al.*, 2006; Ellett *et al.*, 2011; Nguyen-Chi *et al.*, 2015). Following injury, neutrophils and then macrophages migrate towards the site of injury (Mathias *et al.*, 2006). Apoptotic neutrophils are then subsequently phagocytosed by macrophages (Ellett *et al.*, 2011), and the remaining neutrophils undergo a process of retrogradation, migrating away from the injured region (Mathias *et al.*, 2006). During this time, macrophages switch from a pro- to anti-inflammatory phenotype characterized by the suppression of key pro-inflammatory signals (TNF-α and IL-6; Nguyen-Chi *et al.*, 2015). The key role of macrophage infiltration for tissue repair has been demonstrated in zebrafish (Hasegawa *et al.*, 2015; Morales and Allende, 2019). Mutants such as *Panther*

(Morales and Allende, 2019) and *clo* (Hasegawa *et al.*, 2015), or zebrafish treated with *pu.*1 MO (Hasegawa *et al.*, 2015) have demonstrated that a loss of macrophages leads to perturbed blastemal cell proliferation (Hasegawa *et al.*, 2015). This loss of macrophages is associated with a prolonged neutrophilic response and increased cell apoptosis. Although macrophages are key in regulating the proliferative response of pax3-expressing cells (Ratnayake *et al.*, 2021), the importance of the inflammatory microenvironment for the activity of Pax7-expressing muSCs towards injury has not yet been explored in zebrafish. I predicted that a loss of macrophage recruitment, following muscle injury, would result in a similar disruption in the expansion of the Pax7-expressing muSC population. Contrastingly, following continuous macrophage ablation, I found that more Pax7-expressing muSCs were present following muscle injury (Fig. 5.1) resulting in more myofibers later in regeneration (Fig. 5.2). Ratnayake *et al.,* (2021) define two sub-populations of macrophages contributing towards zebrafish muscle repair. They showed that initially 'transient' macrophages present within the injured region subsequently switch towards a 'dwelling' macrophage (Ratnayake *et al.*, 2021). Furthermore, the dwelling macrophage sub-population expresses anti-inflammatory markers (*arg-1* and *mmp9*), making contacts with muSCs. The ablation of macrophages between 1.75-2 dpi showed that dwelling macrophages promote muSC proliferation (Ratnayake *et al.*, 2021). It is possible that the early (< 1.75 dpi) pro- and late (> 1.75 dpi) anti-inflammatory macrophages differentially control muSC populations following injury. Therefore, I asked whether pro-inflammatory immune cells are important to limit muSC proliferation following injury in zebrafish.

The switch from a pro- to anti-inflammatory microenvironment has been well characterized during tissue repair (Thornton, 1949; Mathew *et al.*, 2007). Initial studies in Xenopus and zebrafish demonstrated that tissue repair relies on both pro- and anti-inflammatory mechanisms (Thornton, 1949; Mathew *et al.*, 2007). It has been shown *in vitro* and *in vivo,* that the different polarisation states of macrophages control myoblast survival, proliferation, migration, and fusion (Chazaud *et al.*, 2003; Saclier, Cuvellier, *et al.*, 2013). Moreover, a loss of pro- or anti-inflammatory macrophages results in a failure to repair damaged muscle (Warren *et al.*, 2005; Arnold *et al.*, 2007; Contreras-Shannon *et al.*, 2007; Sun *et al.*, 2009; Martinez *et al.*,

2010; Lu, Huang, Ransohoff, *et al.*, 2011; Deng *et al.*, 2012; Mounier *et al.*, 2013; Akahori *et al.*, 2015). It is not known whether an altered inflammatory microenvironment modulates Pax7-expressing muSC response to injury in zebrafish. Therefore, to understand whether the increased muSC number, following injury and in the absence of macrophages, results from a skewed anti-inflammatory microenvironment, I treated larvae with DEX (Hasegawa *et al.*, 2015) and used a TNF-α receptor mutant line (*tnfrsf1a*). DEX is a glucocorticoid which has been demonstrated to inhibit the production of pro-inflammatory cytokines (IL-1b and TNF-α) during tail-fin regeneration, reducing neutrophil and macrophage recruitment (Sharif *et al.*, 2015; Hasegawa *et al.*, 2017; Xie *et al.*, 2019). Corticosteroid have also been shown to skew helper T-cells towards an anti-inflammatory phenotype (IL-4+; Derijk and Sternberg, 1994). I noted that DEX treatment also reduced the number of macrophages and neutrophils following muscle damage (Fig. 9.6), abrogating the pro-longed neutrophilic response following macrophage ablation (Fig. 9.7). I found that both DEX treatment (Fig. 5.19) and *tnfrsf1a-/-* (Fig. 5.21) resulted in more Pax7-expressing muSCs following injury. My data highlights the importance of a pro-inflammatory microenvironment for the control of muSC number, limiting Pax7-expressing muSC expansion within the first 24 hours following injury.

6.2 Macrophages control muSC activity following injury

Muscle regeneration is highly conserved between mammals and zebrafish. In zebrafish, a population of muSCs activate, migrate, clonally proliferate, differentiate and fuse into myofibers (Knappe *et al.*, 2015; Gurevich *et al.*, 2016; Pipalia *et al.*, 2016). This process is co-ordinated by the temporal expression of commitment- (*Myf5* and *Myod*) and differentiation (*Myog*)-associated transcription factors, completed by ~3 dpi (Gurevich *et al.*, 2016). Muscle repair occurs within the changing inflammatory environment, and in a recent study by Ratnayake *et al.,* (2021), macrophages have been shown to control muSC activity. They found that macrophages make direct contact with pax3-expressing muSCs later in the regenerative programme (11 hpi), promoting muSC proliferation (Ratnayake *et al.*,

2021). As previously discussed, this study presents a discrepancy with my findings. I demonstrated that there are more Pax7-expressing muSCs following injury in the absence of macrophage. Ratnayake *et al.,* (2021) induce larger injuries using a 30g needle (Ratnayake *et al.*, 2021). This method of injury damages multiple myotomes in addition to the surrounding myosepta. Nguyen *et al.,* (2017) described a population of low-cycling *meox*-expressing muSCs residing in the horizontal myosepta. A sub-set of these cells subsequently migrate to the vertical myosepta, where they expand and contribute to muscle growth (Nguyen *et al.*, 2017). Moreover, the myosepta are enriched with ECM molecules such as laminin and fibronectin, and have been described as potential muSC niche in zebrafish (Seger *et al.*, 2011; Knappe *et al.*, 2015; Gurevich *et al.*, 2016; Pipalia *et al.*, 2016). The role of the niche to promote muSC maintenance has been demonstrated in mouse, where the disruption of the niche leads to muSC activation (Bjornson *et al.*, 2012; Bröhl *et al.*, 2012; Baghdadi, Castel, *et al.*, 2018; Low *et al.*, 2018; Verma *et al.*, 2018). Moreover, following tail fin amputation in zebrafish, the type and extent of injury modulates immune cell activity and blastema cells expansion (Niethammer *et al.*, 2009; Miskolci *et al.*, 2019). It is unknown whether the size of injury affects the muSC response to muscle damage in zebrafish. To examine the effect of injury size on *pax7a*-expressing muSC response, I used Evans blue staining to measure the initial injured volume (Fig. 3.1) and live-imaged the subsequent *pax7a*-expressing muSC response (Fig. 3.2). I found that the number of muSCs scaled with injury size as more muSCs responded towards a larger injury (Fig. 3.2). Knappe *et al.,* (2015) discussed a similar concept, showing that *pax7a*-expressing muSCs do not contribute towards the repair of smaller muscle injuries in zebrafish (Knappe *et al.*, 2015). I then examined the effect of scaling the injury size on muSC response following macrophage ablation. I found that, at both 24 hpi (Fig. 5.3) and 48 hpi (Fig. 5.4), the number of muSCs increased following small injuries in the absence of macrophages. In contrast, following large injuries, the number of muSC decreases following macrophage ablation. Modelling of innate immune cell responses to varying injury sizes in *Drosophila* revealed a positive correlation between the injury size and number of cells responding (Weavers *et al.*, 2016). It has also been shown following tail fin amputation that the type of injury affects the blastemal cells responses to

injury (Miskolci *et al.*, 2019). Comparing burn and transection-induced injuries, Miskolci *et al.,* (2019) found that burn-induced injuries elicit a stronger prolonged pro-inflammatory macrophage and neutrophil response (Miskolci *et al.*, 2019). This prolonged pro-inflammatory response results in more vimentin-expressing blastemal cells over time at the site of injury (Miskolci *et al.*, 2019). Currently, a multitude of injury methods are used to damage muscle, including injection of CTX (Seger *et al.*, 2011) or application of a sharp needle (Gurevich *et al.*, 2016; Pipalia *et al.*, 2016; Nguyen *et al.*, 2017; Ratnayake *et al.*, 2021) in zebrafish. Although these methods elicit a robust cellular response, many studies do not control for injury size. It is possible that, like in the tail fin, the type and extent of injury can modulate immune cell recruitment to damaged muscle, affecting muSC response. Therefore, my results reveal that injury extent dictates the response of the muSC response to injury.

6.3 Notch signalling is conserved for maintenance of the muSC niche in zebrafish muscle during homeostasis and regeneration

In mouse, Pax7-expressing muSC lineage is critical for muscle repair (Lepper *et al.*, 2011). Lepper *et al.,* (2011) shows that following Pax7-specific muSC ablation, mice are unable to repair damaged muscle, stating that no other resident population is able to compensate for the loss of Pax7-expressing cells (Lepper *et al.*, 2011). Moreover, studies in mouse have investigated the activity of Notch signalling within Pax7-expressing muSCs following injury, demonstrating that following tamoxifen-induced loss of Rbp-jk in Pax7-expressing cells, mice fail to repair injured muscle (Bjornson *et al.*, 2012; Mourikis, Sambasivan, *et al.*, 2012). These studies also revealed that in the absence of Notch signalling, muSCs undergo premature S-phase-independent differentiation, perturbing muscle regeneration (Bjornson *et al.*, 2012; Mourikis, Sambasivan, *et al.*, 2012). It was not known whether Notch signalling shows a conserved function between mammals and zebrafish. Therefore, I tested the role of Notch signalling for muSC responses to injury in zebrafish. Using both pharmacological (DAPT) and genetic (HS:dnsu[h]) tools to inhibit Notch signalling, I found that following injury, there were fewer Pax7- and *pax7a*-expressing muSCs in the absence of Notch within the myotome (Fig. 3.4-3.7). This phenotype was

associated with decreased proliferation (Fig. 3.9) and an increased proportion of differentiating muSCs (Fig. 3.10). These findings are consistent with results from mice, demonstrating that Notch signalling is key for limiting muSC differentiation to allow proliferation in response to injury in zebrafish.

In mouse, muSCs can interact with adjacent committed myoblasts (Zhang *et al.*, 2021), myofibers (Low *et al.*, 2018) and blood vessels (Verma *et al.*, 2018) via Notch to maintain quiescence. I then asked whether myofibers or myosepta signal to muSCs to maintain quiescence in zebrafish. Using the DeltaD zebrafish reporter line, I did not identify DeltaD expression in myofibers or myosepta (Fig. 5.13). This suggests that committed myoblasts or myosepta do not signal to muSCs via DeltaD in zebrafish. It is important to also assess the expression of other Notch ligands, such as Jagged or DeltaC, to understand if committed myoblasts or myosepta interact with muSCs via Notch in zebrafish.

Studies investigating the effect of Notch inhibition and over-activation in murine Pax7-expressing muSCs have shown that Notch is important for muSC quiescence (Kopan *et al.*, 1994; Bjornson *et al.*, 2012; Mourikis, Gopalakrishnan, *et al.*, 2012; Yefei Wen *et al.*, 2012). Rbp-jk-/- Pax7+ cells reside above the basement membrane suggesting they have exited quiescence (Bjornson *et al.*, 2012). Contrastingly, forced NICD expression results in the upregulation of CalcR and laminin expression (Mourikis, Gopalakrishnan, *et al.*, 2012), maintaining proliferation (Yefei Wen *et al.*, 2012), and inhibiting differentiation of MPCs (Kopan *et al.*, 1994). As discussed previously, the myoseptum is often described as a niche, analogous to the adult mammalian muSC niche (Seger *et al.*, 2011; Knappe *et al.*, 2015; Gurevich *et al.*, 2016; Pipalia *et al.*, 2016). It is also unknown whether muSCs within myosepta of zebrafish are controlled by Notch activity. Therefore, I tested the importance of Notch signalling for muSC responses to injury within zebrafish myosepta. I found that following Notch inhibition, there were more proliferating *pax7a*-expressing cells (Fig. 3.9) and more differentiating myoblasts (Fig. 3.10) within the vertical myosepta in an absence of injury. Moreover, I found that there were fewer *pax7a*-expressing muSCs within the vertical myosepta following injury in the presence of constitutively active Notch signalling (Fig. 3.8). Therefore, my results suggest that the myosepta is

analogous to the mammalian muSC niche as I found that Pax7-expressing muSCs, residing within zebrafish muSC niche, are controlled by Notch signalling.

6.4 Identification of a novel *Tp1*-expressing muscle progenitor cell type responding to Notch in zebrafish

Studies investigating the importance of Notch activity in muSCs revealed that following injury, Pax7-expressing muSCs downregulate Notch target genes (Bjornson *et al.*, 2012; Mourikis, Sambasivan, *et al.*, 2012). This allows muSCs to activate, proliferate and differentiate down the myogenic lineage. Notch activity is expressed at low levels during the proliferative phase of muSC activation, and subsequently upregulated in differentiated myoblasts to signal to undifferentiated MPCs, keeping them in a quiescent state (Zhang *et al.*, 2021). Although Notch activity is initially downregulated in muSCs following injury, these studies removed the muSCs from their niche by isolated Pax7-expressing cells 3.5-4 dpi (Bjornson *et al.*, 2012; Mourikis, Sambasivan, *et al.*, 2012). Furthermore, while it has been shown that prolonged tamoxifen treatment to induce Pax7-specific Rbp-jk-/- results in disrupted repair of damaged muscle *in vivo*, the reduction in proliferation and increase in differentiation were measured *in vitro* (Bjornson *et al.*, 2012; Mourikis, Sambasivan, *et al.*, 2012). The importance of Notch activity in proliferating muSCs following injury *in vivo* is currently unknown. As I have shown that DAPT treatment leads to fewer proliferating muSCs following injury, similar to mice, I predict that proliferating muSCs display Notch activity following injury. Therefore, to test whether proliferating Pax7-expressing cells express a reporter for Notch activity, I used zebrafish expressing H2BmCherry (Parsons *et al.*, 2009; Ninov *et al.*, 2012) or VenusPEST (Aulehla *et al.*, 2008; Ninov *et al.*, 2012) under the control of *Tp1* promotor (multiple Rbp-jk binding sites). Using these *Tp1* reporter lines allowed me to identify cells showing Notch activity *in vivo*. By live imaging both *Tp1:H2BmCherry*- and *Tp1*:VenusPEST-expressing cells, I identified a population of *Tp1*:VenusPEST-expressing cells which upregulates *Tp1:H2BmCherry* over time before subsequently losing *Tp1*:VenusPEST expression (Fig. 4.1). Moreover, by live imaging, I found that proliferating *pax7a*-expressing cells express *Tp1*:VenusPEST (Fig. 4.4) demonstrating

that *pax7a*-expressing cells show Notch activity immediately after muscle injury in zebrafish. Following on this result I propose that, although Notch activity may be reduced in Pax7-expressing cells to facilitate the exit from quiescence, Notch activity is still needed to limit differentiation and promote proliferation during the early stages of muscle repair. This is in accordance with published work showing that Pax7-specific Rbp-jk-/- results in premature S-phase-independent differentiation (Bjornson *et al.*, 2012; Mourikis, Sambasivan, *et al.*, 2012).

In vivo analysis has shown that the duration of tamoxifen induction of Pax7-specific Rbp-jk-/-affects the contribution of Rbpj null SCs towards muscle regeneration. Short-term tamoxifen treatment (16 days), results in overtly normal tissue repair (Mourikis, Sambasivan, *et al.*, 2012; Mourikis and Tajbakhsh, 2014), and prolonged tamoxifen treatment (28-32 days) results in inhibition of repair muscle (Bjornson *et al.*, 2012; Mourikis, Sambasivan, *et al.*, 2012). Although Notch activity in Pax7-expressing cells is key for muscle repair, the contribution *in vivo* of Notch active Pax7-expressing cells to muscle repair remains unknown. Therefore, I wanted to determine whether *pax7a*+ cells express the *Tp1:H2BmCherry* transgene after injury, and if these cells contribute to muscle repair in zebrafish. By immunostaining, I found that both uninjured and injured larvae have very few *pax7a:eGFP*;*Tp1:H2BmCherry*-expressing cells at 24 hpi (Fig. 4.2), 48 hpi (Fig. 4.5) and 72 hpi (Fig. 4.6). Similar results were obtained when labelling cells with Pax7 immunoreactivity (Fig. 4.8) or when using the *pax7b* reporter line (Fig. 4.7) 24 hpi. I found that most *Tp1*-expressing nuclei are in myofibers, and do not respond to muscle injury. I also found that a motile population *Tp1*-expressing cells responds to injury, increasing *pax7a* expression over time (Fig. 4.5-4.6).

Teleost muSCs are a heterogenous population. It has been shown by *in situ* hybridization in black rockfish (*Sebastes schlegelii*) that teleost muSCs express pax3a/b and *pax7a*/b (Wang *et al.*, 2021). *pax3a*, *pax7a*, and *pax7b* genes are expressed following injury, whereas *pax3b* does not change (Wang *et al.*, 2021). Following injury in zebrafish, *pax7a*+, but not pax3a+ cells expand, proliferating more in response to injury (Seger *et al.*, 2011). Investigating the role of *pax7a*- and *pax7b*-expressing cells following zebrafish muscle injury, Pipalia *et al.,* (2016) found that these populations respond differently. *pax7a*-expressing cells fuse to one another to

form *de novo* myofibers, whereas *pax7b*-expressing cells fuse to existing damaged myofibers (Pipalia *et al.*, 2016). Additionally, studies have also shown that Pax3-expressing cells also express Meox-1 (Nguyen *et al.*, 2017) and c-met (Gurevich *et al.*, 2016), important for growth and regeneration, respectively. Interestingly, c-met co-labels only 10 % of Pax7-expressing cells and 15 % of Pax3-expressing cells (Gurevich *et al.*, 2016). This low proportion is similar to the proportion of *Tp1*+ cells expressing *pax7a* which I observed following injury. Moreover, Gurevich *et al.,* (2016) observed asymmetrical division of c-met-expressing cells into a c-met^{high}pax7^{low} stem cell population and a c-met^{low}pax7^{high} progenitor population following injury. It has been shown in mouse that Notch activity is important for asymmetrical division of MPCs (Conboy and Rando, 2002; Shinin *et al.*, 2006; Kuang *et al.*, 2007). Altogether, this suggests that the *Tp1*-expressing population may be part of the c-met population described by Gurevich *et al.,* (2016).

Using a reporter for c-met, Gurevich *et al.,* (2016) also showed that the number of c-met-expressing cells increases in the myotome until metamorphosis, after which, the number of c-met-expressing cells remained constant throughout adulthood. Therefore, I aimed to understand if the *Tp1:H2BmCherry*-expressing population is restricted to the developing larval zebrafish. I acquired images of *Tp1*:VenusPEST and *Tp1:H2BmCherry* expression at 24 hpf and 48 hpf. I found that although *Tp1*:VenusPEST is lost through development, *Tp1:H2BmCherry* persists (Fig. 4.9). Moreover, by 30 dpf, all *Tp1:H2BmCherry*-expressing cells are co-localised with *pax7a:eGFP* (Fig. 4.9). Notch signalling has been shown to be essential during the development of muscle in mammals (Delfini *et al.*, 2000; Hirsinger *et al.*, 2001; Bröhl *et al.*, 2012; Mourikis, Gopalakrishnan, *et al.*, 2012; Fujimaki *et al.*, 2018). Although the role of Notch signalling during zebrafish myotome development is unknown, studies investigating the development of pectoral fin musculature have shown that Notch signalling has a conserved requirement for muscle development (Pascoal *et al.*, 2013; Lleras-Forero *et al.*, 2020). I propose that during muscle development, cells with Notch activity contribute to myofiber development in the myotome, expressing both the *Tp1* reporters. By 48 hpi, most of the *Tp1:H2BmCherry*-nuclei are in myofibers, and do not contribute to muscle repair. Contrastingly, a smaller population of migratory *Tp1:H2BmCherry*-expressing cells exist, which can respond

to injury. These cells may be part of the c-met-expressing muSC population described by Gurevich *et al.,* (2016), asymmetrically proliferating following injury, generating a Pax7-expressing daughter cell. This accounts for the increased proportion of *Tp1*+ cells expressing *pax7a* I observed following injury (Fig. 4.5-4.6)

6.5 Macrophages control muSCs which show Notch activity

Macrophages have been shown to control muSC behaviour through the release of trophic factors such as, IL-6 (Zhang *et al.*, 2013), IL-1β (Luo *et al.*, 2003; Saclier, Yacoub-Youssef, *et al.*, 2013), TNF-α (Warren *et al.*, 2002; Li, 2003; Chen *et al.*, 2005), IFN-γ (Cheng *et al.*, 2008; Villalta, Deng, *et al.*, 2011), TGF-β (Saclier, Yacoub-Youssef, *et al.*, 2013), VEGF (Saclier, Yacoub-Youssef, *et al.*, 2013), and Oncostatin M (Latroche *et al.*, 2017). Macrophages have also been shown to make direct contacts with non-immune cells in zebrafish pigment migration (Eom and Parichy, 2017), angiogenesis (Gurevich *et al.*, 2018) and more recently muSC proliferation (Ratnayake *et al.*, 2021). Investigations in mouse have shown that both pro- (Ly6C^{high}CD11b+F4/80+) and anti-inflammatory (CD163+) macrophages can supress Notch signalling following muscle damage (Akahori *et al.*, 2015; Du *et al.*, 2017). It was unknown whether macrophages control Notch expressing cells following injury in zebrafish. Therefore, I asked whether macrophages could regulate the Notch active myoblast population (*Tp1*+) in zebrafish following injury. I found that following Notch inhibition, more proliferating *Tp1*-expressing myoblasts are observed at the site of injury (Fig. 4.10). This result suggests that *Tp1*-expressing cells are activated in the absence of Notch. Moreover, following macrophage ablation there were more proliferating (Fig. 5.6) and differentiating (Fig. 5.12) *Tp1*-expressing cells at the site of injury. Following injury, this increase in number of *Tp1*:H2B-mCherry-expressing cell was phenocopied following DEX treatment (Fig. 5.20), suggesting that *Tp1*-expressing cells are also controlled by pro-inflammatory macrophages like Pax7-expressing cell population.

In zebrafish, the proportion of *fms*+ macrophages is reduced when larvae are injected with a *notch1a* MO (Bugeon *et al.*, 2011). It has also been shown that Notch signalling skews macrophages towards a pro-inflammatory phenotype, leading to fewer recruited macrophages in skin wound healing (Hamilton Outtz *et al.*, 2010; Lin *et al.*,

2018). I found that macrophage recruitment is blunted following Notch inhibition (Fig. 5.19). It is possible that a global loss of Notch signalling potentiates the induction of an anti-inflammatory microenvironment, further controlling *Tp1*-expressing cell activity following injury.

During zebrafish pigment migration, macrophages can detect and tether to DeltaC-expressing protrusions on xanthoblasts (Eom and Parichy, 2017). Contrastingly, there is no description of the expression of Notch ligands on macrophages in zebrafish. Therefore, I aimed to examine if macrophages express the Notch ligand, DeltaD, in zebrafish following muscle injury. Using the DeltaD zebrafish reporter line, I found that macrophages express DeltaD following injury in zebrafish (Fig. 5.13). To examine if macrophage regulation of muSCs is lost following Notch inhibition, I co-treated larvae with MTZ and DAPT to ablate macrophages and Notch signalling, respectively. I have previously shown that Notch inhibition and macrophage ablation have opposing effects on the number of Pax7-expressing muSCs following injury. I predicted that loss of macrophages would result in reduced proliferation, as shown by Ratnayake *et al.,* (2021) in zebrafish. I also predicted that Notch inhibition would result in reduced muSC proliferation. I found that following macrophage ablation, there were more Pax7-expressing cells, which was reduced following Notch inhibition (Fig. 5.15). This result suggests that both macrophages and Notch signalling control muSC response to injury in zebrafish.

In zebrafish spinal neuron differentiation, progenitors rarely activate and differentiate when in close contact due to a Notch-Delta mediated lateral inhibition between adjacent cells (Hadjivasiliou *et al.*, 2019). It is possible that macrophages are contributing to Notch activity in Pax7+ and *Tp1*+ cell populations via DeltaD, inducing a mechanism of lateral inhibition between cells (Fig. 6.1). Therefore, I propose that macrophages signal to *Tp1*+ and Pax7+ cells via DeltaD to activate Notch signalling, inducing lateral inhibition (Fig. 6.1). Ablation of macrophages removes the macrophage-derived DeltaD signal, reducing lateral inhibition between cells. This then results in increased myoblast activation and proliferation (Fig. 6.1). Furthermore, my data suggest that Notch signalling is also important for limiting differentiation and allowing proliferation of Pax7-expressing muSCs. Therefore, my

results suggest that Notch activity in muSCs is regulated by macrophage mediated lateral inhibition to regulate proliferation (Fig. 6.1).

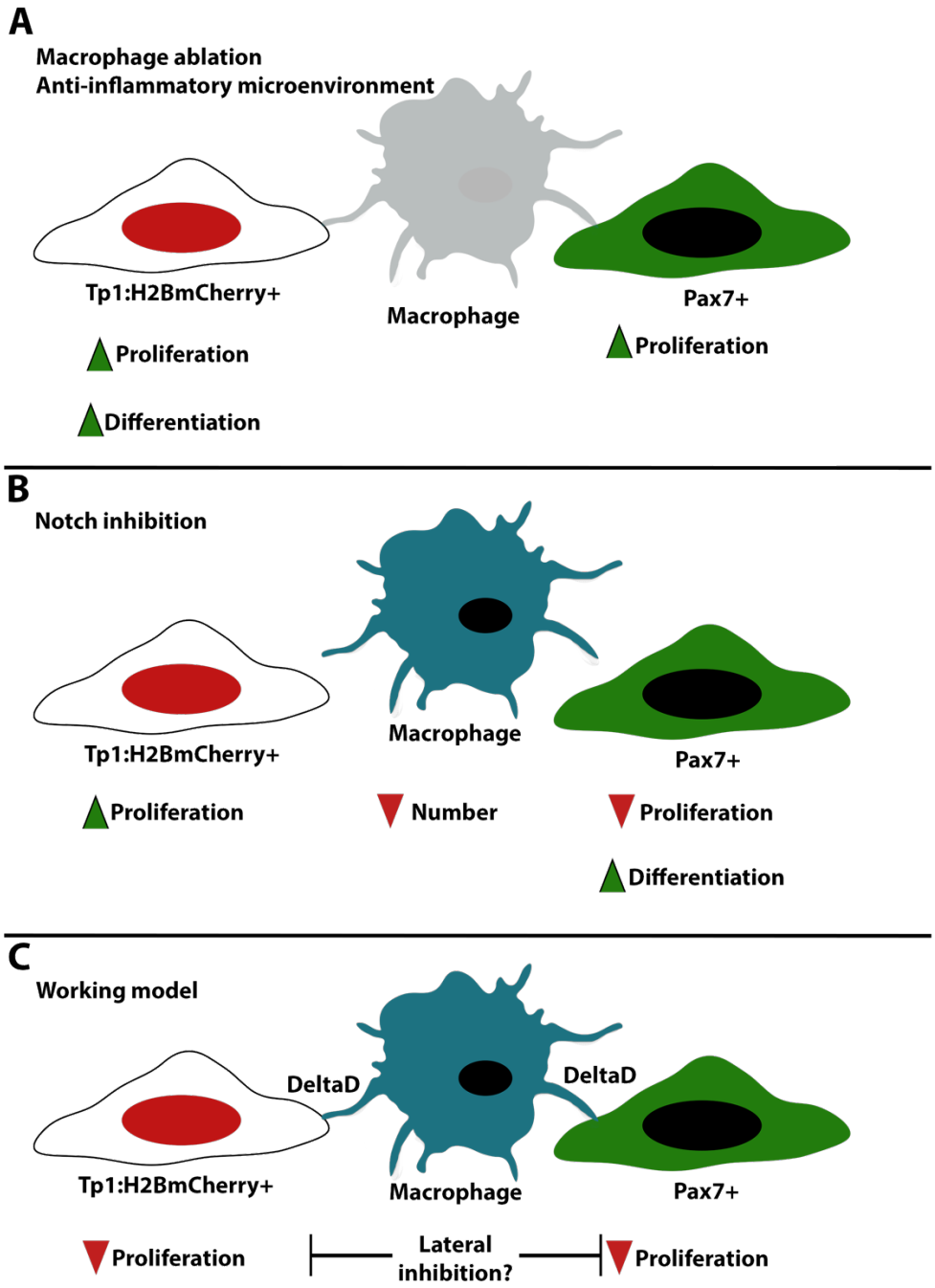

Figure 6.1. Schematic depicting control of *Tp1*+ and Pax7+ cell proliferation and differentiation by macrophages and Notch signalling.
Following macrophage ablation or dexamethasone treatment, there were more *Tp1*+ and Pax7+ cells after injury (A). Both *Tp1*+ and Pax7+ cells hyper-proliferate in the absence of macrophages following injury, and there were more differentiating *Tp1*+ cells (A). Following Notch inhibition, *Tp1*+ cells hyper-proliferate and Pax7+ cells proliferate less after injury (B). In the absence of Notch, Pax7+ cells also differentiate more (B). Macrophages express DeltaD (C), and fewer macrophages are recruited to injury following Notch inhibition (B). Macrophages have been shown to control *Tp1*+ and Pax7+ cells in a Notch dependent manner. Therefore, the proposed model hypothesis that macrophages regulate *Tp1*+ and Pax7+ cells via DeltaD, supressing cell proliferation (C). This then promotes Notch signalling in the stem cell population which results in lateral inhibition, further inhibiting muSC activation (C).

6.6 Limitations and future work

Statistical framework

Throughout this study I developed and refined a robust statistical framework to detect changes in muSC number, assessing the effect of age, injury and drug treatment. I concluded that only 5 and 4 animals are needed to discriminate differences in muSC number in response to injury and drug treatment, at 4 (Table. 3.2) and 8 dpf (Table. 3.3), respectively. In contrast, to determine muSC response following drug treatment in the absence of injury, 23 and 26 animals are needed, at 4 dpf (Table. 3.2) and 8 dpf (Table. 3.3), respectively. Injury results in large changes in the number of cells, and so, leads to high power (>99 %), whereas in the absence of injury, the low number of cells and high variability between animals leads to low power (4dpf: 39.2 %, 8dpf: 21.4 %). Therefore, it is hard to identify significant differences due to age and drug treatment between uninjured animals. Furthermore, increasing the number of animals to detect differences would increase the probability of a type I error (false positive), and so, has limited my ability to conduct investigations in the absence of injury.

Studies exploring changes to the proliferation of pax3-expressing muSCs with age in the horizontal and vertical myosepta identified significant changes using 8-9 animals (Nguyen *et al.*, 2017). Similarly, using 3-4 larvae, Roy *et al.,* (2017) identified a significant increase in the number of Pax7+ muSCs within vertical myosepta due to larvae age (Roy *et al.*, 2017). While pax3 reporter line and Pax7 antibody label many muSCs within vertical and horizontal myosepta, *pax7a* reporter line marks far fewer muSCs (~5 cells per structure). This small cell number within the myosepta, and high variability between animals drastically lowered the power. This has made it challenging to measure significant differences in the number of *pax7a*-expressing cells within the vertical and horizontal myosepta following injury or drug treatment.

Throughout my work I have shown that most *Tp1:H2BmCherry*-expressing nuclei are in myofibers within zebrafish muscle, which do not respond towards injury. This has made it challenging to make conclusions on the *Tp1:H2BmCherry*-cells which respond to injury. It is possible that, following quantification of all *Tp1:H2BmCherry*-expresing nuclei within the myotome, the large number of nuclei found within myofibers lowers the effect size between conditions and therefore power of analysis. This has

limited my ability to detect significant changes. To circumvent this, I also quantified *Tp1:H2BmCherry*-expressing nuclei at the site of injury to reduce the impact of quantifying *Tp1:H2BmCherry*-expressing myofibers.

Inflammatory microenvironment

I demonstrated that in the absence of macrophage, more muSCs respond towards an injury (Fig. 5.1). Moreover, skewing the inflammatory response towards an anti-inflammatory microenvironment following DEX treatment (Fig. 5.20) or, with the use of *tnfrsf1a* mutant fish (Fig. 5.22), I showed a similar increase in the number of muSCs. I also showed that the recruitment of macrophages towards muscle injury was reduced following Notch inhibition (Fig. 5.19). Therefore, my data implies that pro-inflammatory macrophages are important for limiting muSC proliferation.

Previous investigations measuring the immune response towards tail-fin amputation showed that pro-inflammatory macrophages (TNF-α+) migrate to the site of wounding, which subsequently switch to an anti-inflammatory state (TNF-α-; Nguyen-Chi *et al.*, 2015). Ratnayake *et al.,* (2021) demonstrated a similar paradigm, showing that transient macrophages migrate towards muscle injury in zebrafish, subsequently switching to a dwelling phenotype, expressing anti-inflammatory markers (*arg-1* and *mmp9*; Ratnayake *et al.*, 2021). Moreover, they found that following dwelling macrophage ablation at 1.75 dpi, *pax3*-expressing cells proliferate less (Ratnayake *et al.*, 2021). Contrastingly, I demonstrated that, by continuously ablating macrophage before and after injury, there are more Pax7-expressing muSCs following injury. As this increase in Pax7-expressing muSCs was also identified following DEX treatment and in *tnfrsf1a* mutant, I proposed that early pro-inflammatory macrophages are important for limiting muSC proliferation following injury. However, it remains unknown whether pro-inflammatory macrophages regulate muSCs to limit their proliferation. Therefore, using the TNF-α and NF-κβ reporter zebrafish, it would be possible to demonstrate the inflammatory state of macrophages following injury, assessing the effects of drug treatment (DAPT and DEX) or *tnfrsf1a* mutation.

Scaling of the injury-macrophage phenotype

Studies investigating blastema cell proliferation following tail-fin amputation revealed the importance of the type and size injury (Niethammer *et al.*, 2009; Miskolci *et al.*, 2019). These studies demonstrated that, both the type and size of injury modulate the recruitment and pro-inflammatory state of immune cells (Niethammer *et al.*, 2009; Miskolci *et al.*, 2019). They also found that a prolonged inflammatory response was associated with increased blastemal cell number (Miskolci *et al.*, 2019). Results from Ratnayake *et al.,* (2021) suggest that anti-inflammatory (dwelling) macrophages promote muSC proliferation (Ratnayake *et al.*, 2021), and my data suggest that pro-inflammatory macrophages limit muSC proliferation (Fig. 5.1, 5.20, 5.22). Moreover, I have shown how different injury sizes modify the muSC response to injury in the absence of macrophage (Fig. 5.3, 5.4). Following larger injuries, macrophages promote muSC expansion whereas following smaller injuries, macrophages limit muSC expansion. It has been shown in the *Drosophila* that the immune response is positively correlated with the injury size (Weavers *et al.*, 2016). It is possible that injury size skews the inflammatory response during muscle repair, affecting the proliferation of muSCs. To understand if the degree of inflammation affects the muSC response to injury, the Fms (macrophages) zebrafish reporter line could be used in conjunction with the TNF-α and NF-κβ zebrafish reporter lines. This would allow me to assess the inflammatory state of recruited macrophages to different injury sizes, investigating how this affects muSC proliferation.

The importance of Notch signalling

Although I demonstrated that Notch inhibition affects the number of proliferating (Fig. 3.9) and the proportion of differentiating (Fig. 3.10) muSCs following injury, I have not explored the activation state of muSCs. In zebrafish, pax3-expressing muSCs within the niche arrest at G2 (Nguyen *et al.*, 2017). Therefore, by assessing cyclin gene expression by qPCR (*ccna2, ccnb1, ccnb2, ccnd1,* and *ccne*), I predict that following Notch inhibition, muSCs within the myoseptum will upregulate cyclin gene expression. In contrast, I predict that following NICD over-expression, muSCs will downregulate cyclin gene expression.

Throughout my work I have shown that pax7- and *Tp1*-expressing muSC populations are largely independent, responding differently to Notch signalling (Fig. 4.10). Although I have shown that *Tp1*-expressing cells express Myog following injury (Fig. 5.12) and can therefore contribute to myogenesis, I have not examined if this novel *Tp1*-expressing population derived from Pax3, Myf5, c-met, or Meox1 population (Ruparelia *et al.*, 2020). I found that the proportion of *Tp1*+ cells expressing *pax7a* increased following injury, reminiscent of the mammalian *Twist2* interstitial cells (Liu *et al.*, 2017) and zebrafish c-met muSCs (Gurevich *et al.*, 2016). Therefore, it would be important to also understand if *Tp1:H2BmCherry* cells derived from an existing muSC population, such as the c-met population (Gurevich *et al.*, 2016), or the novel *Twist2*-expressing cell (Liu *et al.*, 2017) within the muscle myotome.

Macrophages control muSC behaviour via Notch signalling

I proposed that pro-inflammatory macrophages contribute to Notch activity in Pax7+ and *Tp1*+ cells via DeltaD, inducing a mechanism of lateral inhibition (Fig. 6.1). This mechanism of lateral inhibition between progenitor cells has been described in zebrafish spinal neuron differentiation (Hadjivasiliou *et al.*, 2019). Hadjivasiliou *et al.,* (2019) demonstrated that *Tp1*:VenusPEST-expressing spinal neurons extend Delta expressing processes to maintain quiescence in adjacent cells (Hadjivasiliou *et al.*, 2019). Although I have shown that macrophages express DeltaD, and macrophage ablation and DEX treatment leads to more Pax7+ and *Tp1*+ cells following injury, I have not directly demonstrated that macrophages regulate muSCs via DeltaD. I propose that macrophages regulate muSCs through DeltaD activation of Notch. Therefore, it would be important to examine first if macrophage ablation affects the activity of Notch in Pax7+ and *Tp1*+ cells. Following injury, quantifying the number of *Tp1:H2BmCherry*+ and *pax7a:eGFP*+ cells expressing the *Tp1*:VenusPEST transgene in the presence or absence of macrophages would demonstrate whether macrophage ablation affects Notch activity in Pax7+ and *Tp1*+ cells. It may also be possible to visualise *Tp1*:VenusPEST-expressing cells making contacts with adjacent cells, laterally inhibiting Notch activity and supressing *Tp1*:VenusPEST expression (as described by Hadjivasiliou *et al.*, 2019). Additionally, induction of constitutively active NICD by heat shock, following macrophage ablation, would demonstrate if

Notch activity is responsible for maintaining Pax7+ and *Tp1*+ cells in a quiescent state. I predict that following macrophage ablation, there will be more Pax7+ and *Tp1*+ cells which will be subsequently reduced following NICD over-expression.

To assess whether macrophages might interact and modulate muSC activity via Notch following injury, it would be crucial to manipulate macrophages to prevent them from activating Notch in muSCs. Mind bomb is important for the processing and expression of Notch ligands (reviewed by Guo *et al.*, 2016). Therefore, to specifically prevent macrophages-derived Notch signals, one could overexpress a dominant negative version of Mind bomb in Fms:Gal4-expressing macrophages. I predict that following expression of dominant negative version of Mind bomb in macrophages, more Pax7+ and *Tp1*+ cells would be present following injury, similarly to the observations made following macrophage ablation, DEX treatment and in *tnfrsf1a* mutants.

Chapter 7 Conclusion

I aimed to demonstrate 1) whether zebrafish muSCs are controlled by Notch signalling during homeostasis and regeneration, 2) how the inflammatory microenvironment controls the response of muSCs to injury, and 3) if macrophages control muSCs displaying Notch activity following injury. I found that, following muscle injury, *pax7a*-expressing muSC proliferation and differentiation is controlled by Notch signalling. Moreover, using the *Tp1*:VenusPEST reporter, I found that proliferating *pax7a*-expressing cells activate Notch. Together my data demonstrate a conserved role of Notch signalling in controlling both mammalian and zebrafish muSC proliferation and differentiation. Throughout my work, I also identified a novel *Tp1:H2BmCherry*-expressing population within zebrafish muscle. I noted that most of the *Tp1:H2BmCherry*-expressing nuclei are found in myofibers and do not respond to muscle injury. Contrastingly, *Tp1:H2BmCherry*-expressing cells respond to injury, which upregulate *pax7a* over time. Although these injury-responsive *Tp1*+ cells express Myog post-muscle damage, it is still unclear if these cells contribute to myofiber formation following injury. Moreover, the identity of these *Tp1*-expressing cells is still unknown; however, they show similarities to both, the c-met+ muSCs identified in zebrafish, and the *Twist2* interstitial cell identified in mouse (Gurevich *et al.*, 2016; Liu *et al.*, 2017). The c-met+ muSC asymmetrically divides generating a *c-met*^{low}*pax7*^{high} population and the *Twist2*+ interstitial cell downregulates *Twist2* and upregulates Pax7 following injury (Gurevich *et al.*, 2016; Liu *et al.*, 2017).

I found that macrophage ablation, DEX treatment and *tnfrsf1a* mutation resulted in more Pax7-expressing cells following injury. Macrophage ablation and DEX treatment also resulted in more *Tp1:H2BmCherry*-expressing cells. Therefore, my data suggest that the proliferation of both Pax7- and *Tp1*-expressing populations are limited by pro-inflammatory macrophages following injury. Exploring the role of macrophages in regulating pax3-expressing muSC proliferation, Ratnayake *et al.,* (2021) found that following large injuries, anti-inflammatory macrophages (dwelling) promote muSC proliferation. I demonstrated that the muSC response scales with injury, showing that following macrophages ablation, larger injuries resulted in fewer Pax7-expressing muSCs, whereas smaller injures resulted in more Pax7-expressing muSCs.

My data therefore suggests that the size of injury modulates the effect of macrophage ablation on muSC activity. I propose that the size of injury skews the immune response, which may modulate the proliferation muSC response following injury.

Together, my data show that *pax7a*-and *Tp1*-expressing cells are regulated by Notch activity. Moreover, as macrophages also express DeltaD, I propose that pro-inflammatory macrophages maintain Notch activity via DeltaD in both, Pax7+ and *Tp1*+ cells, following injury. This increased Notch activity promotes a mechanism of lateral inhibition between adjacent cells. Moreover, Notch signalling is still required to limit differentiation in injury responsive *pax7a*-expressing cells, promoting proliferation.

Zebrafish larvae have a remarkable ability to repair damaged tissue, completely regenerating muscle within 3 days (Gurevich *et al.*, 2016). In contrast, following exercise-induced injury in human, muscle repair takes approximately 4 weeks, associated with fibrosis (reviewed by Laumonier and Menetrey, 2016). My work has demonstrated for the first time that, following injury, Notch activity is important for promoting muSC proliferation in zebrafish. I have also shown that macrophages limit muSC proliferation, which I predict is facilitated by macrophage expressed DeltaD. Together, my data will help us understand how zebrafish larvae repair muscle so efficiently.

Chapter 8 Bibliography

Acharyya, S., Sharma, S.M., Cheng, A.S., Ladner, K.J., He, W., Kline, W., Wang, H., Ostrowski, M.C., Huang, T.H. and Guttridge, D.C. (2010) 'TNF inhibits notch-1 in skeletal muscle cells by Ezh2 and DNA methylation mediated repression: Implications in Duchenne muscular dystrophy', *PLoS ONE*, 5(8). doi:10.1371/journal.pone.0012479.

Akahori, H., Karmali, V., Polavarapu, R., Lyle, A.N., Weiss, D., Shin, E., Husain, A., Naqvi, N., Van Dam, R., Habib, A., Choi, C.U., King, A.L., Pachura, K., Taylor, W.R., Lefer, D.J. and Finn, A. V. (2015) 'CD163 interacts with TWEAK to regulate tissue regeneration after ischaemic injury', *Nature Communications*, 6. doi:10.1038/ncomms8792.

Alexander, R.M.N. (1969) 'The orientation of muscle fibres in the myomeres of fishes', *Journal of the Marine Biological Association of the United Kingdom*, 49(2), pp. 263–290. doi:10.1017/S0025315400035906.

Aoyama, H. and Asamoto, K. (1988) 'Determination of somite cells: Independence of cell differentiation and morphogenesis', *Development*, 104(1), pp. 15–28. doi:10.1242/dev.104.1.15.

Arnold, L., Henry, A., Poron, F., Baba-Amer, Y., Van Rooijen, N., Plonquet, A., Gherardi, R.K. and Chazaud, B. (2007) 'Inflammatory monocytes recruited after skeletal muscle injury switch into antiinflammatory macrophages to support myogenesis', *Journal of Experimental Medicine*, 204(5), pp. 1057–1069. doi:10.1084/jem.20070075.

Arnold, L., Perrin, H., De Chanville, C.B., Saclier, M., Hermand, P., Poupel, L., Guyon, E., Licata, F., Carpentier, W., Vilar, J., Mounier, R., Chazaud, B., Benhabiles, N., Boissonnas, A., Combadiere, B. and Combadiere, C. (2015) 'CX3CR1 deficiency promotes muscle repair and regeneration by enhancing macrophage ApoE production', *Nature Communications*, 6. doi:10.1038/ncomms9972.

Atit, R., Sgaier, S.K., Mohamed, O.A., Taketo, M.M., Dufort, D., Joyner, A.L., Niswander, L. and Conlon, R.A. (2006) 'B-Catenin Activation Is Necessary and Sufficient To Specify the Dorsal Dermal Fate in the Mouse', *Developmental Biology*, 296(1), pp. 164–176. doi:10.1016/j.ydbio.2006.04.449.

Aulehla, A. and Pourquié, O. (2006) 'On periodicity and directionality of somitogenesis', *Anatomy and Embryology*, 211(SUPPL. 1), pp. 3–8. doi:10.1007/s00429-006-0124-y.

Aulehla, A. and Pourquié, O. (2010) 'Signaling gradients during paraxial mesoderm development.', *Cold Spring Harbor perspectives in biology*, 2(2), pp. 1–17. doi:10.1101/cshperspect.a000869.

Aulehla, A., Wiegraebe, W., Baubet, V., Wahl, M.B., Deng, C., Taketo, M., Lewandoski, M. and Pourquié, O. (2008) 'A β-catenin gradient links the clock and wavefront systems in mouse embryo segmentation', *Nature Cell Biology*, 10(2), pp. 186–193. doi:10.1038/ncb1679.

Bae, H., Zmijewski, J.W., Deshane, J.S., Tadie, J., Chaplin, D.D., Takashima, S. and Abraham, E. (2011) 'AMP-activated protein kinase enhances the phagocytic ability of macrophages and neutrophils', *The FASEB Journal*, 25(12), pp. 4358–4368. doi:10.1096/fj.11-190587.

Baghdadi, M.B., Castel, D., Machado, L., Fukada, S.I., Birk, D.E., Relaix, F., Tajbakhsh, S. and Mourikis, P. (2018) 'Reciprocal signalling by Notch–Collagen V–CALCR retains muscle stem cells in their niche', *Nature* [Preprint]. doi:10.1038/s41586-018-0144-9.

Baghdadi, M.B., Firmino, J., Soni, K., Evano, B., Di Girolamo, D., Mourikis, P., Castel, D. and Tajbakhsh, S. (2018) 'Notch-Induced miR-708 Antagonizes Satellite Cell Migration and Maintains Quiescence', *Cell Stem Cell*, 23(6), pp. 859-868.e5. doi:10.1016/j.stem.2018.09.017.

Balla, K.M., Lugo-Villarino, G., Spitsbergen, J.M., Stachura, D.L., Hu, Y., Bañuelos, K., Romo-Fewell, O., Aroian, R. V. and Traver, D. (2010) 'Eosinophils in the zebrafish: Prospective isolation, characterization, and eosinophilia induction by helminth determinants', *Blood*, 116(19), pp. 3944–3954. doi:10.1182/blood-2010-03-267419.

Ballotta, V., Driessen-Mol, A., Bouten, C.V.C. and Baaijens, F.P.T. (2014) 'Strain-dependent modulation of macrophage polarization within scaffolds', *Biomaterials*, 35(18), pp. 4919–4928. doi:10.1016/j.biomaterials.2014.03.002.

Banerjee, A., Chitnis, U., Jadhav, S., Bhawalkar, J. and Chaudhury, S. (2009) 'Hypothesis testing, type I and type II errors', *Industrial Psychiatry Journal*, 18(2), p. 127. doi:10.4103/0972-6748.62274.

Barresi, M.J.F., D'Angelo, J.A., Hernández, L.P. and Devoto, S.H. (2001) 'Distinct mechanisms regulate slow-muscle development', *Current Biology*, 11(18), pp. 1432–1438. doi:10.1016/S0960-9822(01)00428-6.

Baxendale, S., Davison, C., Muxworthy, C., Wolff, C., Ingham, P.W. and Roy, S. (2004) 'The B-cell maturation factor Blimp-1 specifies vertebrate slow-twitch muscle fiber identity in response to Hedgehog signaling', *Nature Genetics*, 36(1), pp. 88–93. doi:10.1038/ng1280.

Belcastro, A.N., Arthur, G.D., Albisser, T.A. and Raj, D.A. (1996) 'Heart, liver, and skeletal muscle myeloperoxidase activity during exercise', *Journal of Applied Physiology*, 80(4), pp. 1331–1335. doi:10.1152/jappl.1996.80.4.1331.

Ben-Yair, R. and Kalcheim, C. (2005) 'Lineage analysis of the avian dermomyotome sheet reveals the existence of single cells with both dermal and muscle progenitor fates', *Development*, 132(4), pp. 689–701. doi:10.1242/dev.01617.

Benjamini, Y. and Hochberg, Y. (1995) 'Controlling the False Discovery Rate: A Practical and Powerful Approach to Multiple Testing', *Journal of the Royal Statistical Society: Series B (Methodological)* [Preprint]. doi:10.1111/j.2517-6161.1995.tb02031.x.

Bennett, C.M., Kanki, J.P., Rhodes, J., Liu, T.X., Paw, B.H., Kieran, M.W., Langenau, D.M., Delahaye-Brown, A., Zon, L.I., Fleming, M.D. and Thomas Look, A. (2001) 'Myelopoiesis in the zebrafish, Danio rerio', *Blood*, 98(3), pp. 643–651. doi:10.1182/blood.V98.3.643.

Bentzinger, C.F., Wang, Y.X., Dumont, N.A. and Rudnicki, M.A. (2013) 'Cellular dynamics in the muscle satellite cell niche', *EMBO Reports*, 14(12), pp. 1062–1072. doi:10.1038/embor.2013.182.

Bentzinger, C.F., Wang, Y.X., Von Maltzahn, J., Soleimani, V.D., Yin, H. and Rudnicki, M.A. (2013) 'Fibronectin regulates Wnt7a signaling and satellite cell expansion', *Cell Stem Cell*, 12(1), pp. 75–87. doi:10.1016/j.stem.2012.09.015.

Bentzinger, C.F., Wang, Y.X. and Rudnicki, M.A. (2012) 'Building muscle: molecular regulation of myogenesis.', *Cold Spring Harbor perspectives in biology*, 4(2). doi:10.1101/cshperspect.a008342.

Berberoglu, M.A., Gallagher, T.L., Morrow, Z.T., Talbot, J.C., Hromowyk, K.J., Tenente, I.M., Langenau, D.M. and Amacher, S.L. (2017) 'Satellite-like cells

contribute to pax7-dependent skeletal muscle repair in adult zebrafish', *Developmental Biology*, 424(2), pp. 162–180. doi:10.1016/j.ydbio.2017.03.004.
Bertrand, J.Y., Kim, A.D., Teng, S. and Traver, D. (2008) 'CD41+ cmyb+ precursors colonize the zebrafish pronephros by a novel migration route to initiate adult hematopoiesis', *Development*, 135(10), pp. 1853–1862. doi:10.1242/dev.015297.
Bi, P., Yue, F., Sato, Y., Wirbisky, S., Liu, W., Shan, T., Wen, Y., Zhou, D., Freeman, J. and Kuang, S. (2016) 'Stage-specific effects of Notch activation during skeletal myogenesis', *eLife*, 5, pp. 1–22. doi:10.7554/eLife.17355.
Birbrair, A., Zhang, T., Wang, Z.M., Messi, M.L., Mintz, A. and Delbono, O. (2013) 'Type-1 pericytes participate in fibrous tissue deposition in aged skeletal muscle', *American Journal of Physiology - Cell Physiology*, 305(11), pp. 1098–1113. doi:10.1152/ajpcell.00171.2013.
Bjornson, C.R.R., Cheung, T.H., Liu, L., Tripathi, P. V., Steeper, K.M. and Rando, T.A. (2012) 'Notch signaling is necessary to maintain quiescence in adult muscle stem cells', *Stem Cells*, 30(2), pp. 232–242. doi:10.1002/stem.773.
Bladt, F., Rlethmacher, D., Aguzzl, A. and Blrchmelert, C. (1995) 'Into the llmb bud', 376(August), pp. 768–771.
Bober, E., Franz, T., Arnold, H.H., Gruss, P. and Tremblay, P. (1994) 'Pax-3 is required for the development of limb muscles: A possible role for the migration of dermomyotomal muscle progenitor cells', *Development*, 120(3), pp. 603–612. doi:10.1242/dev.120.3.603.
Borello, U., Berarducci, B., Murphy, P., Bajard, L., Buffa, V., Piccolo, S., Buckingham, M. and Cossu, G. (2006) 'The Wnt/β-catenin pathway regulates Gli-mediated Myf5 expression during somitogenesis', *Development*, 133(18), pp. 3723–3732. doi:10.1242/dev.02517.
Borello, U., Buffa, V., Sonnino, C., Melchionna, R., Vivarelli, E. and Cossu, G. (1999) 'Differential expression of the Wnt putative receptors Frizzled during mouse somitogenesis', *Mechanisms of Development*, 89(1–2), pp. 173–177. doi:10.1016/S0925-4773(99)00205-1.
Borello, U., Coletta, M., Tajbakhsh, S., Leyns, L., De Robertis, E.M., Buckingham, M. and Cossu, G. (1999) 'Transplacental delivery of the Wnt antagonist Frzb1 inhibits development of caudal paraxial mesoderm and skeletal myogenesis in mouse

embryos', *Development*, 126(19), pp. 4247–4255. doi:10.1242/dev.126.19.4247.
Borycki, A.G., Mendham, L. and Emerson, C.P. (1998) 'Control of somite patterning by Sonic hedgehog and its downstream signal response genes', *Development*, 125(4), pp. 777–790. doi:10.1242/dev.125.4.777.
Brack, A.S., Conboy, I.M., Conboy, M.J., Shen, J. and Rando, T.A. (2008) 'A Temporal Switch from Notch to Wnt Signaling in Muscle Stem Cells Is Necessary for Normal Adult Myogenesis', *Cell Stem Cell*, 2(1), pp. 50–59. doi:10.1016/j.stem.2007.10.006.
Braun, T., Bober, E., Winter, B., Rosenthal, N. and Arnold, H.H. (1990) 'Myf-6, a new member of the human gene family of myogenic determination factors: Evidence for a gene cluster on chromosome 12', *EMBO Journal*, 9(3), pp. 821–831. doi:10.1002/j.1460-2075.1990.tb08179.x.
Braun, T., Buschhausen-Denker, G., Bober, E., Tannich, E. and Arnold, H.H. (1989) 'A novel human muscle factor related to but distinct from MyoD1 induces myogenic conversion in 10T1/2 fibroblasts', *EMBO Journal*, 8(3), pp. 701–709. doi:10.1002/j.1460-2075.1989.tb03429.x.
Braun, T., Rudnicki, M.A., Arnold, H.H. and Jaenisch, R. (1992) 'Targeted inactivation of the muscle regulatory gene Myf-5 results in abnormal rib development and perinatal death', *Cell*, 71(3), pp. 369–382. doi:10.1016/0092-8674(92)90507-9.
Bray, S.J. (2006) 'Notch signalling: A simple pathway becomes complex', *Nature Reviews Molecular Cell Biology*, 7(9), pp. 678–689. doi:10.1038/nrm2009.
Brennand, K., Huangfu, D. and Melton, D. (2007) 'All β cells contribute equally to islet growth and maintenance', *PLoS Biology*, 5(7), pp. 1520–1529. doi:10.1371/journal.pbio.0050163.
Brigitte, M., Schilte, C., Plonquet, A., Baba-Amer, Y., Henri, A., Charlier, C., Tajbakhsh, S., Albert, M., Gherardi, R.K. and Chrétien, F. (2010) 'Muscle resident macrophages control the immune cell reaction in a mouse model of notexin-induced myoinjury', *Arthritis and Rheumatism*, 62(1), pp. 268–279. doi:10.1002/art.27183.
Bröhl, D., Vasyutina, E., Czajkowski, M.T., Griger, J., Rassek, C., Rahn, H.P., Purfürst, B., Wende, H. and Birchmeier, C. (2012) 'Colonization of the Satellite Cell Niche by Skeletal Muscle Progenitor Cells Depends on Notch Signals', *Developmental Cell*, 23(3), pp. 469–481. doi:10.1016/j.devcel.2012.07.014.

Brunelli, S., Relaix, F., Baesso, S., Buckingham, M. and Cossu, G. (2007) 'Beta catenin-independent activation of MyoD in presomitic mesoderm requires PKC and depends on Pax3 transcriptional activity', *Developmental Biology*, 304(2), pp. 604–614. doi:10.1016/j.ydbio.2007.01.006.

Bryson-Richardson, R.J. and Currie, P.D. (2008) 'The genetics of vertebrate myogenesis', *Nature Reviews Genetics*, 9(8), pp. 632–646. doi:10.1038/nrg2369.

Buckingham, M., Bajard, L., Chang, T., Daubas, P., Hadchouel, J., Meilhac, S., Montarras, D., Rocancourt, D. and Relaix, F. (2003) 'The formation of skeletal muscle: From somite to limb', *Journal of Anatomy*, 202(1), pp. 59–68. doi:10.1046/j.1469-7580.2003.00139.x.

Buckingham, M. and Relaix, F. (2007) 'The role of Pax genes in the development of tissues and organs: Pax3 and Pax7 regulate muscle progenitor cell functions', *Annual Review of Cell and Developmental Biology*, 23, pp. 645–673. doi:10.1146/annurev.cellbio.23.090506.123438.

Bugeon, L., Taylor, H.B., Progatzky, F., Lin, M.I., Ellis, C.D., Welsh, N., Smith, E., Vargesson, N., Gray, C., Renshaw, S.A., Chico, T.J.A., Zon, L.I., Lamb, J. and Dallman, M.J. (2011) 'The NOTCH pathway contributes to cell fate decision in myelopoiesis', *Haematologica*, 96(12), pp. 1753–1760. doi:10.3324/haematol.2011.044115.

Burzyn, D., Kuswanto, W., Kolodin, D., Shadrach, J.L., Cerletti, M., Jang, Y., Sefik, E., Tan, T.G., Wagers, A.J., Benoist, C. and Mathis, D. (2013) 'XA Special Population of regulatory T Cells Potentiates muscle repair', *Cell*, 155(6), pp. 1282–1295. doi:10.1016/j.cell.2013.10.054.

Cantini, M., Giurisato, E., Radu, C., Tiozzo, S., Pampinella, F., Senigaglia, D., Zaniolo, G., Mazzoleni, F. and Vitiello, L. (2002) 'Macrophage-secreted myogenic factors: A promising tool for greatly enhancing the proliferative capacity of myoblasts in vitro and in vivo', *Neurological Sciences*, 23(4), pp. 189–194. doi:10.1007/s100720200060.

Cantini, M., Massimino, M.L., Bruson, A., Catani, C., Dallalibera, L. and Carraro, U. (1994) 'Macrophages regulate proliferation and differentiation of satellite cells', *Biochemical and Biophysical Research Communications*, pp. 1688–1696. doi:10.1006/bbrc.1994.2129.

Chal, J. and Pourquié, O. (2017) 'Making muscle: Skeletal myogenesis in vivo and in

vitro', *Development (Cambridge)*, 144(12), pp. 2104–2122. doi:10.1242/dev.151035.

Chazaud, B., Sonnet, C., Lafuste, P., Bassez, G., Rimaniol, A.C., Poron, F., Authier, F.J., Dreyfus, P.A. and Gherardi, R.K. (2003) 'Satellite cells attract monocytes and use macrophages as a support to escape apoptosis and enhance muscle growth', *Journal of Cell Biology*, 163(5), pp. 1133–1143. doi:10.1083/jcb.200212046.

Chen, A.E., Ginty, D.D. and Fan, C.M. (2005) 'Protein kinase A signalling via CREB controls myogenesis induced by Wnt proteins', *Nature*, 433(7023), pp. 317–322. doi:10.1038/nature03126.

Chen, A.T. and Zon, L.I. (2009) 'Zebrafish blood stem cells', *Journal of Cellular Biochemistry*, 108(1), pp. 35–42. doi:10.1002/jcb.22251.

Chen, J.F., Mandel, E.M., Thomson, J.M., Wu, Q., Callis, T.E., Hammond, S.M., Conlon, F.L. and Wang, D.Z. (2006) 'The role of microRNA-1 and microRNA-133 in skeletal muscle proliferation and differentiation', *Nature Genetics*, 38(2), pp. 228–233. doi:10.1038/ng1725.

Cheng, M., Nguyen, M.H., Fantuzzi, G. and Koh, T.J. (2008) 'Endogenous interferon-γ is required for efficient skeletal muscle regeneration', *American Journal of Physiology - Cell Physiology*, 294(5), pp. 1183–1191. doi:10.1152/ajpcell.00568.2007.

Cheung, T.H., Quach, N.L., Charville, G.W., Liu, L., Park, L., Edalati, A., Yoo, B., Hoang, P. and Rando, T.A. (2012) 'Maintenance of muscle stem-cell quiescence by microRNA-489', *Nature*, 482(7386), pp. 524–528. doi:10.1038/nature10834.

Chiang, C., Litingtung, Y., Lee, E., Youngt, K.E., Cordent, J.L., Westphal, H. and Beachyt, P.A. (1996) 'mice lacking Sonic hedgehog gene function', *Nature*, 383, pp. 407–413.

Chiristov, C., Chrétien, F., Abou-Khalil, R., Bassez, G., Vallet, G., Authier, F.J., Bassaglia, Y., Shinin, V., Tajbakhsh, S., Chazaud, B. and Gherardi, R.K. (2007) 'Muscle satellite cells and endothelial cells: Close neighbors and privileged partners', *Molecular Biology of the Cell* [Preprint]. doi:10.1091/mbc.E06-08-0693.

Christ, B., Brand-Saberi, B., Grim, M. and Wilting, J. (1992) 'Local signalling in dermomyotomal cell type specification', *Anatomy and Embryology*, 186(5), pp. 505–510. doi:10.1007/BF00185464.

Chung, P.C., Lin, W.S., Scotting, P.J., Hsieh, F.Y., Wu, H.L. and Cheng, Y.C. (2011) 'Zebrafish her8a is activated by su(h)-dependent notch signaling and is essential for the inhibition of neurogenesis', *PLoS ONE*, 6(4). doi:10.1371/journal.pone.0019394.

Clarkson, M., Taylor, J.F., McStay, E., Palmer, M.J., Clokie, B.G.J. and Migaud, H. (2021) 'A temperature shift during embryogenesis impacts prevalence of deformity in diploid and triploid Atlantic salmon (Salmo salar L.)', *Aquaculture Research*, 52(3), pp. 906–923. doi:10.1111/are.14945.

Cohen, J. (1988) 'Statistical power analysis for the social sciences (2nd ed.)', *Hillsdale NJ: Erlbaum.* [Preprint].

Collins, C.A., Olsen, I., Zammit, P.S., Heslop, L., Petrie, A., Partridge, T.A. and Morgan, J.E. (2005) 'Stem cell function, self-renewal, and behavioral heterogeneity of cells from the adult muscle satellite cell niche', *Cell*, 122(2), pp. 289–301. doi:10.1016/j.cell.2005.05.010.

Colucci-Guyon, E., Tinevez, J.Y., Renshaw, S.A. and Herbomel, P. (2011) 'Strategies of professional phagocytes in vivo: Unlike macrophages, neutrophils engulf only surface-associated microbes', *Journal of Cell Science*, 124(18), pp. 3053–3059. doi:10.1242/jcs.082792.

Conboy, I.M. and Rando, T.A. (2002) 'The regulation of Notch signaling controls satellite cell activation and cell fate determination in postnatal myogenesis', *Developmental Cell*, 3(3), pp. 397–409. doi:10.1016/S1534-5807(02)00254-X.

Conboy, M.J., Karasov, A.O. and Rando, T.A. (2007) 'High incidence of non-random template strand segregation and asymmetric fate determination in dividing stem cells and their progeny', *PLoS Biology*, 5(5), pp. 1120–1126. doi:10.1371/journal.pbio.0050102.

Conerly, M.L., Yao, Z., Zhong, J.W., Groudine, M. and Tapscott, S.J. (2016) 'Distinct Activities of Myf5 and MyoD Indicate Separate Roles in Skeletal Muscle Lineage Specification and Differentiation', *Developmental Cell*, 36(4), pp. 375–385. doi:10.1016/j.devcel.2016.01.021.

Contreras-Shannon, V., Ochoa, O., Reyes-Reyna, S.M., Sun, D., Michalek, J.E., Kuziel, W.A., McManus, L.M. and Shireman, P.K. (2007) 'Fat accumulation with altered inflammation and regeneration in skeletal muscle of CCR2-/- mice following ischemic injury', *American Journal of Physiology - Cell Physiology*, 292(2), pp. 953–

967. doi:10.1152/ajpcell.00154.2006.
Cordani, N., Pisa, V., Pozzi, L., Sciorati, C. and Clementi, E. (2014) 'Nitric oxide controls fat deposition in dystrophic skeletal muscle by regulating fibro-adipogenic precursor differentiation', *Stem Cells* [Preprint]. doi:10.1002/stem.1587.
Cornelison, D.D.W., Olwin, B.B., Rudnicki, M.A. and Wold, B.J. (2000) 'MyoD(-/-) satellite cells in single-fiber culture are differentiation defective and MRF4 deficient', *Developmental Biology*, 224(2), pp. 122–137. doi:10.1006/dbio.2000.9682.
Cossu, G., Kelly, R., Di Donna, S., Vivarelli, E. and Buckingham, M. (1995) 'Myoblast differentiation during mammalian somitogenesis is dependent upon a community effect', *Proceedings of the National Academy of Sciences of the United States of America*, 92(6), pp. 2254–2258. doi:10.1073/pnas.92.6.2254.
Crist, C.G., Montarras, D. and Buckingham, M. (2012) 'Muscle satellite cells are primed for myogenesis but maintain quiescence with sequestration of Myf5 mRNA targeted by microRNA-31 in mRNP granules', *Cell Stem Cell*, 11(1), pp. 118–126. doi:10.1016/j.stem.2012.03.011.
Cusella-De Angelis, M.G., Lyons, G., Sonnino, C., De Angelis, L., Vivarelli, E., Farmer, K., Wright, W.E., Molinaro, M., Bouché, M., Buckingham, M. and Cossu, G. (1992) 'MyoD, myogenin independent differentiation of primordial myoblasts in mouse somites', *Journal of Cell Biology*, 116(5), pp. 1243–1255. doi:10.1083/jcb.116.5.1243.
Da'as, S., Teh, E.M., Dobson, J.T., Nasrallah, G.K., McBride, E.R., Wang, H., Neuberg, D.S., Marshall, J.S., Lin, T.J. and Berman, J.N. (2011) 'Zebrafish mast cells possess an Fce{open}RI-like receptor and participate in innate and adaptive immune responses', *Developmental and Comparative Immunology*, 35(1), pp. 125–134. doi:10.1016/j.dci.2010.09.001.
Delfini, M.C., Hirsinger, E., Pourquie, O. and Duprez, D. (2000) 'Delta 1-activated Notch inhibits muscle differentation without affecting Myf5 and Pax3 expression in chick limb myogenesis', *Development*, 127(23), pp. 5213–5224.
Dellavalle, A., Sampaolesi, M., Tonlorenzi, R., Tagliafico, E., Sacchetti, B., Perani, L., Innocenzi, A., Galvez, B.G., Messina, G., Morosetti, R., Li, S., Belicchi, M., Peretti, G., Chamberlain, J.S., Wright, W.E., Torrente, Y., Ferrari, S., Bianco, P. and Cossu, G.

(2007) ‘Pericytes of human skeletal muscle are myogenic precursors distinct from satellite cells’, *Nature Cell Biology*, 9(3), pp. 255–267. doi:10.1038/ncb1542.
Denetclaw, W.F., Berdougo, E., Venters, S.J. and Ordahl, C.P. (2001) ‘Denetclaw e tal 2001 morphogenetic cell movements middle region dermomyo’, 1755, pp. 1745–1755.
Deng, B., Wehling-Henricks, M., Villalta, S.A., Wang, Y. and Tidball, J.G. (2012) ‘IL-10 Triggers Changes in Macrophage Phenotype That Promote Muscle Growth and Regeneration’, *The Journal of Immunology*, 189(7), pp. 3669–3680. doi:10.4049/jimmunol.1103180.
Derijk, R. and Sternberg, E.M. (1994) ‘Corticosteroid action and neuroendocrine-immune interactions’, *Annals of the New York Academy of Sciences*, 746, pp. 33–41. doi:10.1111/j.1749-6632.1994.tb39208.x.
Detrich, H.W., Kieran, M.W., Chan, F.Y., Barone, L.M., Yee, K., Rundstadler, J.A., Pratt, S., Ransom, D. and Zon, L.I. (1995) ‘Intraembryonic hematopoietic cell migration during vertebrate development’, *Proceedings of the National Academy of Sciences of the United States of America*, 92(23), pp. 10713–10717. doi:10.1073/pnas.92.23.10713.
Devoto, S.H., Melançon, E., Eisen, J.S. and Westerfield, M. (1996) ‘Identification of separate slow and fast muscle precursor cells in vivo, prior to somite formation’, *Development*, 122(11), pp. 3371–3380.
Dinno, A. (2015) ‘Nonparametric pairwise multiple comparisons in independent groups using Dunn’s test’, *Stata Journal*, 15(1), pp. 292–300. doi:10.1177/1536867x1501500117.
Dinno, A. (2017) ‘dunn.test: Dunn’s Test of Multiple Comparisons Using Rank Sums’, *R package version 1.3.5* [Preprint].
Dobson, J.T., Seibert, J., Teh, E.M., Da’as, S., Fraser, R.B., Paw, B.H., Lin, T.J. and Berman, J.N. (2008) ‘Carboxypeptidase A5 identifies a novel mast cell lineage in the zebrafish providing new insight into mast cell fate determination’, *Blood*, 112(7), pp. 2969–2972. doi:10.1182/blood-2008-03-145011.
Dort, J., Fabre, P., Molina, T. and Dumont, N.A. (2019) ‘Macrophages Are Key Regulators of Stem Cells during Skeletal Muscle Regeneration and Diseases’, *Stem Cells International*, 2019(Dmd), pp. 1–20. doi:10.1155/2019/4761427.

Du, H., Shih, C.H., Wosczyna, M.N., Mueller, A.A., Cho, J., Aggarwal, A., Rando, T.A. and Feldman, B.J. (2017) 'Macrophage-released ADAMTS1 promotes muscle stem cell activation', *Nature Communications*, 8(1). doi:10.1038/s41467-017-00522-7.

Dufaux, B. and Order, U. (1989) 'Complement activation after prolonged exercise', *Clinica Chimica Acta*, 179(1), pp. 45–49. doi:10.1016/0009-8981(89)90021-1.

Dumont, N., Bouchard, P. and Frenette, J. (2008) 'Neutrophil-induced skeletal muscle damage: A calculated and controlled response following hindlimb unloading and reloading', *American Journal of Physiology - Regulatory Integrative and Comparative Physiology*, 295(6), pp. 1831–1838. doi:10.1152/ajpregu.90318.2008.

Dumont, N. and Frenette, J. (2010) 'Macrophages protect against muscle atrophy and promote muscle recovery in vivo and in vitro: A mechanism partly dependent on the insulin-like growth factor-1 signaling molecule', *American Journal of Pathology*, 176(5), pp. 2228–2235. doi:10.2353/ajpath.2010.090884.

Dumont, N.A., Wang, Y.X. and Rudnicki, M.A. (2015) 'Intrinsic and extrinsic mechanisms regulating satellite cell function', *Development (Cambridge)*, 142(9), pp. 1572–1581. doi:10.1242/dev.114223.

Dunty, W.C., Biris, K.K., Chalamalasetty, R.B., Taketo, M.M., Lewandoski, M. and Yamaguchi, T.P. (2008) 'Wnt3a/β-catenin signaling controls posterior body development by coordinating mesoderm formation and segmentation', *Development*, 135(1), pp. 85–94. doi:10.1242/dev.009266.

Dyer, C., Linker, C., Graham, A. and Knight, R. (2014) 'Specification of sensory neurons occurs through diverse developmental programs functioning in the brain and spinal cord', *Developmental Dynamics* [Preprint]. doi:10.1002/dvdy.24184.

Eliceiri, B.P., Gonzalez, A.M. and Baird, A. (2011) 'Zebrafish model of the blood-brain barrier: morphological and permeability studies.', *Methods in molecular biology (Clifton, N.J.)* [Preprint]. doi:10.1007/978-1-60761-938-3_18.

Elks, P.M., Van Eeden, F.J., Dixon, G., Wang, X., Reyes-Aldasoro, C.C., Ingham, P.W., Whyte, M.K.B., Walmsley, S.R. and Renshaw, S.A. (2011) 'Activation of hypoxia-inducible factor-1α (hif-1α) delays inflammation resolution by reducing neutrophil apoptosis and reverse migration in a zebrafish inflammation model', *Blood*, 118(3), pp. 712–722. doi:10.1182/blood-2010-12-324186.

Ellett, F., Pase, L., Hayman, J.W., Andrianopoulos, A. and Lieschke, G.J. (2011)

'Mpeg1 Promoter Transgenes Direct Macrophage-Lineage Expression in Zebrafish', *Blood*, 117(4), pp. 49–56. doi:10.1182/blood-2010-10-314120.

Eom, D.S. and Parichy, D.M. (2017) 'A macrophage relay for long-distance signaling during postembryonic tissue remodeling', *Science* [Preprint]. doi:10.1126/science.aal2745.

Epstein, J.A., Shapiro, D.N., Cheng, J., Lam, P.Y.P. and Maas, R.L. (1996) 'Pax3 modulates expression of the c-met receptor during limb muscle development', *Proceedings of the National Academy of Sciences of the United States of America*, 93(9), pp. 4213–4218. doi:10.1073/pnas.93.9.4213.

Fan, C.M., Lee, C.S. and Tessier-Lavigne, M. (1997) 'A role for WNT proteins in induction of dermomyotome', *Developmental Biology*, 191(1), pp. 160–165. doi:10.1006/dbio.1997.8713.

Fan, C.M., Li, L., Rozo, M.E. and Lepper, C. (2012) 'Making skeletal muscle from progenitor and stem cells: Development versus regeneration', *Wiley Interdisciplinary Reviews: Developmental Biology*, 1(3), pp. 315–327. doi:10.1002/wdev.30.

Feng, X., Adiarte, E.G. and Devoto, S.H. (2006) 'Hedgehog acts directly on the zebrafish dermomyotome to promote myogenic differentiation', *Developmental Biology*, 300(2), pp. 736–746. doi:10.1016/j.ydbio.2006.08.056.

Feng, Y., Santoriello, C., Mione, M., Hurlstone, A. and Martin, P. (2010) 'Live imaging of innate immune cell sensing of transformed cells in zebrafish larvae: Parallels between tumor initiation and wound inflammation', *PLoS Biology*, 8(12). doi:10.1371/journal.pbio.1000562.

Fielding, R.A., Manfredi, T.J., Ding, W., Fiatarone, M.A., Evans, W.J. and Cannon, J.G. (1993) 'Acute phase response in exercise III. Neutrophil and IL-1β accumulation in skeletal muscle', *American Journal of Physiology - Regulatory Integrative and Comparative Physiology*, 265(1 34-1). doi:10.1152/ajpregu.1993.265.1.r166.

Finsterbusch, M., Hall, P., Li, A., Devi, S., Westhorpe, C.L.V., Kitching, A.R., Hickey, M.J. and Kubes, P. (2016) 'Patrolling monocytes promote intravascular neutrophil activation and glomerular injury in the acutely inflamed glomerulus', *Proceedings of the National Academy of Sciences of the United States of America*, 113(35), pp. E5172–E5181. doi:10.1073/pnas.1606253113.

Fong, A.P., Yao, Z., Zhong, J.W., Cao, Y., Ruzzo, W.L., Gentleman, R.C. and Tapscott, S.J. (2012) 'Genetic and Epigenetic Determinants of Neurogenesis and Myogenesis', *Developmental Cell*, 22(4), pp. 721–735. doi:10.1016/j.devcel.2012.01.015.

Fontenot, J.D., Gavin, M.A. and Rudensky, A.Y. (2017) 'Foxp3 programs the development and function of CD4+CD25+ regulatory T cells', *Journal of Immunology*, 198(3), pp. 986–992. doi:10.1038/ni904.

Frenette, J., Cai, B. and Tidball, J.G. (2000) 'Complement activation promotes muscle inflammation during modified muscle use', *American Journal of Pathology*, 156(6), pp. 2103–2110. doi:10.1016/S0002-9440(10)65081-X.

Fry, C.S., Kirby, T.J., Kosmac, K., McCarthy, J.J. and Peterson, C.A. (2017) 'Myogenic Progenitor Cells Control Extracellular Matrix Production by Fibroblasts during Skeletal Muscle Hypertrophy', *Cell Stem Cell*, 20(1), pp. 56–69. doi:10.1016/j.stem.2016.09.010.

Fu, X., Xiao, J., Wei, Y., Li, S., Liu, Y., Yin, J., Sun, K., Sun, H., Wang, Huating, Zhang, Z., Zhang, B.T., Sheng, C., Wang, Hongyan and Hu, P. (2015) 'Combination of inflammation-related cytokines promotes long-term muscle stem cell expansion', *Cell Research*, 25(6), pp. 655–673. doi:10.1038/cr.2015.58.

Fujimaki, S., Seko, D., Kitajima, Y., Yoshioka, K., Tsuchiya, Y., Masuda, S. and Ono, Y. (2018) 'Notch1 and Notch2 Coordinately Regulate Stem Cell Function in the Quiescent and Activated States of Muscle Satellite Cells', *Stem Cells*, 36(2), pp. 278–285. doi:10.1002/stem.2743.

Ganassi, M., Badodi, S., Wanders, K. and Zammit, P.S. (2020) 'Myogenin is an essential regulator of adult myofibre growth and muscle stem cell homeostasis', *eLife*, 9, pp. 1–23. doi:10.7554/eLife.60445.

Garcia-Concejo, A., Jimenez-Gonzalez, A. and Rodriguez, R.E. (2018) 'Opioid and Notch signaling pathways are reciprocally regulated through miR- 29a and miR-212 expression', *Biochimica et Biophysica Acta - General Subjects*, 1862(12), pp. 2605–2612. doi:10.1016/j.bbagen.2018.07.001.

Geling, A., Plessy, C., Rastegar, S., Strähle, U. and Bally-Cuif, L. (2004) 'Her5 acts as a prepattern factor that blocks neurogenin1 and coe2 expression upstream of Notch to inhibit neurogenesis at the midbrain-hindbrain boundary', *Development*, 131(9), pp. 1993–2006. doi:10.1242/dev.01093.

Geling, A., Steiner, H., Willem, M., Bally-Cuif, L. and Haass, C. (2002) 'A γ-secretase inhibitor blocks Notch signaling in vivo and causes a severe neurogenic phenotype in zebrafish', *EMBO Reports*, 3(7), pp. 688–694. doi:10.1093/embo-reports/kvf124.

George, R.M., Biressi, S., Beres, B.J., Rogers, E., Mulia, A.K., Allen, R.E., Rawls, A., Rando, T.A. and Wilson-Rawls, J. (2013) 'Numb-deficient satellite cells have regeneration and proliferation defects', *Proceedings of the National Academy of Sciences of the United States of America*, 110(46), pp. 18549–18555. doi:10.1073/pnas.1311628110.

Ginhoux, F. and Jung, S. (2014) 'Monocytes and macrophages: Developmental pathways and tissue homeostasis', *Nature Reviews Immunology*, 14(6), pp. 392–404. doi:10.1038/nri3671.

Giordani, J., Bajard, L., Demignon, J., Daubas, P., Buckingham, M. and Maire, P. (2007) 'Six proteins regulate the activation of Myf5 expression in embryonic mouse limbs', *Proceedings of the National Academy of Sciences of the United States of America*, 104(27), pp. 11310–11315. doi:10.1073/pnas.0611299104.

Giordani, L., He, G.J., Negroni, E., Sakai, H., Law, J.Y.C., Siu, M.M., Wan, R., Corneau, A., Tajbakhsh, S., Cheung, T.H. and Le Grand, F. (2019) 'High-Dimensional Single-Cell Cartography Reveals Novel Skeletal Muscle-Resident Cell Populations', *Molecular Cell*, 74(3), pp. 609-621.e6. doi:10.1016/j.molcel.2019.02.026.

Goel, A.J., Rieder, M.K., Arnold, H.H., Radice, G.L. and Krauss, R.S. (2017) 'Niche Cadherins Control the Quiescence-to-Activation Transition in Muscle Stem Cells', *Cell Reports*, 21(8), pp. 2236–2250. doi:10.1016/j.celrep.2017.10.102.

Goody, M.F., Kelly, M.W., Reynolds, C.J., Khalil, A., Crawford, B.D. and Henry, C.A. (2012) 'NAD+ Biosynthesis Ameliorates a Zebrafish Model of Muscular Dystrophy', *PLoS Biology*, 10(10). doi:10.1371/journal.pbio.1001409.

Gordon, J. and Galli, S. (1990) 'Mast Cells as a source of both preformed and immunologicallys inducible TNF-alpha/cachetin', *Nature*, 346(July), pp. 274–6.

Gorospe, J.R.M., Nishikawa, B.K. and Hoffman, E.P. (1996) 'Recruitment of mast cells to muscle after mild damage', *Journal of the Neurological Sciences*, 135(1), pp. 10–17. doi:10.1016/0022-510X(95)00255-Z.

Gray, C., Loynes, C.A., Whyte, M.K.B., Crossman, D.C., Renshaw, S.A. and Chico, T.J.A. (2011) 'Simultaneous intravital imaging of macrophage and neutrophil

behaviour during inflammation using a novel transgenic zebrafish', *Thrombosis and Haemostasis*, 105(5), pp. 811–819. doi:10.1160/TH10-08-0525.
Grifone, R., Demignon, J., Giordani, J., Niro, C., Souil, E., Bertin, F., Laclef, C., Xu, P.X. and Maire, P. (2007) 'Eya1 and Eya2 proteins are required for hypaxial somitic myogenesis in the mouse embryo', *Developmental Biology*, 302(2), pp. 602–616. doi:10.1016/j.ydbio.2006.08.059.
Grifone, R., Demignon, J., Houbron, C., Souil, E., Niro, C., Seller, M.J., Hamard, G. and Maire, P. (2005) 'Six1 and Six4 homeoproteins are required for Pax3 and Mrf expression during myogenesis in the mouse embryo', *Development*, 132(9), pp. 2235–2249. doi:10.1242/dev.01773.
Gros, J., Manceau, M., Thomé, V. and Marcelle, C. (2005) 'A common somitic origin for embryonic muscle progenitors and satellite cells', *Nature*, 435(7044), pp. 954–958. doi:10.1038/nature03572.
Grossman, S.R., Johannsen, E., Tong, X., Yalamanchili, R. and Kieff, E. (1994) 'The Epstein-Barr virus nuclear antigen 2 transactivator is directed to response elements by the Jκ recombination signal binding protein', *Proceedings of the National Academy of Sciences of the United States of America*, 91(16), pp. 7568–7572. doi:10.1073/pnas.91.16.7568.
Guo, B., McMillan, B.J. and Blacklow, S.C. (2016) 'Structure and function of the Mind bomb E3 ligase in the context of Notch signal transduction', *Current Opinion in Structural Biology* [Preprint]. doi:10.1016/j.sbi.2016.05.012.
Gupta, V.A., Kawahara, G., Myers, J.A., Chen, A.T., Hall, T.E., Manzini, M.C., Currie, P.D., Zhou, Y., Zon, L.I., Kunkel, L.M. and Beggs, A.H. (2012) 'A splice site mutation in Laminin-α2 results in a severe muscular dystrophy and growth abnormalities in Zebrafish', *PLoS ONE*, 7(8), pp. 1–9. doi:10.1371/journal.pone.0043794.
Gurevich, D.B., Nguyen, P.D., Siegel, A.L., Ehrlich, O. V., Sonntag, C., Phan, J.M.N., Berger, S., Ratnayake, D., Hersey, L., Berger, J., Verkade, H., Hall, T.E. and Currie, P.D. (2016) 'Asymmetric division of clonal muscle stem cells coordinates muscle regeneration in vivo', *Science*, 353(6295). doi:10.1126/science.aad9969.
Gurevich, D.B., Severn, C.E., Twomey, C., Greenhough, A., Cash, J., Toye, A.M., Mellor, H. and Martin, P. (2018) 'Live imaging of wound angiogenesis reveals macrophage orchestrated vessel sprouting and regression', *The EMBO Journal*,

37(13), pp. 1–23. doi:10.15252/embj.201797786.

Hadjivasiliou, Z., Moore, R.E., McIntosh, R., Galea, G.L., Clarke, J.D.W. and Alexandre, P. (2019) 'Basal Protrusions Mediate Spatiotemporal Patterns of Spinal Neuron Differentiation', *Developmental Cell*, 49(6), pp. 907-919.e10. doi:10.1016/j.devcel.2019.05.035.

Hall, T.E., Wood, A.J., Ehrlich, O., Li, M., Sonntag, C.S., Cole, N.J., Huttner, I.G., Sztal, T.E. and Currie, P.D. (2019) 'Cellular rescue in a zebrafish model of congenital muscular dystrophy type 1A', *npj Regenerative Medicine*, 4(1), pp. 1–13. doi:10.1038/s41536-019-0084-5.

Hamer, P.W., McGeachie, J.M., Davies, M.J. and Grounds, M.D. (2002) 'Evans Blue Dye as an in vivo marker of myofibre damage: Optimising parameters for detecting initial myofibre membrane permeability', *Journal of Anatomy*, 200(1), pp. 69–79. doi:10.1046/j.0021-8782.2001.00008.x.

Hamilton Outtz, H., Wu, J.K., Wang, X. and Kitajewski, J. (2010) 'Notch1 Deficiency Results in Decreased Inflammation during Wound Healing and Regulates Vascular Endothelial Growth Factor Receptor-1 and Inflammatory Cytokine Expression in Macrophages', *The Journal of Immunology*, 185(7), pp. 4363–4373. doi:10.4049/jimmunol.1000720.

Happ, M., Bathke, A.C. and Brunner, E. (2019) 'Optimal sample size planning for the Wilcoxon-Mann-Whitney test', *Statistics in Medicine*, 38(3), pp. 363–375. doi:10.1002/sim.7983.

Hasegawa, T., Hall, C.J., Crosier, P.S., Abe, G., Kawakami, K., Kudo, A. and Kawakami, A. (2017) 'Transient inflammatory response mediated by interleukin-1β is required for proper regeneration in zebrafish fin fold', *eLife*, 6, pp. 1–22. doi:10.7554/eLife.22716.

Hasegawa, T., Nakajima, T., Ishida, T., Kudo, A. and Kawakami, A. (2015) 'A diffusible signal derived from hematopoietic cells supports the survival and proliferation of regenerative cells during zebrafish fin fold regeneration', *Developmental Biology*, 399(1), pp. 80–90. doi:10.1016/j.ydbio.2014.12.015.

Hasty, P., Bradley, A., Morris, J.H., Edmondson, D.G., Venutit, J.M., Olson, E.N. and Kleln, W.H. (1993) 'Mice With a Targeted Mutation in the', *Nature*, 364, pp. 501–506.

He, Q., Zhang, C., Wang, L., Zhang, P., Ma, D., Lv, J. and Liu, F. (2015) 'Inflammatory signaling regulates hematopoietic stem and progenitor cell emergence in vertebrates', *Blood*, 125(7), pp. 1098–1106. doi:10.1182/blood-2014-09-601542.

Henkel, T., Ling, P.D., Hayward, S.D. and Peterson, M.G. (1994) 'Mediation of Epstein-Barr virus EBNA2 transactivation by recombination signal-binding protein Jκ', *Science*, 265(5168), pp. 92–95. doi:10.1126/science.8016657.

Henry, C.A. and Amacher, S.L. (2004) 'Zebrafish slow muscle cell migration induces a wave of fast muscle morphogenesis', *Developmental Cell*, 7(6), pp. 917–923. doi:10.1016/j.devcel.2004.09.017.

Herbomel, P., Thisse, B. and Thisse, C. (1999) 'Ontogeny and behaviour of early macrophages in the zebrafish embryo', *Development*, 126(17), pp. 3735–3745.

Herbomel, P., Thisse, B. and Thisse, C. (2001) 'Zebrafish early macrophages colonize cephalic mesenchyme and developing brain, retina, and epidermis through a M-CSF receptor-dependent invasive process', *Developmental Biology*, 238(2), pp. 274–288. doi:10.1006/dbio.2001.0393.

Heredia, J.E., Mukundan, L., Chen, F.M., Mueller, A.A., Deo, R.C., Locksley, R.M., Rando, T.A. and Chawla, A. (2013) 'Type 2 innate signals stimulate fibro/adipogenic progenitors to facilitate muscle regeneration', *Cell*, 153(2), pp. 376–388. doi:10.1016/j.cell.2013.02.053.

Hinits, Y. and Hughes, S.M. (2007) 'Mef2s are required for thick filament formation in nascent muscle fibres', *Development*, 134(13), pp. 2511–2519. doi:10.1242/dev.007088.

Hinits, Y., Osborn, D.P.S. and Hughes, S.M. (2009) 'Differential requirements for myogenic regulatory factors distinguish medial and lateral somitic, cranial and fin muscle fibre populations', *Development*, 136(3), pp. 403–414. doi:10.1242/dev.028019.

Hinits, Y., Williams, V.C., Sweetman, D., Donn, T.M., Ma, T.P., Moens, C.B. and Hughes, S.M. (2011) 'Defective cranial skeletal development, larval lethality and haploinsufficiency in Myod mutant zebrafish', *Developmental Biology*, 358(1), pp. 102–112. doi:10.1016/j.ydbio.2011.07.015.

Hirsinger, E., Duprez, D., Jouve, C., Malapert, P., Cooke, J. and Pourquié, O. (1997) 'Noggin acts downstream of Wnt and Sonic Hedgehog to antagonize BMP4 in avian

somite patterning', *Development*, 124(22), pp. 4605–4614. doi:10.1242/dev.124.22.4605.

Hirsinger, E., Malapert, P., Dubrulle, J., Delfini, M.C., Duprez, D., Henrique, D., Ish-Horowicz, D. and Pourquié, O. (2001) 'Notch signalling acts in postmitotic avian myogenic cells to control MyoD activation', *Development*, 128(1), pp. 107–116.

Hirsinger, E., Stellabotte, F., Devoto, S.H. and Westerfield, M. (2004) 'Hedgehog signaling is required for commitment but not initial induction of slow muscle precursors', *Developmental Biology*, 275(1), pp. 143–157. doi:10.1016/j.ydbio.2004.07.030.

Hofmann, M., Schuster-Gossler, K., Watabe-Rudolph, M., Aulehla, A., Herrmann, B.G. and Gossler, A. (2004) 'WNT signaling, in synergy with T/TBX6, controls Notch signaling by regulating Dll1 expression in the presomitic mesoderm of mouse embryos', *Genes and Development*, 18(22), pp. 2712–2717. doi:10.1101/gad.1248604.

Hollander, M., A. Wolfe, D. and Chicken, E. (2013) 'Wilcoxon', in *Nonparametric Statistical Methods*.

Hollway, G.E., Bryson-Richardson, R.J., Berger, S., Cole, N.J., Hall, T.E. and Currie, P.D. (2007) 'Whole-Somite Rotation Generates Muscle Progenitor Cell Compartments in the Developing Zebrafish Embryo', *Developmental Cell*, 12(2), pp. 207–219. doi:10.1016/j.devcel.2007.01.001.

Hutcheson, D.A., Zhao, J., Merrell, A., Haldar, M. and Kardon, G. (2009) 'Embryonic and fetal limb myogenic cells are derived from developmentally distinct progenitors and have different requirements for β-catenin', *Genes and Development*, 23(8), pp. 997–1013. doi:10.1101/gad.1769009.

Ikeya, M. and Takada, S. (1998) 'Wnt signaling from the dorsal neural tube is required for the formation of the medial dermomyotome', *Development*, 125(24), pp. 4969–4976. doi:10.1242/dev.125.24.4969.

Jaillon, O., Aury, J.M., Brunet, F., Petit, J.L., Stange-Thomann, N., Maucell, E., Bouneau, L., Fischer, C., Ozouf-Costaz, C., Bernot, A., Nicaud, S., Jaffe, D., Fisher, S., Lutfalla, G., Dossat, C., Segurens, B., Dasilva, C., Salanoubat, M., Levy, M., Houdet, N., Castellano, S., Anthouard, V., Jubin, C., Castelli, V., Katinka, M., Vacherie, B., Blémont, C., Skalli, Z., Cattolico, L., Poulain, J., De Berardinis, V., Cruaud, C., Dupart,

S., Brottler, P., Coutanceau, J.P., Gouzy, J., Parra, G., Lardier, G., Chapple, C., McKernan, K.J., McEwan, P., Bosak, S., Kellis, M., Volff, J.N., Gulgó, R., Zody, M.C., Mesirov, J., Lindblad-Toh, K., Birren, B., Nusbaum, C., Kahn, D., Robinson-Rechavi, M., Laudet, V., Schachter, V., Quétler, F., Saurin, W., Scarpeill, C., Wincker, P., Lander, E.S., Weissenbach, J. and Roest Crollius, H. (2004) 'Genome duplication in the teleost fish Tetraodon nigroviridis reveals the early vertebrate proto-karyotype', *Nature*, 431(7011), pp. 946–957. doi:10.1038/nature03025.

Jarriault S, Brou C, Logeat F, Schroeter Eh, Kopan R and Israel A (1995) 'Signalling downstream of activated mammalian Notch [see comments]', *Nature*, 377(6547), pp. 355–358.

Joe, A.W.B., Yi, L., Natarajan, A., Le Grand, F., So, L., Wang, J., Rudnicki, M.A. and Rossi, F.M.V. (2010) 'Muscle injury activates resident fibro/adipogenic progenitors that facilitate myogenesis', *Nature Cell Biology*, 12(2), pp. 153–163. doi:10.1038/ncb2015.

Johnson, R.L., Laufer, E., Riddle, R.D. and Tabin, C. (1994) 'Ectopic expression of Sonic hedgehog alters dorsal-ventral patterning of somites', *Cell*, 79(7), pp. 1165–1173. doi:10.1016/0092-8674(94)90008-6.

Johnston, I.A., Bower, N.I. and Macqueen, D.J. (2011) 'Growth and the regulation of myotomal muscle mass in teleost fish', *Journal of Experimental Biology*, 214(10), pp. 1617–1628. doi:10.1242/jeb.038620.

Johnston, I.A., Lee, H.T., Macqueen, D.J., Paranthaman, K., Kawashima, C., Anwar, A., Kinghorn, J.R. and Dalmay, T. (2009) 'Embryonic temperature affects muscle fibre recruitment in adult zebrafish: Genome-wide changes in gene and microRNA expression associated with the transition from hyperplastic to hypertrophic growth phenotypes', *Journal of Experimental Biology*, 212(12), pp. 1781–1793. doi:10.1242/jeb.029918.

Joshi, S., Singh, A.R., Zulcic, M., Bao, L., Messer, K., Ideker, T., Dutkowski, J. and Durden, D.L. (2014) 'Rac2 controls tumor growth, metastasis and M1-M2 macrophage differentiation in vivo', *PLoS ONE*, 9(4). doi:10.1371/journal.pone.0095893.

Jostes, B., Walther, C. and Gruss, P. (1990) 'The murine paired box gene, Pax7, is expressed specifically during the development of the nervous and muscular

system', *Mechanisms of Development*, 33(1), pp. 27–37. doi:10.1016/0925-4773(90)90132-6.

Juan, A.H., Derfoul, A., Feng, X., Ryall, J.G., Dell'Orso, S., Pasut, A., Zare, H., Simone, J.M., Rudnicki, M.A. and Sartorelli, V. (2011) 'Polycomb EZH2 controls self-renewal and safeguards the transcriptional identity of skeletal muscle stem cells', *Genes and Development*, 25(8), pp. 789–794. doi:10.1101/gad.2027911.

Kami, K. and Senba, E. (1998) 'Localization of leukemia inhibitory factor and interleukin-6 messenger ribonucleic acids in regenerating rat skeletal muscle', *Muscle and Nerve*, 21(6), pp. 819–822. doi:10.1002/(SICI)1097-4598(199806)21:6<819::AID-MUS20>3.0.CO;2-M.

Karlsson, J., Von Hofsten, J. and Olsson, P.E. (2001) 'Generating transparent zebrafish: A refined method to improve detection of gene expression during embryonic development', *Marine Biotechnology* [Preprint]. doi:10.1007/s1012601-0053-4.

Kassar-Duchossoy, L., Gayraud-Morel, B., Gomès, D., Rocancourt, D., Buckingham, M., Shinin, V. and Tajbakhsh, S. (2004) 'Mrf4 determines skeletal muscle identity in Myf5:Myod double-mutant mice', *Nature*, 431(7007), pp. 466–471. doi:10.1038/nature02876.

Kato, H., Taniguchi, Y., Kurooka, H., Minoguchi, S., Sakai, T., Nomura-Okazaki, S., Tamura, K. and Honjo, T. (1997) 'Involvement of RBP-J in biological functions of mouse Notch1 and its derivatives', *Development*, 124(20), pp. 4133–4141.

Kiefer, J.C. and Hauschka, S.D. (2001) 'Myf-5 is transiently expressed in nonmuscle mesoderm and exhibits dynamic regional changes within the presegmented mesoderm and somites I-IV', *Developmental Biology*, 232(1), pp. 77–90. doi:10.1006/dbio.2000.0114.

Kitamoto, T. and Hanaoka, K. (2010) 'Notch3 null mutation in mice causes muscle hyperplasia by repetitive muscle regeneration', *Stem Cells*, 28(12), pp. 2205–2216. doi:10.1002/stem.547.

Klos, A., Tenner, A.J., Johswich, K.O., Ager, R.R., Reis, E.S. and Köhl, J. (2009) 'The role of the anaphylatoxins in health and disease', *Molecular Immunology*, 46(14), pp. 2753–2766. doi:10.1016/j.molimm.2009.04.027.

Knappe, S., Zammit, P.S. and Knight, R.D. (2015) 'A population of Pax7-expressing

muscle progenitor cells show differential responses to muscle injury dependent on developmental stage and injury extent', *Frontiers in Aging Neuroscience*, 7(AUG), pp. 1–17. doi:10.3389/fnagi.2015.00161.

Kohyama, J., Tokunaga, A., Fujita, Y., Miyoshi, H., Nagai, T., Miyawaki, A., Nakao, K., Matsuzaki, Y. and Okano, H. (2005) 'Visualization of spatiotemporal activation of Notch signaling: Live monitoring and significance in neural development', *Developmental Biology*, 286(1), pp. 311–325. doi:10.1016/j.ydbio.2005.08.003.

Kondo, S. and Sauder, D.N. (1997) 'Tumor necrosis factor (TNF) receptor type 1 (p55) is a main mediator for TNF-α-induced skin inflammation', *European Journal of Immunology*, 27(7), pp. 1713–1718. doi:10.1002/eji.1830270718.

Kondoh, K., Sunadome, K. and Nishida, E. (2007) 'Notch signaling suppresses p38 MAPK activity via induction of MKP-1 in myogenesis', *Journal of Biological Chemistry*, 282(5), pp. 3058–3065. doi:10.1074/jbc.M607630200.

Kopan, R., Nye, J.S. and Weintraub, H. (1994) 'The intracellular domain of mouse Notch: A constitutively activated repressor of myogenesis directed at the basic helix-loop-helix region of MyoD', *Development*, 120(9), pp. 2385–2396. doi:10.1242/dev.120.9.2385.

Korthuis, R.J., Grisham, M.B. and Granger, D.N. (1988) 'Leukocyte depletion attenuates vascular injury in postischemic skeletal muscle', *American Journal of Physiology - Heart and Circulatory Physiology*, 254(5). doi:10.1152/ajpheart.1988.254.5.h823.

Kostallari, E., Baba-Amer, Y., Alonso-Martin, S., Ngoh, P., Relaix, F., Lafuste, P. and Gherardi, R.K. (2015) 'Pericytes in the myovascular niche promote post-natal myofiber growth and satellite cell quiescence', *Development (Cambridge)*, 142(7), pp. 1242–1253. doi:10.1242/dev.115386.

Kuang, S., Kuroda, K., Le Grand, F. and Rudnicki, M.A. (2007) 'Asymmetric Self-Renewal and Commitment of Satellite Stem Cells in Muscle', *Cell*, 129(5), pp. 999–1010. doi:10.1016/j.cell.2007.03.044.

Kuroda, K., Tani, S., Tamura, K., Minoguchi, S., Kurooka, H. and Honjo, T. (1999) 'Delta-induced Notch signaling mediated by RBP-J inhibits MyoD expression and myogenesis', *Journal of Biological Chemistry*, 274(11), pp. 7238–7244. doi:10.1074/jbc.274.11.7238.

Lachin, J.M. (1981) 'Introduction to sample size determination and power analysis for clinical trials', *Controlled Clinical Trials*, 2(2), pp. 93–113. doi:10.1016/0197-2456(81)90001-5.

Laclef, C., Hamard, G., Demignon, J., Souil, E., Houbron, C. and Maire, P. (2003) 'Altered myogenesis in Six1-deficient mice', *Development*, 130(10), pp. 2239–2252. doi:10.1242/dev.00440.

Lassar, A.B., Paterson, B.M. and Weintraub, H. (1986) 'Transfection of a DNA locus that mediates the conversion of 10T1 2 fibroblasts to myoblasts', *Cell*, 47(5), pp. 649–656. doi:10.1016/0092-8674(86)90507-6.

Latimer, A.J., Shin, J. and Appel, B. (2005) 'Her9 Promotes Floor Plate Development in Zebrafish', *Developmental Dynamics*, 232(4), pp. 1098–1104. doi:10.1002/dvdy.20264.

Latroche, C., Weiss-Gayet, M., Muller, L., Gitiaux, C., Leblanc, P., Liot, S., Ben-Larbi, S., Abou-Khalil, R., Verger, N., Bardot, P., Magnan, M., Chrétien, F., Mounier, R., Germain, S. and Chazaud, B. (2017) 'Coupling between Myogenesis and Angiogenesis during Skeletal Muscle Regeneration Is Stimulated by Restorative Macrophages', *Stem Cell Reports*, 9(6), pp. 2018–2033. doi:10.1016/j.stemcr.2017.10.027.

Laumonier, T. and Menetrey, J. (2016) 'Muscle injuries and strategies for improving their repair', *Journal of Experimental Orthopaedics*, 3(1). doi:10.1186/s40634-016-0051-7.

LeBert, D., Squirrell, J.M., Freisinger, C., Rindy, J., Golenberg, N., Frecentese, G., Gibson, A., Eliceiri, K.W. and Huttenlocher, A. (2018) 'Damage-induced reactive oxygen species regulate vimentin and dynamic collagen- based projections to mediate wound repair', *eLife*, 7, pp. 1–26. doi:10.7554/eLife.30703.

Van Leeuwen, J.L., Van Der Meulen, T., Schipper, H. and Kranenbarg, S. (2008) 'A functional analysis of myotomal muscle-fibre reorientation in developing zebrafish Danio rerio', *Journal of Experimental Biology*, 211(8), pp. 1289–1304. doi:10.1242/jeb.012336.

Lemos, D.R., Babaeijandaghi, F., Low, M., Chang, C.K., Lee, S.T., Fiore, D., Zhang, R.H., Natarajan, A., Nedospasov, S.A. and Rossi, F.M.V. (2015) 'Nilotinib reduces muscle fibrosis in chronic muscle injury by promoting TNF-mediated apoptosis of

fibro/adipogenic progenitors', *Nature Medicine*, 21(7), pp. 786–794. doi:10.1038/nm.3869.

Lepper, C., Conway, S.J. and Fan, C.M. (2009) 'Adult satellite cells and embryonic muscle progenitors have distinct genetic requirements', *Nature*, 460(7255), pp. 627–631. doi:10.1038/nature08209.

Lepper, C. and Fan, C.M. (2010) 'Inducible lineage tracing of Pax7-descendant cells reveals embryonic origin of adult satellite cells', *Genesis*, 48(7), pp. 424–436. doi:10.1002/dvg.20630.

Lepper, C., Partridge, T.A. and Fan, C.M. (2011) 'An absolute requirement for pax7-positive satellite cells in acute injury-induced skeletal muscle regeneration', *Development*, 138(17), pp. 3639–3646. doi:10.1242/dev.067595.

Lewis, F.C., Cottle, B.J., Shone, V., Marazzi, G., Sassoon, D., Tseng, C.C.S., Dankers, P.Y.W., Chamuleau, S.A.J., Nadal-Ginard, B. and Ellison-Hughes, G.M. (2017) 'Transplantation of Allogeneic PW1pos/Pax7neg Interstitial Cells Enhance Endogenous Repair of Injured Porcine Skeletal Muscle', *JACC: Basic to Translational Science*, 2(6), pp. 717–736. doi:10.1016/j.jacbts.2017.08.002.

Li, Y.P. (2003) 'TNF-α is a mitogen in skeletal muscle', *American Journal of Physiology - Cell Physiology*, 285(2 54-2), pp. 370–376. doi:10.1152/ajpcell.00453.2002.

Lieschke, G.J., Oates, A.C., Crowhurst, M.O., Ward, A.C. and Layton, J.E. (2001) 'Morphologic and functional characterization of granulocytes and macrophages in embryonic and adult zebrafish', *Blood*, 98(10), pp. 3087–3096. doi:10.1182/blood.V98.10.3087.

de Lima, J.E., Bonnin, M.A., Birchmeier, C. and Duprez, D. (2016) 'Muscle contraction is required to maintain the pool of muscle progenitors via yap and notch during fetal myogenesis', *eLife*, 5(AUGUST), pp. 1–25. doi:10.7554/eLife.15593.

Lin, Y., Zhao, J.L., Zheng, Q.J., Jiang, X., Tian, J., Liang, S.Q., Guo, H.W., Qin, H.Y., Liang, Y.M. and Han, H. (2018) 'Notch Signaling Modulates Macrophage Polarization and Phagocytosis Through Direct Suppression of Signal Regulatory Protein α Expression', *Frontiers in Immunology*, 9(July), pp. 1–12. doi:10.3389/fimmu.2018.01744.

Liu, N., Garry, G.A., Li, S., Bezprozvannaya, S., Sanchez-Ortiz, E., Chen, B., Shelton, J.M., Jaichander, P., Bassel-Duby, R. and Olson, E.N. (2017) 'A Twist2-dependent progenitor cell contributes to adult skeletal muscle', *Nature Cell Biology*, 19(3), pp. 202–213. doi:10.1038/ncb3477.

Lleras-Forero, L., Newham, E., Teufel, S., Kawakami, K., Hartmann, C., Hammond, C.L., Knight, R.D. and Schulte-Merker, S. (2020) 'Muscle defects due to perturbed somite segmentation contribute to late adult scoliosis', *Aging*, 12(18), pp. 18603–18621. doi:10.18632/aging.103856.

Londhe, P. and Davie, J.K. (2011) 'Gamma Interferon Modulates Myogenesis through the Major Histocompatibility Complex Class II Transactivator, CIITA', *Molecular and Cellular Biology*, 31(14), pp. 2854–2866. doi:10.1128/mcb.05397-11.

Londhe, P. and Davie, J.K. (2013) 'Interferon-γ resets muscle cell fate by stimulating the sequential recruitment of JARID2 and PRC2 to promoters to repress myogenesis', *Science Signaling*, 6(305), pp. 1–15. doi:10.1126/scisignal.2004633.

Low, S.H., Barnes, J.L., Zammit, P.S. and Beauchamp, J.R. (2018) 'Delta-Like 4 Activates Notch 3 to Regulate Self-Renewal in Skeletal Muscle Stem Cells', *Stem Cells*, 36(3), pp. 458–466. doi:10.1002/stem.2757.

Lu, H., Huang, D., Ransohoff, R.M. and Zhou, L. (2011) 'Acute skeletal muscle injury: CCL2 expression by both monocytes and injured muscle is required for repair', *The FASEB Journal*, 25(10), pp. 3344–3355. doi:10.1096/fj.10-178939.

Lu, H., Huang, D., Saederup, N., Charo, I.F., Ransohoff, R.M. and Zhou, L. (2011) ' Macrophages recruited via CCR2 produce insulin-like growth factor-1 to repair acute skeletal muscle injury ', *The FASEB Journal*, 25(1), pp. 358–369. doi:10.1096/fj.10-171579.

Lukjanenko, L., Karaz, S., Stuelsatz, P., Gurriaran-Rodriguez, U., Michaud, J., Dammone, G., Sizzano, F., Mashinchian, O., Ancel, S., Migliavacca, E., Liot, S., Jacot, G., Metairon, S., Raymond, F., Descombes, P., Palini, A., Chazaud, B., Rudnicki, M.A., Bentzinger, C.F. and Feige, J.N. (2019) 'Aging Disrupts Muscle Stem Cell Function by Impairing Matricellular WISP1 Secretion from Fibro-Adipogenic Progenitors', *Cell Stem Cell*, 24(3), pp. 433-446.e7. doi:10.1016/j.stem.2018.12.014.

Luo, D., Renault, V.M. and Rando, T.A. (2005) 'The regulation of Notch signaling in muscle stem cell activation and postnatal myogenesis', *Seminars in Cell and*

Developmental Biology, 16(4–5), pp. 612–622. doi:10.1016/j.semcdb.2005.07.002.
Luo, G., Hershko, D.D., Robb, B.W., Wray, C.J. and Hasselgren, P.O. (2003) 'IL-1β stimulates IL-6 production in cultured skeletal muscle cells through activation of MAP kinase signaling pathway and NF-κB', *American Journal of Physiology - Regulatory Integrative and Comparative Physiology*, 284(5 53-5), pp. 1249–1254. doi:10.1152/ajpregu.00490.2002.
Macqueen, D.J., Robb, D.H.F., Olsen, T., Melstveit, L., Paxton, C.G.M. and Johnston, I.A. (2008) 'Temperature until the "eyed stage" of embryogenesis programmes the growth trajectory and muscle phenotype of adult Atlantic salmon', *Biology Letters*, 4(3), pp. 294–298. doi:10.1098/rsbl.2007.0620.
Mahalwar, P., Walderich, B., Singh, A.P. and Volhard, C.N. (2014) 'Local reorganization of xanthophores fine-tunes and colors the striped pattern of zebrafish', *Science* [Preprint]. doi:10.1126/science.1254837.
Malecova, B., Gatto, S., Etxaniz, U., Passafaro, M., Cortez, A., Nicoletti, C., Giordani, L., Torcinaro, A., De Bardi, M., Bicciato, S., De Santa, F., Madaro, L. and Puri, P.L. (2018) 'Dynamics of cellular states of fibro-adipogenic progenitors during myogenesis and muscular dystrophy', *Nature Communications*, 9(1). doi:10.1038/s41467-018-06068-6.
Von Maltzahn, J., Jones, A.E., Parks, R.J. and Rudnicki, M.A. (2013) 'Pax7 is critical for the normal function of satellite cells in adult skeletal muscle', *Proceedings of the National Academy of Sciences of the United States of America*, 110(41), pp. 16474–16479. doi:10.1073/pnas.1307680110.
Manceau, M., Gros, J., Savage, K., Thomé, V., McPherron, A., Paterson, B. and Marcelle, C. (2008) 'Myostatin promotes the terminal differentiation of embryonic muscle progenitors', *Genes and Development*, 22(5), pp. 668–681. doi:10.1101/gad.454408.
Mantovani, A., Sica, A., Sozzani, S., Allavena, P., Vecchi, A. and Locati, M. (2004) 'The chemokine system in diverse forms of macrophage activation and polarization', *Trends in Immunology*, 25(12), pp. 677–686. doi:10.1016/j.it.2004.09.015.
Maroto, M., Bone, R.A. and Kim Dale, J. (2012) 'Somitogenesis', *Development (Cambridge)*, 139(14), pp. 2453–2456. doi:10.1242/dev.069310.

Marschallinger, J., Obermayer, A., Sänger, A.M., Stoiber, W. and Steinbacher, P. (2009) 'Postembryonic fast muscle growth of teleost fish depends upon a nonuniformly distributed population of mitotically active Pax7+ precursor cells', *Developmental Dynamics*, 238(9), pp. 2442–2448. doi:10.1002/dvdy.22049.

Martinez, C.O., McHale, M.J., Wells, J.T., Ochoa, O., Michalek, J.E., McManus, L.M. and Shireman, P.K. (2010) 'Regulation of skeletal muscle regeneration by CCR2-activating chemokines is directly related to macrophage recruitment', *American Journal of Physiology - Regulatory Integrative and Comparative Physiology*, 299(3), pp. 832–842. doi:10.1152/ajpregu.00797.2009.

Mathew, L.K., Sengupta, S., Kawakami, A., Andreasen, E.A., Löhr, C. V., Loynes, C.A., Renshaw, S.A., Peterson, R.T. and Tanguay, R.L. (2007) 'Unraveling tissue regeneration pathways using chemical genetics', *Journal of Biological Chemistry*, 282(48), pp. 35202–35210. doi:10.1074/jbc.M706640200.

Mathias, J.R., Perrin, B.J., Liu, T.-X., Kanki, J., Look, A.T. and Huttenlocher, A. (2006) 'Resolution of inflammation by retrograde chemotaxis of neutrophils in transgenic zebrafish', *Journal of Leukocyte Biology*, 80(6), pp. 1281–1288. doi:10.1189/jlb.0506346.

Mauro, A. (1961) 'Satellite cell of skeletal muscle fibers.', *The Journal of biophysical and biochemical cytology*, 9(2), pp. 493–495. doi:10.1083/jcb.9.2.493.

Maves, L., Waskiewicz, A.J., Paul, B., Cao, Y., Tyler, A., Moens, C.B. and Tapscott, S.J. (2007) 'Pbx homeodomain proteins direct Myod activity to promote fast-muscle differentiation', *Development*, 134(18), pp. 3371–3382. doi:10.1242/dev.003905.

McLennan, I.S. (1996) 'Degenerating and regenerating skeletal muscles contain several subpopulations of macrophages with distinct spatial and temporal distributions.', *Journal of anatomy*, 188 (Pt 1, pp. 17–28. Available at: http://www.ncbi.nlm.nih.gov/pubmed/8655404%0Ahttp://www.pubmedcentral.nih.gov/articlerender.fcgi?artid=PMC1167629.

McMahon, J.A., Takada, S., Zimmerman, L.B., Fan, C.M., Harland, R.M. and McMahon, A.P. (1998) 'Noggin-mediated antagonism of BMP signaling is required for growth and patterning of the neural tube and somite', *Genes and Development*, 12(10), pp. 1438–1452. doi:10.1101/gad.12.10.1438.

Megeney, L.A., Kablar, B., Garrett, K., Anderson, J.E. and Rudnicki, M.A. (1996)

'MyoD is required for myogenic stem cell function in adult skeletal muscle', *Genes and Development*, 10(10), pp. 1173–1183. doi:10.1101/gad.10.10.1173.
Melançon, E., Liu, D.W.C., Westerfield, M. and Eisen, J.S. (1997) 'Pathfinding by identified zebrafish motoneurons in the absence of muscle pioneers', *Journal of Neuroscience*, 17(20), pp. 7796–7804. doi:10.1523/jneurosci.17-20-07796.1997.
De Micheli, A.J., Laurilliard, E.J., Heinke, C.L., Ravichandran, H., Fraczek, P., Soueid-Baumgarten, S., De Vlaminck, I., Elemento, O. and Cosgrove, B.D. (2020) 'Single-Cell Analysis of the Muscle Stem Cell Hierarchy Identifies Heterotypic Communication Signals Involved in Skeletal Muscle Regeneration', *Cell Reports*, 30(10), pp. 3583-3595.e5. doi:10.1016/j.celrep.2020.02.067.
Minchin, J.E.N. and Hughes, S.M. (2008) 'Sequential actions of Pax3 and Pax7 drive xanthophore development in zebrafish neural crest', *Developmental Biology*, 317(2), pp. 508–522. doi:10.1016/j.ydbio.2008.02.058.
Miskolci, V., Squirrell, J., Rindy, J., Vincent, W., Sauer, J.D., Gibson, A., Eliceiri, K.W. and Huttenlocher, A. (2019) 'Distinct inflammatory and wound healing responses to complex caudal fin injuries of larval zebrafish', *eLife*, 8, pp. 1–18. doi:10.7554/eLife.45976.
Mitchell, K.J., Pannérec, A., Cadot, B., Parlakian, A., Besson, V., Gomes, E.R., Marazzi, G. and Sassoon, D.A. (2010) 'Identification and characterization of a non-satellite cell muscle resident progenitor during postnatal development', *Nature Cell Biology*, 12(3), pp. 257–266. doi:10.1038/ncb2025.
Molkentin, J.D., Black, B.L., Martin, J.F. and Olson, E.N. (1995) 'Cooperative activation of muscle gene expression by MEF2 and myogenic bHLH proteins', *Cell*, 83(7), pp. 1125–1136. doi:10.1016/0092-8674(95)90139-6.
Mollan, K.R., Trumble, I.M., Reifeis, S.A., Ferrer, O., Bay, C.P., Baldoni, P.L. and Hudgens, M.G. (2019) 'Exact power of the rank-sum test for a continuous variable', *arXiv*, pp. 1–15. Available at: http://arxiv.org/abs/1901.04597.
Montarras, D., Morgan, J., Colins, C., Relaix, F., Zaffran, S., Cumano, A., Partridge, T. and Buckingham, M. (2005) 'Developmental biology: Direct isolation of satellite cells for skeletal muscle regeneration', *Science*, 309(5743), pp. 2064–2067. doi:10.1126/science.1114758.
Morales, R.A. and Allende, M.L. (2019) 'Peripheral macrophages promote tissue

regeneration in zebrafish by fine-tuning the inflammatory response', *Frontiers in Immunology*, 10(FEB). doi:10.3389/fimmu.2019.00253.

Mori, R., Kondo, T., Ohshima, T., Ishida, Y. and Mukaida, N. (2002) 'Accelerated wound healing in tumor necrosis factor receptor p55-deficient mice with reduced leukocyte infiltration', *The FASEB Journal*, 16(9), pp. 963–974. doi:10.1096/fj.01-0776com.

Morris, A.C., Beresford, G.W., Mooney, M.R. and Boss, J.M. (2002) 'Kinetics of a Gamma Interferon Response: Expression and Assembly of CIITA Promoter IV and Inhibition by Methylation', *Molecular and Cellular Biology*, 22(13), pp. 4781–4791. doi:10.1128/mcb.22.13.4781-4791.2002.

Mounier, R., Théret, M., Arnold, L., Cuvellier, S., Bultot, L., Göransson, O., Sanz, N., Ferry, A., Sakamoto, K., Foretz, M., Viollet, B. and Chazaud, B. (2013) 'AMPKα1 regulates macrophage skewing at the time of resolution of inflammation during skeletal muscle regeneration', *Cell Metabolism*, 18(2), pp. 251–264. doi:10.1016/j.cmet.2013.06.017.

Mourikis, P., Gopalakrishnan, S., Sambasivan, R. and Tajbakhsh, S. (2012) 'Cell-autonomous notch activity maintains the temporal specification potential of skeletal muscle stem cells', *Development (Cambridge)*, 139(24), pp. 4536–4548. doi:10.1242/dev.084756.

Mourikis, P., Sambasivan, R., Castel, D., Rocheteau, P., Bizzarro, V. and Tajbakhsh, S. (2012) 'A critical requirement for notch signaling in maintenance of the quiescent skeletal muscle stem cell state', *Stem Cells*, 30(2), pp. 243–252. doi:10.1002/stem.775.

Mourikis, P. and Tajbakhsh, S. (2014) 'Distinct contextual roles for Notch signalling in skeletal muscle stem cells', *BMC Developmental Biology*, 14(1), pp. 1–8. doi:10.1186/1471-213X-14-2.

Muñoz-Cánoves, P., Scheele, C., Pedersen, B.K. and Serrano, A.L. (2013) 'Interleukin-6 myokine signaling in skeletal muscle: A double-edged sword?', *FEBS Journal*, 280(17), pp. 4131–4148. doi:10.1111/febs.12338.

Nathan, C. (2006) 'Neutrophils and immunity: Challenges and opportunities', *Nature Reviews Immunology*, 6(3), pp. 173–182. doi:10.1038/nri1785.

Nguyen-Chi, M., Laplace-Builhé, B., Travnickova, J., Luz-Crawford, P., Tejedor, G.,

Lutfalla, G., Kissa, K., Jorgensen, C. and Djouad, F. (2017) 'TNF signaling and macrophages govern fin regeneration in zebrafish larvae', *Cell death & disease*, 8(8), p. e2979. doi:10.1038/cddis.2017.374.

Nguyen-Chi, M., Laplace-Builhe, B., Travnickova, J., Luz-Crawford, P., Tejedor, G., Phan, Q.T., Duroux-Richard, I., Levraud, J.P., Kissa, K., Lutfalla, G., Jorgensen, C. and Djouad, F. (2015) 'Identification of polarized macrophage subsets in zebrafish', *eLife*, 4(JULY 2015), pp. 1–14. doi:10.7554/eLife.07288.

Nguyen, P.D., Gurevich, D.B., Sonntag, C., Hersey, L., Alaei, S., Nim, H.T., Siegel, A., Hall, T.E., Rossello, F.J., Boyd, S.E., Polo, J.M. and Currie, P.D. (2017) 'Muscle Stem Cells Undergo Extensive Clonal Drift during Tissue Growth via Meox1-Mediated Induction of G2 Cell-Cycle Arrest', *Cell Stem Cell*, 21(1), pp. 107-119.e6. doi:10.1016/j.stem.2017.06.003.

Niethammer, P., Grabher, C., Look, A.T. and Mitchison, T.J. (2009) 'A tissue-scale gradient of hydrogen peroxide mediates rapid wound detection in zebrafish', *Nature*, 459(7249), pp. 996–999. doi:10.1038/nature08119.

Ninov, N., Borius, M. and Stainier, D.Y.R. (2012) 'Different levels of Notch signaling regulate quiescence, renewal and differentiation in pancreatic endocrine progenitors', *Development*, 139(9), pp. 1557–1567. doi:10.1242/dev.076000.

Nord, H., Skalman, L.N. and Von Hofsten, J. (2013) 'Six1 regulates proliferation of Pax7-positive muscle progenitors in zebrafish', *Journal of Cell Science*, 126(8), pp. 1868–1880. doi:10.1242/jcs.119917.

Novoa, B. and Figueras, A. (2012) 'Zebrafish: Model for the Study of Inflammation and the Innate Immune Response to Infectious Diseases BT - Current Topics in Innate Immunity II', in Lambris, J.D. and Hajishengallis, G. (eds). New York, NY: Springer New York, pp. 253–275. doi:10.1007/978-1-4614-0106-3_15.

O'Neill, L.A.J. and Grahame Hardie, D. (2013) 'Metabolism of inflammation limited by AMPK and pseudo-starvation', *Nature*, 493(7432), pp. 346–355. doi:10.1038/nature11862.

Ogston, S.A., Lemeshow, S., Hosmer, D.W., Klar, J. and Lwanga, S.K. (1991) 'Adequacy of Sample Size in Health Studies.', *Biometrics*, 47(1), p. 347. doi:10.2307/2532527.

Olson, E.N. (1990) 'MyoD family: a paradigm for development?', *Genes and*

Development, 4(9), pp. 1454–1461. doi:10.1101/gad.4.9.1454.

Orso, S.D., Juan, A.H., Ko, K., Naz, F., Perovanovic, J., Gutierrez-cruz, G., Orso, S.D., Juan, A.H., Ko, K., Naz, F. and Perovanovic, J. (2019) 'Correction: Single cell analysis of adult mouse skeletal muscle stem cells in homeostatic and regenerative conditions (Development, (2019) 146, 12, 10.1242/dev.174177)', *Development (Cambridge)*, 146(13). doi:10.1242/dev.181743.

Osipo, C., Golde, T.E., Osborne, B.A. and Miele, L.A. (2008) 'Off the beaten pathway: The complex cross talk between Notch and NF-κB', *Laboratory Investigation*, 88(1), pp. 11–17. doi:10.1038/labinvest.3700700.

Ott, M.O., Bober, E., Lyons, G., Arnold, H. and Buckingham, M. (1991) 'Early expression of the myogenic regulatory gene, myf-5, in precursor cells of skeletal muscle in the mouse embryo', *Development*, 111(4), pp. 1097–1107. doi:10.1242/dev.111.4.1097.

Oustanina, S., Hause, G. and Braun, T. (2004) 'Pax7 directs postnatal renewal and propagation of myogenic satellite cells but not their specification', *EMBO Journal*, 23(16), pp. 3430–3439. doi:10.1038/sj.emboj.7600346.

Palacios, D., Mozzetta, C., Consalvi, S., Caretti, G., Saccone, V., Proserpio, V., Marquez, V.E., Valente, S., Mai, A., Forcales, S. V., Sartorelli, V. and Puri, P.L. (2010) 'TNF/p38α/polycomb signaling to Pax7 locus in satellite cells links inflammation to the epigenetic control of muscle regeneration', *Cell Stem Cell*, 7(4), pp. 455–469. doi:10.1016/j.stem.2010.08.013.

Palstra, A.P., Rovira, M., Rizo-Roca, D., Torrella, J.R., Spaink, H.P. and Planas, J. V. (2014) 'Swimming-induced exercise promotes hypertrophy and vascularization of fast skeletal muscle fibres and activation of myogenic and angiogenic transcriptional programs in adult zebrafish', *BMC Genomics*, 15(1), pp. 1–20. doi:10.1186/1471-2164-15-1136.

Parslow, A., Cardona, A. and Bryson-Richardson, R.J. (2014) 'Sample drift correction following 4D confocal time-lapse Imaging', *Journal of Visualized Experiments*, (86), pp. 1–4. doi:10.3791/51086.

Parsons, M.J., Pisharath, H., Yusuff, S., Moore, J.C., Siekmann, A.F., Lawson, N. and Leach, S.D. (2009) 'Notch-responsive cells initiate the secondary transition in larval zebrafish pancreas', *Mechanisms of Development*, 126(10), pp. 898–912.

doi:10.1016/j.mod.2009.07.002.
Pascoal, S., Esteves de Lima, J., Leslie, J.D., Hughes, S.M. and Saúde, L. (2013) 'Notch Signalling Is Required for the Formation of Structurally Stable Muscle Fibres in Zebrafish', *PLoS ONE*, 8(6), pp. 1–10. doi:10.1371/journal.pone.0068021.
Patsalos, A., Pap, A., Varga, T., Trencsenyi, G., Contreras, G.A., Garai, I., Papp, Z., Dezso, B., Pintye, E. and Nagy, L. (2017) 'In situ macrophage phenotypic transition is affected by altered cellular composition prior to acute sterile muscle injury', *Journal of Physiology*, 595(17), pp. 5815–5842. doi:10.1113/JP274361.
Pedersen, B.K. (2011) 'Exercise-induced myokines and their role in chronic diseases', *Brain, Behavior, and Immunity*, 25(5), pp. 811–816. doi:10.1016/j.bbi.2011.02.010.
Perdiguero, E., Ruiz-Bonilla, V., Gresh, L., Hui, L., Ballestar, E., Sousa-Victor, P., Baeza-Raja, B., Jardí, M., Bosch-Comas, A., Esteller, M., Caelles, C., Serrano, A.L., Wagner, E.F. and Mũoz-Cánoves, P. (2007) 'Genetic analysis of p38 MAP kinases in myogenesis: Fundamental role of p38α in abrogating myoblast proliferation', *EMBO Journal*, 26(5), pp. 1245–1256. doi:10.1038/sj.emboj.7601587.
Perdiguero, E., Sousa-Victor, P., Ruiz-Bonilla, V., Jardí, M., Caelles, C., Serrano, A.L. and Muñoz-Cánoves, P. (2011) 'p38/MKP-1-regulated AKT coordinates macrophage transitions and resolution of inflammation during tissue repair', *Journal of Cell Biology*, 195(2), pp. 307–322. doi:10.1083/jcb.201104053.
Picard, C.A. and Marcelle, C. (2013) 'Two distinct muscle progenitor populations coexist throughout amniote development', *Developmental Biology*, 373(1), pp. 141–148. doi:10.1016/j.ydbio.2012.10.018.
Pillon, N.J., Bilan, P.J., Fink, L.N. and Klip, A. (2013) 'Cross-talk between skeletal muscle and immune cells: Muscle-derived mediators and metabolic implications', *American Journal of Physiology - Endocrinology and Metabolism*, 304(5). doi:10.1152/ajpendo.00553.2012.
Pipalia, T.G., Koth, J., Roy, S.D., Hammond, C.L., Kawakami, K. and Hughes, S.M. (2016) 'Cellular dynamics of regeneration reveals role of two distinct Pax7 stem cell populations in larval zebrafish muscle repair', *DMM Disease Models and Mechanisms*, 9(6), pp. 671–684. doi:10.1242/dmm.022251.
Plotnikov, S. V., Millard, A.C., Campagnola, P.J. and Mohler, W.A. (2006)

'Characterization of the myosin-based source for second-harmonic generation from muscle sarcomeres', *Biophysical Journal*, 90(2), pp. 693–703. doi:10.1529/biophysj.105.071555.

Porpiglia, E., Samusik, N., Van Ho, A.T., Cosgrove, B.D., Mai, T., Davis, K.L., Jager, A., Nolan, G.P., Bendall, S.C., Fantl, W.J. and Blau, H.M. (2017) 'High-resolution myogenic lineage mapping by single-cell mass cytometry', *Nature Cell Biology*, 19(5), pp. 558–567. doi:10.1038/ncb3507.

Pourquié, O., Coltey, M., Bréant, C. and Le Douarin, N.M. (1995) 'Control of somite patterning by signals from the lateral plate', *Proceedings of the National Academy of Sciences of the United States of America*, 92(8), pp. 3219–3223. doi:10.1073/pnas.92.8.3219.

Pownall, M.E., Gustafsson, M.K. and Emerson, C.P. (2002) 'Myogenic regulatory factors and the specification of muscle progenitors in vertebrate embryos', *Annual Review of Cell and Developmental Biology*, 18, pp. 747–783. doi:10.1146/annurev.cellbio.18.012502.105758.

Radley, H.G. and Grounds, M.D. (2006) 'Cromolyn administration (to block mast cell degranulation) reduces necrosis of dystrophic muscle in mdx mice', *Neurobiology of Disease*, 23(2), pp. 387–397. doi:10.1016/j.nbd.2006.03.016.

Ratnayake, D., Nguyen, P.D., Rossello, F.J., Wimmer, V.C., Tan, J.L., Galvis, L.A., Julier, Z., Wood, A.J., Boudier, T., Isiaku, A.I., Berger, S., Oorschot, V., Sonntag, C., Rogers, K.L., Marcelle, C., Lieschke, G.J., Martino, M.M., Bakkers, J. and Currie, P.D. (2021) 'Macrophages provide a transient muscle stem cell niche via NAMPT secretion', *Nature*, 591(7849), pp. 281–287. doi:10.1038/s41586-021-03199-7.

Rayagiri, S.S., Ranaldi, D., Raven, A., Mohamad Azhar, N.I.F., Lefebvre, O., Zammit, P.S. and Borycki, A.G. (2018) 'Basal lamina remodeling at the skeletal muscle stem cell niche mediates stem cell self-renewal', *Nature Communications*, 9(1). doi:10.1038/s41467-018-03425-3.

Relaix, F., Bencze, M., Borok, M.J., Der Vartanian, A., Gattazzo, F., Mademtzoglou, D., Perez-Diaz, S., Prola, A., Reyes-Fernandez, P.C., Rotini, A. and Taglietti (2021) 'Perspectives on skeletal muscle stem cells', *Nature Communications*, 12(1), pp. 1–11. doi:10.1038/s41467-020-20760-6.

Relaix, F., Montarras, D., Zaffran, S., Gayraud-Morel, B., Rocancourt, D., Tajbakhsh,

S., Mansouri, A., Cumano, A. and Buckingham, M. (2006) 'Pax3 and Pax7 have distinct and overlapping functions in adult muscle progenitor cells', *Journal of Cell Biology*, 172(1), pp. 91–102. doi:10.1083/jcb.200508044.

Relaix, F., Rocancourt, D., Mansouri, A. and Buckingham, M. (2004) 'Divergent functions of murine Pax3 and Pax7 in limb muscle development', *Genes and Development*, 18(9), pp. 1088–1105. doi:10.1101/gad.301004.

Relaix, F., Rocancourt, D., Mansouri, A. and Buckingham, M. (2005) 'A Pax3/Pax7-dependent population of skeletal muscle progenitor cells', *Nature*, 435(7044), pp. 948–953. doi:10.1038/nature03594.

Renshaw, S.A., Loynes, C.A., Trushell, D.M.I., Elworthy, S., Ingham, P.W. and Whyte, M.K.B. (2006) 'Atransgenic zebrafish model of neutrophilic inflammation', *Blood*, 108(13), pp. 3976–3978. doi:10.1182/blood-2006-05-024075.

Renshaw, S.A. and Trede, N.S. (2012) 'A model 450 million years in the making: Zebrafish and vertebrate immunity', *DMM Disease Models and Mechanisms*, 5(1), pp. 38–47. doi:10.1242/dmm.007138.

Rhodes, J., Hagen, A., Hsu, K., Deng, M., Liu, T.X., Look, A.T. and Kanki, J.P. (2005) 'Interplay of pu.1 and Gata1 determines myelo-erythroid progenitor cell fate in zebrafish', *Developmental Cell*, 8(1), pp. 97–108. doi:10.1016/j.devcel.2004.11.014.

Rhodes, S.J. and Konieczny, S.F. (1989) 'Identification of MRF4: A new member of the muscle regulatory factor gene family', *Genes and Development*, 3(12 B), pp. 2050–2061. doi:10.1101/gad.3.12b.2050.

Rocheteau, P., Gayraud-Morel, B., Siegl-Cachedenier, I., Blasco, M.A. and Tajbakhsh, S. (2012) 'A subpopulation of adult skeletal muscle stem cells retains all template DNA strands after cell division', *Cell* [Preprint]. doi:10.1016/j.cell.2011.11.049.

Rodgers, J.T., King, K.Y., Brett, J.O., Cromie, M.J., Charville, G.W., Maguire, K.K., Brunson, C., Mastey, N., Liu, L., Tsai, C.R., Goodell, M.A. and Rando, T.A. (2014) 'MTORC1 controls the adaptive transition of quiescent stem cells from G 0 to GAlert', *Nature*, 510(7505), pp. 393–396. doi:10.1038/nature13255.

Rodgers, J.T., Schroeder, M.D., Ma, C. and Rando, T.A. (2017) 'HGFA Is an Injury-Regulated Systemic Factor that Induces the Transition of Stem Cells into GAlert', *Cell Reports*, 19(3), pp. 479–486. doi:10.1016/j.celrep.2017.03.066.

Rooney, J.E., Gurpur, P.B., Yablonka-Reuveni, Z. and Burkin, D.J. (2009) 'Laminin-111

restores regenerative capacity in a mouse model for α7 integrin congenital myopathy', *American Journal of Pathology*, 174(1), pp. 256–264. doi:10.2353/ajpath.2009.080522.

Rooney, J.E., Welser, J. V., Dechert, M.A., Flintoff-Dye, N.L., Kaufman, S.J. and Burkin, D.J. (2006) 'Severe muscular dystrophy in mice that lack dystrophin and α7 integrin', *Journal of Cell Science*, 119(11), pp. 2185–2195. doi:10.1242/jcs.02952.

Rossi, G. and Messina, G. (2014) 'Comparative myogenesis in teleosts and mammals', *Cellular and Molecular Life Sciences*, 71(16), pp. 3081–3099. doi:10.1007/s00018-014-1604-5.

Rowlerson, A., Radaelli, G., Mascarello, F. and Veggetti, A. (1997) 'Regeneration of skeletal muscle in two teleost fish: Sparus aurata and Brachydanio rerio', *Cell and Tissue Research*, 289(2), pp. 311–322. doi:10.1007/s004410050878.

Roy, S.D., Williams, V.C., Pipalia, T.G., Li, K., Hammond, C.L., Knappe, S., Knight, R.D. and Hughes, S.M. (2017) 'Myotome adaptability confers developmental robustness to somitic myogenesis in response to fibre number alteration', *Developmental Biology*, 431(2), pp. 321–335. doi:10.1016/j.ydbio.2017.08.029.

Rudnicki, M.A., Braun, T., Hinuma, S. and Jaenisch, R. (1992) 'Inactivation of MyoD in mice leads to up-regulation of the myogenic HLH gene Myf-5 and results in apparently normal muscle development', *Cell*, 71(3), pp. 383–390. doi:10.1016/0092-8674(92)90508-A.

Rudnicki, M.A., Schnegelsberg, P.N.J., Stead, R.H., Braun, T., Arnold, H.H. and Jaenisch, R. (1993) 'MyoD or Myf-5 is required for the formation of skeletal muscle', *Cell*, 75(7), pp. 1351–1359. doi:10.1016/0092-8674(93)90621-V.

Ruparelia, A.A., Ratnayake, D. and Currie, P.D. (2020) 'Stem cells in skeletal muscle growth and regeneration in amniotes and teleosts: Emerging themes', *Wiley Interdisciplinary Reviews: Developmental Biology*, 9(2), pp. 1–20. doi:10.1002/wdev.365.

Sacco, A., Doyonnas, R., Kraft, P., Vitorovic, S. and Blau, H.M. (2008) 'Self-renewal and expansion of single transplanted muscle stem cells', *Nature*, 456(7221), pp. 502–506. doi:10.1038/nature07384.

Saclier, M., Cuvellier, S., Magnan, M., Mounier, R. and Chazaud, B. (2013) 'Monocyte/macrophage interactions with myogenic precursor cells during skeletal

muscle regeneration', *FEBS Journal*, 280(17), pp. 4118–4130. doi:10.1111/febs.12166.

Saclier, M., Yacoub-Youssef, H., Mackey, A.L., Arnold, L., Ardjoune, H., Magnan, M., Sailhan, F., Chelly, J., Pavlath, G.K., Mounier, R., Kjaer, M. and Chazaud, B. (2013) 'Differentially activated macrophages orchestrate myogenic precursor cell fate during human skeletal muscle regeneration', *Stem Cells*, 31(2), pp. 384–396. doi:10.1002/stem.1288.

Sambasivan, R., Yao, R., Kissenpfennig, A., Wittenberghe, L. Van, Paldi, A., Gayraud-morel, B., Guenou, H., Malissen, B., Tajbakhsh, S., Galy, A., Sambasivan, R., Yao, R., Kissenpfennig, A. and Wittenberghe, L. Van (2011) 'Erratum to Pax7-expressing satellite cells are indispensable for adult skeletal muscle regeneration (Development (2011), 138 (3647-3656))', *Development*, 138(19), p. 4333. doi:10.1242/dev.073601.

Sanderson, L.E., Chien, A.T., Astin, J.W., Crosier, K.E., Crosier, P.S. and Hall, C.J. (2015) 'An inducible transgene reports activation of macrophages in live zebrafish larvae', *Developmental and Comparative Immunology*, 53(1), pp. 63–69. doi:10.1016/j.dci.2015.06.013.

Sassoon, D., Lyons, G., Wright, W.E., Lin, V., Lassar, A., Weintraub, H. and Buckingham, M. (1989) 'Expression of two myogenic regulatory factors myogenin and MyoDl during mouse embryogenesis', *Nature*, 341(6240), pp. 303–307. doi:10.1038/341303a0.

Scapini, P., Lapinet-Vera, J.A., Gasperini, S., Calzetti, F., Bazzoni, F. and Cassatella, M.A. (2000) 'The neutrophil as a cellular source of chemokines', *Immunological Reviews*, 177(4), pp. 195–203. doi:10.1034/j.1600-065X.2000.17706.x.

Scheer, N., Groth, A., Hans, S. and Campos-Ortega, J.A. (2001) 'An instructive function for Notch in promoting gliogenesis in the zebrafish retina', *Development* [Preprint]. doi:10.1242/dev.128.7.1099.

Schienda, J., Engleka, K.A., Jun, S., Hansen, M.S., Epstein, J.A., Tabin, C.J., Kunkel, L.M. and Kardon, G. (2006) 'Somitic origin of limb muscle satellite and side population cells', *Proceedings of the National Academy of Sciences of the United States of America*, 103(4), pp. 945–950. doi:10.1073/pnas.0510164103.

Schindelin, J., Arganda-Carreras, I., Frise, E., Kaynig, V., Longair, M., Pietzsch, T.,

Preibisch, S., Rueden, C., Saalfeld, S., Schmid, B., Tinevez, J.Y., White, D.J., Hartenstein, V., Eliceiri, K., Tomancak, P. and Cardona, A. (2012) 'Fiji: An open-source platform for biological-image analysis', *Nature Methods*, 9(7), pp. 676–682. doi:10.1038/nmeth.2019.

Schmidt, M., Schüler, S.C., Hüttner, S.S., von Eyss, B. and von Maltzahn, J. (2019) 'Adult stem cells at work: regenerating skeletal muscle', *Cellular and Molecular Life Sciences*, 76(13), pp. 2559–2570. doi:10.1007/s00018-019-03093-6.

Schultz, E. (1996) 'Satellite cell proliferative compartments in growing skeletal muscles', *Developmental Biology*, 175(1), pp. 84–94. doi:10.1006/dbio.1996.0097.

Schuster-Gossler, K., Cordes, R. and Gossler, A. (2007) 'Premature myogenic differentiation and depletion of progenitor cells cause severe muscle hypotrophy in Delta1 mutants', *Proceedings of the National Academy of Sciences of the United States of America*, 104(2), pp. 537–542. doi:10.1073/pnas.0608281104.

Seale, P., Sabourin, L.A., Girgis-Gabardo, A., Mansouri, A., Gruss, P. and Rudnicki, M.A. (2000) 'Pax7 is required for the specification of myogenic satellite cells', *Cell*, 102(6), pp. 777–786. doi:10.1016/S0092-8674(00)00066-0.

Segawa, M., Fukada, S. ichiro, Yamamoto, Y., Yahagi, H., Kanematsu, M., Sato, M., Ito, T., Uezumi, A., Hayashi, S., Miyagoe-Suzuki, Y., Takeda, S., Tsujikawa, K. and Yamamoto, H. (2008) 'Suppression of macrophage functions impairs skeletal muscle regeneration with severe fibrosis', *Experimental Cell Research*, 314(17), pp. 3232–3244. doi:10.1016/j.yexcr.2008.08.008.

Seger, C., Hargrave, M., Wang, X., Chai, R.J., Elworthy, S. and Ingham, P.W. (2011) 'Analysis of Pax7 expressing myogenic cells in zebrafish muscle development, injury, and models of disease', *Developmental Dynamics*, 240(11), pp. 2440–2451. doi:10.1002/dvdy.22745.

Seo, H.C., Sætre, B.O., Håvik, B., Ellingsen, S. and Fjose, A. (1998) 'The zebrafish Pax3 and Pax7 homologues are highly conserved, encode multiple isoforms and show dynamic segment-like expression in the developing brain', *Mechanisms of Development*, 70(1–2), pp. 49–63. doi:10.1016/S0925-4773(97)00175-5.

Sharif, F., Steenbergen, P.J., Metz, J.R. and Champagne, D.L. (2015) 'Long-lasting effects of dexamethasone on immune cells and wound healing in the zebrafish', *Wound Repair and Regeneration*, 23(6), pp. 855–865. doi:10.1111/wrr.12366.

Sharma, P., Saraswathy, V.M., Xiang, L. and Fürthauer, M. (2019) 'Notch-mediated inhibition of neurogenesis is required for zebrafish spinal cord morphogenesis', *Scientific Reports*, 9(1), pp. 1–18. doi:10.1038/s41598-019-46067-1.

Shieh, G., Jan, S.L. and Randles, R.H. (2006) 'On power and sample size determinations for the Wilcoxon-Mann-Whitney test', *Journal of Nonparametric Statistics*, 18(1), pp. 33–43. doi:10.1080/10485250500473099.

Shinin, V., Gayraud-Morel, B., Gomès, D. and Tajbakhsh, S. (2006) 'Asymmetric division and cosegregation of template DNA strands in adult muscle satellite cells', *Nature Cell Biology*, 8(7), pp. 677–682. doi:10.1038/ncb1425.

Smith, S.J., Horstick, E.J., Davidson, A.E. and Dowling, J. (2015) 'Analysis of zebrafish larvae skeletal muscle integrity with evans blue dye', *Journal of Visualized Experiments*, 2015(105), pp. 2–7. doi:10.3791/53183.

Snider, D.R. and Clegg, E.D. (1975) 'Alteration of phospholipids in porcine spermatozoa during in vivo uterus and oviduct incubation.', *Journal of animal science*, 40(2), pp. 269–274. doi:10.2527/jas1975.402269x.

Stainier, D.Y.R., Weinstein, B.M., Iii, H.W.D., Zon, L.I. and Fishman, M.C. (1995) 'Stainier et all 1995 Cloche an early acting ZF gene is reqd by both endothelial and hematopoietic lineages', 3150, pp. 3141–3150.

Stellabotte, F., Dobbs-McAuliffe, B., Fernández, D.A., Feng, X. and Devoto, S.H. (2007) 'Dynamic somite cell rearrangements lead to distinct waves of myotome growth', *Development*, 134(7), pp. 1253–1257. doi:10.1242/dev.000067.

Sun, D., Martinez, C.O., Ochoa, O., Ruiz-Willhite, L., Bonilla, J.R., Centonze, V.E., Waite, L.L., Michalek, J.E., McManus, L.M. and Shireman, P.K. (2009) 'Bone marrow-derived cell regulation of skeletal muscle regeneration', *Faseb J*, 23(2), pp. 382–395. doi:10.1096/fj.07-095901.

Tajbakhsh, S., Borello, U., Vivarelli, E., Kelly, R., Papkoff, J., Duprez, D., Buckingham, M. and Cossu, G. (1998) 'Differential activation of Myf5 and MyoD by different Wnts in explants of mouse paraxial mesoderm and the later activation of myogenesis in the absence of Myf5', *Development*, 125(21), pp. 4155–4162. doi:10.1242/dev.125.21.4155.

Tajbakhsh, S., Rocancourt, D., Cossu, G. and Buckingham, M. (1997) 'Redefining the genetic hierarchies controlling skeletal myogenesis: Pax- 3 and Myf-5 act upstream

of MyoD', *Cell*, 89(1), pp. 127–138. doi:10.1016/S0092-8674(00)80189-0.
Thayer, M.J., Tapscott, S.J., Davis, R.L., Wright, W.E., Lassar, A.B. and Weintraub, H. (1989) 'Positive autoregulation of the myogenic determination gene MyoD1', *Cell*, 58(2), pp. 241–248. doi:10.1016/0092-8674(89)90838-6.
Thornton, C.S. (1949) 'Beryllium inhibition of regeneration. I. Morphological effects of beryllium on amputated fore limbs of larval Amblystoma', *Journal of Morphology* [Preprint]. doi:10.1002/jmor.1050840305.
Tidball, J.G. (2017) 'Regulation of muscle growth and regeneration by the immune system', *Nature Reviews Immunology*, 17(3), pp. 165–178. doi:10.1038/nri.2016.150.
Tidball, J.G. and Wehling-Henricks, M. (2007) 'Macrophages promote muscle membrane repair and muscle fibre growth and regeneration during modified muscle loading in mice in vivo', *Journal of Physiology*, 578(1), pp. 327–336. doi:10.1113/jphysiol.2006.118265.
Troy, A., Cadwallader, A.B., Fedorov, Y., Tyner, K., Tanaka, K.K. and Olwin, B.B. (2012) 'Coordination of satellite cell activation and self-renewal by par-complex-dependent asymmetric activation of p38α/β MAPK', *Cell Stem Cell*, 11(4), pp. 541–553. doi:10.1016/j.stem.2012.05.025.
Vainshtein, A. and Sandri, M. (2020) 'Signaling pathways that control muscle mass', *International Journal of Molecular Sciences*, 21(13), pp. 1–32. doi:10.3390/ijms21134759.
Varga, T., Mounier, R., Horvath, A., Cuvellier, S., Dumont, F., Poliska, S., Ardjoune, H., Juban, G., Nagy, L. and Chazaud, B. (2016) 'Highly Dynamic Transcriptional Signature of Distinct Macrophage Subsets during Sterile Inflammation, Resolution, and Tissue Repair', *The Journal of Immunology*, 196(11), pp. 4771–4782. doi:10.4049/jimmunol.1502490.
Der Vartanian, A., Quétin, M., Michineau, S., Auradé, F., Hayashi, S., Dubois, C., Rocancourt, D., Drayton-Libotte, B., Szegedi, A., Buckingham, M., Conway, S.J., Gervais, M. and Relaix, F. (2019) 'PAX3 Confers Functional Heterogeneity in Skeletal Muscle Stem Cell Responses to Environmental Stress', *Cell Stem Cell* [Preprint]. doi:10.1016/j.stem.2019.03.019.
Vasyutina, E. and Birchmeier, C. (2006) 'The development of migrating muscle

precursor cells', *Anatomy and Embryology*, 211(SUPPL. 1), pp. 37–41. doi:10.1007/s00429-006-0118-9.

Vasyutina, E., Lenhard, D.C., Wende, H., Erdmann, B., Epstein, J.A. and Birchmeier, C. (2007) 'RBP-J (Rbpsuh) is essential to maintain muscle progenitor cells and to generate satellite cells', *Proceedings of the National Academy of Sciences of the United States of America*, 104(11), pp. 4443–4448. doi:10.1073/pnas.0610647104.

Verma, M., Asakura, Y., Murakonda, B.S.R., Pengo, T., Latroche, C., Chazaud, B., McLoon, L.K. and Asakura, A. (2018) 'Muscle Satellite Cell Cross-Talk with a Vascular Niche Maintains Quiescence via VEGF and Notch Signaling', *Cell Stem Cell*, 23(4), pp. 530-543.e9. doi:10.1016/j.stem.2018.09.007.

Villalta, S.A., Deng, B., Rinaldi, C., Wehling-Henricks, M. and Tidball, J.G. (2011) ' IFN-γ Promotes Muscle Damage in the mdx Mouse Model of Duchenne Muscular Dystrophy by Suppressing M2 Macrophage Activation and Inhibiting Muscle Cell Proliferation ', *The Journal of Immunology*, 187(10), pp. 5419–5428. doi:10.4049/jimmunol.1101267.

Villalta, S.A., Rinaldi, C., Deng, B., Liu, G., Fedor, B. and Tidball, J.G. (2011) 'Interleukin-10 reduces the pathology of mdx muscular dystrophy by deactivating M1 macrophages and modulating macrophage phenotype', *Human Molecular Genetics*, 20(4), pp. 790–805. doi:10.1093/hmg/ddq523.

Walton, E.M., Cronan, M.R., Beerman, R.W. and Tobin, D.M. (2015) 'The macrophage-specific promoter mfap4 allows live, long-term analysis of macrophage behavior during mycobacterial infection in zebrafish', *PLoS ONE*, 10(10), pp. 1–17. doi:10.1371/journal.pone.0138949.

Wang, M., Song, W., Jin, C., Huang, K., Yu, Q., Qi, J., Zhang, Q. and He, Y. (2021) 'Pax3 and pax7 exhibit distinct and overlapping functions in marking muscle satellite cells and muscle repair in a marine teleost, sebastes schlegelii', *International Journal of Molecular Sciences*, 22(7). doi:10.3390/ijms22073769.

Wang, Xiaobin, Shen, Q.W., Wang, J., Zhang, Z., Feng, F., Chen, T., Zhang, Y., Wei, H., Li, Z., Wang, Xinxia and Wang, Y. (2016) 'KLF7 Regulates Satellite Cell Quiescence in Response to Extracellular Signaling', *Stem Cells* [Preprint]. doi:10.1002/stem.2346.

Wang, Y., Wehling-Henricks, M., Samengo, G. and Tidball, J.G. (2015) 'Increases of

M2a macrophages and fibrosis in aging muscle are influenced by bone marrow aging and negatively regulated by muscle-derived nitric oxide', *Aging Cell*, 14(4), pp. 678–688. doi:10.1111/acel.12350.

Warren, G.L., Hulderman, T., Jensen, N., McKinstry, M., Mishra, M., Luster, M.I. and Simeonova, P.P. (2002) 'Physiological role of tumor necrosis factor alpha in traumatic muscle injury.', *The FASEB journal : official publication of the Federation of American Societies for Experimental Biology*, 16(12), pp. 1630–1632. doi:10.1096/fj.02-0187fje.

Warren, G.L., Hulderman, T., Mishra, D., Gao, X., Millecchia, L., O'Farrell, L., Kuziel, W.A. and Simeonova, P.P. (2005) 'Chemokine receptor CCR2 involvement in skeletal muscle regeneration', *The FASEB Journal*, 19(3), pp. 1–23. doi:10.1096/fj.04-2421fje.

Weavers, H., Liepe, J., Sim, A., Wood, W., Martin, P. and Stumpf, M.P.H. (2016) 'Systems Analysis of the Dynamic Inflammatory Response to Tissue Damage Reveals Spatiotemporal Properties of the Wound Attractant Gradient', *Current Biology*, 26(15), pp. 1975–1989. doi:10.1016/j.cub.2016.06.012.

Webster, M.T., Manor, U., Lippincott-Schwartz, J. and Fan, C.M. (2016) 'Intravital Imaging Reveals Ghost Fibers as Architectural Units Guiding Myogenic Progenitors during Regeneration', *Cell Stem Cell*, 18(2), pp. 243–252. doi:10.1016/j.stem.2015.11.005.

Weinberg, E.S., Allende, M.L., Kelly, C.S., Abdelhamid, A., Murakami, T., Andermann, P., Doerre, O.G., Grunwald, D.J. and Riggleman, B. (1996) 'Developmental regulation of zebrafish MyoD in wild-type, no tail and spadetail embryos', *Development*, 122(1), pp. 271–280. doi:10.1242/dev.122.1.271.

Welch, B.L. (1938) 'The Significance of the Difference Between Two Means when the Population Variances are Unequal', *Biometrika*, 29(3/4), p. 350. doi:10.2307/2332010.

Wen, Y., Bi, P., Liu, W., Asakura, A., Keller, C. and Kuang, S. (2012) 'Constitutive Notch Activation Upregulates Pax7 and Promotes the Self-Renewal of Skeletal Muscle Satellite Cells', *Molecular and Cellular Biology*, 32(12), pp. 2300–2311. doi:10.1128/mcb.06753-11.

Wen, Yefei, Bi, P., Liu, W., Asakura, A., Keller, C. and Kuang, S. (2012) 'Constitutive

Notch Activation Upregulates Pax7 and Promotes the Self-Renewal of Skeletal Muscle Satellite Cells', *Molecular and Cellular Biology*, 32(12), pp. 2300–2311. doi:10.1128/mcb.06753-11.

Westerfield, M. (2007) 'The Zebrafish Book. A Guide for the Laboratory Use of Zebrafish (Danio rerio), 5th Edition', *University of Oregon Press, Eugene (Book)* [Preprint].

Wobbrock, J.O., Findlater, L., Gergle, D. and Higgins, J.J. (2011) 'The Aligned Rank Transform for nonparametric factorial analyses using only ANOVA procedures', *Conference on Human Factors in Computing Systems - Proceedings*, pp. 143–146. doi:10.1145/1978942.1978963.

Wolff, C., Roy, S. and Ingham, P.W. (2003) 'Multiple muscle cell identities induced by distinct levels and timing of Hedgehog activity in the zebrafish embryo', *Current Biology* [Preprint]. doi:10.1016/S0960-9822(03)00461-5.

Woodhouse, S., Pugazhendhi, D., Brien, P. and Pell, J.M. (2013) 'Ezh2 maintains a key phase of muscle satellite cell expansion but does not regulate terminal differentiation', *Journal of Cell Science*, 126(2), pp. 565–579. doi:10.1242/jcs.114843.

Xie, Y., Tolmeijer, S., Oskam, J.M., Tonkens, T., Meijer, A.H. and Schaaf, M.J.M. (2019) 'Glucocorticoids inhibit macrophage differentiation towards a pro-inflammatory phenotype upon wounding without affecting their migration', *DMM Disease Models and Mechanisms*, 12(5). doi:10.1242/dmm.037887.

Yang, W. and Hu, P. (2018) 'Skeletal muscle regeneration is modulated by inflammation', *Journal of Orthopaedic Translation*, 13, pp. 25–32. doi:10.1016/j.jot.2018.01.002.

Yartseva, V., Goldstein, L.D., Rodman, J., Kates, L., Chen, M.Z., Chen, Y.J.J., Foreman, O., Siebel, C.W., Modrusan, Z., Peterson, A.S. and Jovičić, A. (2020) 'Heterogeneity of Satellite Cells Implicates DELTA1/NOTCH2 Signaling in Self-Renewal', *Cell Reports*, 30(5), pp. 1491-1503.e6. doi:10.1016/j.celrep.2019.12.100.

Yoo, S.K., Deng, Q., Cavnar, P.J., Wu, Y.I., Hahn, K.M. and Huttenlocher, A. (2010) 'Differential Regulation of Protrusion and Polarity by PI(3)K during Neutrophil Motility in Live Zebrafish', *Developmental Cell*, 18(2), pp. 226–236. doi:10.1016/j.devcel.2009.11.015.

Zammit, P.S., Golding, J.P., Nagata, Y., Hudon, V., Partridge, T.A. and Beauchamp, J.R. (2004) 'Muscle satellite cells adopt divergent fates: A mechanism for self-renewal?', *Journal of Cell Biology*, 166(3), pp. 347–357. doi:10.1083/jcb.200312007.

Zhan, M., Jin, B., Chen, S.E., Reecy, J.M. and Li, Y.P. (2007) 'TACE release of TNF-α mediates mechanotransduction-induced activation of p38 MAPK and myogenesis', *Journal of Cell Science*, 120(4), pp. 692–701. doi:10.1242/jcs.03372.

Zhang, C., Li, Y., Wu, Y., Wang, L., Wang, X. and Du, J. (2013) 'Interleukin-6/signal transducer and activator of transcription 3 (STAT3) pathway is essential for macrophage infiltration and myoblast proliferation during muscle regeneration', *Journal of Biological Chemistry*, 288(3), pp. 1489–1499. doi:10.1074/jbc.M112.419788.

Zhang, C., Wang, C., Li, Y., Miwa, T., Liu, C., Cui, W., Song, W.C. and Du, J. (2017) 'Complement C3a signaling facilitates skeletal muscle regeneration by regulating monocyte function and trafficking', *Nature Communications*, 8(1). doi:10.1038/s41467-017-01526-z.

Zhang, H., Shang, R. and Bi, P. (2021) 'Feedback regulation of Notch signaling and myogenesis connected by MyoD–Dll1 axis', *PLoS Genetics*, 17(8), pp. 1–25. doi:10.1371/journal.pgen.1009729.

Zhang, J., Xiao, Z., Qu, C., Cui, W., Wang, X. and Du, J. (2014) ' CD8 T Cells Are Involved in Skeletal Muscle Regeneration through Facilitating MCP-1 Secretion and Gr1 high Macrophage Infiltration ', *The Journal of Immunology*, 193(10), pp. 5149–5160. doi:10.4049/jimmunol.1303486.

Zhang, S. and Cui, P. (2014) 'Complement system in zebrafish', *Developmental and Comparative Immunology*, 46(1), pp. 3–10. doi:10.1016/j.dci.2014.01.010.

Zhang, X.M., Ramalho-Santos, M. and McMahon, A.P. (2001) 'Smoothened mutants reveal redundant roles for Shh and Ihh signaling including regulation of L/R asymmetry by the mouse node', *Cell*, 105(6), pp. 781–792. doi:10.1016/S0092-8674(01)00385-3.

Zhu, Y.P., Brown, J.R., Sag, D., Zhang, L. and Suttles, J. (2015) 'Adenosine 5'-Monophosphate–Activated Protein Kinase Regulates IL-10–Mediated Anti-Inflammatory Signaling Pathways in Macrophages', *The Journal of Immunology*, 194(2), pp. 584–594. doi:10.4049/jimmunol.1401024.

Chapter 9 Appendix

9.1 Figures

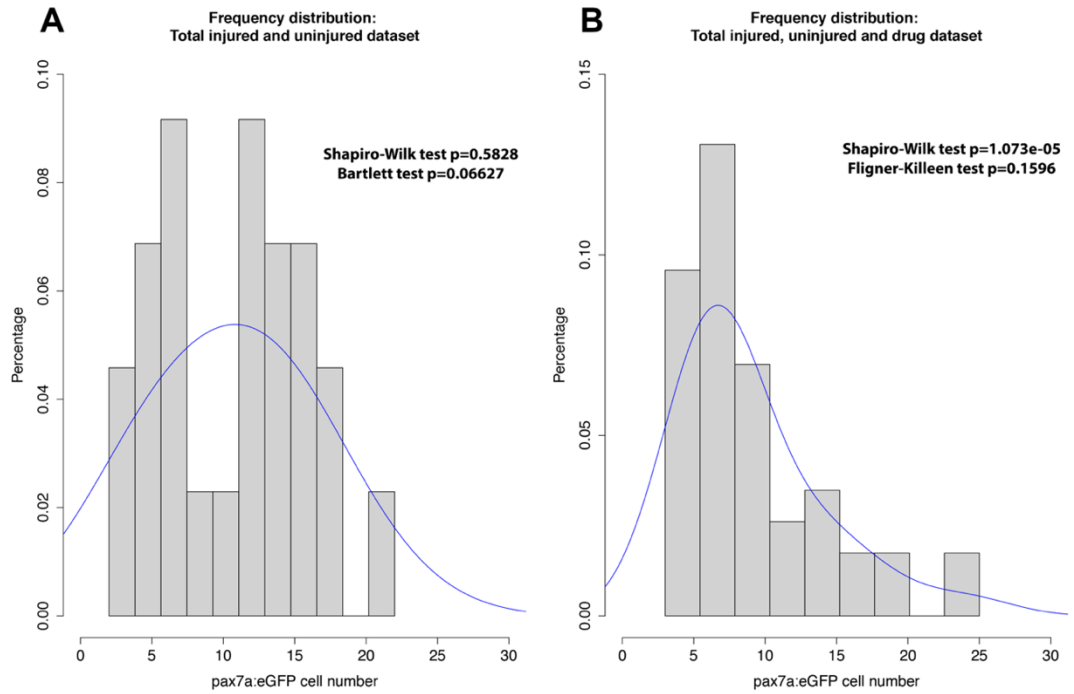

Figure 9.1. Normality and scedasticity.
Histograms with density curves illustrating the frequency distribution of *pax7a:eGFP*$^{+}$ cell number across the datasets analysed. Datasets were grouped as follows: animals at 4 and 8 dpf, with or without injury (**A**, n=24); animals at 4 and 8 dpf, with or without injury, treated with DAPT or DMSO (**B**, n=47). The Shapiro-Wilk test was used to assess for normality. To assess scedasticity, a Bartlett test (**A**) or Fligner-Killeen test (**B**) was used.

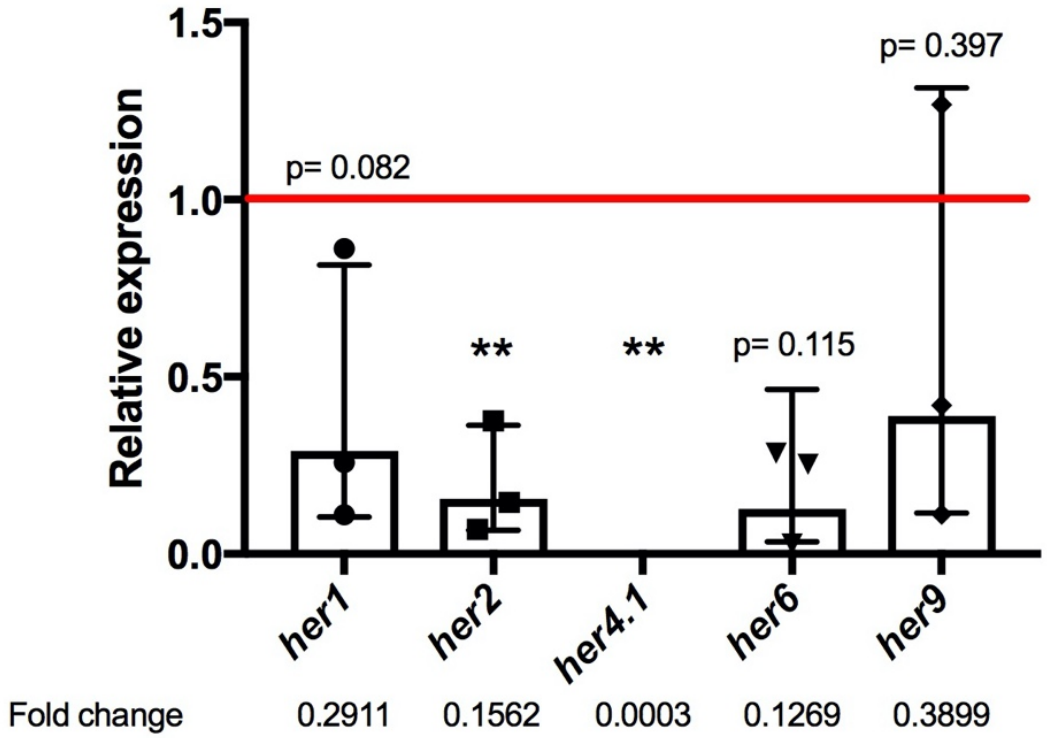

Figure 9.2. DAPT treatment partially supresses the expression of Notch target genes.
3 dpf wild type larvae were treated with 100 µM DAPT or 1% v/v DMSO for 18 hours. 500ng/µl total RNA from whole larvae was used to synthesis cDNA of which 2ng cDNA were used per qPCR reaction. Expression of *her1*, *her2*, *her4.1*, *her6* and *her9* was determined relative to *Elf1a* housekeeping gene. Mean fold change has been reported relative to DMSO controls (red line). All Notch target genes are downregulated, of which *her2*, *her4.1* are significantly suppressed. Errors bars represent SEM and statistical significance was determined by Student's t-test.

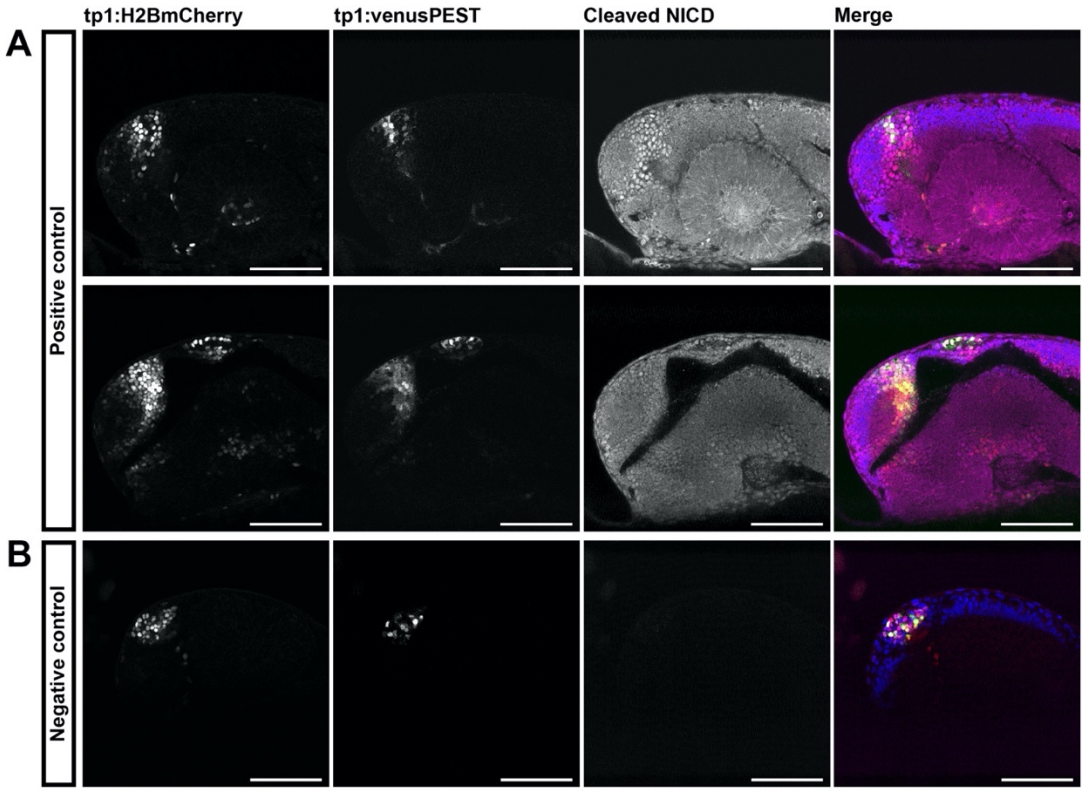

Figure 9.3. The *Tp1* reporter lines are expressed within a small proportion of Notch expressing cells.

24 hpf *Tp1:H2BmCherry*; *Tp1*:VenusPEST+ larvae were fixed and Venus, mCherry and cleaved NICD were detected by immunofluorescence (**A**). Controls with only secondary antibody (**B**) were used to validate the staining, so ensure that the staining observed was not a consequence of non-specific secondary antibody binding. A large population of cells expressing cleaved NICD were present in the developing zebrafish midbrain. Cleaved NICD-expressing was also express in a subset of mCherry+ cells, and a smaller subset of Venus+ cells.

Scale bars: 100 μm (**A-B**).

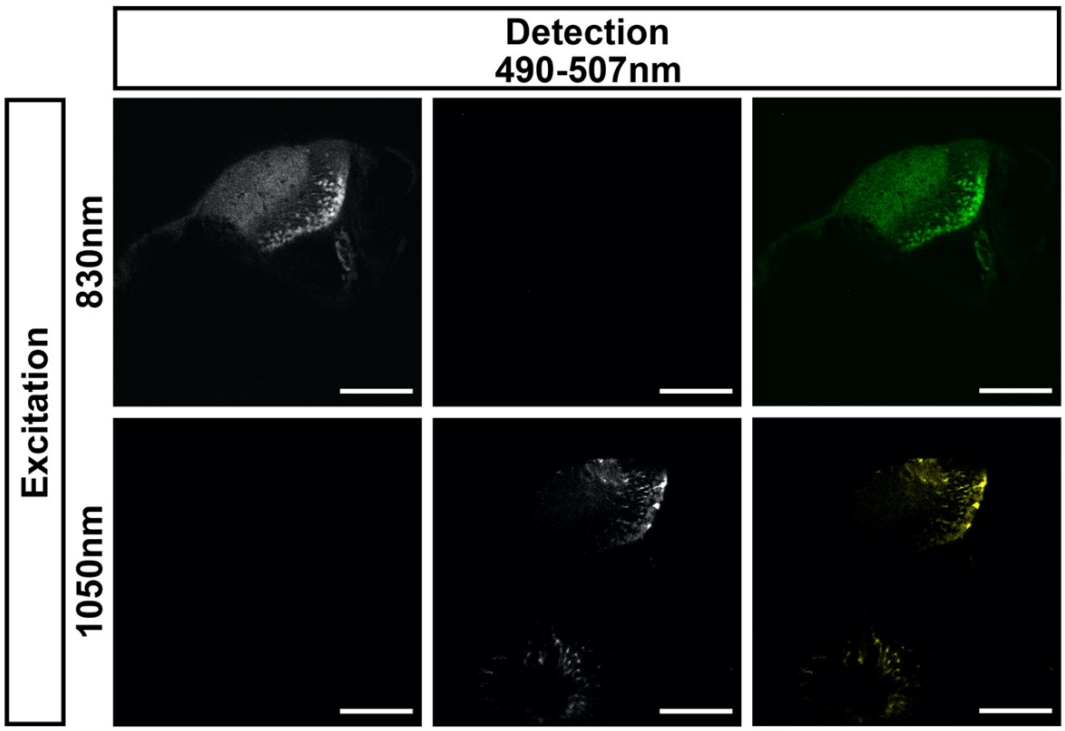

Figure 9.4. Optimisation of multi-photon imaging setup to sequentially acquire eGFP and Venus signal.

5 dpf *pax7a:eGFP*; *Tp1*:VenusPEST- expressing larvae were imaged on a multi-photon system. The ti:sapphire laser was tuned to 830 nm to excite eGFP and the OPO was tuned to 1050 nm to excite Venus. Both fluorophores were sequentially detected using a detector specific for 490-507 nm. Representative z-projections demonstrating non-overlapping signals of eGFP and Venus in the zebrafish midbrain.
Scale bars: 100 µm

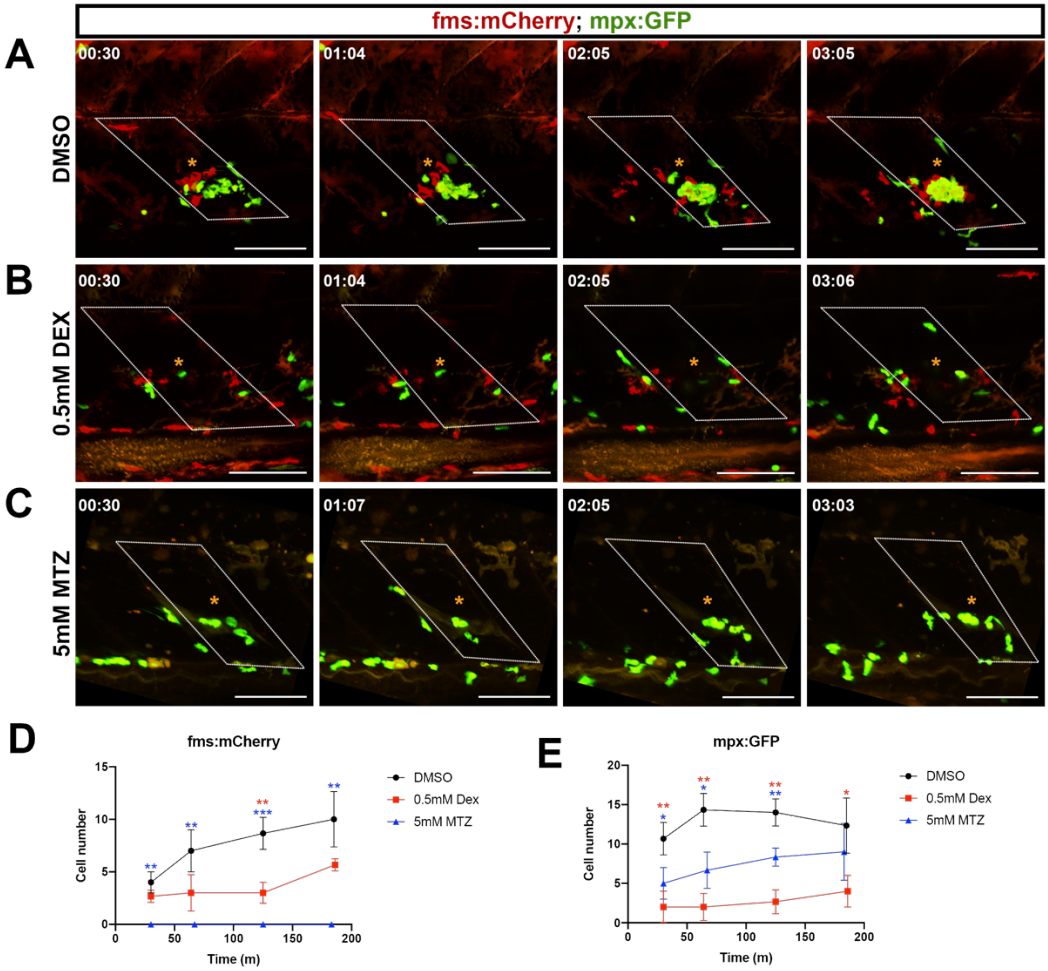

Figure 9.5. Optimisation of dexamethasone and metronidazole treatment.
5 dpf *mpx:GFP*; *fms:mCherry*+ larvae were injured and treated with DMSO (**A**), DEX (**B**) or MTZ (**C**). Larvae were then live imaged on a multi-photon system over a 3.4-hour time period. Representative z-projections (**A-C**) show migratory mCherry+ macrophages and GFP+ neutrophils responding to injury (asterisk). The number of mCherry+ (**D**) and GFP+ cells were quantified. DEX treatment resulted in fewer mCherry+ (**D**) and GFP+ cells. MTZ treatments abolished mCherry+ macrophage numbers (**D**) and reduced the number of recruited GFP+ neutrophils. Significant differences were tested by Student's t-test (* $p < 0.05$, ** $p < 0.01$, *** $p < 0.001$).
Scale bars: 100 µm

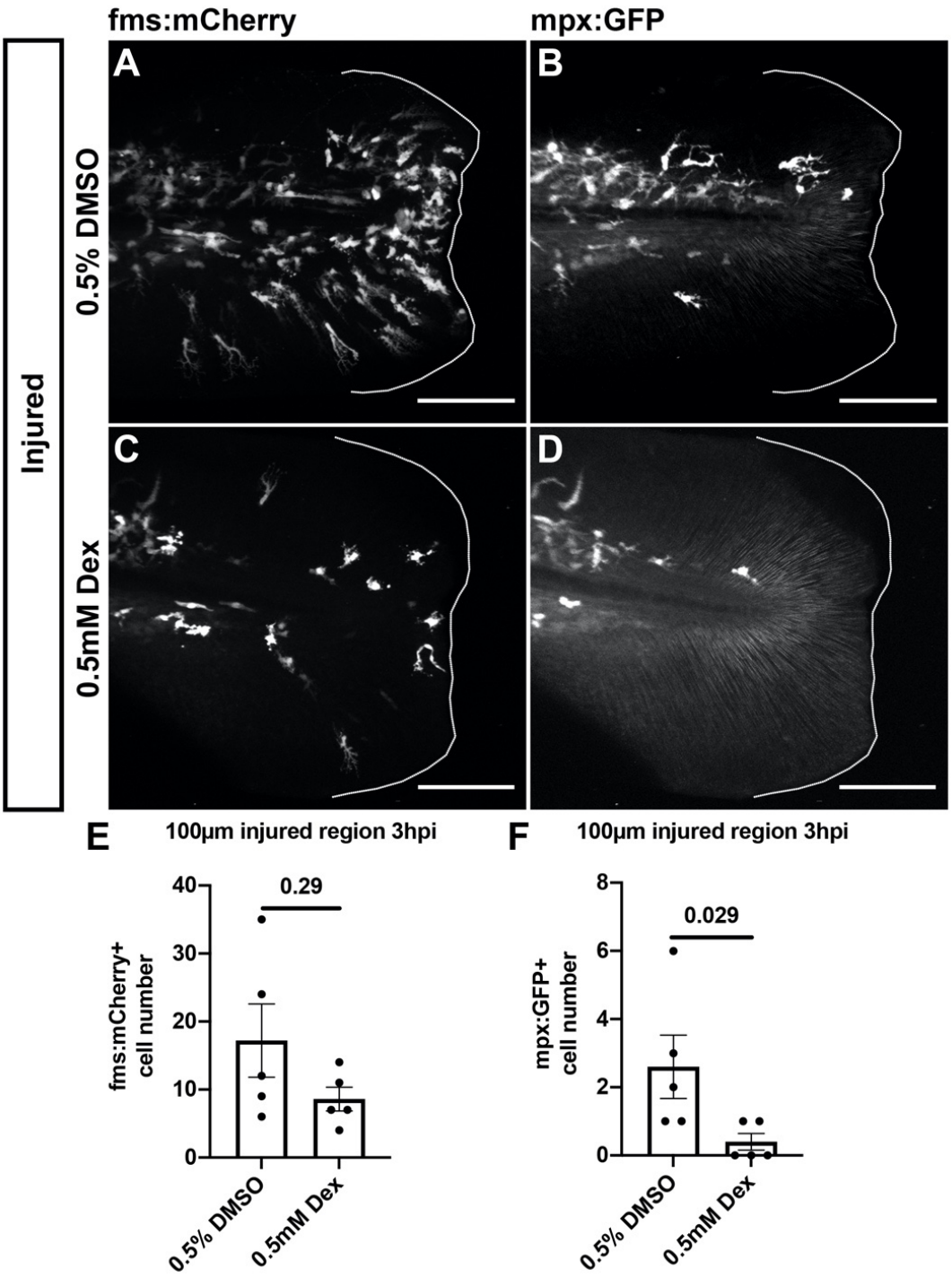

Figure 9.6. Fewer inflammatory cell recruited towards caudal fin amputation 3 hpa following dexamethasone treatment.

Representative projections from confocal z-stacks of the amputated caudal fin (dotted line) of 2 dpf *mpx:GFP*; *fms:mCherry*+ larvae treated with DMSO (**A-B**) or DEX (**C-D**). The number of mCherry+ macrophages and GFP+ neutrophils (**F**) were quantified within a 100 µm injured region 3 hpa. Although there were fewer mCherry+ cells following DEX treatment, this was non-significant ($p > 0.05$; **E**). There were fewer GFP+ cells following DEX treatment (**F**). Significant differences were tested by Wilcoxon Mann Whitney U rank sum test. Error bars represent standard deviation, and values above comparison bars represent significance (p-values).

Scale bars: 100 µm

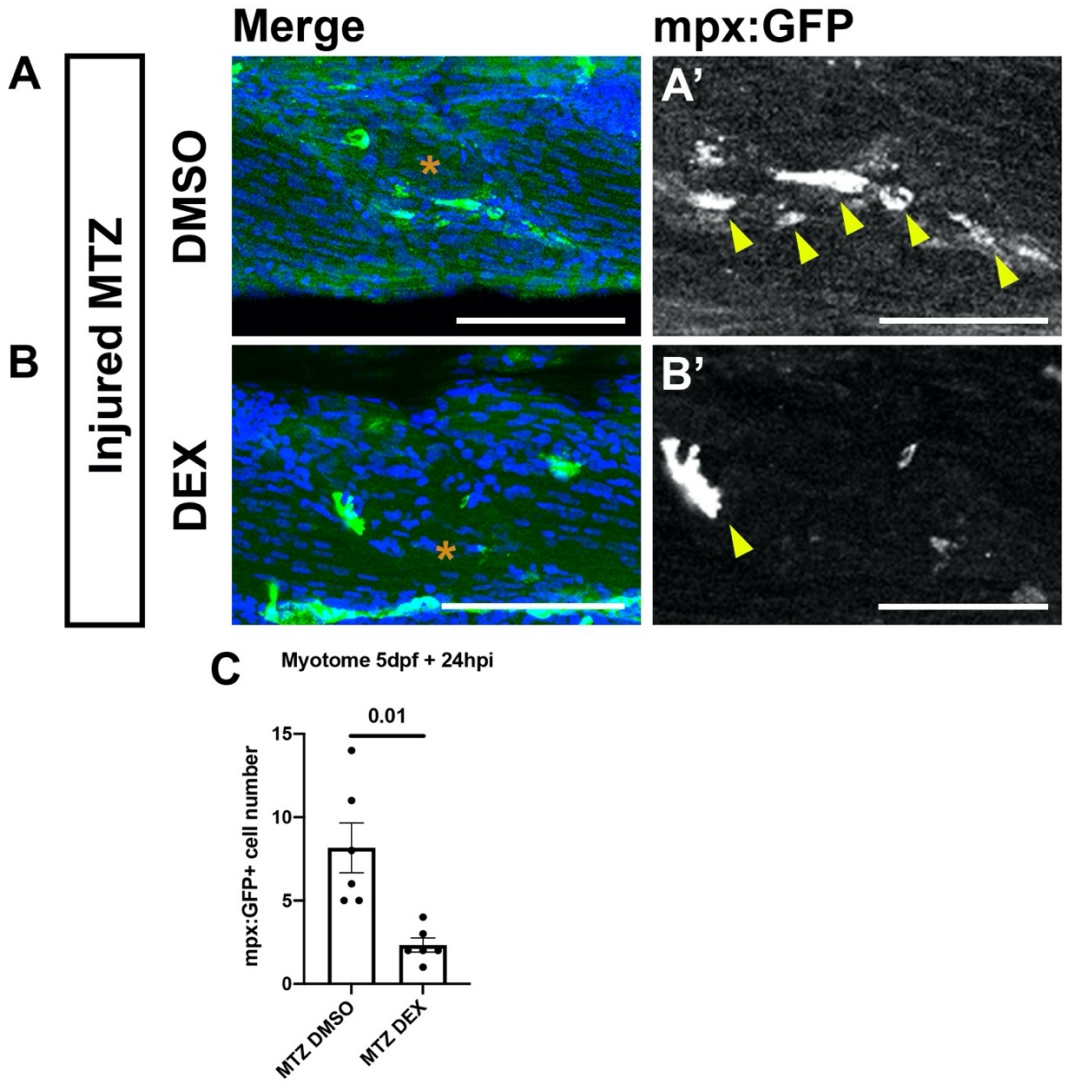

Figure 9.7. Dexamethasone treatment reduces the number of neutrophils which perdure following macrophage ablation 24 hpi.

Representative projections from confocal z-stacks of the injured myotome of 5dpf *mpx:GFP*-expressing larvae 24 hpi. Larvae were treated with MTZ (A) or co-treated with MTZ and DEX (B). eGFP+ neutrophils were detected (**A'-B'**), and the number of cells were quantified in the injured myotome (**C**). Injury denoted by an asterisk. There were fewer GFP+ neutrophils when larvae were co-treated with MTZ and DEX. Significant differences were tested by Welch's t-test. Error bar represents standard deviation, and the value above the comparison bars represents significance (p-values).

Scale bars: 100 µm (**A-B**), 50 µm (**A'-B'**).

9.2 Tables

Stage (dpf)	Injury (Y/N)	DAPT (µM)	DMSO (%)	Mean number of *pax7a:eGFP*+ cells	SD
4	N	0	0	5.5	1.52
4	Y	0	0	11.67	1.86
8	N	0	0	8.33	4.68
8	Y	0	0	17.17	2.48
4	N	0	1	5.83	2.14
4	Y	0	1	14	1.61
4	N	100	0	7.5	1.87
4	Y	100	0	7.83	2.71
8	N	0	1	6.8	1.92
8	Y	0	1	17.33	6.19
8	N	100	0	5.5	1.52
8	Y	100	0	6.33	1.75

Table 9.1. Summary of experimental datasets
Experimental parameters for each data set have been listed showing the mean number of *pax7a:eGFP*+ muSCs and standard deviation (SD). Parameters include the age of the larvae (4 or 8 dpf) if the larvae were injured (yes or no) and treated with DAPT (0 µM or 100 µM) or DMSO (0% or 1% v/v).

9.3 USB files

9.3.1 Movies

Movie 9.1. Evans blue labelling co-localised with a second harmonic signal from myofibers throughout the extent of the injury field.
7dpf *pax7a pax7a:eGFP* larvae were submerged in 0.1% Evans blue for 1h, injured and then imaged on a multiphoton microscope. Visualisation of Evans blue in damaged myofibers (magenta), second harmonic generation (SHG) in myofibers (cyan) and *pax7a:eGFP* (muSC; green) reveals extensive co-localisation of the Evans Blue and SHG signal.
Scale bar: 100µm.

Movie 9.2. muSC response to single myotome injury.
Injured 3 dpf *pax7a:eGFP*$^{+}$ larvae were imaged by multiphoton microscopy from 1-16.83 hpi with 10 minute intervals between frames. Acquisition encompassed the entire injured myotome and z-stack projections, reveals the migration of muSCs in response to injury.
Scale bar: 50µm. Time stamp in minutes post injury.

Movie 9.3. *Tp1:H2BmCherry*; *Tp1*:VenusPEST-expressing cells respond to muscle injury.
5 dpf *Tp1:H2BmCherry*; *Tp1*:VenusPEST+ larvae were injured and live imaged on a multi-photon system from 1-18.75 hpi with 15 minute intervals between frames. Live imaging reveals a population of migratory mCherry+Venus+ cells responding towards muscle injury.
Scale bar: 50 µm. time stamp in minutes post injury.

Movie 9.4. Activated muSCs do not express *Tp1:H2BmCherry* in response to injury.
7 dpf *pax7a:eGFP*; *Tp1:H2BmCherry*- expressing larvae were injured and live imaged on a multi-photon system from 1-10.2 hpi with 25 minute intervals between frames. Live imaging reveals that proliferating and migrating *pax7a:eGFP*-expressing muSCs did not express the *Tp1:H2BmCherry* transgene following injury.
Scale bar: 50 µm. time stamp in minutes post injury.

Movie 9.5. *pax7a:eGFP*-expressing muSCs express *Tp1*:VenusPEST in response to injury.
5 dpf *pax7a:eGFP*; *Tp1*:VenusPEST- expressing larvae were injured and live imaged on a multi-photon system from 1.5-18.3 hpi with 21 minute intervals between frames. Live imaging reveals proliferating and migrating eGFP+Venus+ in response to injury.
Scale bar: 50 µm. time stamp in minutes post injury.

Movie 9.6. Proliferating *pax7a:eGFP*-expressing muSCs express *Tp1*:VenusPEST in response to injury.
5 dpf *pax7a:eGFP*; *Tp1*:VenusPEST- expressing larvae were injured and live imaged on a multi-photon system from 1.5-18.3 hpi with 21 minute intervals between frames. Live imaging highlights that proliferating *pax7a:eGFP*-expressing muSCs and the subsequent daughter cells expressed *Tp1*:VenusPEST in response to injury.
Scale bar: 10 µm. time stamp in minutes post injury.

Movie 9.7. Neutrophils and macrophages are recruited towards muscle injury.
5 dpf *mpx:GFP*; *fms:mCherry*+ larvae were injured and treated with DMSO and live imaged on a multi-photon system from 0.5-3.4 hpi with 8.6 minute intervals between frames. Live imaging demonstrates recruitment of GFP+ neutrophils and mCherry+ macrophages towards muscle injury.
Scale bar: 50 µm. time stamp in minutes post injury.

Movie 9.8. Fewer neutrophils and macrophages are recruited towards muscle injury following dexamethasone treatment.
5 dpf *mpx:GFP*; *fms:mCherry*+ larvae were injured and treated with DEX. Larvae where then live imaged on a multi-photon system from 0.5-3.4 hpi with 6.8 minute intervals between frames. Live imaging revealed fewer GFP+ neutrophils and mCherry+ macrophages were recruited towards muscle injury.
Scale bar: 50 µm. time stamp in minutes post injury.

Movie 9.9. Fewer neutrophils and no macrophages are recruited towards muscle injury following metronidazole treatment.
5 dpf *mpx:GFP*; *fms:mCherry*+ larvae were injured and treated with MTZ. Larvae where then live imaged on a multi-photon system from 0.5-3.4 hpi with 7.3 minute intervals between frames. Live imaging revealed fewer GFP+ neutrophils and no mCherry+ macrophages were recruited towards muscle injury.
Scale bar: 50 µm. time stamp in minutes post injury.

Movie 9.10. Migratory *Tp1:H2BmCherry*+ cells observed following injury in an absence of macrophages.
5 dpf *Tp1:H2BmCherry*; *fms:mCherry*+ larvae were injured and treated with MTZ. Larvae where then live imaged on a multi-photon system from 1-18.3 hpi with 15 minute intervals between frames. Live imaging revealed many migratory mCherry+ cells following injury.
Scale bas: 50 µm. time stamp in minutes post injury.

Movie 9.11. Recruited neutrophils express *Tp1:H2BmCherry* following injury in an absence of macrophages.
5 dpf *mpx:GFP*; *Tp1:H2BmCherry*; *fms:mCherry*+ larvae were injured and treated with MTZ. Larvae where then live imaged on a multi-photon system from 1.5-18.3 hpi with 10 minute intervals between frames. Live imaging revealed eGFP+mCherry+ neutrophils were recruited towards muscle injury.
Scale bar: 50 µm. time stamp in minutes post injury.

Movie 9.12. Macrophages are recruited to injured muscle.
5 dpf *fms:mCherry*+ larvae were injured and live imaged on a multi-photon system from 1-3.7 hpi with 10 minute intervals between frames. Live imaging demonstrates recruitment of mCherry+ macrophages towards muscle injury. Injury can be visualised in SHG signal.
Scale bar: 50 µm. time stamp in minutes post injury.

Movie 9.13. Fewer macrophages are recruited to muscle injury following DAPT treatment.
5 dpf *fms:mCherry*+ larvae were injured and treated with DAPT. Larvae where then live imaged on a multi-photon system from 1-3.5 hpi with 10 minute intervals between frames. Live imaging revealed fewer mCherry+ macrophages were recruited towards muscle injury. Injury can be visualised in SHG signal.
Scale bar: 50 µm. time stamp in minutes post injury.

9.3.2 Excel files

File 9.1. Summary of datasets and significance chapter 3.
Excel workbook containing statistical results and the means and standard deviations from each dataset. Workbook has been separated in function of the figure number. ANOVA results section includes the comparisons made (condition, cell type and anatomic position), the type of ANOVA conducted (Classical or ART) and the p-value. Pair-wise results section includes the comparisons made, the type of pair-wise test (monovariable: Student's t-test, Welch's t-test, Wilcoxon-Mann-Whitney [WMW] test; multivariable: Tukey or Dunn's test with Benjamini and Hochberg (bh) correction) and the p-value. The pair-wise results section also includes results from a normality test (Shapiro–Wilk test) and test for equal variance (Bartlett test, Fligner-Killeen test or F-test). For each worksheet, the mean and standard deviation for each condition has also been listed to understand any significant changes.

File 9.2. Summary of datasets and significance chapter 4.
Excel workbook containing statistical results and the means and standard deviations from each dataset. Workbook has been separated in function of the figure number. ANOVA results section includes the comparisons made (condition, cell type and anatomic position), the type of ANOVA conducted (Classical or ART) and the p-value. Pair-wise results section includes the comparisons made, the type of pair-wise test (monovariable: Student's t-test, Welch's t-test, Wilcoxon-Mann-Whitney [WMW] test; multivariable: Tukey or Dunn's test with Benjamini and Hochberg (bh) correction) and the p-value. The pair-wise results section also includes results from a normality test (Shapiro–Wilk test) and test for equal variance (Bartlett test, Fligner-Killeen test or F-test). For each worksheet, the mean and standard deviation for each condition has also been listed to understand any significant changes.

File 9.3. Summary of datasets and significance chapter 5.
Excel workbook containing statistical results and the means and standard deviations from each dataset. Workbook has been separated in function of the figure number. ANOVA results section includes the comparisons made (condition, cell type and anatomic position), the type of ANOVA conducted (Classical or ART) and the p-value. Pair-wise results section includes the comparisons made, the type of pair-wise test (monovariable: Student's t-test, Welch's t-test, Wilcoxon-Mann-Whitney [WMW] test; multivariable: Tukey or Dunn's test with Benjamini and Hochberg (bh) correction) and the p-value. The pair-wise results section also includes results from a normality test (Shapiro–Wilk test) and test for equal variance (Bartlett test, Fligner-Killeen test or F-test). For each worksheet, the mean and standard deviation for each condition has also been listed to understand any significant changes.

Publications

Sultan, S.H., Dyer, C. and Knight, R.D., 2021. Notch Signaling Regulates Muscle Stem Cell Homeostasis and Regeneration in a Teleost Fish. *Frontiers in cell and developmental biology*, *9*.

Pipalia, T., **Sultan, S.,** Koth, J., Knight, R. and Hughes, S., 2020. Skeletal muscle regeneration in zebrafish. In *Methods in Molecular Biology*. Humana Press Inc.